## DOCTOR OF PHILOSOPHY

# A large scale analysis of chemoattractant induced cytoskeletal dynamics in Dictyostelium discoideum by means of proteomic and imaging approach

Sobczyk, Grzegorz Jerzy

*Award date:*
2012

DOCTOR OF PHILOSOPHY

# A large scale analysis of chemoattractant induced cytoskeletal dynamics in Dictyostelium discoideum by means of proteomic and imaging approach

Grzegorz Jerzy Sobczyk

2012

University of Dundee

# A Large Scale Analysis of Chemoattractant Induced Cytoskeletal Dynamics in *Dictyostelium discoideum* by Means of Proteomic and Imaging Approach

PhD thesis

Grzegorz Jerzy Sobczyk

Supervisor

Professor Cornelis Jan Weijer

Division of Cell and Developmental Biology

College of Life Sciences

University of Dundee

# Summary

Chemotaxis is a fundamental process involved in a diverse range of biological phenomena such as nutrient finding in unicellular organisms, development and morphogenesis of multicellular organisms, wound healing and immune response. It is also related to a number of diseases including immunological disorders and cancer metastasis. It is a complex cellular process which is composed of several steps including signal detection and amplification, cell polarisation and cytoskeleton reorganisation. There are several signal transduction pathways working in parallel to control chemotaxis, which involve a multitude of regulatory factors and effectors modulating the cytoskeletal dynamics. The final outcome is actin polymerisation at the leading edge, depolymerisation at the trailing edge and myosin II filament assembly and contraction in the back of the cell, which together drive the directional cell movement in the direction of the chemotactic gradient.

One of the poorly understood aspects of the chemotactic response is a biphasic character of the chemoattractant-induced actin polymerisation. The two temporally distinct phases of actin polymerisation reveal very different characteristics and regulation, but the exact mechanisms responsible for these differences have not been determined.

We have taken advantage of recent advances in a quantitative proteomic technique and adapted the SILAC experimental approach to analyse the fast translocation dynamics of proteins associated with a crude cytoskeleton preparation after stimulation with the chemoattractant in *Dictyostelium discoideum.* These experiments detected, among many other proteins, a wide range of cytoskeletal components including structural constituents, actin binding proteins and regulatory factors associated with the cortical cytoskeleton. The SILAC results provide valuable quantitative information about the translocation dynamics for

hundreds of cytoskeletal components in the same experiment. Most of those proteins follow the generic biphasic profile of enrichment reflecting actin dynamics, but subsets of proteins show specific incorporation during only one of the two phases of actin polymerisation. We identify several positive regulators of actin polymerisation showing enrichment specific to the first phase of chemotactic response and other regulatory components incorporated to the cytoskeleton exclusively during the second phase of cAMP-induced actin polymerisation. Detailed analysis of the major structural components of the actin cytoskeleton reveal that about 25% of the primary actin nucleator – Arp2/3 complex, incorporated to the cortex during the first phase, do not trigger formation of a new filament.

In order to verify the proteomic analysis 55 known cytoskeletal proteins, which showed strong enrichment in the SILAC experiments, were selected for tagging with GFP followed by *in vivo* fluorescence microscopy imaging. Their analyses served as positive controls validating the translocation dynamics patterns measured with the SILAC experiments and also provided further detailed spatio-temporal characterisation of the cAMP-mediated protein translocation. Regulatory factors involved in the first phase of actin polymerisation can be classified into two groups exhibiting distinct incorporation dynamics detected by TIRFM imaging. The first group includes DocA, DocB and GacR proteins, which show very rapid and transient translocation to the cortex and are most likely involved in the earliest events following cAMP stimulation. The second group, which is composed of Roco7, PakB, XacB and GacA proteins, shows slower enrichment and longer occupancy at the cortex. TIRFM analysis also led to characterisation of a new class of cytoskeletal components, which bind exclusively to the pre-existing actin filaments and do not associate with the structures formed during response to cAMP stimulation. These proteins, which include MhcA, ZizA, RapGAP1 and two novel cytoskeletal components, translocate only to the inner cortex upon cAMP stimulation and are likely involved in regulation of the actin depolymerisation phase.

In order to identify novel components of the cytoskeleton 54 uncharacterised proteins showing response to cAMP stimulation in the SILAC experiments, were cloned and tagged with GFP. Most of those proteins showed specific localisations to various cellular compartments including the nucleus, contractile vacuoles and various types of vesicles. 12 of the selected proteins showed colocalisation with the cortical structures and clear translocation in response to cAMP stimulation. A small number of these proteins contain actin binding domains identified by sequence homology analysis, but none of them were previously characterised. These novel cytoskeletal components need to be further investigated in order to determine their functions in the cytoskeleton and chemotaxis.

# Table of Contents

**1. INTRODUCTION - 8 -**

1.1. *DICTYOSTELIUM DISCOIDEUM* AS AN IDEAL MODEL ORGANISM TO INVESTIGATE CHEMOTAXIS - 9 -

1.2. PRINCIPLES OF CHEMOTACTIC MOVEMENT - 13 -

1.3. COMPONENTS OF THE CYTOSKELETON - 15 -

1.4. REGULATION OF CHEMOTAXIS - 20 -

1.4.1. Ras GTPases - 20 -

1.4.2. Directional sensing and cell polarity - 22 -

1.4.3. Signal transduction pathways - 25 -

1.5. BIPHASIC CHARACTER OF CAMP-INDUCED ACTIN POLYMERISATION - 32 -

1.6. EXPERIMENTAL APPROACH FOR INVESTIGATING FUNCTION AND REGULATION OF THE CYTOSKELETON DURING CHEMOTAXIS - 35 -

1.6.1. Mass spectrometry-based proteomics - 37 -

1.6.2. *In vivo* fluorescence microscopy - 44 -

**2. MATERIALS AND METHODS - 50 -**

2.1. BUFFERS - 50 -

2.2. SILAC PROTOCOL - 51 -

2.2.1. Cell stimulation and lysis conditions - 51 -

2.2.2. Sample preparation - 52 -

2.2.3. In-gel digest and peptide extraction - 53 -

2.3. CROSS-LINKED SILAC PROTOCOL - 54 -

2.4. DATA ANALYSIS - 55 -

2.5. PHALLOIDIN ACTIN POLYMERISATION ASSAY - 56 -

2.6. MOLECULAR CLONING - 57 -

2.6.1. Vectors for protein GFP tagging and overexpression - 57 -

2.6.2. Cloning procedures - 58 -

2.7. *DICTYOSTELIUM* CELLS TRANSFECTION - 60 -

2.8. *IN VIVO* FLUORESCENCE MICROSCOPY - 61 -

2.8.1. Confocal microscopy - 61 -

2.8.2. TIRF microscopy - 62 -

**3. PROTEOMIC ANALYSIS OF THE CYTOSKELETON - 63 -**

3.1. EXPERIMENTAL APPROACH - 63 -

3.2. GENERAL PROTEIN DETECTION - 69 -

3.3. CYTOSKELETAL PROTEINS - 71 -

3.3.1. Structural components of the cytoskeleton - 74 -

3.3.2. Regulatory components of the cytoskeleton - 77 -

3.4. PROTEINS FROM OTHER CELLULAR COMPONENTS - 80 -

3.5. CROSS-LINKED SILAC EXPERIMENT - 85 -

3.6. SELECTION OF PROTEINS FOR TAGGING WITH GFP - 92 -

**4. *IN VIVO* MICROSCOPY ANALYSIS OF THE CYTOSKELETAL DYNAMICS - 98 -**

4.1. GENERAL LOCALISATION GROUPS - 99 -

4.1.1. Strong cortical proteins - 99 -

4.1.2. Weak cortical proteins - 101 -

4.1.3. Microtubular proteins - 105 -

4.1.4. Contractile vacuole proteins - 108 -

4.1.5. Vesicular proteins - 110 -

4.1.6. Nuclear proteins - 113 -

4.2. DETAILED CHARACTERISATION OF SELECTED INDIVIDUAL PROTEINS - 116 -

4.2.1. Structural components of the cytoskeleton - 118 -

4.2.1.1. Coronin A; CorA - 118 -

4.2.1.2. Subunit of actin capping protein Cap32/34; AcpA - 121 -

4.2.1.3. Myosin II heavy chain; MhcA - 125 -

4.2.1.4. Kinesin Family member; Kif5 - 128 -

4.2.2. Regulatory components of the cytoskeleton - 131 -

4.2.2.1. Unconventional Rac GEFs; DocA and DocB - 131 -

4.2.2.2. Zizimin-related protein; ZizA - 135 -

4.2.2.3. Ras-like GTPase; Roco7 - 137 -

4.2.2.4. p21-activated protein kinase; PakB - 141 -

4.2.2.5. Rac GAP; GacR - 143 -

4.2.2.6. Rho GAP; GacA - 146 -

4.2.2.7. Rho GEF / Rho GAP; XacB - 148 -

4.2.3. Uncharacterised cytoskeletal factors - 150 -

4.2.3.1. DDB_G0283827; WASP-related protein - 150 -

4.2.3.2. DDB_G0295683; ADF-H dcp - 153 -
4.2.3.3. DDB_G0277615; ADF-H dcp - 156 -
4.2.3.4. DDB_G0267974; CH dcp - 158 -
4.2.3.5. DDB_G0284825; Rap/Ran GAP dcp - 161 -
4.2.3.6. DDB_G0275305; Fry homolog - 164 -
4.2.3.7. DDB_G0292230 - 167 -
4.2.3.8. DDB_G0293032 - 170 -

**5. DISCUSSION - 173 -**

5.1. SILAC ALLOWS SIMULTANEOUS QUANTITATIVE MEASUREMENTS OF TRANSLOCATION DYNAMICS FOR HUNDREDS OF PROTEINS - 175 -

5.2. *IN VIVO* MICROSCOPY ANALYSIS VALIDATE THE SILAC RESULTS AND PROVIDE ADDITIONAL CHARACTERISATION OF THE CYTOSKELETAL COMPONENTS TRANSLOCATION DYNAMICS - 188 -

5.3. *IN VIVO* MICROSCOPY ANALYSIS VALIDATE THE DYNAMICS OF SEVERAL NOVEL CYTOSKELETAL COMPONENTS DETECTED IN THE SILAC EXPERIMENTS - 208 -

**6. REFERENCES - 216 -**

# Abbreviations:

**AA – arachidonic acid;**
**ACA – adenylyl cyclase of aggregation stage;**
**ADF-H – actin depolymerising factor homology;**
**ARM – Armadillo repeat;**
**Arp2/3 – actin related protein 2/3 complex;**
**cAMP – cyclic adenosine monophosphate;**
**cAR1 – cyclic AMP receptor 1;**
**cGMP – cyclic guanosine monophosphate;**
**CH – calponin homology;**
**CRAC – cytosolic regulator of ACA;**
**CZH – CDM-zizimin homology;**
**DAG – diacylglycerol;**
**DH – Dbl homology;**
**FFA – free fatty acid;**
**F-actin – filamentous actin;**
**G-actin – globular actin monomer;**
**GAP – GTPase-activating protein;**
**Gbp – cGMP binding protein;**
**GDI – GDP-dissociation inhibitor;**
**GEF – guanine nucleotide exchange factor;**
**GPCR – G-protein-coupled receptor;**
**$IP_3$ – inositol (1,4,5) triphosphate;**
**LPA – lysophosphatidic acid;**
**MHCK – myosin heavy chain kinase;**
**MLCK – myosin light chain kinase;**
**PAKa – p21 activated kinase A;**
**PH – pleckstrin homology;**
**PI – phosphatidylinositol;**
**PI3K – phosphatidylinositol (PI) 3 kinases;**
**Pia – Pianissimo;**
**$PI(4,5)P_2$ – phosphatidylinositol (4,5) bisphosphate;**
**$PI(3,4,5)P_3$ – phosphatidylinositol (3,4,5) trisphosphate;**
**PKB – protein kinase B;**
**PL – phospholipid;**
**$PLA_2$ – phospholipase $A_2$;**
**PLC – phospholipase C;**
**PTEN – phosphatase and tensin homolog;**
**RIP3 – Ras interacting protein 3;**
**Scar – suppressor of cyclic AMP receptor;**
**sGC – soluble guanylyl cyclase;**
**TORC2 – Target of rapamycin complex 2;**
**VHP – villin headpiece;**
**WASP – Wiskott-Aldrich syndrome protein;**
**WAVE – WASP family verprolin homology proteins;**
**WIP – WASP interacting protein;**

# 1. Introduction

# 1.1. *Dictyostelium discoideum* as an ideal model organism to investigate chemotaxis

Chemotaxis, the directed movement up or down a chemical concentration gradient of a chemoattractant/repellent, is an essential process which plays a crucial role in a multitude of biological responses and organisms. In single celled organisms it is involved in many aspects of survival such as nutrient sourcing, avoidance of predators and finding optimal environmental conditions. In higher organisms it plays major roles during development by guiding cells in different tissues to their destination, especially during gastrulation [1]. Chemotaxis of axonal growthcones is also critical for the correct wiring of the nervous system in the growing embryo [2]. In adult life chemotaxis plays important roles in processes responsible for tissue maintenance and repair, wound healing and angiogenesis [3]. Chemotaxis is essential for a proper functioning of many cell types in the immune system, such as neutrophils and macrophages, which circulate between vascular and lymphatic systems and migrate toward the sites of infection or inflammation guided by chemoattractants [4, 5].

Due to its involvement in this diverse range of physiological functions, aberrations in chemotaxis are linked to development and progression of several disorders such as asthma, arthritis and other chronic inflammatory diseases [6-9]. Improper cell migration is also the primary cause of one of the most severe pathological phenomena, which is the cancer metastasis [10, 11]. This process occurs when the cancer cells in the primary tumour mutate genes involved in the control of the cell movement. Some of those cells will acquire the ability to invade into the surrounding tissues and also penetrate into the vascular system and spread around the whole organism, generating secondary tumours [12].

Because of this great importance in development and disease, chemotaxis has been a subject of extensive research for a few decades, yet there are still many aspects of this process that are not fully understood.

Since chemotaxis is such a fundamental process, it was developed and optimised very early in the evolution of life in ancient unicellular eukaryotes. Once established, this process was highly conserved throughout the evolution of higher organisms, and the principal mechanisms controlling chemotactic cell movement are virtually identical in all the eukaryotes from simple amoebas to mammalian cells such as leucocytes, especially neutrophils [13]. This universal character allows us to investigate this process in a simple model organism and then translate the results of this research into understanding the basis of development and disease in humans.

*Dictyostelium discoideum* is a simple organism, which was proven to be a powerful system for investigating mechanisms of eukaryotic chemotaxis and other cytoskeletal functions. In fact many of the regulatory components, including Roco proteins [14, 15], and signalling pathways, such as phospholipase $A_2$ [16, 17], mediating chemoattractant-induced motility in eukaryotes have been described in this experimental system. Also many cytoskeletal proteins, such as coronins [18], were first identified in *Dictyostelium* cells.

*Dictyostelium discoideum* is a social amoeba, which spends most of its life as a single cell organism feeding on bacteria in the soil. *Dictyostelium* cells chase bacteria by chemotaxing towards folic acid secreted by those prokaryotes. When the cells divide and multiply they start to deplete their food source and eventually starve. Starvation triggers a fascinating developmental process leading to aggregation of cells to form a motile slug and transform into a fruiting body, which allows them to spread over a new territory (Fig. 1).

**Figure 1.** The lifecycle of *Dictyostelium discoideum.* Vegetative cells are spread uniformly while feeding on bacteria (on the left). Upon food source depletion they starve and start aggregating into multicellular mounds. These structures are transformed into motile slugs (in the middle) which migrate out before developing into a mature fruiting body (on the right). During development cells undergo differentiation into prestalk and prespore cell types which are sorted into different compartments of the multicellular structures and play different roles during the entire developmental process.

Aggregation initiates by individual cells starting to secrete cAMP (cyclic AMP), which is a primary chemoattractant used during the remainder of the developmental process. Other cells in close proximity detect this signal and respond by moving in the direction of its source and by synthesizing and secreting more cAMP themselves [19]. This in turn is then detected by other cells. This process results in the formation of periodic waves of cAMP travelling through the cell mass from the aggregation centre outward, which guide the cells towards the aggregation centre. Up to several hundred thousand cells aggregate during this process by chemotaxing to cAMP, initially individually and later in streams formed by many cells connected in a head-to-tail manner. They form a multicellular mound, which transforms into a slug and which moves to the surface of the soil by a phototactic process. The cells continue to move in response to spiral cAMP waves initiated at the tip [20].

*Dictyostelium* cells differentiate during the developmental process and form two major types of cells, prespore and prestalk, which have very different functions and fates. Prestalk cells drive the developmental process at the multicellular level and they eventually form the stalk

of the fruiting body and die. Prespore cells on the other hand, only follow the guidance provided by the prestalk cells and slowly switch off their metabolism, preparing to form spores, which will go to the next generation [21].

This simple developmental process places the social amoebas on the threshold of the transition between unicellularity and multicellularity. The mounds and slugs formed during development are not true multicellular organisms, since their morphogenesis depends on cell aggregation rather than cell division. In this sense, it may be more adequate to describe those multicellular stages as superorganisms, similarly to social insects like ants or termites. There are several parallel characteristics between those different groups of organisms. Both aggregates of social amoebas and colonies of social insects are formed by closely related, fully independent individuals, which lose their own identity and are willing to sacrifice their lives for the sake of the entire superorganism. In both of those systems there is a specialisation of individuals to perform different functions, which in amoebas involves different genetic programs and cellular composition, while in insects it involves differential development and morphology. The collective behaviour of those superorganisms is controlled by self-organising emergent processes, which give them capabilities far exceeding the summed potential of all the components acting independently.

*Dictyostelium* cells use chemotaxis during their whole life cycle, which means that they are very motile and have highly developed cytoskeletal machinery. The complexity of the actin cytoskeleton and the signalling pathways regulating it in *Dictyostelium* is comparable with that of mammalian leucocytes and other highly motile cells [22]. This organism is biochemically and genetically tractable. Most of the molecular genetic techniques, such as homologous recombination, insertional mutagenesis and RNA interference are available and highly efficient in this system. The *Dictyostelium discoideum* genome has been sequenced and is being annotated [23], which enables all the high-throughput genomic, transcriptomic

and proteomic analysis to be performed. All those characteristics make this model organism a perfect system to use for investigation of chemotaxis and cytoskeletal dynamics.

## 1.2. Principles of chemotactic movement

The dynamic process of chemotactic movement can be divided into several interconnected events such as directional sensing, signal amplification, cell polarisation and force generation driving the motility [24, 25]. It has been proposed that the directional sensing of the chemoattractant coupled with the signal amplification and transduction acts as a compass guiding cells towards the source of stimulus [26].

Directional movement requires a defined cell polarity with differential organisation of the cortical cytoskeleton at two distinct cellular poles. This polarised morphology and localisation of cytoskeletal components is necessary for performing distinct functions at the front and back of moving cells [24].

Actin polymerisation occurs at the leading edge of chemotaxing cells, where it drives the membrane protrusions. The exact mechanism of actin based force generation is not fully understood, but the best model describing this process involves an actin polymerisation based Brownian ratchet [27]. During movement the cell needs to contract its uropod in order for it to follow the protruding front. This process is driven by the contraction of the actin meshwork through the action of myosin II filaments, which are localised predominantly at the back and sides of polarised cells [28, 29]. This actin-based molecular motor generates contractile force by sliding along actin filaments in an MgATP dependent manner [30].

At the same time the cell needs to establish new connections to the substrate at the leading edge in order to gain traction and brake the cell-substrate contacts at the rear to allow uropod contraction [31]. All of those steps together result in a directional cell movement (Fig. 1.1.).

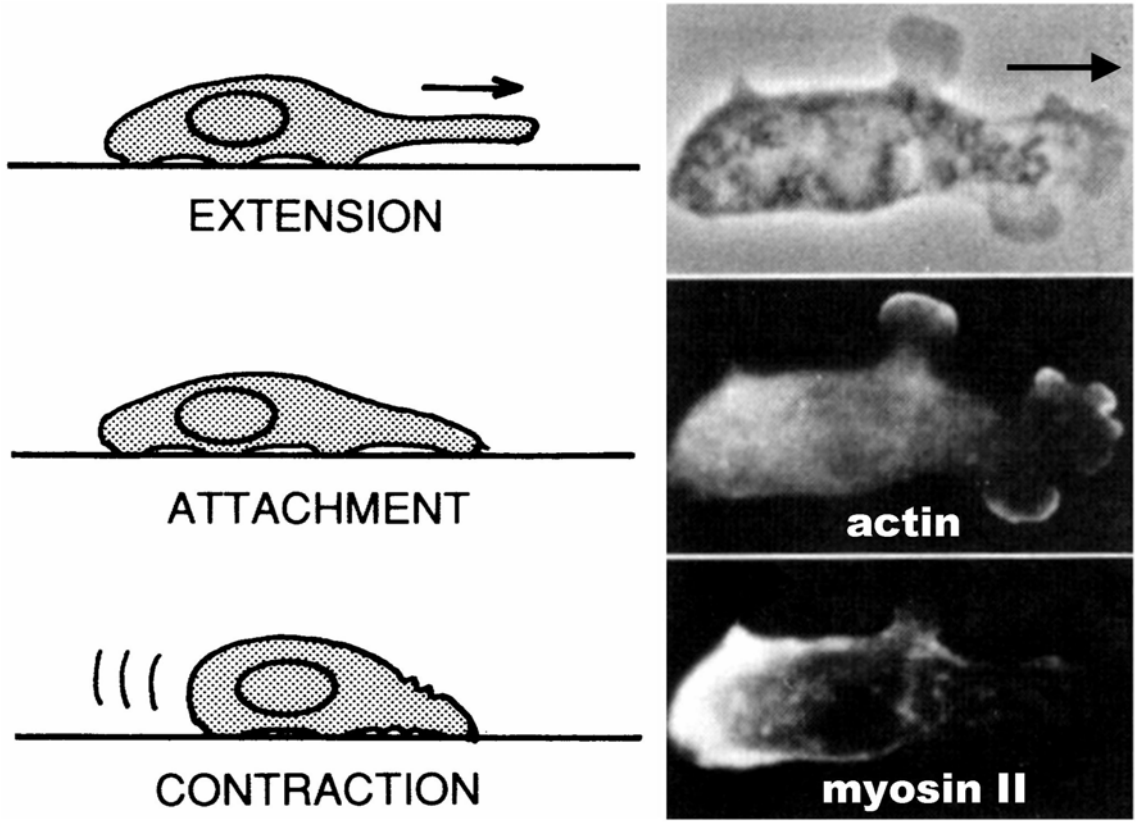


**Figure 1.1.** Basic principles of cellular motility. Directional movement requires a polarised distribution of the cytoskeletal components. Actin polymerisation drives pseudopod formation at the leading edge, while myosin II filaments generate contractile force at the back mediating uropod retraction. During the whole process cell needs to establish new attachment points at the front and disassemble the ones at the rear. Arrows indicate the direction of movement (Based on Fukui *et al.*, 1987).

There are several mechanisms regulating this polarised localisation and activation of different cytoskeletal components leading to F-actin driven pseudopod formation at the front and myosin II mediated contraction at the back of the cell [32, 33]. These mechanisms include positive feedback-loops, which help to maintain the established polarisation and ensure the persistence of cellular movement [34].

# 1.3. Components of the cytoskeleton

The cortical actin cytoskeleton is made of a dense network of actin filaments. Each of those filaments is asymmetric and contains a fast growing barbed end and a slow growing or shrinking pointed end. ATP-bound actin monomers are incorporated into the existing filaments and due to their intrinsic ATPase activity they hydrolyse ATP into ADP + Pi [35]. ATP hydrolysis coupled with the delay in Pi dissociation acts as a molecular clock determining the age of the filament and regulates the kinetics of disassembly and the association of interacting proteins [36].

These cortical actin structures are generated by nucleation processes driven primarily by the Arp2/3 complex [37]. This highly conserved complex was first purified from *Acanthamoeba* [38] and has since emerged as a major eukaryotic actin nucleator of the branched networks of actin filaments at the cortex [39].

The Arp2/3 complex is a stable assembly of 7 subunits including two actin-related proteins, Arp2 and Arp3, which function as an initiation point for the new filament formation [40, 41]. This protein complex binds to the side of an existing actin filament and triggers elongation of a new filament at a roughly 70° branch angle [42]. These two processes of filament-branching and nucleation are tightly coupled [43, 44]. This means that this complex can only generate new filaments as branches emerging from the existing filaments, leading to the formation of a highly branched network of cross-linked actin filaments [45, 46] (Fig. 1.2.).

The Arp2/3 complex possesses very little activity on its own and needs to be activated by the nucleation promoting factors (NPFs) in order to perform its function [44, 47]. Some of the most prominent and best characterised NPFs are proteins belonging to the WASP (Wiskott – Aldrich syndrome protein) family [48, 49]. All the members of this family contain conserved

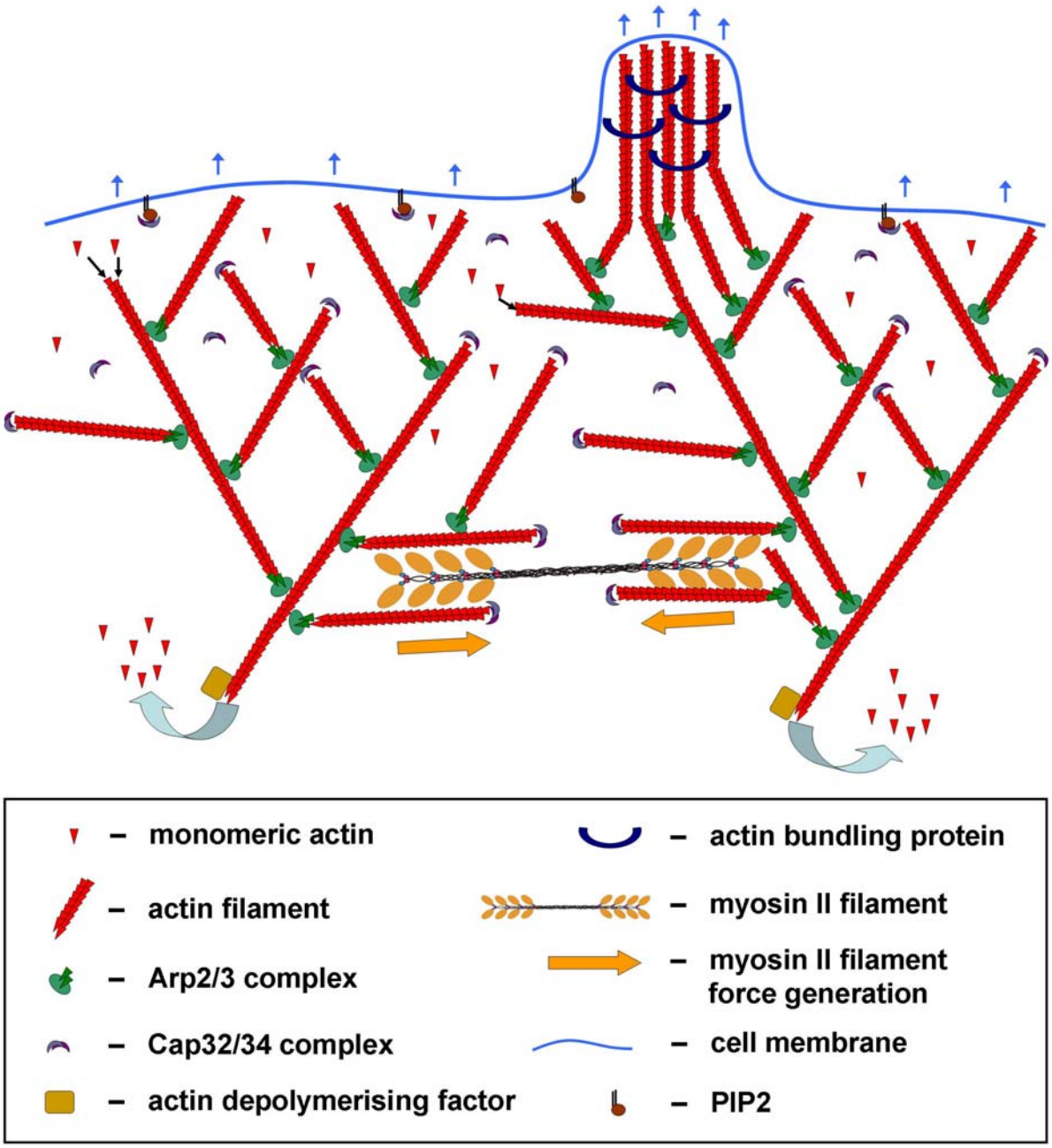


**Figure 1.2.** General scheme of the branched network of actin filaments at the cortex. New filaments are generated by the Arp2/3 complex binding to the side of existing filaments and nucleating a branch emerging at a 70° angle to the mother filament. Filaments are growing at the barbed ends by incorporating G-actin until cupped by the Cap32/34 complex, which is inhibited by $PI(4,5)P_2$ at the membrane. A dense network of the branched filaments drives broad membrane protrusions, while filaments assembled into tight bundles by the bundling proteins generate narrow finger-like extensions. Bipolar myosin II filaments bind to different parts of the cortical actin meshwork and generate contractile force by moving along F-actin and decreasing the distance between those two regions. Actin filaments are being depolymerised by ADFs at the pointed ends.

catalytic WCA domain composed of WH2 (WASP-homology 2) motif responsible for binding actin monomer (G-actin) and a Central and an Acidic region involved in interaction with the Arp2/3 complex [50, 51]. The most basic model of the WASP-mediated Arp2/3

activation is that the WCA domain delivers actin monomer to form a trimer with Arp2 and Arp3 subunits, which functions as a nucleus for the new filament [39, 52].

In a resting condition the WASP family proteins are present in a closed inactive conformation, in which the catalytic domain is inhibited by the interaction with GBD (GTPase Binding Domain) [53, 54]. This autoinhibitory conformation is disrupted by the interaction with activated Rho GTPases allowing the initiation of the Arp2/3-mediated actin polymerisation [55, 56]. This regulatory mechanism couples the WASP-dependent activation of the Arp2/3 complex to the signal transduction pathways that couple the detection of a chemoattractant gradient to localised cytoskeletal dynamics [57].

The Arp2/3 complex generates actin filaments with free fast growing barbed ends, which then elongate in an autocatalytic manner [58]. This filament elongation continues until inhibited by the capping protein binding to the barbed end [59]. One of the most significant capping proteins responsible for the majority of the barbed end capping activity in *Dictyostelium* cells is the heterodimeric Cap32/34 complex [60, 61]. This factor is inhibited by phosphatidylinositol (4,5) bisphosphate ($PI(4,5)P_2$) present in a great abundance on the inner leaflet of the cell membrane, and thus protects the very peripheral actin filaments from being capped [59, 62].

The mechanical properties and the metabolism of the actin cytoskeleton are modulated by a big collection of actin binding proteins (ABPs). These effectors control the turn-over cycle of actin networks, regulate their organisation and apply tension, which are required for the diverse actin-driven cellular functions [63]. The regulation of various mechanical properties is mediated, among others, by cross-linking proteins forming a loose network of actin filaments, bundling proteins generating a tight bundle, factors anchoring filaments to the membranes and actin based motors. The major regulators of actin dynamics and turn-over include nucleating factors, depolymerising factors, proteins capping actin filaments and

proteins sequestering G-actin or regulating ADP/ATP exchange in those monomers [64]. The ABPs can be divided into 7 major groups, based on their functions (Table 1.1.). However this arbitrary classification does not always reflect the biological complexity, since many proteins are exhibiting several activities and belong to more than one group [63]. One such example is cofilin, which can bind both actin monomers and filaments and mediates both depolymerisation and severing of F-actin [65, 66].

1. **Monomer binding proteins** sequester G-actin and prevent its conversion to F-actin (e.g., thymosin) or catalyse exchange of ADP to ATP (e.g., profilin).
2. **Actin depolymerising factors** promote conversion of F-actin to G-actin preferentially at the pointed end of the filaments containing ADP-bound actin subunits (e.g., cofilin).
3. **Actin capping proteins** bind to the free ends of the filaments and inhibit their further elongation. They can cap the pointed ends (e.g., tropomodulin) or the barbed ends (e.g., Cap32/34, CapZ) of actin filaments.
4. **Filament severing proteins** bind to the sides of actin filaments and cut them into two separate pieces (e.g., gelsolin, severin).
5. **Cross-linking proteins** contain more than one binding site for F-actin and lead to the formation of three-dimentional actin filament networks and filament bundles (e.g., villin, fimbrin).
6. **Stabilising proteins** bind to the side of actin filaments and prevent their depolymerisation (e.g., tropomyosin).
7. **Motor proteins** use actin filaments as a track for movement. They are involved in trafficking and force generation (e.g., myosin family proteins).

**Table 1.1.** Basic classification of the actin binding proteins. Based on their activity, ABPs can be divided into 7 groups of factors performing different functions in the regulation of the actin cytoskeleton. Some of the ABPs exhibit several activities and belong to few groups at the same time.

All of those classes of factors play important roles in the regulation of the actin cytoskeleton functions. They are the final effectors of the signalling pathways controlling actin dynamics. Various ABPs can recognise different binding sites present on the surface of actin filaments,

but most of those components have to compete with several other proteins binding to the same region of F-actin [67].

One of the most important processes during cell movement is a contractile force generation, which is mediated by one of the ABPs group of motor proteins. Conventional filamentous myosin II is the major member of this family driving this process of force generation [68].
Myosin II is a hexamer consisting of 2 myosin heavy chains (MHC), 2 regulatory light chains (RLC) and 2 essential light chains (ELC) [69-71]. These myosin II complexes spontaneously assemble into bipolar filaments, which is the only form in which they can perform their cellular functions (reviewed in [72]).
Myosin II filament assembly in *Dictyostelium* is negatively regulated through MHC phosphorylation by MHC kinases (MHCKs) [73], and induced by dephosphorylation performed by MHC phosphatase PP2A [74]. *Dictyostelium* myosin II filaments are assembled in the cytosol and then translocated to the cortex by two separate and independent mechanisms [75]. Myosin II function and motor activity in *Dictyostelium* are controlled by cGMP signalling pathway [76, 77] and other factors, such as p-21 activated kinase PakA [78, 79].

# 1.4. Regulation of chemotaxis

## 1.4.1. Ras GTPases

The Ras superfamily of small GTPases is present in all eukaryotes and plays a key role in a regulation of a wide range of cellular processes including proliferation [80], differentiation [81], cell polarity [82] and motility [83, 84] and subcellular trafficking [85, 86].

These proteins act as molecular switches cycling between active GTP-bound and inactive GDP-bound states [87]. This activation/inactivation cycle is controlled by specific regulatory factors (Fig. 1.3.). Activation is mediated by GEFs (Guanine-nucleotide Exchange Factors), which promote dissociation of the GDP allowing binding of GTP and transition to the active state [88, 89]. Inactivation is directed by GAPs (GTPase-Activating Proteins), which stimulate the intrinsic GTPase activity leading to GTP hydrolysis into GDP [90, 91]. Additional regulation comes from GDIs (GDP-Dissociation Inhibitors), which can lock GTPases in an inactive GDP-bound state and inhibit activation by GEFs [92]. Only activated small GTPases can interact with downstream effectors and regulate their function. This simple and easily controlled mode of action makes small GTPases extremely versatile components of various signal transduction pathways [93].

The Ras superfamily can be divided into five broad subfamilies: Ras, Rho, Ran, Rab and Arf [94]. The Ras and Rho subfamilies, which are involved in the regulation of the cytoskeleton are overrepresented in *Dictyostelium* relatively to the small genome size of this organism [95]. Two members of the Ras subfamily, RasC and RasG, play a central role in the regulation of chemotaxis and development in *Dictyostelium* [96, 97]. These two proteins are acting directly downstream of the G-protein-coupled cAMP receptor and activate several

signalling pathways controlling chemotactic movement and cAMP relay response. They exhibit certain overlap in function, but RasG was shown to be more important in chemotaxis while RasC functions predominantly in ACA (adenylyl cyclase) activation [98].

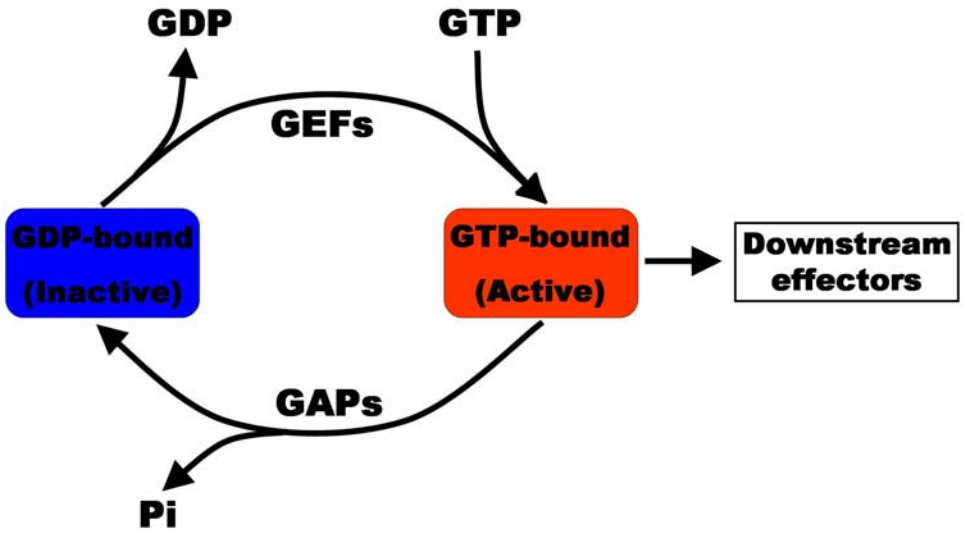


**Figure 1.3.** Regulation of small GTPases. Inactive GDP-bound small GTPases (blue) are activated by GEFs, which catalyse exchange of GDP into GTP. This exchange is inhibited by GDIs. Active GTP-bound form (red) can interact with downstream effectors and mediate the regulatory function. The intrinsic GTPase activity is greatly enhanced by GAPs leading to GTP hydrolysis and transition to the inactive state.

Members of the Rho subfamily are specialised regulators of the actin cytoskeleton functions, working as a components of the signalling pathways downstream of RasG and RasC [99]. The Rho subfamily can be further divided into three major groups called Rac, Rho and Cdc42. Among 18 Rho GTPases identified in *Dictyostelium* 7 are classified as members of the Rac subfamily based on the phylogenetic analysis, while the rest do not belong to any of those groups. There are no clear homologs of Rho and Cdc42 proteins in *Dictyostelium,* which suggests that they diverged later in evolution [100, 101].

The Rho GTPases are regulated by a surprisingly large number of factors in *Dictyostelium*. There are 42 proteins containing Rho GEF domain, 43 with Rho GAP domain and 3 proteins containing both, encoded in the *Dictyostelium* genome. Additionally there are 8 proteins belonging to the Dock180/Zizimin-related unconventional family of Rho GEFs identified in

this organism [100]. This relatively big number of regulatory factors involved in the cytoskeletal functions is related to the complexity of the microfilament apparatus and the requirement for highly diverse and complex cellular functions during the *Dictyostelium* life cycle. It also suggests considerable redundancy in this highly important regulatory system.

## 1.4.2. Directional sensing and cell polarity

Chemotaxis is a complex cellular process involving several signalling pathways with a variety of regulatory steps, signal amplification and very precise fine tuning enabling response to a very shallow gradients on the edge of physical limits of detection [102-104].

The initial step is the binding of the chemoattractant to cell surface receptors, which then transduce this signal via G proteins to a complex network of signalling pathways, resulting in a gradient of cellular components [105]. There is a big collection of proteins and molecules that specifically localise to the front or to the back of cells moving in the gradient of chemoattractant (reviewed in [102]). Factors showing increased localisation to the front include phosphatidylinositol 3 kinase (PI3K) and its product phosphatidylinositol (3,4,5) trisphosphate ($PI(3,4,5)P_3$) [106]; furthermore $PI(3,4,5)P_3$ binding proteins such as CRAC [107], PKB/Akt [108], Rho GEFs and others described below. Components found at the back and sides of chemotaxing cells include PTEN [109], ACA [110] and others (Fig. 1.4.).

This internal gradient is translated into coordinated remodelling of the cytoskeleton and leads to the formation of actin filaments in the front, which drives the extension of filopodia and pseudopodia [111], and myosin thick filaments at the back of the cell [75], which inhibit pseudopodia formation and drive uropod retraction [112]. The final outcome is cell polarisation and cellular movement up the gradient of chemoattractant [113].

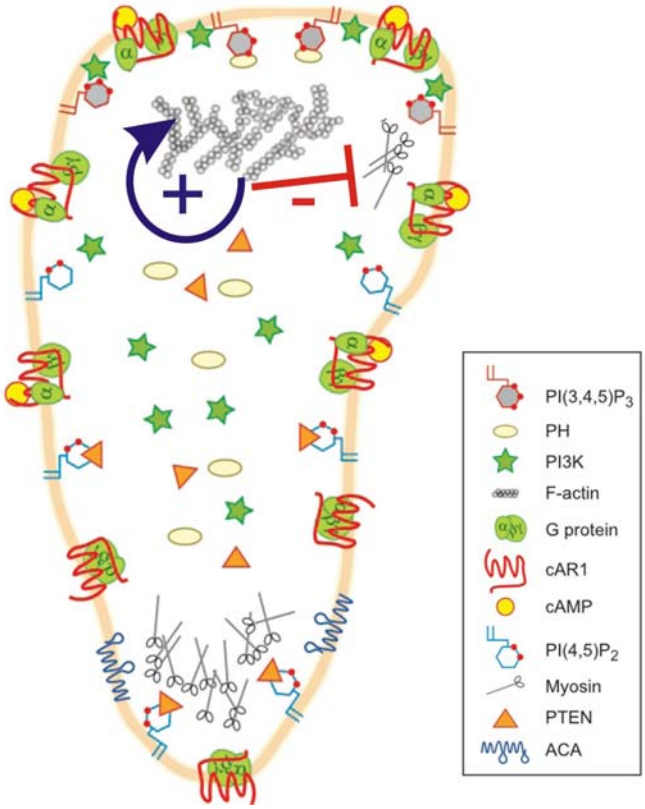


**Figure 1.4.** Spatial localisation of different proteins in polarised cell. cAMP receptor cAR1 is distributed uniformly but gradient of external cAMP is translated into localised production of $PI(3,4,5)P_3$ by PI3K at the front of the cell, which determinates localization of proteins containing PH domain. $PI(3,4,5)P_3$ gradient is formed and maintained by the specific localisation of PI3K to the front and PTEN to the back and sides of the cell. This leads to spatially determined rearrangements: actin is being polymerised at the front while myosin filaments assembled at the back.
Actin polymerisation process is amplified by a positive feedback loop, which stabilizes initiated pseudopodia. At the same time actin polymerisation and the positive feedback loop that it triggers lead to the inhibition of myosin filament assembly at the front of the cell. (Based on Manahan *et al.*, 2004)

Cytoskeleton reorganisation at the front of the cell is driven by the Arp2/3 dependent autocatalytic polymerisation of actin filaments and actin dependent inhibition of myosin II filament assembly [114, 115]. Localised stimulation of *Dictyostelium* cells with chemoattractant results in activation of Ras and PI3K signalling leading to actin polymerisation and newly polymerised actin results in further recruitment of PI3K signalling which in turn triggers more actin polymerisation forming a positive feed-back loop [34, 116-118]. At the same time activated Ras stimulates signalling pathways that locally activate MHC kinase A, which results in phosphorylation of the myosin II heavy chain and disassembly of myosin filaments at those sites in *Dictyostelium* [75, 119].

Both of those events fit in the LEGI (Local Excitation Global Inhibition) model, which explains regulation of actin cytoskeleton by local activation of polymerisation at the front of polarised *Dictyostelium* cells and global inhibition at the rest of cell surface [26, 120]. On the

contrary, myosin II filament assembly is globally activated and only locally inhibited at the front of the *Dictyostelium* cells [15, 77, 121], which complements the regulation of actin cytoskeleton, since myosin II filaments at the cell cortex suppress actin-driven protrusions [113]. This model predicts different diffusion rates of factors mediating global and local response. For example cGMP which is a small and highly diffusible molecule, leads to global activation of myosin II filament assembly and therefore inhibition of actin-based pseudopodia [122, 123], while local activation of actin polymerisation and myosin II disassembly is mediated by local accumulation of $PI(3,4,5)P_3$ and several proteins at the sites of activation in *Dictyostelium* cells [103, 124, 125].

The localisation and functional role of $PI(3,4,5)P_3$ and the mode of cell movement may differ depending on the strength of the gradient that the *Dictyostelium* cells are exposed to. In shallow gradients of chemoattractant $PI(3,4,5)P_3$ is almost uniformly distributed along the cell membrane, while in the steep gradients it is strongly localised at the leading edge [126]. Detailed analysis of phenotypes exhibited by various *Dictyostelium* mutants in PI3K signalling revealed that in shallow gradients $PI(3,4,5)P_3$ plays more global role of increasing the frequency of new pseudopodia formation rather than their localisation [127]. These and other observations resulted in a model of chemotaxis, in which pseudopodia are constantly produced spontaneously in random directions, similarly to the random motion observed in the absence of chemoattractant stimulation [128, 129]. In these models the steering process is thought to be a separate event mediated by other pathways, which stabilise and maintain only those pseudopodia pointing in the direction of the gradient while retracting the others [130]. On the other hand, in steep chemoattractant gradients $PI(3,4,5)P_3$ is almost exclusively localised to the leading edge of *Dictyostelium* cells, where it plays more direct role in mediating the chemotaxis, by driving localised production of new pseudopodia in the direction of the gradient [126, 127].

## 1.4.3. Signal transduction pathways

*Dictyostelium* can detect several chemoattractants like cAMP, folic acid or lysophosphatidic acid (LPA), with cAMP being the major signalling molecule during development. Cyclic AMP is detected by a family of serpentine G-protein-coupled receptors (GPCRs) cAR1 – 4 [131]. Binding of cAMP triggers the activation and dissociation of heterotrimeric G proteins into cytosolic Gα-GTP subunits and membrane bound Gβγ subunits, both of which can regulate a diverse set of downstream effectors [116, 132].

The main signal transduction pathway from cAMP GPCRs goes through Gβγ subunits via Ras GEFs to Ras GTPases. The Ras superfamily of small G proteins and especially members of the Rho family within this superfamily as described earlier, are the major regulators of cytoskeletal dynamics in eukaryotic cells and play substantial role in chemotaxis [98, 116, 117]. Different Ras GEFs (e.g., GefR, GefA) activate different Ras GTPases (e.g., RasG, RasC) which then activate several signalling pathways leading in parallel to the effectors in the cytoskeleton (Figures 1.5. and 1.6.).

The first pathway discovered to play a crucial role in *Dictyostelium* chemotaxis was class I phosphatidylinositol 3 kinase (PI3K) signalling [106]. Upon cAMP stimulation RasG is locally activated, which then recruits PI3K to the membrane. PI3K phosphorylates $PI(4,5)P_2$ to form $PI(3,4,5)P_3$ leading to local accumulation of this molecule at the membrane. At the same time $PI(3,4,5)P_3$ is degraded to $PI(4,5)P_2$ by a membrane bound phosphatase – PTEN [125]. Therefore dissociation of PTEN from the membrane at the site of cAMP stimulus is a necessary step in order to efficiently accumulate $PI(3,4,5)P_3$. Evidence has been presented that this dissociation event is driven by a cAMP activated phospholipase C (PLC) activity, which hydrolyses $PI(4,5)P_2$ to form diacylglycerol (DAG) and inositol(1,4,5) triphosphate ($IP_3$) [133]. $PI(4,5)P_2$ is not only a substrate for PI3K and a product of PTEN but it is also an

important factor regulating PTEN binding to the membrane [134]. This binding may depend on PI(4,5)$P_2$ both directly and indirectly, since PTEN binds to PI(4,5)$P_2$ via several charged residues at its N terminus, but this alone is not sufficient to drive PTEN localisation. Therefore other mechanisms, which are yet unknown, must take part in this process but could also require presence of PI(4,5)$P_2$ [133, 135].

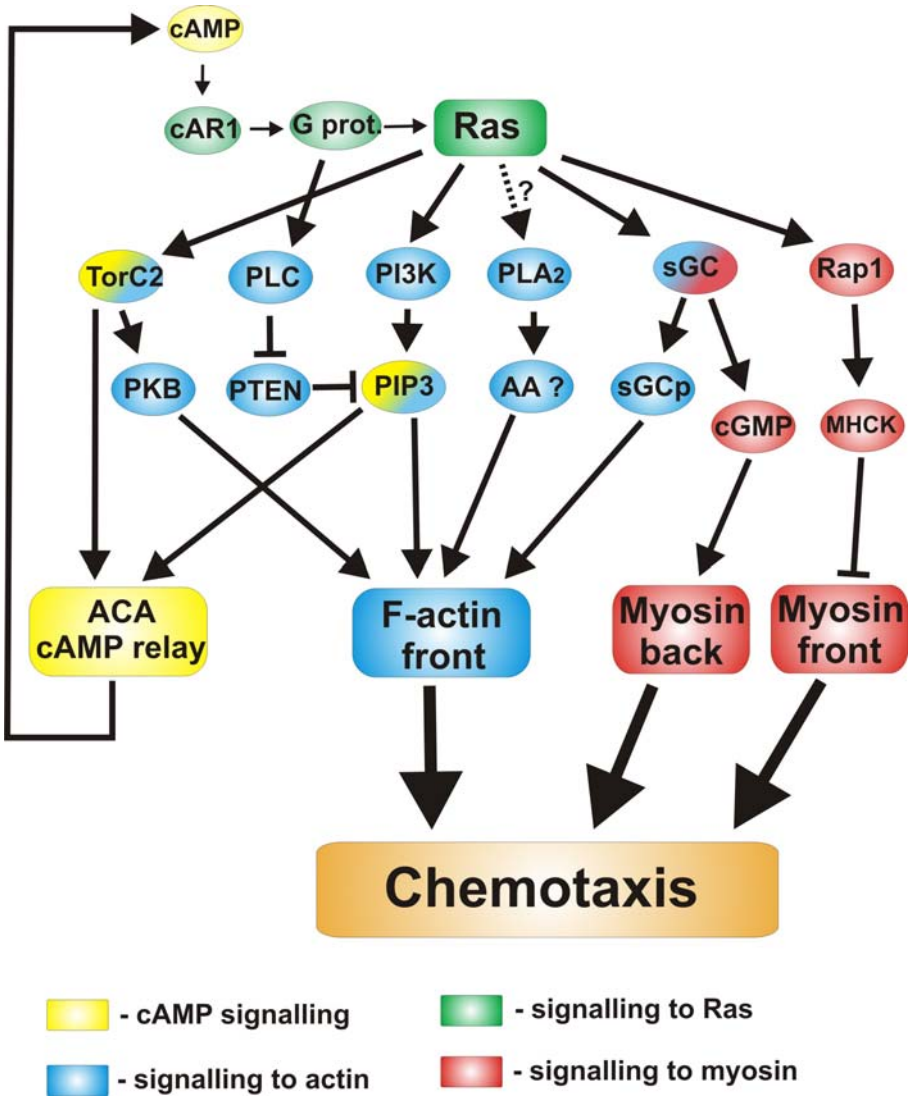


**Figure 1.5.** The general overview of the signalling pathways triggered by cAMP in *Dictyostelium.* Binding of cAMP to cAR1 leads to dissociation of G protein which then activates Ras proteins and also PLC. Ras signalling leads directly or indirectly to activation of several pathways transducing the signal to the cytoskeleton in parallel. TORC2 mediates both cAMP relay response and actin polymerisation; PLC, PTEN and PI3K contribute to PI(3,4,5)$P_3$ signalling which is the central factor in chemotaxis. $PLA_2$ is a parallel pathway to PI3K and can control chemotaxis in the absence of PI(3,4,5)$P_3$. sGC is another parallel pathway that can alone mediate chemotaxis in highly polarised cells. It generates two independent signals by binding to the actin filaments at the front where it regulates formation of new pseudopodia and production of cGMP which globally promotes myosin filament assembly. Rap1 activates MHCK which inhibits myosin filaments assembly at the front.

The mechanism of PLC activation is not fully understood but it is mediated by the $G\alpha_2$ at the site of cAR1 stimulation [136]. This activation leads to local degradation of $PI(4,5)P_2$ and dissociation of PTEN from the membrane. The remaining pool of $PI(4,5)P_2$ is sufficient as a substrate for PI3K and at the absence of PTEN an effective accumulation of $PI(3,4,5)P_3$ can be achieved. The proper level of PLC activity is necessary for building a functional gradient of $PI(3,4,5)P_3$ during chemotaxis. Mutants lacking PLC activity are unable to accumulate $PI(3,4,5)P_3$ at the front of the cell and exhibit chemotaxis defects, while overexpression of PLC leads to global dissociation of PTEN from the membrane and $PI(3,4,5)P_3$ production, which also disrupts PI3K signalling and chemotaxis in *Dictyostelium* [133, 135].

$PI(3,4,5)P_3$ is a key player in the regulation of chemotaxis. Local accumulation of this molecule in the membrane can alone drive the pseudopodia formation and protrusion by stimulating actin polymerisation [137]. Accumulation of $PI(3,4,5)P_3$ at the leading edge and building a steep gradient of $PI(3,4,5)P_3$ within the cell is crucial for efficient chemotaxis and is a major characteristic of polarised cells [33, 125]. $PI(3,4,5)P_3$ acts as a binding site for proteins containing $PI(3,4,5)P_3$ specific Plekstrin Homology (PH) domains and therefore mediate their translocation to the membrane after cAMP stimulation. There is a great variety of proteins binding to $PI(3,4,5)P_3$, which play part in different aspects of chemotaxis and the cAMP relay response. One of those proteins is CRAC (Cytosolic Regulator of Adenylyl Cyclase) which regulates activation of ACA (Adenylyl Cyclase of Aggregation stage) and mediates signalling to cAMP relay response [107, 110]. There is a multitude of PH domain containing proteins which lead to activation of actin polymerisation or contribute to cytoskeleton structure and dynamics in other way. Many Rac GEFs and also Rac GAPs, bind to $PI(3,4,5)P_3$ and regulate Rac GTPases – a subfamily within Rho family involved in regulation of the actin cytoskeleton [99, 100, 138].

Rac small G proteins directly activate Scar/WAVE complex and WASP protein, two main NPFs acting on the Arp2/3 complex, which is a key nucleator of actin polymerisation [41,

48]. Scar/WAVE is inhibited by other components of the complex – PIR121 and Nap, and after Rac activation it is released from these interactions and can bind Arp2/3 and trigger actin polymerisation [139]. WASP is present in an inactive form due to auto-inhibition, which is released after conformational change mediated by binding of activated RacC, allowing activation of the Arp2/3 complex [49, 52, 56]. Each of those factors activates the Arp2/3 complex in a different context and leads to formation of different actin based structures. The Scar/WAVE complex induces formation of pseudopodia and lamellipodia – broad membrane protrusions filled with dense meshwork of branched actin filaments [139, 140], while the WASP protein is involved in clathrin based endocytosis and vesicle trafficking [50, 141]. Some of the other proteins that bind to $PI(3,4,5)P_3$ and regulate actin cytoskeleton are: PhdA a PH domain containing adaptor protein regulating filamentous actin (F-actin) localisation and organisation [106], PDKa, Akt/PKB and PKBA protein kinases involved in signal transduction to both actin and myosin cytoskeleton [140, 142] and PAKa which regulates assembly of the myosin thick filaments [72].

There is an intrinsic positive feedback loop in the PI3K signalling, which leads to strong signal amplification and maintenance of the polarisation at the leading edge. The model of this feedback loop is based on the ability of PI3K to bind to newly polymerised, ATP-rich actin filaments. Once activated PI3K pathway leads to formation of new actin filaments, which then recruit more PI3K to the site of activation [126, 143]. Ras signalling is also involved in this feedback loop. Even though activation of Ras is PI3K and F-actin independent, it is strongly amplified by factors contributing not only to PI3K signalling but also to other pathways regulated by Ras [117, 140, 143]. The result of this feedback loop is strong amplification of the initial signal, which maintains the persistence of chemotactic response and enables detection of very shallow gradients, which is enhanced by the localisation of PTEN at the sides and back of chemotaxing cells through a mechanism

described above. Both of these mechanisms help to establish and maintain an internal gradient of $PI(3,4,5)P_3$ and other factors between the front and the back of chemotaxing cells, which is translated into organised response to chemoattractant stimulation [144].

Even though $PI(3,4,5)P_3$ plays a central role in the chemotactic response it is not essential for this process. Mutant lacking all five genes encoding class I PI3 kinases in *Dictyostelium* as well as PTEN still exhibit good chemotaxis in steep gradients of cAMP with orientation efficiencies close to that of wild type, however they move at reduced speed [145]. This suggests that at least one other pathway acting in parallel with PI3K can independently drive chemotactic movement. Two research groups using two different approaches found that phospholipase $A_2$ ($PLA_2$) plays a role of additional compass in chemotaxis and is required for directed cell movement in the absence of PI3K signalling [16, 17].

The mechanism of $PLA_2$ pathway is not well understood. $PLA_2$ is a cytosolic enzyme that cleaves the second acyl chain in phospholipids (PLs) and forms lysoPLs and free fatty acids (FFA) such as arachidonic acid (AA) [17]. The mediator of $PLA_2$ signalling in chemotaxis is unknown but AA is one of the candidates, another possible factor is lysophosphatidic acid (LPA) – a product of further processing of lysoPL. The mechanism of $PLA_2$ activation is also unsolved, but it must go through cAR1 and therefore is probably dependent on a G protein signalling pathway [146]. $PLA_2$ activity is dependent on $Ca^{2+}$ signalling, which is controlled by $IP_3$ and the $IP_3$ receptor [147]. $IP_3$ is a product of PLC which is a regulator of $PI(3,4,5)P_3$ signalling as described before, and therefore it could be a point of crosstalk between the two pathways. But $Ca^{2+}$ signalling is not entirely dependent on PLC activity since there are other sources of $IP_3$ in the cell and *plc*-null mutants have close to wild type levels of $IP_3$ [146].

The $PLA_2$ and PI3K pathways act in parallel to regulate chemotaxis and either one of them is sufficient to generate chemotactic movement, while cells lacking both of those pathways cannot move up gradients of cAMP [16, 17]. But this is still not the end of the story. It was recently shown that inhibition of both $PLA_2$ and PI3K blocks chemotaxis completely only in

unpolarised not fully developed cells after 4-5 h of pulsing with cAMP. If the cells are developed for longed time, 7-9 h, they become highly polarised and establish stable internal gradients of many cellular components. These cells are able to move in gradient of cAMP after inhibiting both the $PLA_2$ and PI3K pathways [148]. This implies existence of a third pathway that could independently drive the chemotactic response, present only in polarised cells. It was determined that soluble guanylyl cyclase (sGC) is responsible for this rescue of chemotaxis defect in polarised cells [148]. Further investigation revealed that sGC signalling has an interesting bipolar character. sGC protein localises to the front of chemotaxing cells where it binds to F-actin and regulates dynamics and orientation of pseudopodia formation. On the other hand the product of sGC catalytic activity – cGMP, regulates myosin assembly and motor activity at the back of the cell [76, 148]. Myosin assembly and activity is regulated by cGMP which activates cGMP binding protein C (GbpC) that initiates myosin filaments translocation to the cortex. GbpC also phosphorylates myosin light chain kinase A (MLCK-A) which activates myosin motor activity in the acto-myosin filaments and generates driving force for uropod retraction during cell movement [72]. Interestingly mutants lacking only catalytic activity of sGC could still induce chemotaxis to some extent, while catalytically active sGC lacking ability to bind to F-actin could not, indicating that actin binding is required for the primary function of sGC in chemotaxis [148].

Another component contributing to the complexity of the whole system is Target Of Rapamycin Complex 2 (TORC2). This complex consists of the TOR protein, which is highly conserved in evolution and contains structural similarities to the PI3 kinase family, Ras interacting protein 3 (RIP3), Pianissimo (Pia) and few other proteins [149]. TORC2 is activated after cAMP stimulation by Ras pathway via RIP3 [150] and then phosphorylates several proteins involved in signal transduction to chemotaxis. TORC2 regulates cAMP relay response since it is an essential component for ACA activation both directly and indirectly through PKB [149]. The major contribution of TORC2 signalling to the cytoskeleton

regulation is through activation of protein kinases B – PKBA and PKBR1 at the leading edge [151]. PKBA binds to PI(3,4,5)$P_3$ and activates another PI(3,4,5)$P_3$ bound kinase – PAKa which regulates the myosin cytoskeleton. PKBR1 is constitutively bound to the membrane and after activation by TORC2, phosphorylates downstream effectors such as Rac GEFs and GAPs and TalinB, which play important roles in regulation of actin cytoskeleton [142, 149].

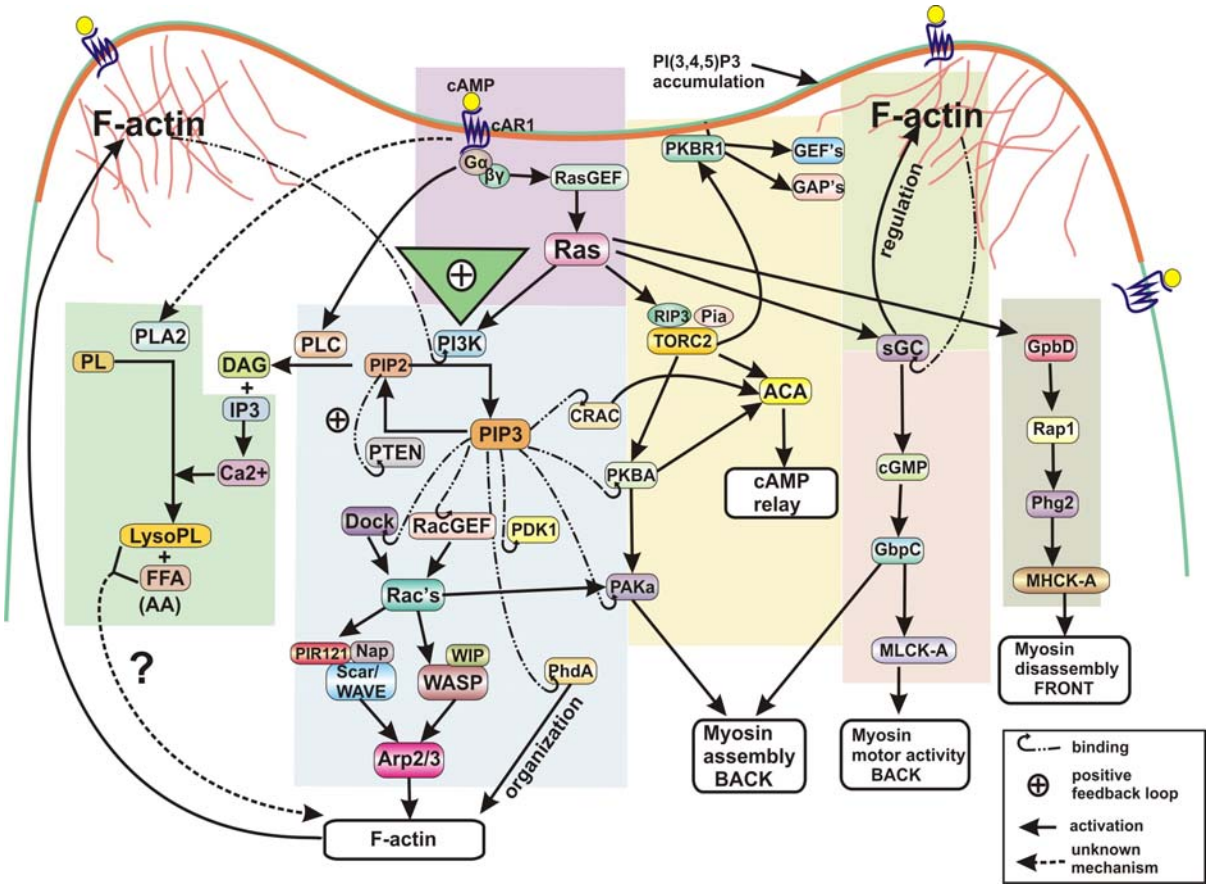


**Figure 1.6.** Detailed model of signal transduction pathways from cAR1 to the cytoskeleton. Separate pathways are indicated by different colours of the background.
Ras GTPases are master regulators of signalling in chemotaxis. They independently activate PI3K, TORC2, sGC and Rap1 pathways. Activation of PLC is mediated by Gα subunit, the mechanism of $PLA_2$ activation remains unknown. PI3K, PTEN and PLC all contribute to the formation of PI(3,4,5)$P_3$ gradient, which is the major factor in chemotaxis. It is a binding site for the PH domain containing proteins, and therefore mediates their localisation to the front of the cell. Rac GEFs bind to PI(3,4,5)$P_3$ and locally activate Rac GTPases, which trigger WASP and Scar activity, the main regulators of the Arp2/3 complex. This leads to actin polymerisation and formation of pseudopodia. There is a positive feedback loop between Ras, PI3K and actin polymerisation shown as green triangle. TORC2 is a regulator of ACA and also regulates cytoskeleton by acting on PKB's. sGC mediates two independent signals to actin at the front by binding to F-actin, and to myosin at the back by producing cGMP. GpbD contains GEF domain which activates Rap1 and leads to myosin filament disassembly at the front, mediated by MHCK-A activity.

therefore in order to generate new protrusions at the leading edge myosin filaments need to be disassembled at the front of chemotaxing cell [68]. This process is mediated by Rap1 GTPase which is rapidly activated by GEF domain of GbpD at the leading edge upon cAMP stimulation. Activated Rap1 binds and activates Phg2 kinase, which then phosphorylates myosin heavy chain kinase A (MHCK-A) that leads to inhibition of myosin filament assembly at the front [116].

All the pathways described here form a highly complex network of regulation of chemotaxis. Studying roles of different components and mechanisms acting in separate pathways is difficult because of their redundant character. There are still many parts of the system that need to be covered with extensive analysis and presumably also novel functional components remain to be discovered.

## 1.5. Biphasic character of cAMP-induced actin polymerisation

Stimulation of cells with cAMP results in two temporally distinct phases of actin polymerisation (Fig. 1.7. B). The first phase is very rapid and peaks at about 5 s after stimulation at room temperature and 10 s at 12°C. This phase is not dependent on PI3K activity and it leads to uniform actin polymerisation at the cortex, which is followed by a phase of rapid actin depolymerisation [152]. During this rapid phase of actin polymerisation cells stop moving and soon after the depolymerisation phase, they retract all their pseudopodia and round up (Fig. 1.7. A 25 s). This is referred to as a cringe response and it is

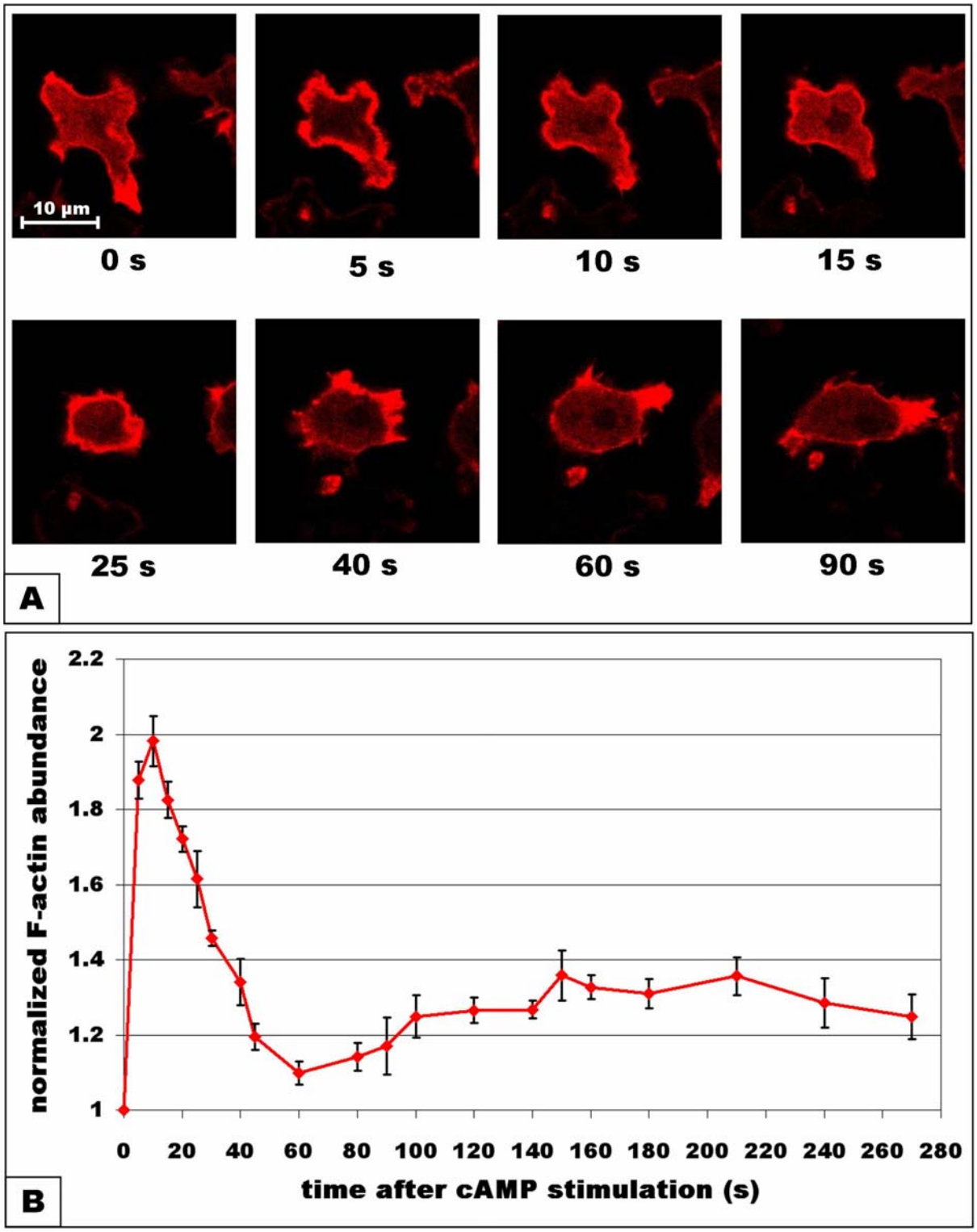


**Figure 1.7.** Two phases of actin polymerisation in response to cAMP stimulation. **A)** Confocal images of the cell expressing RFP-lifeact F-actin probe stimulated with cAMP at room temperature. **B)** Phalloidin assay analysis of actin dynamics after cAMP stimulation at 12°C. The graph shows the relative F-actin abundance. It is a representation of 16 separate measurements.
The first uniform burst of actin polymerisation peaks at about 10 seconds after stimulation at 12°C. During the second phase actin polymerisation is localised to generated protrusions. It shows much slower kinetics and lower amplitude, peaking between 2-3 min after cAMP stimulation at 12°C.

driven by myosin II mediated contraction. The F-actin level goes back to almost prestimulation level after the depolymerisation phase is finished and then slowly increases during the second long-lasting phase of polymerisation. The second phase, which peaks at around 2-3 min at 12°C, is dependent on PI3K/PTEN activity. During this phase actin polymerisation becomes confined to pseudopodia, which are extended at the front of moving cells [152]. This phase leads to pseudopodia formation and therefore drives the actual chemotactic movement.

Both of those phases are dependent on Arp2/3 activity since mutants with disrupted function of this complex have strongly decreased response in each of those two phases [153]. The fact, that both phases of actin polymerisation require the Arp2/3 complex, but only the second phase is dependent on PI3K signalling, suggests that there have to be diverse paths of signal transduction and regulatory factors involved in each of those phases.

The mechanisms regulating the actin polymerisation during the second phase have been relatively well characterised and are closely related to the mechanisms involved in the random motion in the absence of chemoattractants [26, 143]. However the exact mechanisms leading to the activation of actin polymerisation during the first phase, as well as the regulation of the depolymerisation phase, have not yet been described.

This biphasic nature of chemoattractant-induced actin polymerisation is a universal characteristic, which can be detected with certain variability in both *Dictyostelium* amoebas and human cells such as neutrophils and fibroblasts [154]. The physiological relevance of this feature is not fully understood. It is thought that such temporal differentiation of actin polymerisation response could enhance spatial detection of stimulation source. In natural conditions cells might be exposed to oscillatory chemoattractant stimulation such as the periodic waves of cAMP during *Dictyostelium* development. In these conditions the travelling wave of stimulus will induce the first rapid response with a spatio-temporal gradient at the cortex. The actin polymerisation will first occur at the side of the cell that first

experiences the chemoattractant, which might leave some biochemical trace indicating the direction of the source. This type of behaviour can be observed by looking at actin dynamics at streaming *Dictyostelium* cells, but it cannot be detected during uniform cAMP stimulation.

## 1.6. Experimental approach for investigating function and regulation of the cytoskeleton during chemotaxis

There are two main approaches to identify components involved in any biological process and to study mechanisms functioning in it. The first one is a genetic approach, which can be applied in a forward or reverse manner. Forward genetics is used for identification of factors playing role in the process analysed. It is always based on some form of mutagenesis followed by screening for mutants displaying mutant phenotypes in the process of interest. Usually the most challenging part of this approach is the identification of mutations responsible for the observed phenotypes. Reverse genetics is useful for discovering function of a certain component by introducing a disruption or various mutations to the gene of interest and analysing the effects of those manipulations. Both of those techniques are extensively used in many fields of biological research including the investigation of chemotaxis.

The major limitation of these approaches is the redundancy of function exhibited by the components involved in the process analysed. Disruption of a single factor will generate only a very limited phenotype, since its function can be often provided by other redundant components. This often causes a necessity to introduce several disruptions simultaneously, in order to detect a clear phenotype.

This limitation in utilising the genetic approach has proven to be of a crucial significance in the chemotactic research. Many of the molecules involved in the cytoskeletal dynamics are known to have redundant functions and to be somehow able to substitute for each other. This redundancy of certain factors as well as the parallel regulation of the whole process by independent signalling pathways makes this system surprisingly adaptive and resistant to disruption by genetic modifications, as is to be expected of process crucial for life. There are very few essential components of this system, which could not be deleted, such as major subunits of the Arp2/3 complex [153]. From the list of all the mutants ever analysed, that had single cytoskeletal factors knocked-out, only a relatively small proportion was displaying severe defects in chemotaxis. These severe defects usually affect cells lacking factors that act at the initial stages of the signal transduction, upstream of the multiple parallel pathways, such as *car1* [131] or *rasG* null cells [155]. Most of other mutants with disruptions of further downstream signalling factors such as GEFs and GAPs, or effectors like many ABPs, had only minor aberrations, slightly decreased motility rates or even no observable phenotypes at all. Some mutants lacking the whole signalling pathway involved in the regulation of the cytoskeleton could still perform efficient chemotaxis, such as cells lacking all the genes for PI3K's and PTEN [17, 145, 156].

Another approach of identifying components and their functions is a proteomic analysis. This biochemical approach also comes in a variety of forms and has its own limitations. The major difference of this technique, compared to the one previously described, is that it does not need to disturb the process in order to investigate it. Proteomic analysis can be performed in a wild type system, which allows us to observe the biological processes the way they really work in native conditions. This approach can detect various aspects of protein dynamics, changes in protein abundance and protein-protein interactions. It can determine the composition of various cellular structures and protein complexes. The great advantage of

proteomic analysis is the ability to analyse many factors involved in a certain process during a single experiment. The major limitation of this approach is that, although it can be used to analyse dynamics and interactions, it cannot determine the function of analysed proteins, which needs to be investigated in follow up experiments. Both genetic and proteomic methods are highly complementary.

### 1.6.1. Mass spectrometry-based proteomics

Mass spectrometry (MS) is an analytical method used for a very precise measurement of the molecular mass of the analysed sample. There are different types of measuring instruments, such as time-of-flight (TOF), Orbitrap or quadrupole mass analysers, which can be used for various applications including analysis of biomolecules. This technology has emerged as a central tool for in-depth characterisation of proteins in biological systems. A wide range of MS-based experimental strategies have been developed and successfully applied in different fields of proteomic research having a great impact on the life sciences in general [157].

The field of proteomic research has experienced a true revolution in the last decade. Due to remarkable advances in MS technology the MS-based proteomics has evolved from mainly qualitative analytical tool into a truly quantitative method [158]. During this time we could observe constant increase in precision and sensitivity of mass spectra acquisition, which allowed in-depth analysis of highly complex protein samples. This has been driven mainly by development of the Orbitrap technology by Alexander Makarov [159]. This new type of mass analyser operates by trapping ions in a stable orbit around a spindle-like electrode inside an outer barrel-like electrode. The ions orbiting the central electrode also oscillate along its axis in the electric field. The mass-to-charge (m/z) ratios are obtained by Fourier transforms of the frequencies of those axial oscillations measured for all peptide ions. Since the frequency

of ion axial oscillations can be measured very precisely, the corresponding m/z values are also determined with extremely high precision and accuracy [160]. It also generates a very high mass spectrometric resolution which allows distinguishment and precise quantification of peptides with very small differences in m/z ratio values. Another advantage of the Orbitrap in the proteomic research is the large dynamic range of ion abundance in which it can operate. All of those qualities are very important for the analysis of complex biological samples [161]. This technology has become a powerful tool which allowed development of a truly quantitative MS-based proteomics bringing it to a whole new level.

In MS-based proteomics proteins can be characterised by their unique mass which depends on their amino acid composition ("top down" proteomics). This approach is however challenging because the mass difference between proteins with similar composition is small comparing to their total mass and also because entire proteins are difficult to measure [162]. This is why in most applications proteins are first digested with proteases such as trypsin, and the derived peptides are then analysed ("bottom up" proteomics).

Mass spectrometer cannot measure the peptide mass directly but only its mass-to-charge ratio. In order to calculate the mass of those molecules we need to determine the charge state of the ions by analysing their isotopic distribution peaks. Since stable heavy carbon isotope $^{13}C$ contributes to about 1.1% of all the natural carbon on Earth it is always present in large biomolecules which contain hundreds if not thousands of carbon residues. Each peptide is therefore present in several isotopic forms containing either 0 or 1 or 2 etc. of $^{13}C$ isotopes and the mass difference between the neighbouring forms is exactly 1Da (Fig. 1.8. [MS] and Fig. 3.2. A,B). We can determine the charge state of each peptide ion since it is directly related to the distance between different isotopic forms on the m/z scale. For example if the distance between different isotopic forms is 1 mass unit on the m/z scale the peptide ion has charge z=1, if the distance is 0.5 mass units the ion has charge z=2 etc.

A modern MS-based proteomics provides a variety of applications for different aspects of proteomic analysis. Apart from basic protein sequence identification, mass spectrometry is used for mapping and detailed characterisation of post-translational modifications (PTMs) which play a key role in the regulation function and turn-over of proteins [163]. This technique serves as an exceptional tool for studying signal transduction pathways and complex networks of protein regulation by analysing dynamics of protein phosphorylation [164] and other PTMs such as acetylation [165], ubiquitination [166], SUMOlylation [167] and others [168, 169]. Mass spectrometry is also widely used for identification of both stable and transient protein-protein interactions [170-172] and subunits of protein complexes [173, 174] or even analysis of protein composition and turn-over in different organelles and cellular compartments [175, 176].

The quantitative character of modern MS-based proteomics allows for all those analysis to be performed in a quantitative manner revealing the dynamics of the underlying regulatory networks. It also enables studying dynamic changes of protein abundance during cell cycle [177], development [178] or any other biological processes, and also during response to various stimulations and treatments tested in the experimental system [179, 180].

The difficulty in reliable quantification of peptides in any MS measurement comes from the fact that the signal intensity of a peptide ion does not always reflect the peptide abundance in the analysed sample. This is caused by the variability in ionisation efficiency between different peptides and also by the influence of other ions in the sample on the measured intensity of a particular peptide ion. A reliable quantification requires therefore a good internal standard in the sample to normalise quantitative variability between different MS measurements. An ideal internal standard should have identical chemical and physical properties to the analysed molecule. The best solution is to have for each peptide a separate internal standard made from peptide with identical sequence but labelled with different stable isotopes allowing for distinguishment of the two species on MS. This has led to the

development of several techniques for peptide labelling with stable isotope tags both *in vitro* and *in vivo*.

The *in vitro* labelling is done by chemical modifications of proteins or peptides leading to incorporation of stable isotopic tags onto selected sites. There are several different methods which use different types of tags with various isotopic labelling and specificity of reactive groups (reviewed in [181]). The advantage of chemical labelling is that it can be performed on any type of protein sample including tissue biopsies and body fluids. The disadvantage is that the analysed sample and the internal standard have to be processed individually and are mixed together at the late stage before the MS measurement, which can lead to quantitative variability affecting the final results.

The *in vivo* labelling involves metabolic incorporation of stable heavy isotopes into proteins of cells grown in special media containing those isotopes. This can be done by growing bacteria or yeast cells in media containing nitrogen source with $^{15}N$ isotopes, which will be incorporated into all the amino acids, or by growing cell cultures or even whole organisms on media containing essential amino acids labelled with $^{13}C$ and $^{15}N$. The approach of metabolic incorporation has the great advantage that the proteins are tagged in the very early stages. This allows for the samples to be mixed with internal standards at the cell level or straight after the lysis, which reduces the variability caused by sample preparation and yields highly accurate quantification. The disadvantage is that it can only be used for systems, which can be grown on a defined media, which excludes human or environmental samples.

Stable Isotope Labelling by Amino acids in Cell culture (SILAC) is a straightforward approach for labelling the whole proteomes by metabolic incorporation of essential amino acids from the culture medium into the newly synthesised proteins. After a minimum of five cell doublings all the proteins are labelled with ‘heavy’ forms of lysine and arginine containing $^{13}C$ and $^{15}N$ stable isotopes. By choosing various forms of labelled amino acids up

to three different cell populations can be generated, which can be subjected to various treatments and then analysed simultaneously in a single MS measurement [182].

Labelling proteins with 'heavy' forms of lysine and arginine is compatible with tryptic digest during downstream sample preparation. Since trypsin cleaves proteins only after lysine and arginine residues, all the peptides generated by this enzyme will have at least one labelled amino acid (some will have more than one due to missed cleavage sites). This means that all the peptides in the analysed sample will be present in both 'light' and 'heavy' forms, one of which will serve as an internal standard and will allow for precise quantification.

Even though MS technology is rapidly improving and already allows for in-depth analysis of highly complex samples, the level of complexity and dynamic range of protein samples from the whole cell lysate or even a particular purified cellular fraction is still too large to allow comprehensive coverage of the whole proteome. In order to decrease this complexity and dynamic range and therefore increase the protein detection, samples need to be divided into fractions. This can be performed at a protein level by using one dimensional SDS-PAGE when proteins are separated according to their size. Gel lanes containing separated proteins are then cut into individual fractions and the tryptic digest is performed in-gel and followed by peptide extraction [183]. Other ways of sample fractionation can be performed on the peptide level using OFFGEL electrophoresis [184] or anion exchange (SAX) or cation exchange (SCX) columns [185, 186] for peptide separation according to their isoelectric points.

Even such fractionated samples represent a highly complex mixture of peptides which cannot be analysed simultaneously in MS. This is why in modern proteomics mass spectrometers are coupled with liquid chromatography (LC) columns which separate all the peptides usually by reverse-phase chromatography. Peptides need to be ionised and transferred into the gas phase before entering mass spectrometer. The most common method used for performing both of those tasks in proteomics is electrospray ionisation (ESI) [187] developed by John Fenn who

was awarded a share of the Nobel Prize in Chemistry in 2002 for this invention. Peptides are eluted from the LC column with a very low flow and continuously enter the electrospray which injects them already as ions directly into the mass spectrometer (Fig. 1.8.).

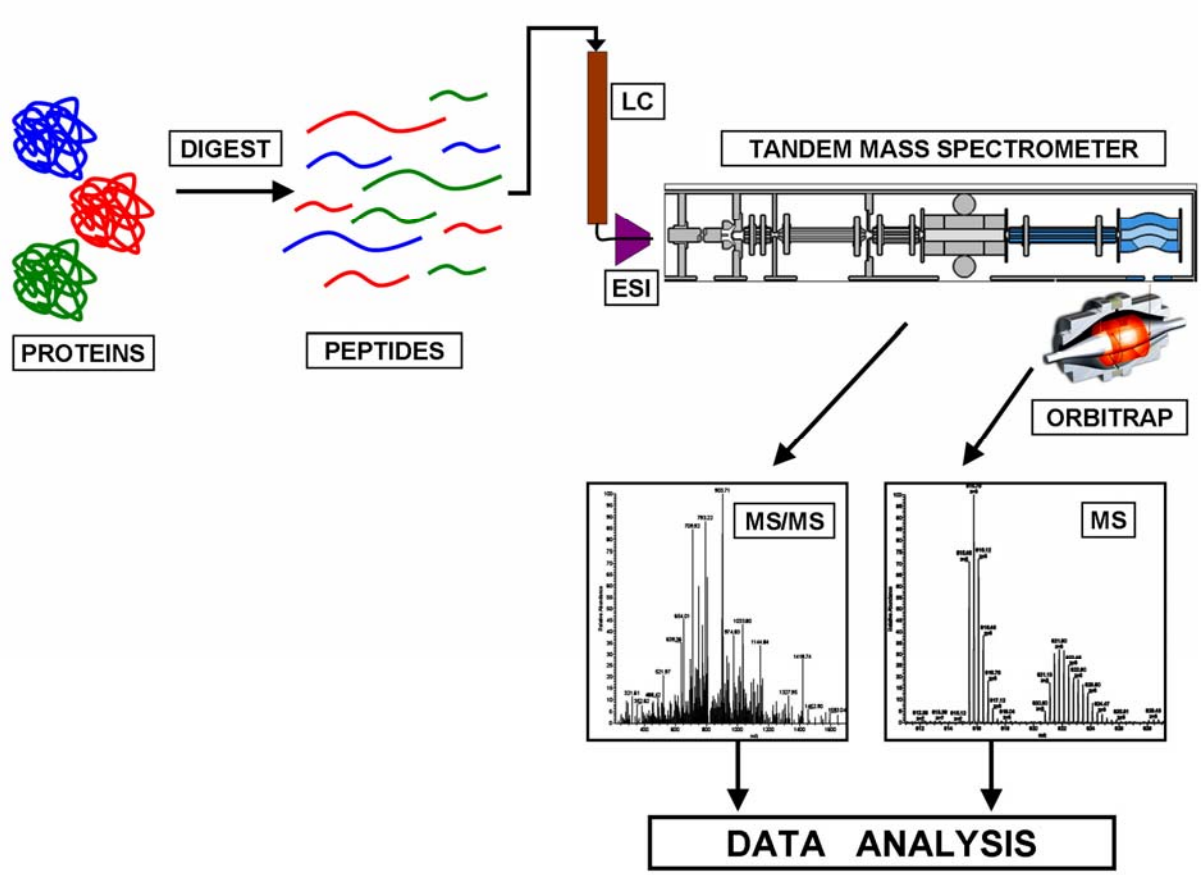


**Figure 1.8.** A general workflow scheme in MS-based proteomics. The analysed sample containing a mixture of different proteins (e.g. cell lysate, cellular fractions or purified complexes) is subjected to a digest with proteolytic enzyme such as trypsin. Generated peptides are separated on a liquid chromatography (LC) column just before entering the mass spectrometer via electrospray ionisation (ESI). Peptide ions are analysed by a tandem mass spectrometer containing at least two mass analysers, the most advanced instruments include an Orbitrap mass analyser shown on the graph. During analysis two types of mass spectra are generated for each peptide ion - MS for the whole peptide and MS/MS for its degradation products. Both of them are used for downstream data analysis including identification and quantitation of analysed peptides.

The challenges of modern proteomics generate requirement for the usage of complex tandem mass spectrometers as core instrumentation. These machines are composed of several different mass analysers and ion traps, which select and manipulate peptide ions for m/z ratio measurement and sequence determination. Peptide ions are precisely controlled inside the vacuum of a mass spectrometer by static and dynamic electromagnetic fields. Individual peptide ions can be selected by quadrupole mass analysers which tune the electromagnetic

field so that only ions with a particular m/z ratio can pass through. Selected peptide ions can then be captured in a field of a linear or three dimensional ion traps where they can be accumulated [188, 189]. After a certain accumulation a cloud of selected peptide ions can be injected into the Orbitrap mass analyser on a stable orbit around inner electrode for a very accurate m/z ratio measurement. In another round of tandem mass spectrometry a sequence of selected peptide ion is determined. For this purpose peptide ions are subjected to some form of fragmentation, usually by collision with an inert gas such as helium at low pressure, which is called collision-induced dissociation (CID). Peptides usually break along the backbone and the m/z ratios of the fragmentation products called MS/MS can be used for sequence determination by matching the masses of fragments and the entire peptide with the database of all the known protein sequences from the analysed specie [190].

MS-based proteomic analysis generate enormous amount of raw data containing MS and MS/MS spectra for all the peptides detected in each sample. These data need to be processed by specialised software which will identify and quantify proteins based on several detected peptides. One example of such software package is MaxQuant - an open source program developed in the Mann Lab [191].

The aim of this study is to adapt this technique of quantitative proteomic analysis to investigate the dynamics of fast protein translocation to the cytoskeleton after chemoattractant stimulation. This type of analysis could bring new insight into the mechanisms regulating cytoskeletal dynamics during chemotaxis and elucidate the differential regulation of the two phases of actin polymerisation. I also want to discover novel and uncharacterised proteins which are expected to be identified with this approach and to start to define their role in the regulation of the cytoskeleton.

## 1.6.2. *In vivo* fluorescence microscopy

Since proteomic analysis can only be applied to a whole cell population it will always generate averaged data from the entire analysed population. In order to gain further insight into function and regulation of proteins on cellular level the proteomic approach needs to be complemented with other methods.

The best way to investigate subcellular localisation and dynamic behaviour of proteins, such as trafficking or stimulation induced translocation, is by using *in vivo* fluorescence microscopy [192]. In this technique a protein of interest is tagged with a fluorescent protein (FP) and expressed in cells or organisms of interest [193]. This is usually done by cloning a gene encoding the selected protein into a vector containing a coding sequence of fluorescent protein directly upstream or downstream of the insertion site. Expression of such a construct will lead to formation of a fusion protein with FP tag at the N- or C-terminus.

Fluorescent proteins like all fluorophores can be excited by absorbing a photon. The exited state is very transient and the absorbed energy is either dispersed in a non-radiative way or emitted as another photon. Due to energy dissipation during a short life-time of the excited state, the emitted photon has lower energy and therefore longer wavelength than the excitation photon. This means that the light emitted by any fluorophore can be detected and measured independently from the light used for excitation [194].

The first fluorescent protein discovered was a green fluorescent protein (GFP) which was isolated from the jellyfish *Aequorea victoria* by Osamu Shimomura in 1962 [195]. It took another 30 years before the gene encoding the GFP was cloned [196] and demonstrated to create fluorescence in other organisms [197, 198]. After that point the GFP was extensively studied and started being used as a tool in molecular biology.

Even though the wild type GFP can generate fluorescence in other organisms it has several disadvantages for the practical use as a fluorescent molecular tag. These include a dual

picked excitation spectrum with a major peak at 395 nm, a low fluorescence quantum yield and low photostability and also poor folding at 37°C. A single point mutation (S65T) was found to dramatically improve the spectral characteristics of the GFP by shifting the excitation spectrum to a single peak at 488 nm while keeping the emission spectrum peak at 509 nm [199]. Eventually all of these qualities were significantly improved by directed and random mutagenesis [200]. After obtaining the crystal structure of the GFP [201, 202] the crucial information about the chromofore formation and neighbouring residues was provided, which allowed for directed engineering of the fluorescent properties of this protein [203]. All these genetic modifications of the GFP led to formation of several different derivatives with various spectral characteristics and other specialised features. Some of those mutants have shifted excitation and emission spectra which include blue fluorescent proteins (BFPs) cyan fluorescent proteins (CFPs) and yellow fluorescent proteins (YFPs) [200, 203]. Other derivatives include super-fast folding fluorescent proteins [204, 205], photoactivatable fluorescent proteins [206-208] and few others [209-211], which can all be used for various specialised applications. In 2008 Martin Chalfie, Osamu Shimomura and Roger Y. Tsien were awarded a Nobel Prize in Chemistry for their discovery and development of the GFP.

Several other fluorescent proteins from different aquatic organisms were isolated and characterised, many of which were also engineered to improve their qualities such as brightness, photostability and folding and to reduce their tendency for oligomerisation [212]. The whole process of developing GFP derivatives and isolating other fluorescent proteins resulted in formation of a wide range of FPs with different excitation and emission peaks spread over the whole spectrum of visible light (Fig. 1.9.). All these proteins have different characteristics such as brightness, photostability, expression levels, folding efficiency, oligomerisation or toxicity and can have different usefulness in various applications [213].

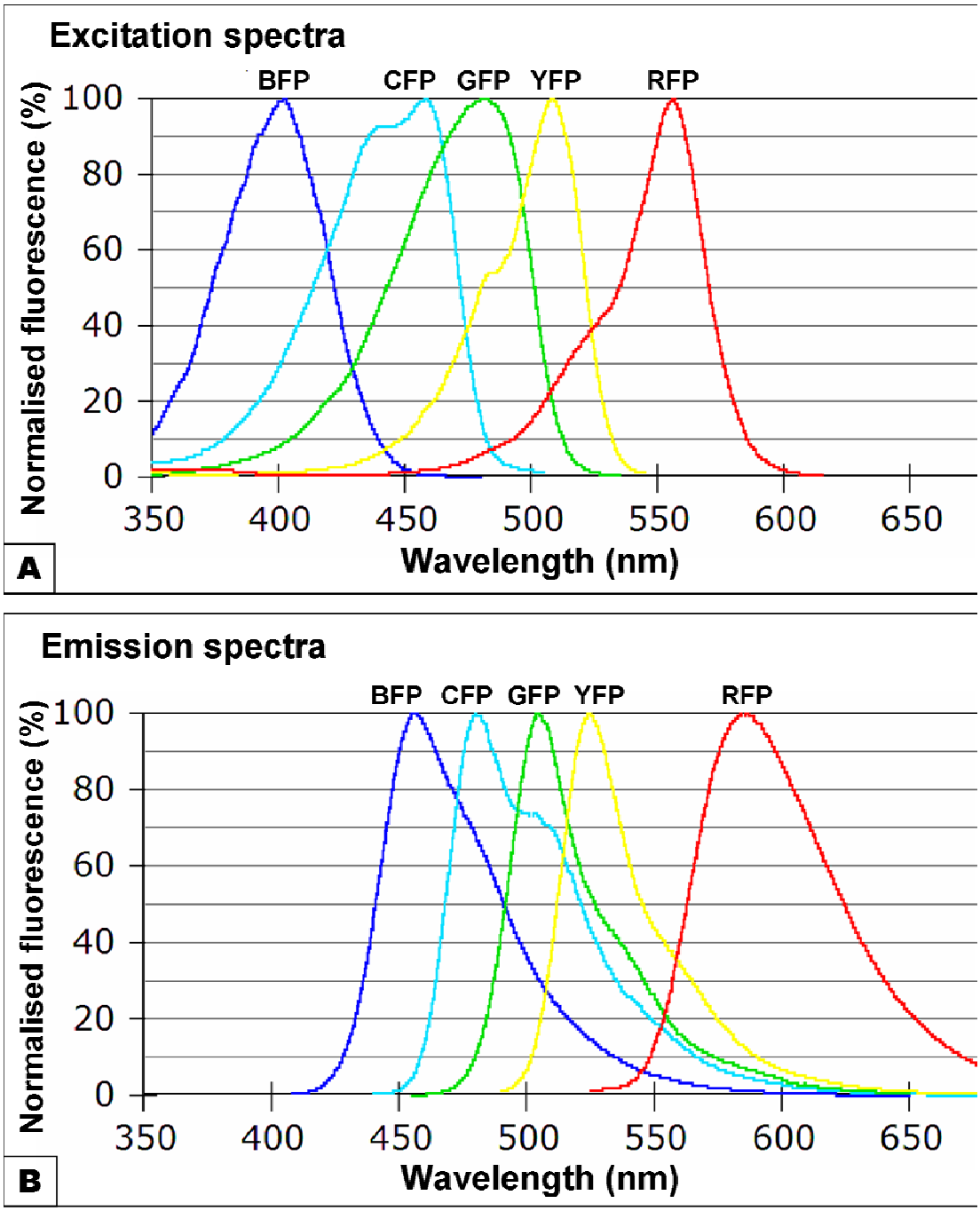


**Figure 1.9.** Excitation **(A)** and emission **(B)** spectra of some of the available fluorescent proteins (FPs) used in fluorescence microscopy. Different FPs can be used simultaneously for multicolour labelling of proteins. The most common combination for double labelling is GFP / RFP and for triple labelling CFP / YFP / RFP. BFP – blue fluorescent protein; CFP – cyan fluorescent protein; GFP – green fluorescent protein; YFP – yellow fluorescent protein; RFP – red fluorescent protein.

Up to three different FPs can be used simultaneously for multiple labelling of different fusion proteins in single cell line, which can be then all imaged independently with hardly any cross-talk between the channels [213-215]. This gives a great opportunity to investigate colocalisation and interaction of different proteins within a cell.

In parallel to the development of fluorescent proteins various techniques in fluorescence microscopy were developed and optimised allowing for quantitative analysis and high resolution imaging of cellular structures and processes. The majority of fluorescence microscopes in life sciences operate in the Epi-illumination mode in which the excitation light passes through the objective lens which is also used to collect the emitted fluorescence. In this method most of the excitation light is transmitted through the specimen and does not enter the microscope which improves the signal-to-noise ratio of the detected image. The reflected fraction of the excitation light, which reaches the objective together with the emitted light, is filtered out using dichroic mirrors and emission filters before the detector.

The most basic design is a wide-field epifluorescence microscope, which collects the emitted light from the whole thickness of the illuminated specimen. This means that an image of visualised structures is always blurred by the light coming from outside of the focal plane. The contribution of out-of-focus light leads to decrease of image clarity and contrast which is most apparent when using objectives with high resolving power. Different ways of dealing with this problem have been developed. One approach is to collect wide-field images and then modify them by using complex computational algorithms which is commonly known as deconvolution process. A nonrestorative or 2D deconvolution improves contrast by removing out-of-focus light form the images while a restorative or 3D deconvolution requires several images from different focal planes of the sample to actually reassigns light to its proper place of origin [216].

Another approach is to collect high contrast images by using more advanced microscope designs. The most common technique developed to obtain high contrast images is Confocal Laser Scanning Microscopy (CLSM). The key feature of a confocal microscope is a controlled and highly limited depth of focus which allows accusation of images from selected focal plane without the background created by the out-of-focus light. In the confocal microscopy the excitation light is transmitted through the specimen and illuminates

fluorophores in its entire depth similarly to the wide-field microscopy. The major difference is that the emitted light collected by the objective lens passes through an aperture with very small diameter which allows only the light from selected focal plane to reach the detector and obstructs all of the out-of-focus light [217, 218]. This technique can obtain images of very high contrast and high resolution and can also be used to generate a 3D image of the analysed structures [219, 220]. The disadvantage of this method is a relatively high exposure of the specimen to the excitation light which leads to increased photobleaching and phototoxicity and which is related to the fact that only small fraction of the emitted light is used to create an image while the rest of generated illumination still causes the negative effects.

Few other techniques in fluorescence microscopy were developed to minimise the photobleaching and phototoxicity while obtaining high contrast images. These techniques utilise sophisticated optical designs to create a thin plane of light used for selective local illumination of the specimen instead of the global excitation by transmitted light. One example of such method is a Digital Scanned Laser Light-sheet Microscopy (DSLM) developed by Philipp Keller, which uses a light-sheet for optical sectioning of the specimen [221]. This type of fluorescence microscopy generates images with very high signal-to-noise ratio and it can be applied for large specimens such as a whole zebrafish developing embryo [222].

Another technique which uses a different kind of restrictive illumination is a Total Internal Reflection Fluorescence Microscopy (TIRFM) developed by Daniel Axelrod [223]. TIRFM uses an evanescent wave created during total internal reflection of the laser light at the glass-water interface to selectively excite fluorophores in a restricted region immediately adjacent to this interface (Fig. 1.10.). The evanescent light wave decays exponentially from the interface and can therefore penetrate only a very thin region of about 200 nm into the specimen which means that the images obtained by the TIRFM contain essentially no background coming from deeper structures [224]. This specialised type of fluorescence

microscopy is therefore particularly useful for investigating the dynamics of events occurring at the cell membrane such as exocytosis [225] and the cell cortex including different aspects of the cytoskeleton organisation [42, 226] and cell-substrate adhesion [227, 228].

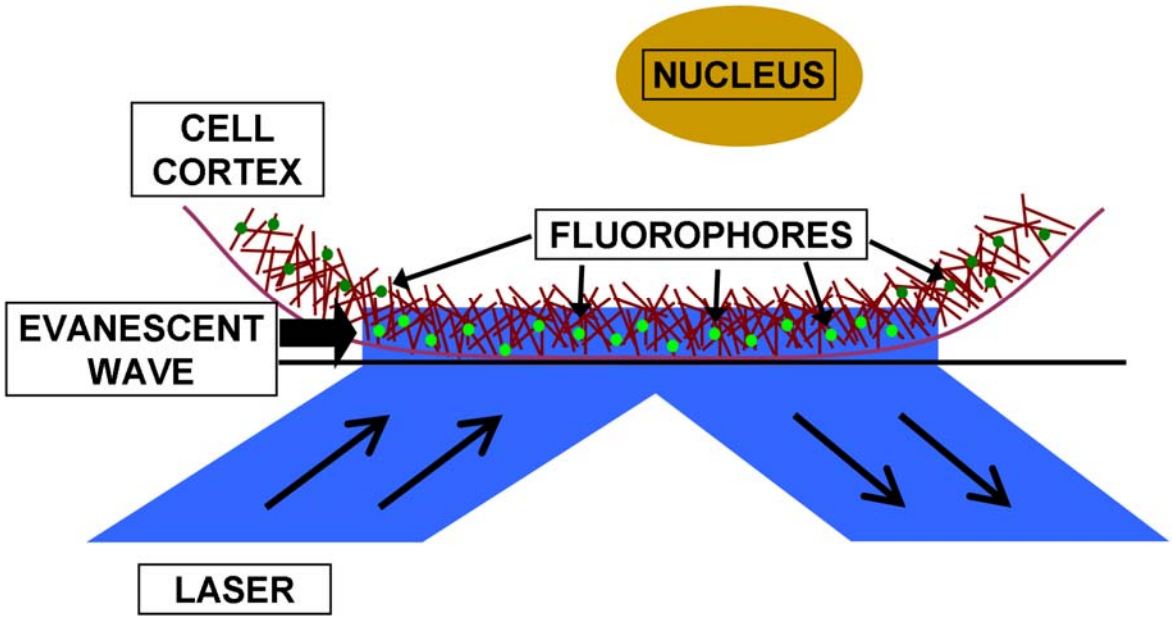


**Figure 1.10.** Total Internal Reflection Fluorescence Microscopy (TIRFM). Excitation laser light is projected at a low angle to the cover glass and totally internally reflected at the glass-water interface. During this process an evanescent wave is formed which penetrates about 200 nm into the specimen. This forms a very spatially restricted illumination zone which leads to selective excitation of only those fluorophores which are present at the membrane and periphery of the cortex of visualised cells. Deeper structures such as nuclei do not get illuminated.

In this study I used the Confocal Scanning Laser Microscopy and the Total Internal Reflection Fluorescence Microscopy to visualise the *in vivo* dynamics of selected proteins which were detected by the quantitative proteomics analysis as factors responding to the chemoattractant stimulation.

# 2. Materials and methods

## 2.1. Buffers

Developmental Buffer (DB) :

5 mM $KH_2PO_4$ 5 mM $Na_2HPO_4$, 2 mM $MgSO_4$, 0.4 mM $CaCl_2$, pH 6.2.

Stimulation Buffer (SM) :

5 mM $KH_2PO_4$ 5 mM $Na_2HPO_4$, 2 mM $MgSO_4$, pH 6.2.

Lysis Buffer (1x) :

20 mM HEPES pH 7.4, 2 mM EGTA pH 8, 2 mM $MgCl_2$, 0.2% Triton X-100, 1x Complete EDTA-free Protease Inhibitors cocktail (Roche, 11873580001).

Fixing Lysis Buffer (1x) :

20 mM HEPES pH 7.4, 2 mM EGTA pH 8, 2 mM $MgCl_2$, 0.2% Triton X-100, 1% formaldehyde.

Wash Buffer :

100 mM HEPES pH 7.4, 2 mM $MgCl_2$, 1x Complete Protease Inhibitors cocktail (Roche).

Sample Buffer (SB, 1x) :

100 mM Tris pH 8, 4% SDS, 25 mM DTT, 5 mM EDTA, 4.5% glycerol.

Urea Buffer (UB, 1x) :

100 mM Tris pH 8, 1% SDS, 2 M urea, 4.5% glycerol, 0.02% bromophenol blue.

H-50 Transformation Buffer :

20 mM HEPES pH 7, 50 mM KCl, 10 mM NaCl, 1 mM $MgSO_4$, 5 mM $NaHCO_3$, 1 mM $NaH_2PO_4$, pH 7.

# 2.2. SILAC protocol

## 2.2.1. Cell stimulation and lysis conditions

Two cultures of *Dictyostelium* $AX_2$ cells were grown in suspension on a horizontal shaker rotating at 170 rpm in a defined SIH medium (Formedium, SIH0310) until the populations went through 6 cell doublings. One population was grown in a light medium with all standard amino acids and the other population was grown in a heavy medium, in which standard K0 L-lysine and R0 L-arginine were substituted with K8 L-lysine (U-13C6, 98%; U-15N2, 98%) and R6 L-arginine (U-13C6, 98%) labelled with stable isotopes of carbon $^{13}C$ and nitrogen $^{15}N$ (Cambridge Isotope Lab, CNLM-291, CLM-2265).

Cells were harvested at the density of $5x10^6$ cells/ml, washed twice with Development Buffer (DB) and resuspended in DB at the density of $1x10^7$ cells/ml. Cells were developed on a rotary shaker for 5 hours by pulsing with 30 nM final concentration of cAMP at 6 min intervals. Developed cells were washed once with Stimulation Buffer (SM) containing 1 mM EGTA in order to dissociate calcium dependent cell clusters formed during development, then once with pure SM and resuspended at the final density of $2x10^7$ cells/ml in a pre-cooled to 12°C SM containing 3 mM caffeine to inhibit endogenous cAMP oscillations.

Both heavy and light cell populations were kept on the rotary shaker in a thermostat at 12°C in the cold room for 20 min. The light cells were transferred to the 50 ml falcon tube with small magnetic bead and placed in a water bath adjusted to 12°C on a magnetic stirrer in the cold room. The cell suspension was stirred at about 300 rpm and 500 µl samples were transferred into 2 ml tubes containing 500 µl of ice cold 2x Lysis Buffer placed on a rotary horizontal mixer (IKA, Vibrax VXR) rotating at 1500 rpm.

Samples were taken before the stimulation and after adding one pulse of cAMP at 500 µM final concentration at 6 time points: 4s, 10s, 20s, 60s, 120s and 180s. The initial one second time point was taken separately by adding 500 µl of unstimulated cells into 2 ml tube containing 5 µl of 50 mM cAMP and after one second adding 500 µl of ice cold 2x Lysis Buffer. The heavy cells lysate was prepared by mixing 5 ml of unstimulated heavy cells suspension with 5 ml of ice cold 2x Lysis Buffer in a 14 ml falcon tube and vortexing for 20 s. One ml of this lysate was transferred into each tube containing previously prepared lysates of stimulated light cells. Mixed lysates were centrifuged for 2 min at 20,000 g at 2°C and the supernatants were discarded. Pellets were resuspended in 1 ml of ice cold Wash Buffer and transferred into 1.5 Protein LoBind tubes (Eppendorf, 2243108-1) and then centrifuged again in the same conditions. Final pellets were frozen and kept at -20°C until further processing.

## 2.2.2. Sample preparation

Frozen pellets (~7 µl) were thawed and resuspended in 12 µl of 1.5x Turbo DNase buffer containing 1x Complete EDTA-free Protease Inhibitors cocktail (Roche, 11873580001) with 2 units of Turbo DNase (Ambion, AM2238) and were incubated at 37°C for 30 min. Samples were then mixed with 7 µl of 4x Sample Buffer (SB) and boiled at 96°C for 6 min. After cooling down to room temperature and short spinning, 3 µl of fresh 1 M iodoacetamide

(Sigma, I1149) were added to the samples which were then incubated at room temperature in the dark for 30 min. After this alkylation step samples were mixed with 10 µl of 4x Urea Buffer (UB) to obtain the final sample volume of ~40 µl.

Samples were run in NuPAGE 4-12% gradient bis-tris gels (Invitrogen, NP0335BOX). The gels were stained with Novex colloidal blue staining kit (Invitrogen, LC6025) for 4 hours in a sterile 14 cm tissue culture dish. After staining and washing the gels, sample lanes were cut into 12 fractions with a single use scalpel blades No.24 (Swann-Morton, 0211). Actin and myosin II bands were cut into individual fractions and the rest of the protein bands were divided into 10 fractions of similar sizes. Each gel fraction was further cut into cubes of about 1x1 mm and transferred into individual 1.5 ml Protein LoBind tube.

## 2.2.3. In-gel digest and peptide extraction

Gel pieces were washed with 500 µl of 40 mM $NH_4CO_3$ (Sigma, A6141) and mixed on a horizontal mixer at 1500 rpm for 15 min. 500 µl of $CH_3CN$ (Sigma, A3396) was added and samples were incubated at 45°C for 2 hours with periodic mixing. Supernatant was discarded and 250 µl of $CH_3CN$ was added to dehydrate the gel pieces for 10 min. Supernatant was discarded and gel pieces were dried in a vacuum centrifuge (Thermo Scientific, Savant SPD131DDA) for 10 min.

Dried gel pieces were covered with 50 µl of 40 mM $NH_4CO_3$ containing 10 µg/ml of Trypsin Gold (Promega, V5280) and incubated at room temperature for 30 min to rehydrate. Between 30 and 100 µl of 40 mM $NH_4CO_3$ was used to cover the gel pieces completely. Samples were incubated at 37°C overnight.

Peptides were extracted with equal volumes (80-150 µl) of 50% $CH_3CN$ / 0.1% trifluoroacetic acid (TFA, Sigma 299537) by incubating at 45°C for 3 h with periodic mixing

on a rotary horizontal mixer at 1500 rpm. Supernatants were transferred to fresh Protein LoBind tubes and 400 µl of 50% $CH_3CN$ / 0.1% TFA was added to the gel pieces. Samples were again incubated at 45°C for 2 h with periodic mixing and supernatants were transferred to the tubes from the previous step. Combined supernatants containing extracted peptides were evaporated in a vacuum centrifuge at 45°C until fully dry.

Dried peptides were resuspended in 15 µl of 0.1% TFA and purified using ZipTip C-18 peptide purification microcolumns (Millipore, ZTC18S096). Each sample was analysed by 100 min run on the LTQ Velos Orbitrap Mass Spectrometer (Thermo Scientific).

## 2.3. Cross-linked SILAC protocol

All the cell growth and development conditions were the same as in the standard SILAC protocol described above.

In the cross-linked version of the SILAC protocol the Lysis Buffer contained formaldehyde (Sigma, 25.254-9) at the final concentration of 1%. Instead of collecting one 500 µl sample for each time point, the stimulation of light cells was repeated 4 times and 125 µl samples were collected for each time point from each stimulation and lysed with equal volume of ice cold 2x Fixing Lysis Buffer. The lysates of corresponding time points from all 4 stimulation series were combined and kept on ice for 30 min. The heavy cells lysate was prepared as described above, but with Fixing Lysis Buffer and was incubated on ice for 30 min before mixing with the combined lysates of the stimulated light cells.

After centrifugation, the pellets were washed two times with 1 ml of Wash Buffer and transferred into 1.5 ml Protein Lo-bind tubes before freezing.

Samples were treated with DNase as described above. For the reversal of formaldehyde cross-linking samples were boiled with SB at 99°C for 40 min. After this step samples were processed as described above for the standard SILAC protocol.

## 2.4. Data analysis

Raw mass-spec data were processed using MaxQuant software developed by Jurgen Cox *et al.* in the Mann Lab, Max Planck Institute for Biochemistry, Martinsried [191]. MaxQuant version 1.0.13.13 was used to quantify peptide peaks and protein Light/Heavy (L/H) ratios, and Mascot Daemon (Matrix Science) version 2.3.2 was used to identify peptides.

Data were analysed with the following variable modifications: Oxidation (M); Acetylation (N-term); Phosphorylation (S,T,Y); and one fixed modification: Carbamidomethylation (C). Maximum Posterior Error Probability (PEP) for each peptide was set at 0.05 and all the other settings were set as default. Protein L/H ratios were quantified, based on a minimum of two peptides per time point, using razor and unique peptides.

Detected proteins were annotated in Excel with Gene Ontology (GO terms) and protein information obtained from the DictyBase web page (http://dictybase.org/Downloads/). Detections were filtered so that only proteins that had ratios present in at least four out of eight time points per experiment were selected for further analysis.

Each protein's series of unnormalised L/H ratios in each experiment were first normalised to their average and then two separate experiments were merged by averaging those ratios for each time point of each protein. Standard errors were calculated for each value. Those protein ratios series from two merged experiments were then normalised to the pre-stimulation time point for each protein separately. Standard errors were recalculated for each time point as a

square root of sum of squares of the standard errors calculated previously for this time point and the pre-stimulation time point. When the protein had no ratio present in the pre-stimulation time point the ratios from the other time points were left normalised to the average with their original standard errors. Unnormalised L/H ratios series from the cross-linked SILAC experiment were normalised to the pre-stimulation time point for each protein. These final protein L/H ratios series normalised to the pre-stimulation time point were analysed by clustering using a Cluster3 software created by Michiel de Hoon, University of Tokyo [229] and based on the earlier Cluster software developed in the Eisen Lab, University of California, Berkeley. We were using City-Block distance as a similarity metric and an average linkage as a clustering method. Clustering results were represented in the form of heat maps with the Java TreeView software developed by Alok Saldanha [230], Stanford University School of Medicine.

# 2.5. Phalloidin actin polymerisation assay

To measure the actin polymerisation in response to cAMP stimulation we used a modified version of the method previously described by Kim *et al.* from the Devreotes Lab [231].
Cells grown in HL-5 medium were harvested at the density of $4x10^6$ cells/ml and were developed and stimulated as described before for the SILAC experiment. Stimulation was performed at 12°C water bath in the cold room. 200 µl samples were collected twice before the stimulation and every 5 s after cAMP stimulation for the first 30 s and then in various time points up to 4.5 min. Samples were lysed with equal volumes of ice cold 2x Fixing Lysis Buffer containing 1 µM Phalloidin – TRITC (Sigma, P1951). Lysates were mixed on a horizontal mixer at 700 rpm in the dark for 2 h at RT or overnight in the cold room. Samples were centrifuged at 20,000 g at 10°C for 10 min and the supernatants were discarded. In

order to extract the phalloidin 500 µl of methanol was added to the samples which were then mixed at RT on a horizontal mixer at 1000 rpm in the dark for 1 h. Samples were centrifuged at 20,000 g at RT for 2 min and two replicas of 200 µl for each time point were transferred to a 96-well microtiter plate with flat transparent bottom. Rhodamine fluorescence was measured using microtiter plate fluorometer (Anthos2001, Anthos Labtech) with 540 nm excitation filter and 575 nm emission filter.

# 2.6. Molecular cloning

## 2.6.1. Vectors for protein GFP tagging and overexpression

We have adapted the comprehensive system of extrachromosomal expression vectors for *Dictyostelium discoideum* developed by Douwe Veltman *et al.* in the van Haastert Lab, University of Groningen [232]. Two vectors with G418 selection cassette, pDM317 with N-terminal GFP tag and pDM323 with C-terminal GFP tag, were modified to fit the particular needs of design for this study. Multiple Cloning Site (MCS) on those vectors was modified by adding AgeI (ACCGGT) restriction site between the two existing sites for BglII (AGATCT) and SpeI (ACTAGT). At the same time the linker fragment between the insert and the C-term GFP tag on pDM323 was extended from 4 amino acids (ThrSerSerGly) to 8 amino acids (ThrSerAlaGlyAlaSerSerGly). 5 amino acids linker (SerGlyLeuArgSer) on pDM317 was not modified. These modifications were made by inserting short fragments of dsDNA with cohesive ends compatible with BglII and SpeI restriction sites present on the vectors. These fragments of dsDNA were generated by aligning two oligos mixed in equimolar ratios. Fragment inserted into the MCS of pDM317 was formed from 18 base long

oligos: GATCTGCTACCGGTAGTA and ACGATGGCCATCATGATC. Fragment inserted into the pDM323 vector was made from 30 base oligos: GATCTGCAACCGGTAGTA-CTAGTGCAGGAG and ACGTTGGCCATCATGATCACGTCCTCGATC.

After these steps both vectors were further modified by inserting expression cassette containing mRFPmars-Lifeact (RFP-lifeact) actin probe construct into the NgoMIV restriction site. First RFP-lifeact probe was generated by inserting dsDNA fragment formed from 61 base oligos, GATCCATGGGTGTTGCTGATTTAATTAAAAAATTTGAATCAA-TTTCAAAAGAAGAAA and GTACCCACAACGACTAAATTAATTTTTTAAAGTTAG-TTAAAGTTTTCTTCTTTGATC, into the BglII and SpeI sites on pDM318 with N-term mRFPmars tag. The whole expression cassette with act15 promotor, RFP-lifeact construct and act8 terminator was amplified by PCR using high fidelity KOD polymerase (Novagen, 71086) with primers intoducing NgoMIV restriction sites at the ends of the cassette. PCR product was purified using PCR clean-up kit (Qiagen, 28106), digested with NgoMIV restriction enzyme (NEB, R0564), and purified again. This construct was ligated using T4 DNA ligase (NEB, M0202) into modified pDM317 and pDM323 vectors digested with NgoMIV and dephosphorylated with Antarctic Phosphatase (NEB, M0289). This insertion of a second expression cassette into the plasmids is a part of the whole vector system design, allowing coexpression of two tagged proteins from a single vector, which ensures similar expression levels in each cell [232]. The final vector based on the pDM323 was called pDG600 and the vector based on the pDM317 was called pDG700.

## 2.6.2. Cloning procedures

Genes selected for cloning were amplified from genomic DNA by PCR using KOD polymerase and primers which introduced restriction sites at the ends of the PCR products.

Each forward primer contained restriction site for BglII or one of the enzymes generating compatible cohesive ends: BamHI and BclI. Several genes which had all of those sites present were cloned using AgeI site on the vectors. Those genes were amplified with forward primers containing recognition sequence for AgeI or XmaI which generates compatible cohesive ends. Reverse primers were carrying restriction sites for SpeI or XbaI or NheI. All the restriction sites on the primers were flanked with 5 base fragments to allow efficient digest of the PCR products. Primers were designed to have the annealing temperature of 54°C. Initially all the genes were amplified using standard PCR conditions with 24 cycles, annealing temperature of 50°C, annealing time of 15 s, extension temperature of 68°C and extension time of 40s/kb. Reactions which did not yield sufficient amount of product or which generated additional non-specific products were further optimised using gradient PCR with annealing temperatures between 45°C and 60°C with 3°C steps. For a few genes the number of cycles was increased up to 28. Reactions were performed in 50 µl with 30 ng of genomic DNA and 0.5 unit of KOD polymerase in Eppendorf Mastercycler ep Gradient S.

PCR products were purified with PCR clean-up kit (Qiagen, 28106) using QG buffer instead of PB buffer to ensure total protein denaturation and prevent potential cohesive ends degradation by any remaining polymerase proofreading activity. Purified samples were digested simultaneously with two restriction enzymes appropriate for each construct's design. After restriction digest samples were purified again with the same method as before and the DNA concentration was measured with NanoDrop ND 1000 spectrophotometer (Thermo Scientific). These final samples were ligated into pDG600 and pDG700 vectors.
Vectors were prepared by digesting first with SpeI (NEB, R0133) for two hours at 37°C, then the enzyme was heat inactivated at 80°C for 20 min and then the vectors were incubated with BglII (NEB, R0144) or with AgeI (NEB, R0522) for two hours at 37°C. After the digests vectors were dephosphorylated with Antarctic Phosphatse (NEB, M0289) at 37°C for 30

min, which was then heat inactivated at 70°C for 5 min, and samples were purified using PCR clean-up kit. 30 ng of plasmid DNA was mixed with approximately two molar excess of insert DNA in 5 µl samples. Ligations were performed using 0.5 unit of T4 DNA ligase (NEB, M0202) at 16°C overnight and the whole sample volumes were used for transformation of chemo-competent DH5 *E. coli* cells.

Initially 6 clones from each transformation were checked by colony PCR and if none of them was positive another 12 clones were screened. If the second round of screening failed to detect positive clones the ligation was repeated. Constructs generated on pDG600 were tested using insert forward primer and GFP reverse primer and constructs on pDG700 were tested with GFP forward primer and insert reverse primer. Whenever available, two positive clones for each construct were purified from bacteria using Plasmid Miniprep kit (Qiagen, 27106). Constructs were validated by restriction analysis with two sets of enzymes: BglII/HindIII and BamHI/SpeI.

## 2.7. *Dictyostelium* cells transfection

$AX_2$ cells were grown in a shaking culture in HL-5 medium up to $4x10^6$ cells/ml. Cells were harvested by centrifugation at 600 g for 2 min, washed two times with H-50 buffer and resuspended in H-50 buffer at the density of $5x10^7$ cells/ml. 100 µl of this cell suspension was mixed with 1 µg of plasmid DNA and transferred to an ice cold 0.1 cm electroporation cuvette. Cells were electroporated with two 0.65kV pulses at 25 µF capacitance with 5 seconds interval. Cuvettes were incubated on ice for 5 min and the cells were transferred to 6-well culture plates with 4 ml of HL-5 medium with Ampicillin and Streptomycin or to 10 cm Petri dishes with 10 ml of HL-5 medium with antibiotics. Selection drug G418 was added

6-18 hours after transfection to a final concentration of 30 µg/ml. Cells were grown for at least 4 days after transfection before being used for *in vivo* imaging.

## 2.8. *In vivo* fluorescence microscopy

About $5x10^6$ cells from each strain were collected and washed twice with 1 ml of DB in 2 ml tubes and resuspended in 0.5 ml of DB. Cells were developed in the dark during 5 hours of starvation in 2 ml tubes on a horizontal mixer at 300 rpm. After development cells were washed once with SM containing 1 mM EGTA then with DB and resuspended in 0.5 ml of DB with 3mM caffeine. 100 µl of these cell suspensions were transferred to separate chambers of 8-chambered cover glass (Nunc, 155411) and mixed with additional 250 µl of DB with 3 mM caffeine. Cells were kept in the dark for 10 min to settle and attach to the bottom and were then used for imaging with confocal and Total Internal Reflection Fluorescence (TIRF) microscopy. During each imaging session cells were stimulated by adding 50 µl of 4 mM cAMP to the chamber.

### 2.8.1. Confocal microscopy

Confocal microscopy was performed using Leica DM IRBE confocal laser scanning microscope with 100x objective. GFP was exited with 488 nm laser and the light emitted from this protein was collected between 500 - 540 nm. mRFPmars was exited with 543 nm laser and the emitted light was collected at 580 - 640 nm. Both channels were scanned at one

frame per second (fps) with 800 Hz scanner speed and 512x512 pixel resolution and the light was detected by a photo multiplier tube.

Confocal images were quantified by ImageJ software by selecting a region of interest (ROI) covering a fragment of cell cortex and reslicing the average signal intensity of those ROI as a function of time. The intensity profile was generated giving a temporal dynamics for both GFP and RFP signals within this fragment of the cortex.

## 2.8.2. TIRF microscopy

Total Internal Reflection Fluorescence microscopy was performed using Nicon Eclipse T*i* TIRF microscope with 100x objective. GFP was exited with 488 nm laser and the emitted light was filtered through a 500-530nm filter. mRFPmars was exited with 594 nm laser and the emitted fluorescence was filtered through a 600 – 630 nm filter. Both channels were detected by a CCD camera with various exposure times between 50 – 300 ms at 1024x1024 pixels resolution. When only green channel was imaged, pictures were collected at a constant rate of 2 fps. When both channels were analysed the image collection speed was limited by a filter changing mechanism which performed with a variable efficiency and resulted in a variable intervals of 2.5 – 4 seconds between the frames.

TIRFM imaging sequences captured only for GFP fluorescence with constant rate of 2 fps were quantified using ImageJ and Time Series Analyser plug-in with ROIs selected in the middle of visualised cells.

# 3. Proteomic analysis of the cytoskeleton

## 3.1. Experimental approach

I have adapted the generic SILAC protocol [182] to analyse fast protein translocation to the cytoskeleton insoluble fraction upon cAMP stimulation (Fig. 3.1.). The cytoskeletal fractions from various time points after cAMP stimulation were prepared using protocol based on the standard cytoskeleton purification procedure. Triton X-100 insoluble fractions were separated by centrifugation and briefly purified with a single washing step. Samples prepared in this way are composed of acto-myosin filaments with all the proteins attached to them, but also other cellular structures resistant to lysis in those conditions, such as the nuclei. This method relies on a fast cell lysis stopping all the biochemical reactions by diluting the necessary cytosolic factors, and on maintaining protein-protein interactions during the entire process of sample preparation. In the course of method development I performed three pilot SILAC experiments with various modifications in preparation and buffer composition. I also analysed kinetics of the cell lysis in various conditions by measuring changes in light scattering after adding the lysis buffer to the cell suspension (data not shown). Several modifications to the protein Sample Buffer and the final sample preparation were tested to establish the best procedure of efficient sample solubilisation and separation on the SDS-PAGE. The lysis conditions were optimized to decrease the delay in cell lysis and the cytoskeleton purification procedure was shortened to a minimum and performed at 0°C. Stimulation with cAMP was performed at 12°C in order to slow down the response allowing reproducible capturing of the first phase of actin polymerisation. The final working protocol is described in detail in the Materials and Methods chapter.

Two independent experiments were analysed and the results were combined. All the proteomic data presented in the heat-maps are protein L/H ratios averaged from two experiments and normalised to pre-stimulation levels. Original data from each experiment are available in Excel files in the Suplementary Materials.

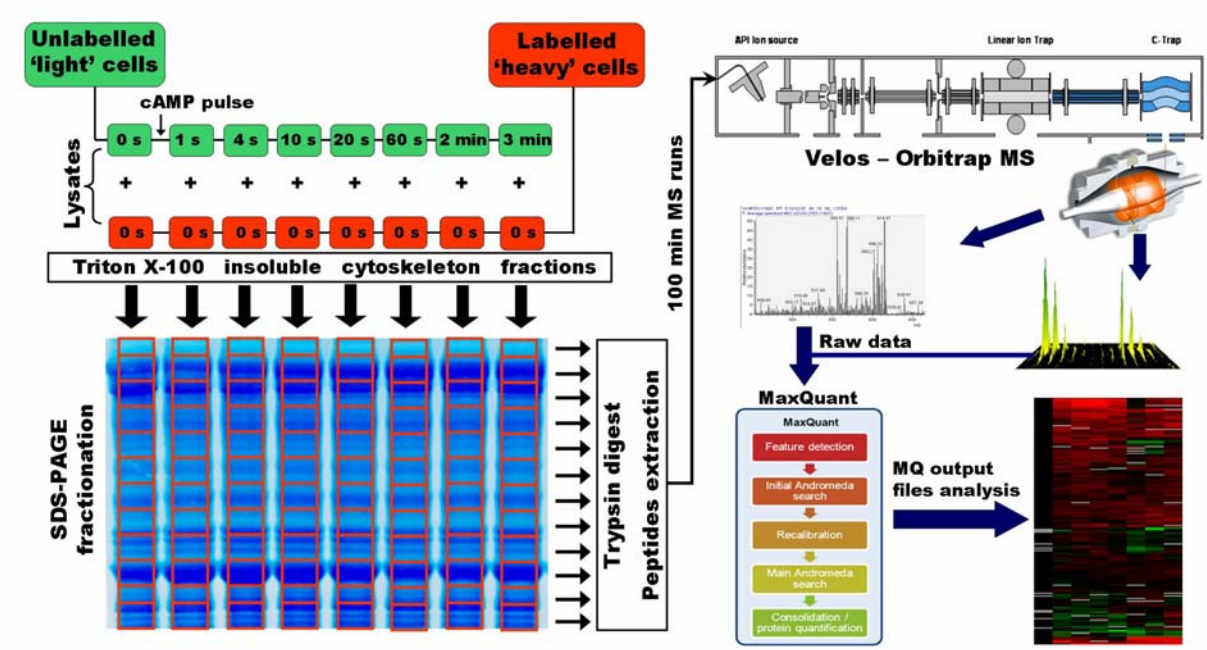


**Figure 3.1.** SILAC experimental workflow. 'Light' cells were stimulated with cAMP and lysed at various time points with Triton X-100 lysis buffer. 'Heavy' cells were lysed without stimulation and served as an internal reference of protein abundance in each time point of stimulated population. Insoluble fractions were fractionated by SDS-PAGE and digested with trypsin. Extracted and purified peptides were analysed by the LTQ Velos Orbitrap MS. Data were processed with the MaxQuant software. The final protein dynamics patterns were clustered and represented in the form of heat maps.

In order for the SILAC experiment to succeed cells need to incorporate 'heavy' forms of lysine and arginine provided in the SILAC medium into their proteins. In optimal conditions after five cell doublings in the 'heavy' SILAC medium about 97% of all the lysine and arginine residues in the entire proteome should contain the labelled forms of those amino acids. Therefore one of the most important controls of the SILAC procedure performed at the initial stages of the protocol development was the analysis of incorporation efficiency of the 'heavy' amino acids into the proteome of *Dictyostelium* cells. Cytoskeleton fraction from the 'heavy' cell population grown in a shaking culture for five cell doublings was analysed separately and the results were used to determine the incorporation efficiency (Fig. 3.2.).

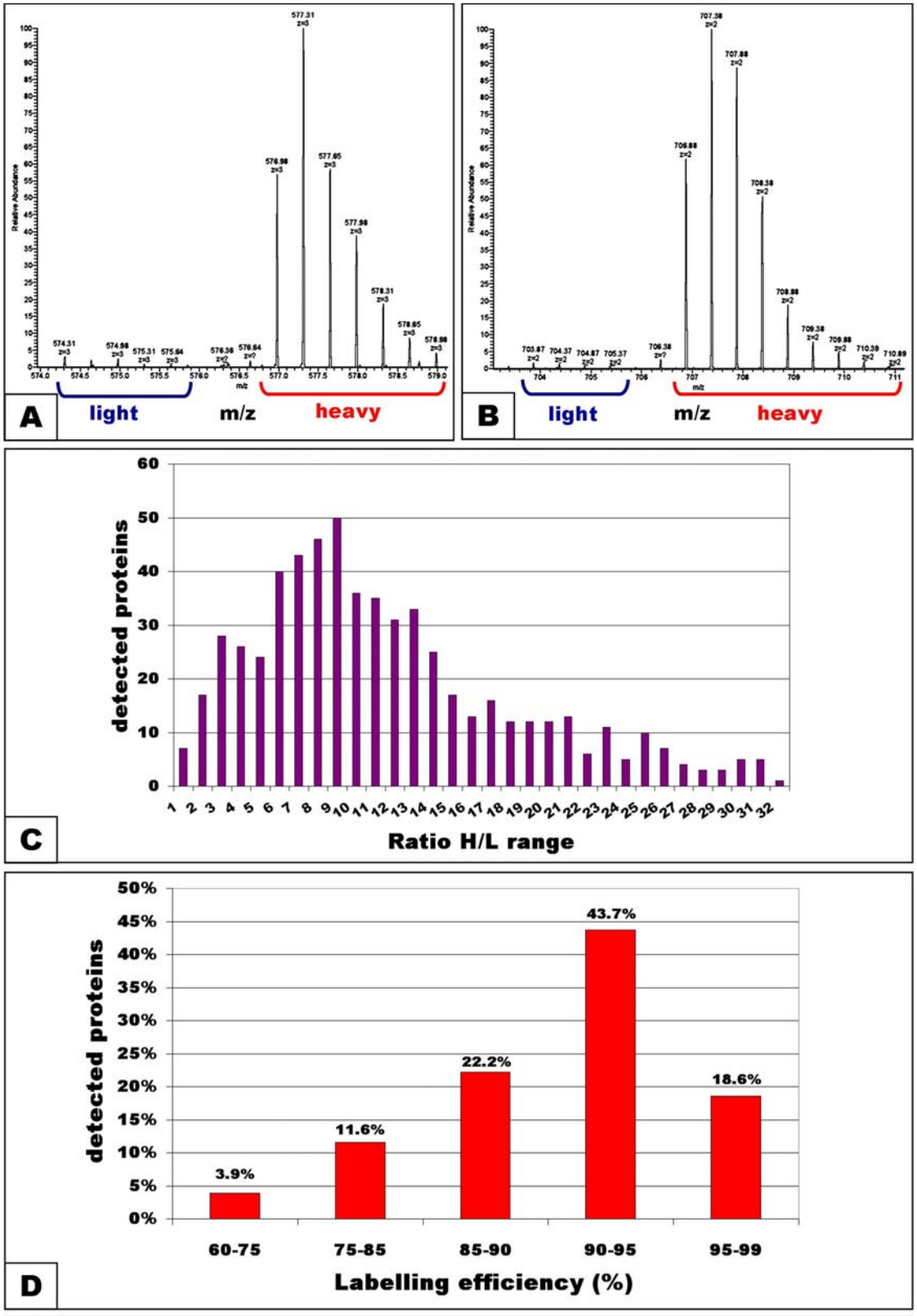


**Figure 3.2.** Results from the labelling efficiency control. **A)** Mass spectrum (MS) of a SILAC pair of a peptide containing a single lysine residue (ALHLFGPTLGYFGEA**K** ) with H/L ratio value of 29.7. **B)** MS of a SILAC pair of a peptide containing a single arginine residue (AAITNDFIGSEI**R** ) with H/L ratio value of 51.9. Blue brackets indicate isotopic distribution peaks belonging to the 'light' forms and red brackets to the 'heavy' forms. **C)** Unnormalised ratio H/L distribution of the 616 detected proteins. Ratio H/L values indicate labeling efficiency of the proteins, e.g. H/L ratio 4 corresponds to 80% of labeling efficiency and H/L ratio 9 corresponds to 90% labeling efficiency. **D)** Labelling efficiency groups of all the detected proteins. The range of labelling efficiency indicates the contribution of 'heavy' forms of lysine and arginine incorporated into the proteins.

The $Ax_2$ axenic strain of *D. discoideum* used in this study is auxotrophic for both lysine and arginine [233] and I observed efficient incorporation for each of those amino acids. Examples of mass spectra for one peptide containing a single lysine residue and one containing a single arginine residue are presented in Figure 3.2. A and B. The H/L ratio values of those peptides correspond to the labelling efficiency of about 97% and 98% respectively.

A general ratio H/L distribution of entire proteins indicates a wide range of labelling efficiencies for different proteins (Fig. 3.2. C). While most of the 616 detected proteins fall in the range of H/L ratio value between 6 and 20 which corresponds to 85-95% labelling efficiency (about 66% of all the proteins) there are some that are labelled with lower than 75% efficiency and some that are labelled with almost 99% efficiency. In total more than 60% of all the proteins are labelled with higher than 90% efficiency and about 85% of all the proteins show labelling efficiency above 85% (Fig. 3.2. D).

There are several reasons for this relatively big variability in the extent of 'heavy' amino acids incorporation between different proteins. One factor might be simply a measurement error which will most likely affect the low abundant proteins represented by very few peptides. Another more specific factor might be a variable protein turn-over rate. Proteins with high turn-over rates and short lifetime will go through more generation cycles than the number of cell doublings and will be therefore labelled with higher efficiency than the most stable proteins with slow turn-over rates. But even the proteins with turn-over rate as slow as the pace of the cell cycle should be labelled with efficiency exceeding 95% after 5 cell doublings. A variable cell doubling time within one cell population might therefore be the most important factor responsible for the presence of proteins labelled with low efficiency. Even though the total cell count indicates 5 cell doublings of the whole population it is likely that some cells will undergo more than 5 doublings while others will divive more slowly. This slowly dividing fraction of the cell population might potentially maintain certain

proteins with significantly lower incorporation factor than the rest of the population, which could affect the final H/L ratio value for those proteins.

Nevertheless the final result with the average labelling efficiency for the whole sample of 93% is satisfactory. Even the proteins exhibiting low incorporation of 'heavy' amino acids of around 80% can still provide informative and fairly quantitative results. In my experimental design 'heavy' cell population serves as an internal reference in the SILAC experiments. Levels of the labelled proteins remain constant in all the time points while only the 'light' forms of the proteins change their abundance levels. The final L/H ratio values from all the time poins are then normalised to the prestimulation time point.

Table 3.1. shows how different labelling efficiencies will affect the SILAC results including initial unnormalised ratios and final ratios normalised to the prestimulation time point ($t_0$). It is noticeable that the normalisation to the prestimulation time point abolishes most of the L/H ratio variabilities coming from differential labelling efficiency of the 'heavy' forms. Low labelling efficiency of proteins in the 'heavy' population leads to overestimation of unnormalised ratios but underestimation of the L/H ratios after normalisation to $t_0$. There is surprisingly little difference between the final normalised L/H ratios quantified for proteins with high and low labelling efficiencies of the 'heavy' form. A three fold increase of the 'light' form normalised to 1 : 1 proportion at the prestimulation time point would be detected as 2.8 fold enrichement for protein labelled with 90% efficiency at the 'heavy' population and as 2.6 fold enrichment for protein showing 75% labelling efficiency (Tab. 3.1.).

This shows that the accuracy of the SILAC ratios quantification is affected by the labelling efficiency lower than 95% but this is a relatively mild effect not exceeding the biological or technical variability and the obtained results can still be analysed in a quantitative manner.

Another factor which needs to be considered during setting up a SILAC procedure is a potential metabolic transition of 'heavy' arginine into proline. This would lead to generation of additional lebelled amino acid in the sample and if occurred on a large scale it could affect

| Labelling efficiency of the 'heavy' form | Actual proportion of 'light' : 'heavy' | Detected L/H ratio unnormalised | Final L/H ratio normalised to $t_0$ (1:1) |
|---|---|---|---|
| **95%** | 1 : 1 | 1.1 | **1** |
| | 2 : 1 | 2.16 | **1.96** |
| | 3 : 1 | 3.21 | **2.92** |
| **90%** | 1 : 1 | 1.22 | **1** |
| | 2 : 1 | 2.33 | **1.9** |
| | 3 : 1 | 3.44 | **2.8** |
| **85%** | 1 : 1 | 1.35 | **1** |
| | 2 : 1 | 2.53 | **1.87** |
| | 3 : 1 | 3.7 | **2.74** |
| **75%** | 1 : 1 | 1.66 | **1** |
| | 2 : 1 | 3 | **1.8** |
| | 3 : 1 | 4.3 | **2.6** |

**Table 3.1** Effects of various labeling efficiencies on the SILAC ratio quantification in the experimental design used in this study. Decreased labeling efficiency of the 'heavy' form used as an internal control, leads to overestimation of detected unnormalised L/H ratios and underestimation of L/H ratios after normalization to the prestimulation time point. All the calculations assume 1 : 1 proportion of 'light' and 'heavy' forms in the prestimulation time point.

significantly the outcome of the experimental results. This issue was addressed by analysing one of the SILAC experiments with variable modifications including labelled forms of proline P(5) and P(6). The obtained results indicated that this transition process is essentially not occurring in the analysed cells. There were 37 labelled residues of proline detected in total which corresponds to only 0.11% of 33,589 proline residues found in the entire experiment. The abundance levels of those few 'heavy' prolines detected were so low that the H/L ratios for those modified peptides were usually not available or very small and it was very difficult to find their peaks at the mass spectra (data not shown).

# 3.2. General protein detection

Total protein detection from the SILAC experiments included about 2500 proteins. Around 30% of those proteins were detected only in one or two time points and were therefore not informative. After filtering out the proteins with detection lower than 4 time points, there were about 1800 proteins left, which were detected with a minimum of 2 peptides/protein in each time point. Proteins were annotated with *Dictyostelium* Gene Ontology Annotations and divided into several groups based on the Cellular Component information (Fig. 3.3). There were more than 200 cytoskeletal proteins which formed a 11% fraction of all the identified proteins. Nuclear proteins had slightly higher contribution of 12% while 5 other protein groups: phagocytic vesicle, centrosome/microtubules, membrane, mitochondria and ribosomes formed smaller fractions of 2-7%. Other characterised proteins which did not have any Cellular Component annotation were put together in a group called 'other', which contained one third of all the proteins detected. Second biggest protein group called 'unknown', which covered almost one quarter of all the proteins detected, was made up from proteins of unknown function. These proteins are predicted from the DNA sequence and some of them have protein domains identified by homology analysis, but they were never characterised and do not have individual names other than the gene/protein IDs.

The general overview of proteins identified in the SILAC experiments shows that cytoskeletal proteins form relatively small portion of all the proteins detected in the insoluble cell fraction analysed. On the other hand out of the first 20 proteins with the highest detection intensity 5 were cytoskeletal factors, including actin, myosin II heavy chain and coronin A described later in detail. This indicates that the analysed samples were significantly enriched in the cytoskeletal fraction, but the exact enrichment factor could only be determined by comparative analysis of those samples and the total cell lysate.

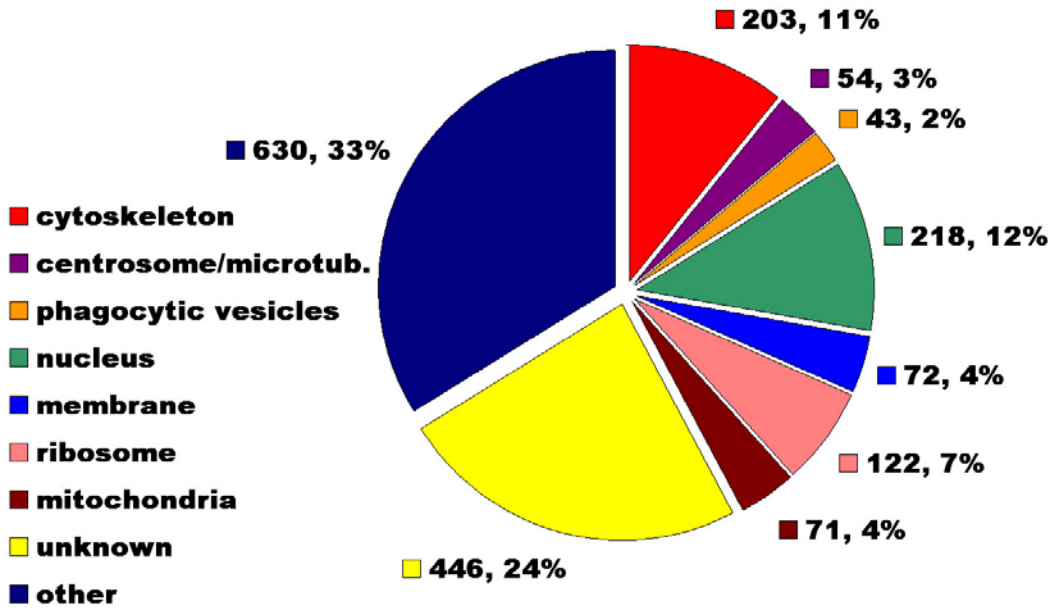


**Figure 3.3.** Protein detection in the SILAC experiments. Proteins were divided into 9 groups based on the Cellular Component information from Gene Ontology Annotations. Cytoskeletal proteins represent 11% of all the proteins identified. 'Other' represents characterized proteins with no Cellular Component information available. 'Unknown' represents proteins of unknown function which have not yet been characterized.

There are few interesting facts to notice in this overview of identified proteins. The substantial part of the whole detection is formed by the nuclear proteins, which is caused by the fact that nuclei stay intact in the lysis conditions used and they get centrifuged and purified at least as efficiently as the cell cortex. Another big class of identified proteins are components of the ribosomal machinery, which suggests that the rough Endoplasmic Reticulum (ER) containing these macrocomplexes is also somewhat resistant to the lysis with Triton X-100 detergent and gets purified with other cellular structures. Presence of many putative membrane proteins in those samples also suggests that some membranous structures are preserved in this purification procedure. It is encouraging to notice that almost 25% of all the molecules identified, are the proteins of unknown function, since besides quantifying the translocation dynamics of the cytoskeletal proteins, one of the main goals of this research project was to identify novel cytoskeletal components.

Results from two SILAC experiments were combined and these final protein L/H ratios series normalised to the pre-stimulation time point were analysed by clustering using a

Cluster3 software created by Michiel de Hoon, University of Tokyo [229]. The purpose of this step was to separate all the proteins into several groups of distinct translocation dynamics patterns. We were using hierarchical clustering with City-Block distance as a similarity metric and an average linkage as a clustering method. These clustering settings were found to generate the best grouping of proteins into clusters with similar dynamics patterns. Clustering results were represented in the form of heat maps with the Java TreeView software developed by Alok Saldanha, Stanford University School of Medicine [230].

## 3.3. Cytoskeletal proteins

As mentioned earlier, a good factor indicating that the analysed fractions were enriched in the cytoskeletal factors, is that the two major structural constituents of the cytoskeleton, actin and myosin II heavy chain, were among the first four most abundant proteins detected.

*Dictyostelium* genome contains 29 genes encoding actin proteins with amino acid identity greater than 83%. 17 of those genes encode identical proteins and another 3 have only few amino acid differences, while the rest are a bit more divergent [22]. This represents a big challenge for proteomic analysis, since the majority of those proteins will generate a pool of identical peptides, which will not be possible to allocate to a single protein, these are the razor peptides. Those actins that do have unique peptides generated in a tryptic digest will have only few of them and the quantification of protein ratios based on those few remaining unique peptides will be less reliable than the one based on all the data available. This is the reason why protein ratios were quantified using both unique and razor peptides.

MaxQuant algorithms allocate the whole pool of razor peptides to a single protein which has the highest unique peptides intensity of all the proteins sharing this pool [191]. In these experiments all the actin razor peptides, which contained most of the actin peptides

altogether, were allocated to Act10 protein, which is therefore a representation of the total combined actin response to cAMP stimulation. It reaches a peak of the first phase at 4 s which lasts until 10 s at a level of about 2.3 L/H. It is followed by depolymerisation phase with the lowest point of 1.2 L/H at 60 s and then rises slowly reaching the highest point of the second phase with 1.7 L/H at 180 s. This is the basic actin dynamics which is in agreement with the data previously collected by phalloidin assay (Fig. 3.5. E).

There were two other actins detected in at least 4 time points, Act17 and Act22, which were both quantified using only the few unique peptides available. Act17 shows higher amplitude in the first phase than Act10, but is not detected in the last two time points, while Act22 shows a bit more noisy pattern than the whole group represented by Act10. This actin dynamics is by far the most commonly represented pattern which is shown in variable amplitude and sometimes slightly different timing by the whole variety of proteins and protein complexes. It is shared by structural components such as Arp2/3 complex, actin filaments effectors like bundling proteins and finally the regulatory factors including GEFs and GAPs (Fig. 3.4.). Another common profile of protein dynamics is the one represented by myosin II complex. It shows slight increase in the early time points followed by depletion at 10 s and 20 s and then reaches the main peak of around 3 L/H in the last 3 time points, which correlate with the second phase of actin polymerisation.

## Abbreviations of protein annotations used in the heat-maps:

**ABP – actin binding protein;**
**adpr – adaptor protein;**
**bd – binding;**
**con – containing;**
**cpx – complex;**
**dcp – domain containing protein;**
**fam – family;**
**gr – group;**
**hom – homology;**
**KIN – kinase;**
**PHOS – phosphatase;**
**put – putative;**
**pr – protein;**
**reg – regulatory;**
**rel – related;**
**rep – repeat;**
**sim – similar;**
**sub – subunit;**

## Cytoskeletal proteins showing strong response


**Figure 3.4.** Protein dynamics of the cytoskeletal proteins. Only proteins with response higher then 1.5 L/H in a minimum of one time point after cAMP stimulation are presented.

### 3.3.1. Structural components of the cytoskeleton

Proteins that follow actin dynamics most closely are the structural components of actin filaments. These include the major actin nucleator – Arp2/3 complex, at the pointed end and the capping protein – Cap32/34 complex, at the barbed end. All 7 components of the Arp2/3 complex share the same actin-like pattern with certain variability in amplitude which is not reproducible between the two experiments and is most likely caused by the measurement errors rather than differential response (Fig. 3.5. B). It is therefore more appropriate to analyse the Arp2/3 complex as a single unity rather than each component separately (Fig. 3.5. C). This primary nucleator of actin filaments has the same timing as actin dynamics but shows higher enrichment reaching more than 3 L/H during the first phase of actin polymerisation. It goes down to almost exactly pre-stimulation levels in the 60 s time point and then reaches similar levels as actin in the last two time points.

Both components of the capping protein complex Cap32/34 also share virtually the same pattern, with variability not exceeding measurement error and should also be analysed together. This major inhibitor of the actin filaments elongation follows the actin dynamics much more closely than the Arp2/3 complex. It reaches almost the same levels in nearly all the time points except for 20 s, which is the beginning of depolymerisation phase, when Cap32/34 shows slower depletion rate than actin. It is interesting to notice that in the first phase the Arp2/3 complex shows much higher enrichment than the Cap32/34 and actin, while in the second phase all of those components share the same ratios.

Myosin II complex reveals a biphasic response to cAMP stimulation as well, but with different timing and pattern than actin. It has a short and low first phase with a peak of 1.6 L/H lasting from 1 s to 4 s followed by a disassembly phase when it goes down close to pre-stimulation levels at 20 s. Myosin II reaches a peak of its second phase at 60 s with amplitude

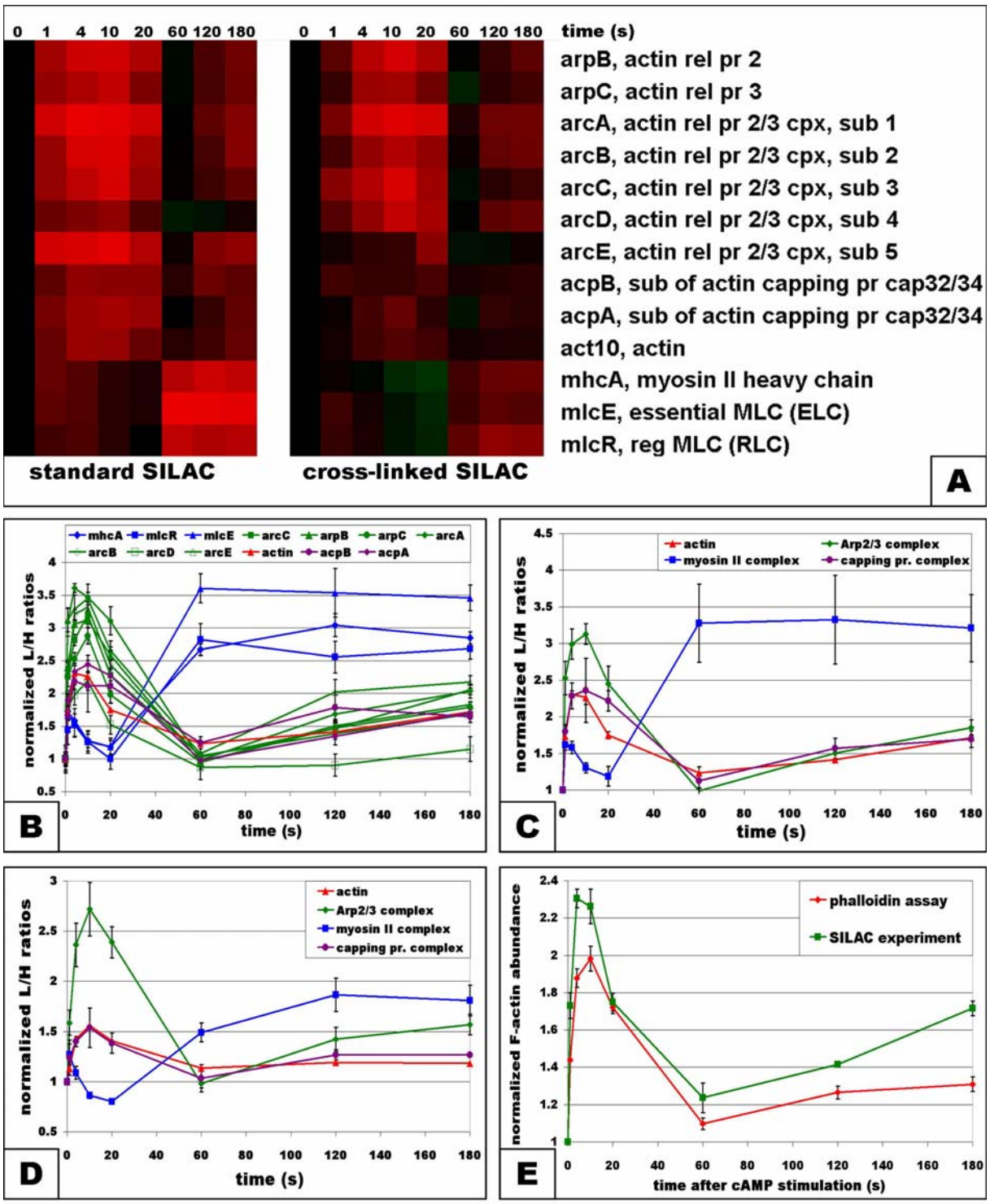


**Figure 3.5.** Protein dynamics of the major structural cytoskeletal components. (A) Heat-map representation of the L/H ratios for standard and cross-linked SILAC experiments. (B) Graph representation of the results from standard SILAC for all the components of protein complexes separately. Actin – red; Arp2/3 subunits – green; Cap32/34 subunits – violet; myosin II subunits – blue. (C) Protein dynamics patterns from the standard SILAC experiment for the whole protein complexes, based on combined results from individual subunits. (D) Protein dynamics patterns from the cross-linked SILAC experiment for the whole protein complexes, based on combined results from individual subunits. (E) Actin dynamics in response to cAMP stimulation measured with phalloidin assay (red) and with SILAC experiment (green).

of about 3 L/H, which stays constant in the following two time points. It is noticable that in the first phase of myosin II filaments assembly all three components of this protein complex show exactly equal levels of enrichment, as we would expect form a stable complex. On the other hand during the second phase of myosin response, essential light chain (ELC) shows higher L/H values than myosin heavy chain (MHC) and regulatory light chain (RLC) (Fig. 3.5. B). Detailed examination of the results for the subunits of myosin II filaments from all the experiments performed revealed however that this tendency is not well reproducible between different biological replicas and is most likely an artefact caused by some form of variability or measurement error.

All of these major structural proteins served as a good positive control of the response to cAMP measured in the SILAC experiments. These results confirmed that this method is capable of analysing protein translocation to the cytoskeleton for multiple proteins in a single experiment. Differences in L/H values between several subunits of a single protein complex indicate the accuracy levels and error range in the MS measurements.

These controls were also used to validate the cross-linked SILAC with formaldehyde fixation during cell lysis. In this experiment all of those structural factors show the same type of dynamics patterns as in native lysis conditions, but with significantly lower amplitudes. Only the Arp2/3 complex reaches similar levels of enrichment as in the standard SILAC experiment with first peak around 2.8 L/H and the second peak of 1.6 L/H (Fig. 3.5. D). Actin and Cap32/34 complex again follow almost identical profile with the first peak at 10 s reaching 1.5 L/H and the second peak hardly noticeable. This generates even greater asymmetry between them and the Arp2/3 complex, which in this experiment shows higher levels of translocation in both phases of stimulation response.

Myosin II complex shows the same biphasic response as in the standard SILAC experiment, but with lower amplitudes reaching 0.8 L/H level during disassembly phase and the second peak around 1.9 L/H at 2 min after cAMP stimulation. Possible reasons for the differences in

the protein dynamics amplitudes between standard and cross-linked SILAC experiments will be discussed later.

## 3.3.2. Regulatory components of the cytoskeleton

There is a big range of cytoskeletal regulatory factors detected in the SILAC experiments, including 14 small GTPases, 24 GEFs, 13 GAPs and a variety of protein kinases. GTPases such as RasG, which is known to be the master regulator of signalling pathways controlling the cytoskeleton [98], did not show any significant changes upon cAMP stimulation (Supplementary Materials). This is consistent with the notion that GTPases form only transient interactions with the downstream effectors. On the other hand proteins responsible for activation and inhibition of their activity, GEFs and GAPs respectively, did reveal temporal translocation to the insoluble fraction after chemoattractant stimulation (Fig. 3.6.).

Most of the GEFs followed, with certain approximation, the general actin dynamics showing early and late peaks (Fig. 3.6. A). The ones that followed actin profile most closely were: ZizA, Roco5, GxcW, GxcDD, GxcA, GefD and DDB_G0280221. Due to low time resolution and relatively high noise fluctuations of those data, it is challenging to divide all the detected activators into unambiguous groups of factors playing major role in triggering the first phase and those responsible for induction of the late response to cAMP stimulation.

There is a set of GEFs which show clear translocation in the early time points but are depleted during the second phase. These proteins which are most likely to be specifically involved in regulation of the first phase of actin polymerisation are: DocA, DocB, GefA, GefR, ZizC and GxcD. DocA and DocB are most significantly enriched in the first phase and most significantly depleted in the second phase within this group. Both of those proteins reach the highest point of their peaks in the earliest 1 s time point. This is a strong indication

that these two proteins might be among the earliest regulators to respond to cAMP stimulation. There is only one GEF – GxcQ, which has significantly higher enrichment in the second phase than in the first phase of actin response detected in the standard SILAC.

The majority of GAPs also show enrichment in time points following cAMP stimulation. Some of them follow patterns similar to actin dynamics, but the resemblance is not as strong as for GEFs. RapGAP1 and Bub2 reveal highest similarity to actin profile, while GacHH has the strongest response from all the GAPs and if follows more myosin-like profile, reaching more than 4 L/H values in the last 3 time points.

There were several other regulatory components sharing the common profiles of protein dynamics. Few PI3Ks were found to follow the generic actin profile, the strongest of which were PikA and PikF. Two kinases known to play roles in signalling to the cytoskeleton, p21-activated protein kinase PakB and Tor, were detected. PakB, which binds to $PI(3,4,5)P_3$, follows the general actin dynamics with amplitudes around 1.7 L/H (Fig. 3.4. and 4.17.). A Tor protein, component of a TORC2 complex playing a central role in one of the signalling pathways described earlier, follows a pattern closely correlated to myosin dynamics with a peak in the second phase of about 2 L/H (Fig. 3.4.).

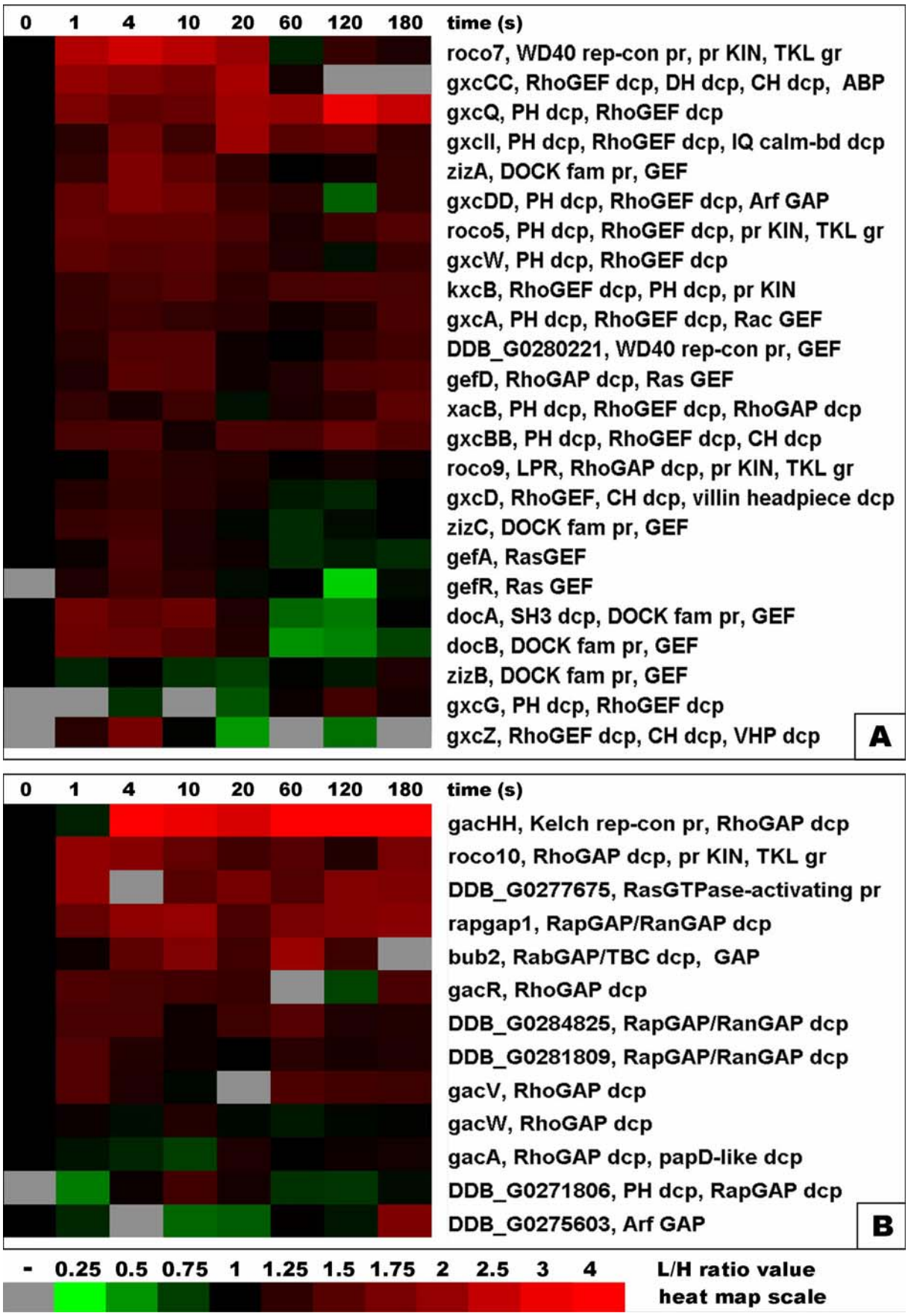


**Figure 3.6.** Protein dynamics of the regulatory cytoskeletal components. (A) Profiles of all GEFs detected in standard SILAC experiment. (B) Profiles of all GAPs detected in standard SILAC experiment.

# 3.4. Proteins from other cellular components

Mixed composition of the analysed samples allowed us to look at the behaviour of proteins from various cellular components. Interestingly most of those proteins do show certain changes in abundance in response to cAMP stimulation. Some of them might represent just the stochastic fluctuations but some are clearly above the noise levels and reveal systematic changes across several time points. These protein groups will be only briefly described here, as they are not in the centre of interest of our analysis. Patterns of protein dynamics for each of the non-cytoskeletal groups are shown in Figures 3.7. and 3.8.

There is a general systematic notion that most of the proteins are enriched after cAMP stimulation and only small proportion of molecules is depleted from the analysed fractions after stimulation. The dynamics patterns are always more reliable if they show persistence within few sequential time points, as this type of pattern is less likely to be caused by noise fluctuations. In other than cytoskeletal protein classes it is more common to see these persistent patterns in later time points, corresponding to the second phase of actin polymerisation. There are few examples of several proteins sharing the same common pattern of translocation dynamics, such as actin-like or myosin-like profile. One example is within phagocytic proteins where few of them share similar pattern of enrichment with a peak at 2 min time point. There is also a group of several membrane proteins showing similar response to cAMP stimulation.

Ribosomal proteins are an interesting example of this collective behaviour, as majority of the proteins in this class share very similar pattern of biphasic dynamics with peaks at 4 s and 2 min and a dip at 10 s and 20 s time points (Fig. 3.8. top left). These patterns have rather small amplitude with the peaks reaching usually not more than 1.5 L/H levels, but it is interesting to see that this pattern resembles actin dynamics. It is not surprising that so many of the

ribosomal proteins share similar pattern, since they form a structurally integral complex, but the similarity of this pattern to the actin dynamics is not something to expect.

One possible simple explanation for this observation is purely mechanistic and it requires assumption that rough ER stays intact during the lysis. With this assumption it is easy to imagine that sheets of this rough ER will be trapped in the cell cortex formed by the meshwork of actin and myosin filaments. This trapping and therefore purification of those structures will be more efficient when the cell cortex is thicker and denser, which is the result of actin polymerisation in response to cAMP. It is important to point out that thickness of the cell cortex will also affect the probability of cell shearing during the lysis and cells in the peaks of actin polymerisation will be more likely to stay intact and trap these structures within them. This mechanism of trapping big cellular structures by the cell cortex would explain the actin-like pattern of the components of these structures without their direct interaction with actin filaments. This example shows that we are dealing not just with a massive background of proteins from the whole cell but that this background can mimic the actual response we are measuring.

There are many uncharacterised proteins that show interesting dynamics in response to cAMP stimulation sometimes reaching high amplitudes (Fig. 3.8. bottom left). Unfortunately these patterns are not very different from the ones displayed by many proteins from all the other protein groups. This characteristic of the background proteins showing response levels similar to the cytoskeletal proteins, makes it particularly difficult to screen for a novel cytoskeletal components from the vast number of unknown proteins.

Even though the majority of detected proteins show changes after cAMP stimulation, not all the dynamics patterns are equally reliable. The level of confidence in the protein ratios present in the SILAC results is directly proportional to the detection level and the number of peptide counts, which these ratios are based on. The general notion is that the protein ratios based on fewer peptides have higher amplitudes and form noisy patterns, while the ratios

based on many peptides show smaller changes, but are more consistent and reproducible. This might be the reason why only small proportion of the proteins does not show any changes throughout the whole experiment. These are the factors which do not display any real translocation in response to cAMP stimulation and are at the same time abundant enough to be resistant to the noise fluctuations. The majority of low abundant proteins which do not respond to cAMP are affected by the measurement errors, which can generate big changes in the SILAC results. The dynamics patterns of some proteins can also be affected by other not specific processes, such as the cortex trapping mechanism proposed for the ribosomal proteins.

It is therefore important to understand that not all the patterns of translocation dynamics detected with the SILAC approach can be interpreted in the same way. The results of analysed proteins need to be individually validated by the level of peptide detection and variability between the biological replicas of the experiment.

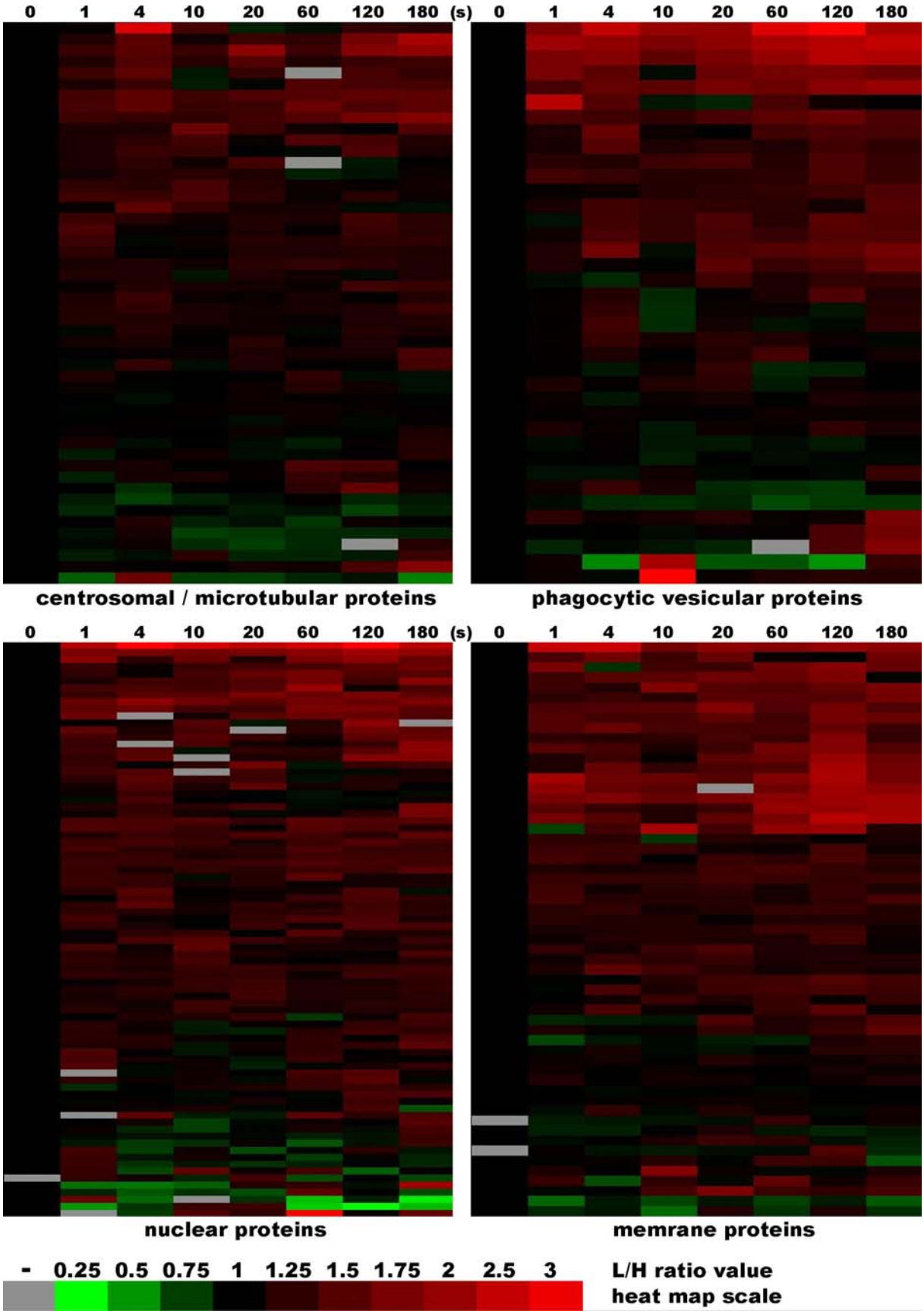


**Figure 3.7.** Protein dynamics of proteins from different cellular components. Only proteins with maximum of one missing time point (gray) are represented. Series of protein L/H ratios are normalized to their prestimulation levels (0 s). Series with prestimulation time point missing are normalized to their average.

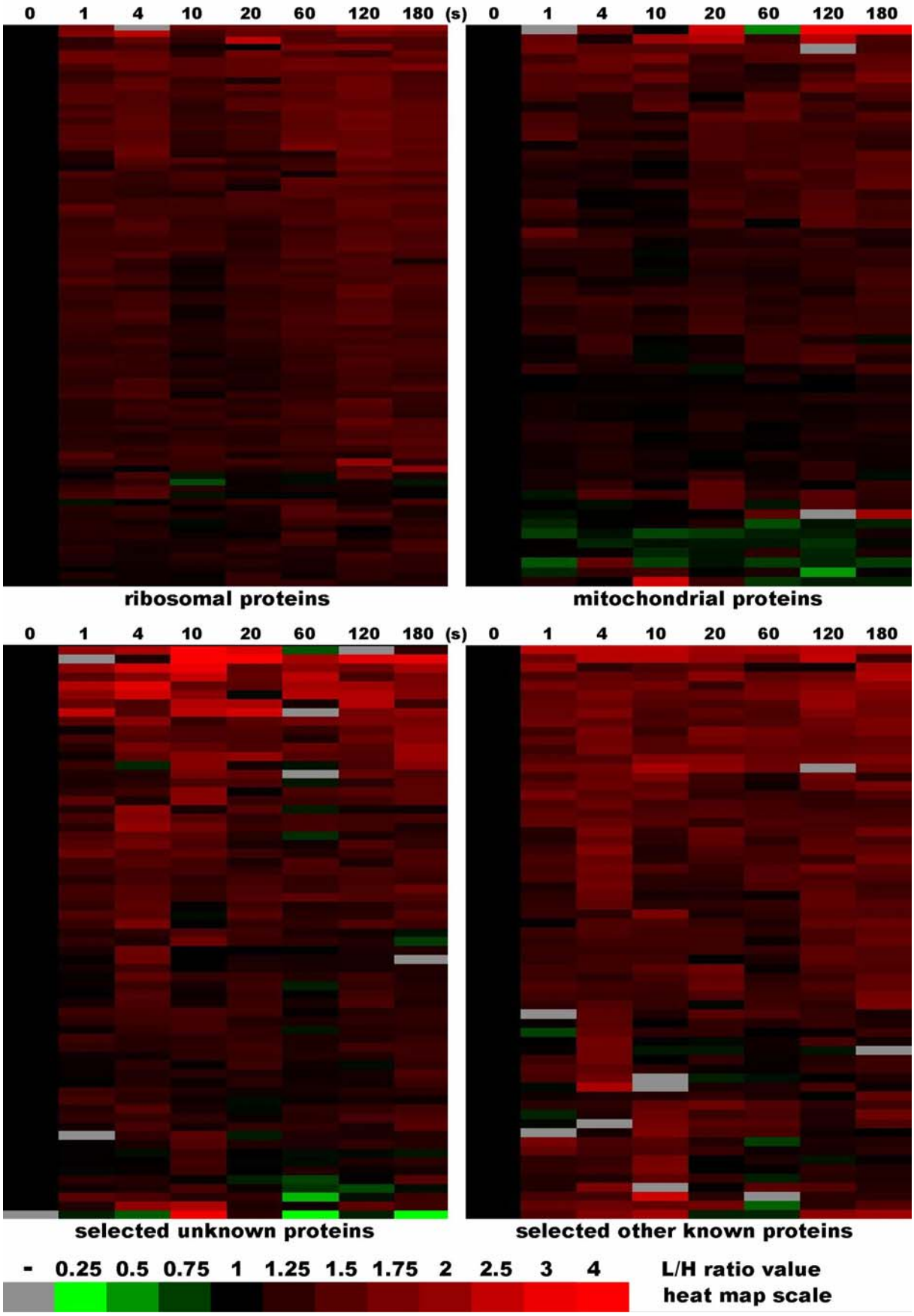


**Figure 3.8.** Protein dynamics of proteins from different cellular components. Only proteins with response higher then 1.5 L/H in a minimum of one time point after cAMP stimulation were selected from the groups of unknown proteins and other known proteins.

# 3.5. Cross-linked SILAC experiment

The proteomic approach to investigate fast protein translocation used in this study depends on maintaining protein-protein interactions throughout the course of sample preparation. In fact using this method for protein dynamics analysis is limited only to those proteins that bind directly or indirectly to the structural core of the cytoskeletal framework. This has been proven to work for a big range of cytoskeletal components, but there were also many known actin binding proteins that were missing in those experiments. Several important regulatory factors such as Scar and WASP proteins, direct activators of the Arp2/3 complex were not detected using the standard SILAC protocol. One explanation for their absence could be that they are present in very small amounts and avoid detection by being covered by more abundant molecules. The other and more likely explanation is that they form only transient and unstable interactions with the structural components of the cytoskeleton and dissociate from the insoluble fraction shortly after cell lysis.

In order to preserve those easily lost proteins, several cross-linking factors compatible with downstream MS analysis were checked. The basic formaldehyde fixation followed by thermal reversal of the cross-linking was found to be the most efficient and practical. Another advantage of fixing the proteins during cell lysis was that the samples did not have to be processed as fast as possible. This allowed us to collect 4 separate stimulation series which were combined in order to average the variability in stimulation response and sampling errors.

The total detection of the cross-linked SILAC was higher than in the standard experiment. There were about 300 new proteins detected out of which 90 were cytoskeleton related. There were also about 40 cytoskeletal proteins missing from the cross-linked SILAC

comparing to the previous results. In this chapter only the cytoskeletal components detected in the cross-linked experiment are described.

Protein dynamics captured in the fixing conditions does not always correlate to the results from the native conditions. Only one third of the cytoskeletal proteins detected in both types of SILAC experiments, showed clearly reproducible dynamics patterns (Fig. 3.9.). This group contains all the structural proteins described before as positive controls of the response to cAMP stimulation. There are also many actin binding proteins and several regulatory factors which have similar dynamics in both experiments. Many of those proteins, which were sharing similar timing of the dynamics profile with the previous experiment, showed different amplitude levels in the peaks of incorporation. The general interpretation of this part of the cross-linked SILAC experiment is straightforward as it validates the results from the standard SILAC experiments.

The remaining two thirds of the cytoskeletal proteins detected in this experiment, showed only weak correlation or even strong negative correlation with the previous results (Fig. 3.10.). These proteins, which show lack of dynamics reproducibility between the two types of experimental preparations, are difficult to interpret and force us to question the reliability of this experimental procedure. There are several factors which might influence the outcome of the cross-linked SILAC experiment, such as the efficiency of formaldehyde cross-linking and its reversal.

One possible explanation of such great variability between the results from those two types of sample preparation, is that formaldehyde fixation will have differential impact on various protein-protein interactions. Formaldehyde, which modifies mostly primary amines present on lysine and arginine residues, is a very small molecule and it forms only 1.2 Å bridge between the two cross-linked proteins. This means that only those protein-protein interactions, which contain lysine and/or arginine side chains in very close proximity, will be efficiently cross-linked with formaldehyde.

## Standard and cross-linked SILAC high correlation results

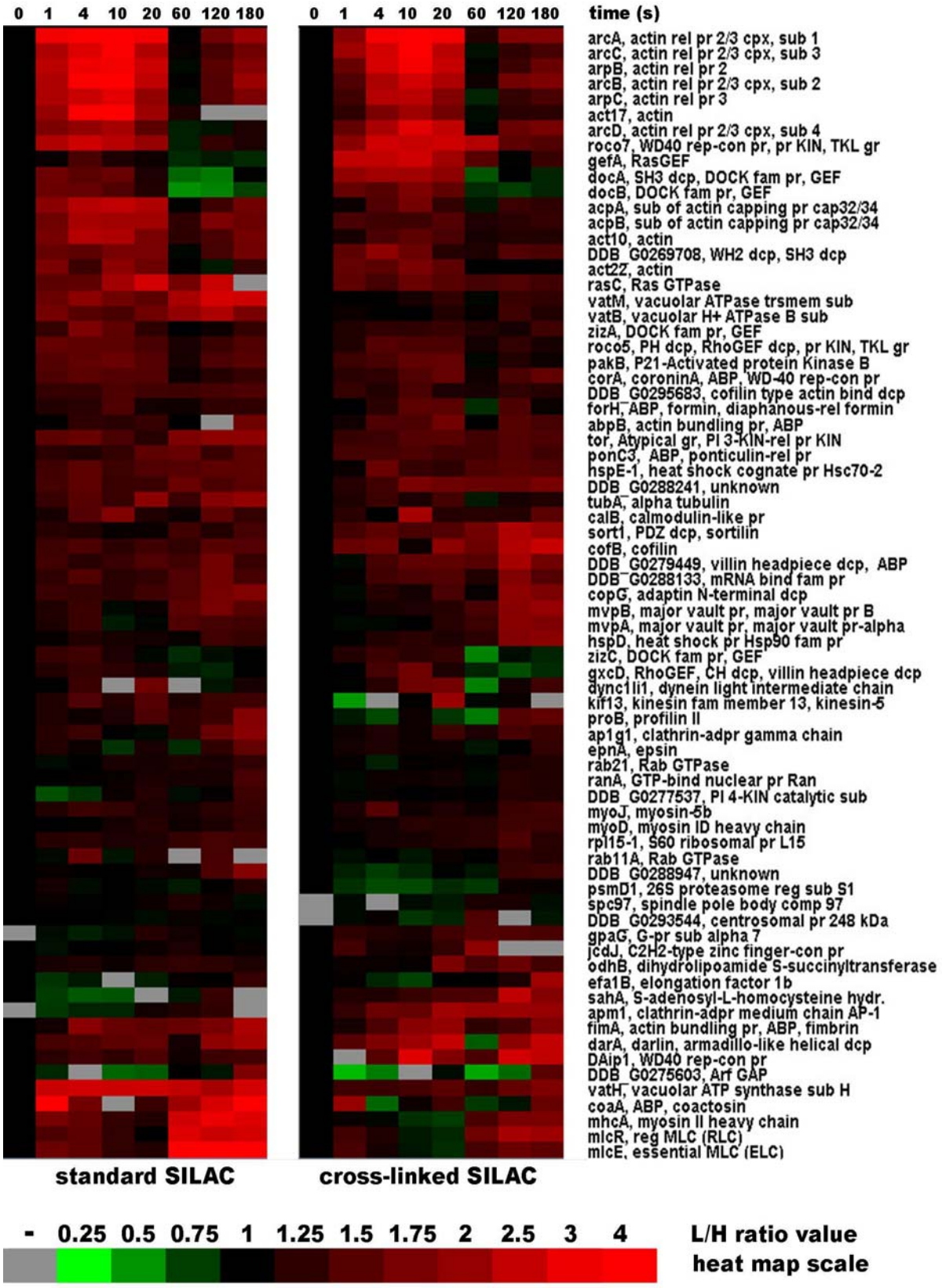


**Figure 3.9.** Comparison of protein dynamics detected in the standard SILAC (left column) and cross-linked SILAC (right column) experiments. Only cytoskeletal proteins showing correlation coefficient higher then 0.5 between the patterns detected in both types of experiments are presented.

Proteins forming interactions which lack this characteristic will have their residues modified without forming cross-linking bridges. In those situations, such modifications will likely interfere with and potentially disrupt the protein-protein interactions they were meant to stabilise. If this explanation is true, then the proteins which can be efficiently cross-linked and preserved in the interactions they form, will show higher enrichment and more reliable dynamics in fixing conditions. All the other proteins, which could be rather disturbed than stabilised by formaldehyde modifications, should be analysed in native conditions.

Unfortunately there is no simple way of predicting which proteins belong to each of those types. The only feature, which we can use to asses this issue, is the dynamics profile in each of those experiments. Assuming that the two most common profiles, actin-like and myosin-like, are more likely to be representing a real protein dynamics than a stochastic noise, we can estimate a sort of weighting factor for the differing profiles. Following this logic, proteins which show pattern similar to actin or myosin dynamics only in one type of SILAC experiment, while the other type gives rather incoherent noisy pattern, the first profile is presumably a better representation of this protein's real translocation dynamics. There are indeed many such examples among the proteins presented in Figure 3.10.

AbpA, GefD and GxcDD are few examples of the proteins that follow the generic actin dynamics in the standard SILAC experiment, while being depleted after cAMP stimulation in the cross-linked preparation. There are also some proteins which reveal strong patterns only in the cross-linked SILAC, such as MyoI and GacA.

Obviously this is a very arbitrary separation based on speculative assumptions and therefore cannot be treated with high dose of confidence. It is discussed in order to illustrate different aspects and complexity of the results obtained with both types of SILAC experiments. It is clear that the cross-linked SILAC cannot replace the standard experimental procedure, but it can provide a complementary data, which have to be analysed cautiously.

## Standard and cross-linked SILAC low correlation results

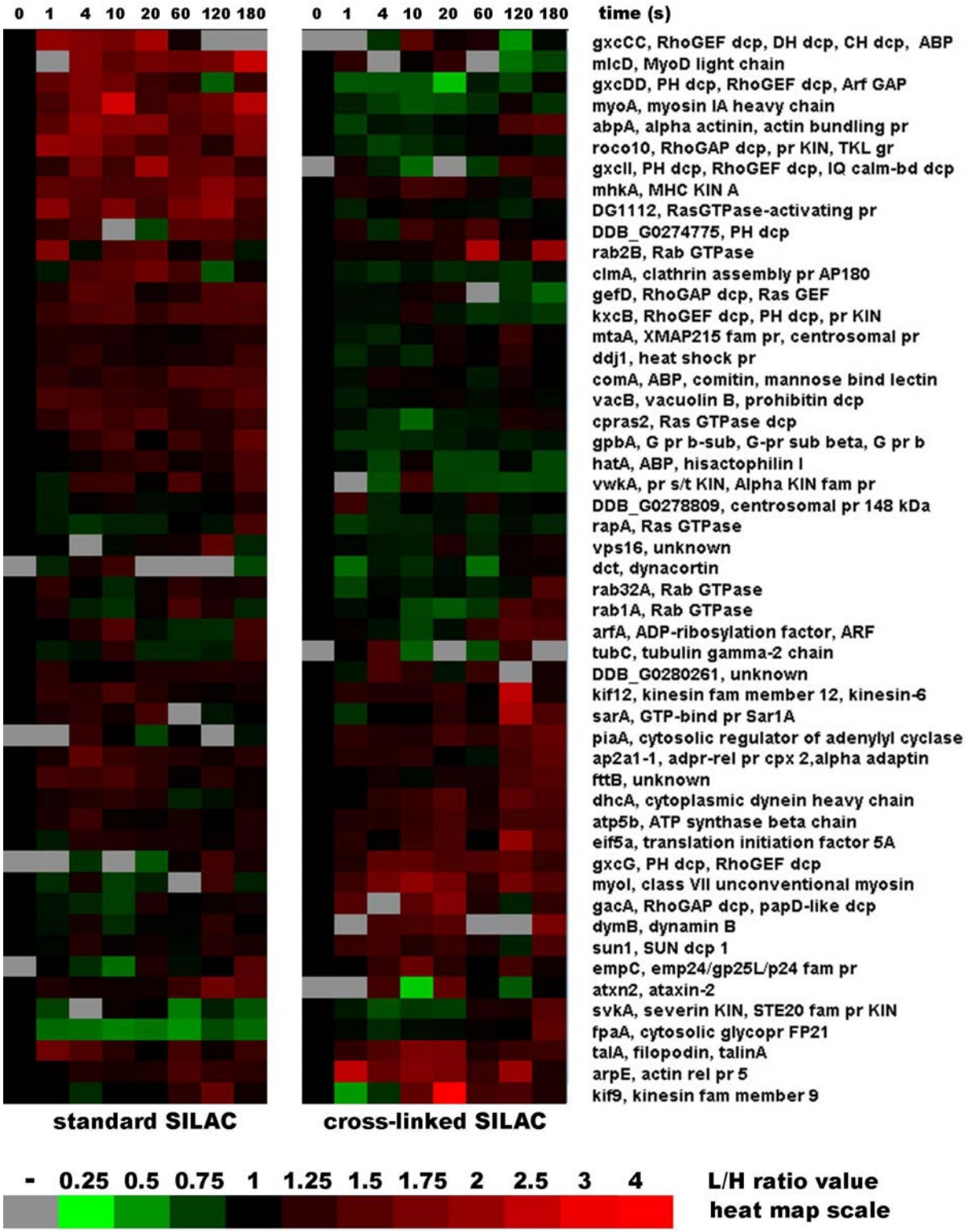


**Figure 3.10.** Comparison of protein dynamics detected in the standard SILAC (left column) and cross-linked SILAC (right column) experiments. Only cytoskeletal proteins showing correlation coefficient from 0.1 to -1 between the patterns detected in both types of experiments are presented.

The most important contribution of the cross-linked type of sample preparation is detection of the proteins that were not found in the standard SILAC procedure. These proteins, which can only be detected in the fixing conditions, are most likely to belong to those factors which are efficiently cross-linked and stabilised by formaldehyde, which implies that their patterns are presumably more reliable. Many of those proteins show patterns with high correlation to the actin dynamics or myosin-like enrichment in the late response, with particularly big number of proteins showing translocation only in the last two time points (Fig. 3.11.).

Some of the most interesting proteins to find here are two components of the Scar protein complex, ScrA and NapA, both of which follow biphasic actin dynamics. There are few other important factors which show resemblance to actin profile, such as component of TORC2 – RipA, or member of Ena/VASP family involved in actin cytoskeleton organisation – VasP. Another interesting observation is DocD protein, showing very little response in the first phase of actin polymerisation and strong enrichment in the late phase, which is very different from the dynamics detected proteinsly for DocA and DocB. There are several unconventional myosins detected only in the cross-linked SILAC, such as MyoB, MyoC, MyoE and MyoK, most of which are incorporated to the cytoskeleton in the later time points similarly to myosin II.

There is a big group of proteins sharing a dynamics pattern which has not been represented in the standard SILAC experiment. These proteins show depletion in almost all the time points within first minute after cAMP stimulation and then show strong enrichment in the last two time points of 2 min and 3 min, corresponding to the second peak of actin polymerisation. This type of translocation pattern suggests a specific function in the second phase of actin response to cAMP stimulation, which involves pseudopod formation and uropod retraction. Proteins showing this type of dynamics include among others: Rho GTPase RacC, Rho GEF GxcC, severin SevA, Ras GAP GapA and phospholipase C (Fig. 3.11.).

## Proteins detected only with cross-linked SILAC

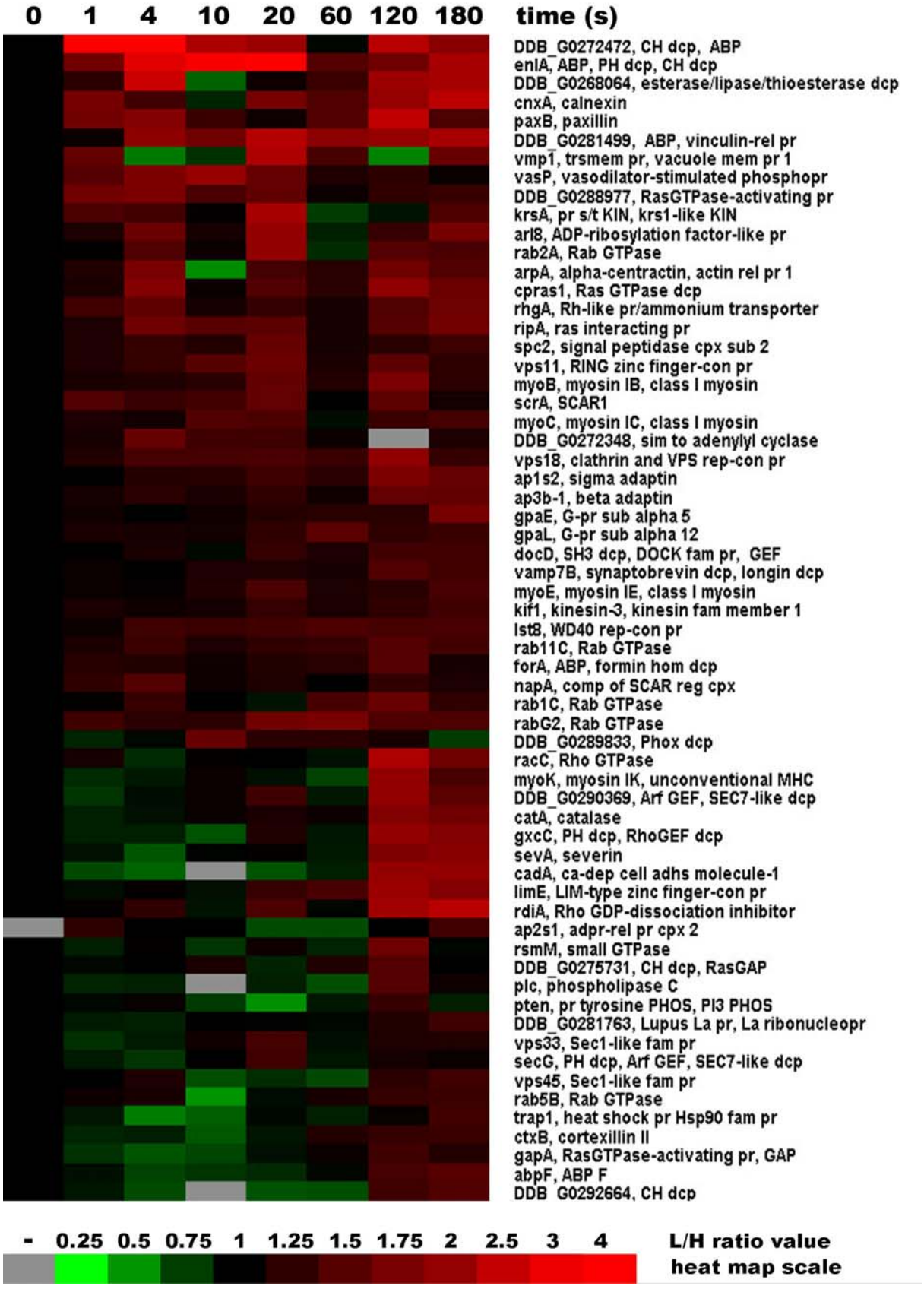


**Figure 3.11.** Proteins detected only in the cross-linked SILAC experiment. Only cytoskeletal proteins with not more then one time point missing are presented.

Cross-linked version of the SILAC experiment had significantly higher detection rate and provided complementary dataset to the one generated with the standard protocol. About one third of the proteins detected in this experiment, including all the major structural components, showed high correlation to the dynamics patterns measured in the standard SILAC. There were many cytoskeletal proteins detected only in this version of the experiment, some of which shared a new pattern of translocation dynamics with specific enrichment only in the second phase of actin polymerisation.

## 3.6. Selection of proteins for tagging with GFP

SILAC experiments provided large scale analysis of protein translocation dynamics in response to cAMP stimulation. Results from these experiments had to be validated by *in vivo* imaging of selected proteins tagged with GFP. This type of analysis is also the only way to confirm the cytoskeletal character of the unknown proteins which showed strong enrichment in the insoluble fraction after cAMP stimulation. For these purposes a group of 120 proteins was selected for cloning and tagging with GFP. About half of them were known cytoskeletal factors such as ABPs, GEFs and GAPs, and another half were proteins of unknown function.
Known cytoskeletal proteins (Fig. 3.12.) were selected based on their dynamics patterns and also their function. Several ABPs such as AbpA, AbpB and coronins were chosen as positive controls to see how the proteomics data correlate with *in vivo* imaging analysis. Most of the GEFs and GAPs which showed strong response in the SILAC results were selected for cloning. Other regulatory proteins such as few PI3Ks and PakB were also selected. Couple of GTPases were selected even though most of them did not show any significant response to stimulation, but they were still interesting to investigate as major regulators of the

cytoskeleton. A number of other known proteins, not directly involved in organisation or regulation of the actin cytoskeleton, were selected due to their strong response or interesting dynamics patterns. These proteins include components of the clathrin endocytic pathway, subunits of vacuolar V-ATPase and few others.

Unknown proteins were selected solely based on the translocation dynamics patterns from the standard SILAC experiment (Fig. 3.13.). Proteins showing various types of patterns were chosen for cloning. Some followed basic actin dynamics while others showed enrichment mostly in the first or the second phase of actin polymerisation and few were most abundant in the time points corresponding to the actin depolymerisation phase. Selection of all those proteins was done with only the first standard SILAC data available. Some of the selected proteins did not show reproducible patterns in the second experiment, therefore after combining the results from both experiments, some profiles were no longer as strong or interesting as in the dataset used for selection. Some of the unknown proteins had various actin binding domains identified by sequence homology analysis. The type of those actin binding domains indicates the character of interaction with actin filaments, but it does not necessarily determine the function of those proteins.

Decision for selecting this relatively big number of proteins for cloning and tagging with GFP was caused by the characteristics of the SILAC results. As described before, proteomic analysis of the cytoskeletal fractions reveal big background of proteins coming from other cellular compartments, which also show certain levels of enrichment after cAMP stimulation. This characteristic combined with relatively high noise fluctuations associated with measurements of protein abundance, made it very difficult to narrow down the selection to a small group of proteins most likely involved in the cytoskeleton dynamics. Instead, a wider range of unknown proteins was chosen for cloning, anticipating that big proportion of them will belong to the background of other cellular components.

## Known proteins selected for cloning


**Figure 3.12.** Known cytoskeletal proteins selected for tagging with GFP and in vivo imaging. Combined results from two standard SILAC experiments are presented. Proteins were chosen based on their function and dynamics pattern.

## Unknown proteins selected for cloning

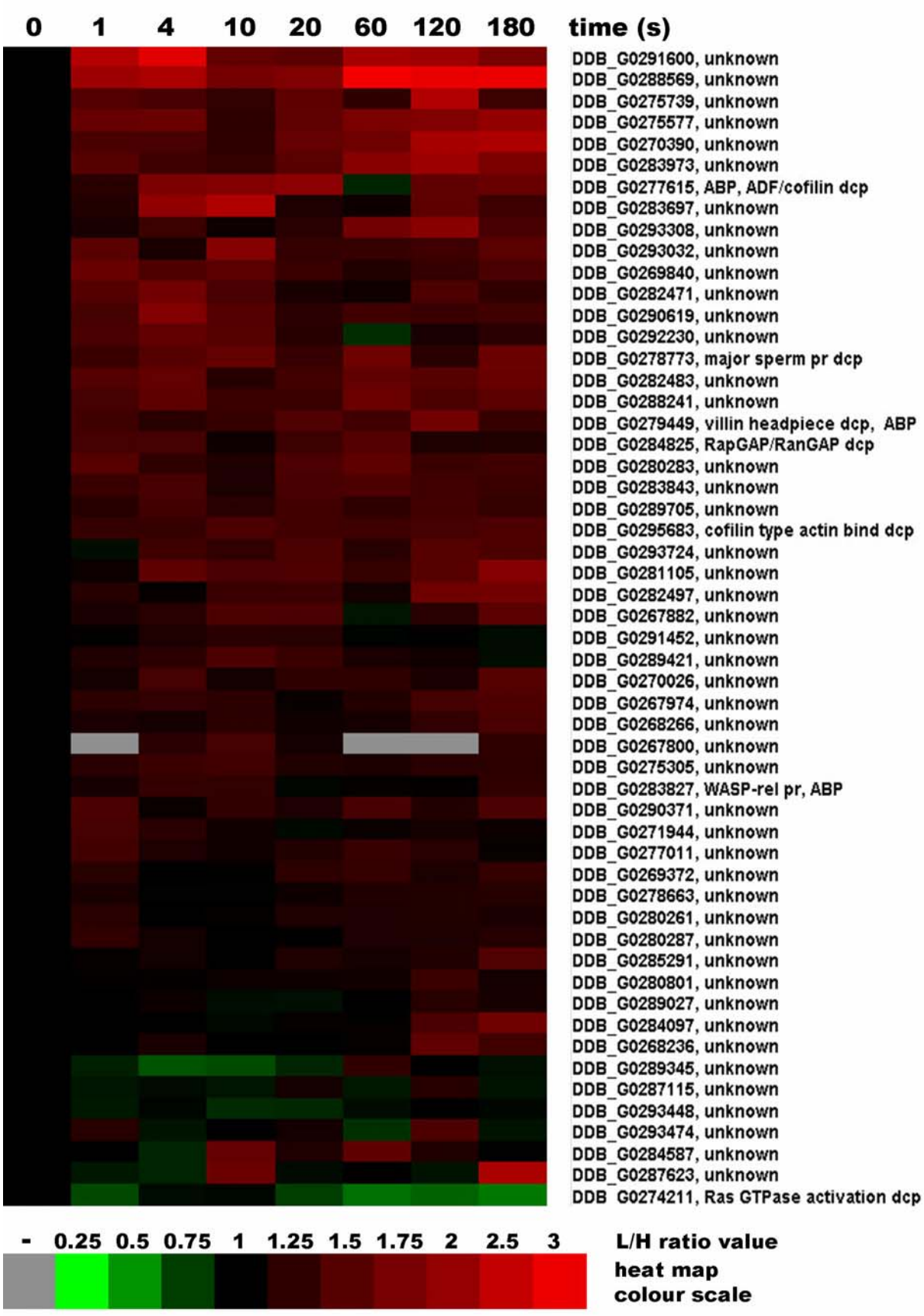


**Figure 3.13.** Proteins of unknown function selected for tagging with GFP and in vivo imaging. Combined results from two standard SILAC experiments are presented. Proteins were chosen based solely on their dynamics pattern.

To minimise the probability of GFP probe interfering with proteins' function and localisation, each of the selected proteins was tagged with GFP on both C-terminus and N-terminus separately. All of those GFP-tagged proteins were coexpressed with RFP-lifeact F-actin probe to analyse their colocalisation with actin structures and correlation with timing of actin response.

In order to generate those constructs we have adapted a comprehensive system of extrachromosomal expression vectors for *Dictyostelium discoideum* developed by Douwe Veltman *et al.* in the van Haastert Lab, University of Groningen [232]. Two vectors containing G418 selection cassette, pDM317 with N-terminal GFP tag and pDM323 with C-terminal GFP tag, were modified to fit the particular needs of design for this study. Multiple Cloning Site (MCS) on those vectors was modified by adding AgeI restriction site between the two existing sites for BglII and SpeI. At the same time the 4 amino acids linker fragment between the insert and the C-terminal GFP tag on the pDM323 was extended to 8 amino acids. These modifications were made by inserting short fragments of dsDNA with cohesive ends compatible with BglII and SpeI restriction sites, which were generated by aligning two oligos mixed in equimolar ratios.

After these steps both vectors were further modified by inserting expression cassette containing RFP-lifeact F-actin probe construct into the NgoMIV restriction site. This insertion of a second expression cassette into the plasmids is a part of the whole vector system design, allowing coexpression of two tagged proteins from a single plasmid, which ensures that both of them are expressed on similar levels for colocalisation analysis [232]. The final modified vector based on the pDM323 was called pDG600 and the vector based on the pDM317 was called pDG700 (Fig. 3.14.).

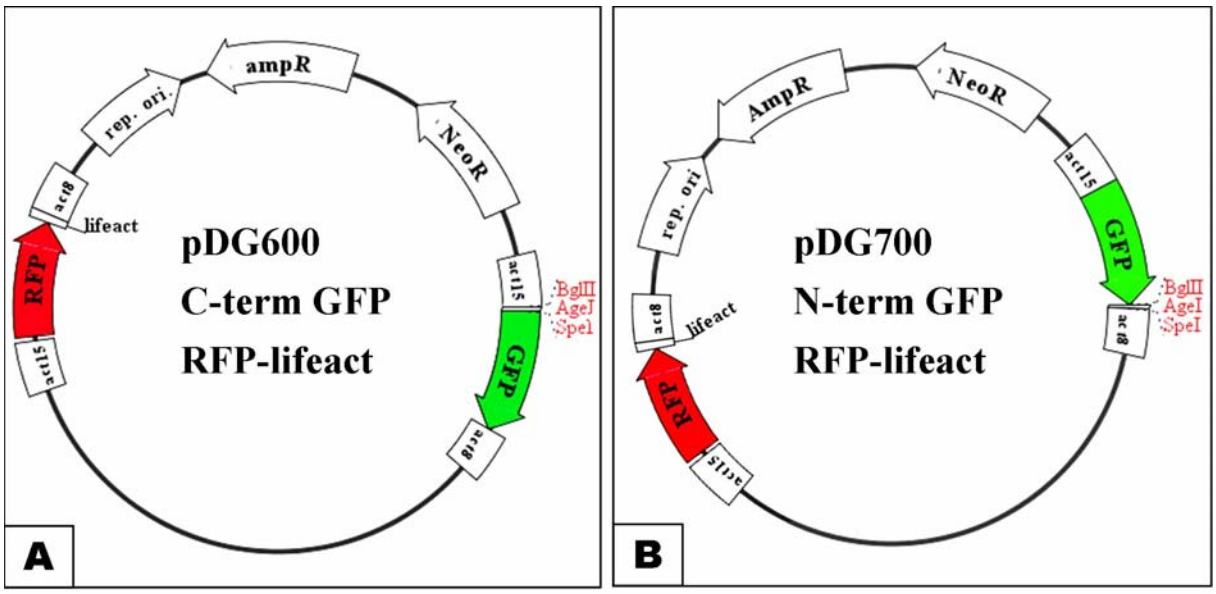


**Figure 3.14.** Extrachromosomal expression vectors for GFP tagging and coexpression with RFP-lifeact probe for filamentous actin. Both GFP and RFP-lifeact expression cassettes contain act15 promoter and act8 terminator. **A)** pDG600 vector with C-terminal GFP tag. **B)** pDG700 with N-terminal GFP tag.

The final cloning efficiency was about 90%. From the initial 120 selected genes 109 were successfully cloned, out of which 103 were cloned into both vectors and 6 genes were present only on one of the two plasmids. The total number of 218 constructs was generated and transfected into *Dictyostelium* cells, which were used for confocal and TIRF microscopy analysis.

# 4. *In vivo* microscopy analysis of the cytoskeletal dynamics

All the GFP-tagged proteins were first visualised using confocal microscopy with both GFP and RFP fluorescence captured at one frame per second. Cells were stimulated with cAMP during each imaging session and the actin polymerisation response was used as a time reference for GFP-tagged protein translocation.

Proteins which showed strong colocalisation with the cortical actin structures were further analysed in greater detail with Total Internal Reflection Fluorescence Microscopy (TIRFM). In this type of fluorescence microscopy only a very thin layer of the cell cortex is illuminated just up to about 200 nm above the cover slip. This technique of cell imaging provides very high spatial resolution, allowing visualisation of individual actin filaments with no background fluorescence from the rest of the cell.

Imaging sessions from both confocal and TIRF microscopy were saved in a movie format and are available in the Supplementary Materials.

# 4.1. General localisation groups

## 4.1.1. Strong cortical proteins

The most important and interesting type of cellular localisation of the analysed proteins was a strong cortical localisation. Proteins in this localisation group were also the ones that showed the strongest translocation from the cytosol to the cortex upon cAMP stimulation. This group of proteins contained many of the known ABPs and regulatory factors selected for cloning (Fig. 4.1.). There were also 6 uncharacterised proteins showing strong cortical localisation, out of which 3 had identified actin binding domain. Most of the proteins in this group had comparatively big changes in the SILAC experiments, usually following actin type of dynamics.

Proteins showing such a strong colocalisation with cortical actin are candidates for playing major roles in regulation and organisation of the actin cytoskeleton. Many of the cytoskeletal positive controls, such as coronins, AbpA, B and C, and myosin II fall into this group. There are 7 GEFs and 3 GAPs, as well as few other regulatory factors like PakB and PikF, exhibiting strong cortical localisation. All the unknown proteins belonging to this group represent a positive identification of novel cytoskeleton associated factors, which is a major outcome of the project.

## Strong cortical proteins

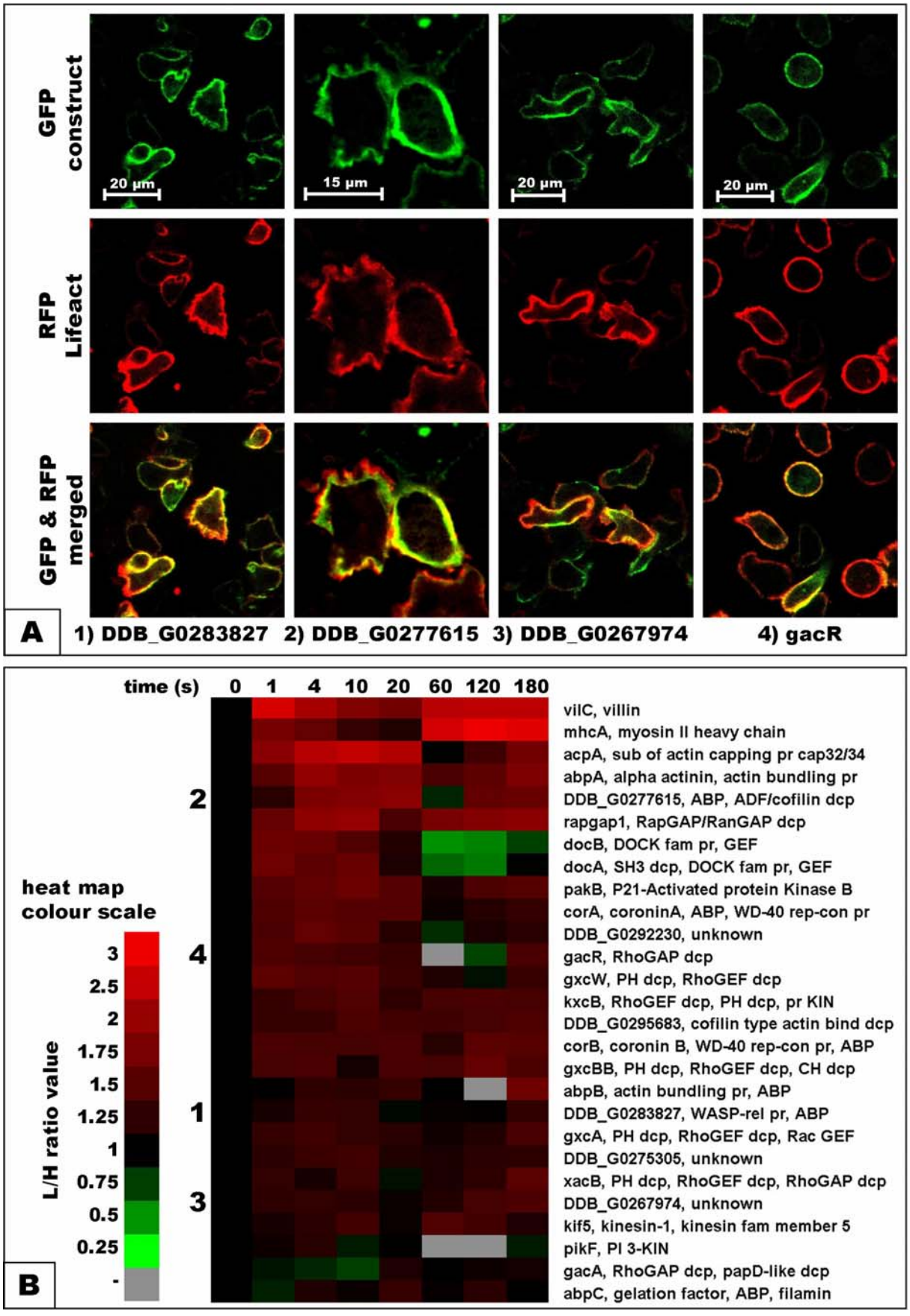


**Figure 4.1.** Proteins exhibiting strong cortical localisation. **A)** Confocal images of four examples of proteins from this group. Images are taken at the peak of the first phase of the actin polymerisation response. **B)** All of the cloned proteins showing this type of localisation. Examples shown in A. are indicated in the heat-map by numbers on the left side. **See also: Supplementary Materials \ Movies \ Strong cortical proteins.**

## 4.1.2. Weak cortical proteins

Another important group of cloned proteins are the ones that show weak cortical localisation. These proteins show some colocalisation with cortical actin but are also found at high levels in the cytosol, even at the peak of their translocation to the cortex (Fig. 4.2.). Only proteins with stronger cortical than cytosolic signal are considered to be part of this group. Different weak cortical proteins show various ratios of cortical to cytosolic signal and therefore this group is composed of proteins showing different levels of cortical localisation. Many of the proteins showing this type of localisation are known actin binding factors. For some of them, such as talin TalA or formin ForH, it is easy to recognise their cortical translocation upon stimulation with cAMP. Some proteins however, like all of the cloned GTPases, show only very slight enrichment in the cortex or in cell protrusions, compared to the signals from the cytosol making it more difficult to detect their weak cortical localisation.

There are a few possible explanations for their weak translocation to the cortex. Their affinity to actin filaments might be lower than that of strong cortical proteins, leading to lower ratio of cortical to cytosolic signal. It might also be caused by the limited availability of specific binding sites recognised by those proteins, which get easily saturated by the overexpressed GFP-tagged proteins, leaving big proportion of them to stay in the cytosol. Alternatively it might be related to the specific character of their function and regulation. This is the explanation for very weak cortical localisation of small GTPases, which are translocated to the cortex only at the activated state forming a small fraction of their whole cytosolic pool. In case of those major regulatory factors, it is not the overall protein localisation but rather the localised regulation of these proteins by GEFs and GAPs that determines their function.

The strength of cortical localisation therefore does not necessarily indicate the importance of a protein's function, but it might suggest that within a class of similar proteins, the ones with

strong cortical localisation play a more substantial role than the ones with weak localisation. Based on this assumption we speculate that both GEFs and GAPs from strong cortical proteins group are more likely to be the main regulators of the cytoskeleton, compared to the proteins of the same families showing weak cortical localisation.

Most of the proteins in this group show actin-like dynamics patterns in the SILAC results, with amplitudes similar to and sometimes higher than those of the strong cortical proteins. Roco7 shows weak cortical localisation, but it has very strong enrichment detected with the SILAC experiment reaching 2.6 L/H in the 4 s time point, which is higher than most of the proteins with strong cortical localisation. Also within the group of strong cortical proteins there are several components, such as examples 1 and 2 from Figure 4.1., showing the same level of translocation to the cortex on confocal imaging analysis, but differing significantly with the levels of enrichment in the SILAC results. This illustrates that there is no direct quantitative correlation between the translocation dynamics measured with the proteomic assay and with *in vivo* imaging analysis.

These two approaches detect slightly different aspects of protein dynamics. The SILAC experiment measures differences in the amount of protein that is bound to the cytoskeleton after cAMP stimulation, which might represent different proportion of the soluble fraction that is not detected in this assay. It might also detect changes in the type of interactions, which do not generate protein translocation. For example the cortical fraction of the protein might change interaction partners and binding stability after cAMP stimulation, but it does not have to lead to recruitment of proteins from the cytosol. In this situation the SILAC experiment would detect changes in dynamics which would not be observable with microscopy analysis. Indeed there are few proteins showing similar differences between the two assays, which will be described in detail in the following chapter.

## Weak cortical proteins

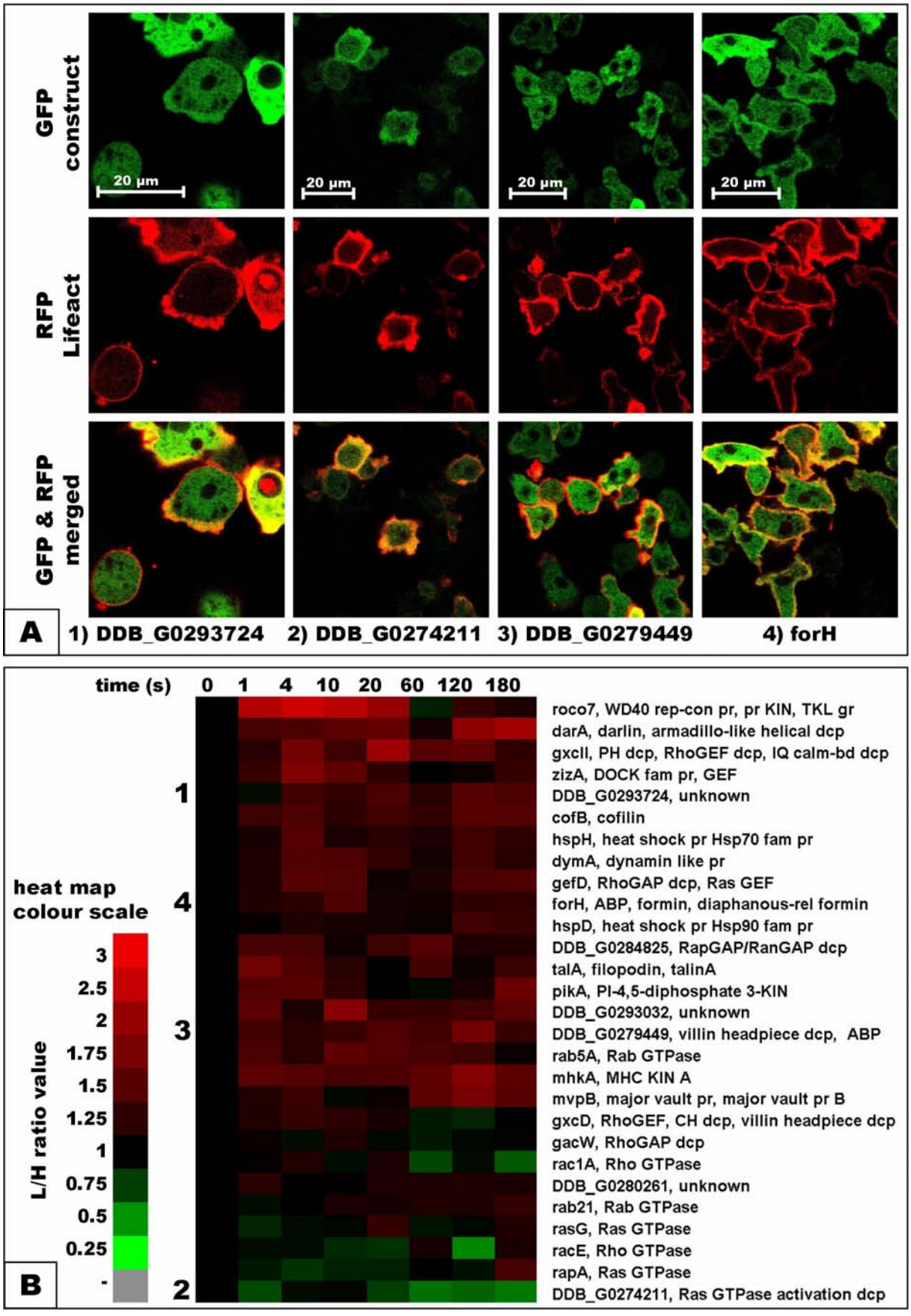


**Figure 4.2.** Proteins exhibiting weak cortical localisation. **A)** Confocal images of four examples of proteins from this group. Images are taken at the peak of the first phase of the actin polymerisation response. **B)** All of the cloned proteins showing this type of localisation. Examples shown in A. are indicated in the heat-map by numbers on the left side. **See also: Supplementary Materials \ Movies \ Strong cortical proteins.**

The cellular imaging on the other hand, can detect proteins present in both cortical and cytosolic fractions and it measures translocation between those two compartments. This translocation has to be mediated by some interactions, but they are not necessarily identical with changes in binding to the cytoskeleton detected by the SILAC experiments. In some cases the cytosolic fraction contains the majority of protein present in the cell, making it difficult to analyse the dynamics of translocation to the cortex.

The fact that the SILAC experiments are performed on the wild type strain while the cells used for imaging are overexpressing the proteins of interest is also likely to generate some differences between the outcome of those two analysis methods.

It is important to state here, that the levels of cytosolic background exhibited by different proteins are gradual and the separation of those proteins into strong and weak cortical groups is arbitrary. Indeed all of the proteins from both groups showed some level of cytosolic localisation in unstimulated cells, which was then depleted to various extents after cAMP stimulation. There were few factors taken into account for dividing proteins into strong and weak cortical localisation groups. The first and most important factor was the level of cytosolic signal depletion coupled with the increase of cortical signal during the first phase of actin polymerisation. The other factors were the width of cortical band and colocalisation with actin structures. Narrow bands of cortical signal, which showed high contrast to the cytosolic fluorescence and colocalised closely with actin structures were considered as characteristic to strong cortical group. Proteins showing broad and somewhat diffused bands of cortical signal, which showed only partial overlapping with cortical actin cytoskeleton, were classified as members of the weak cortical proteins group.

Both of those groups together contain most of the known cytoskeletal proteins which were selected for cloning. All of the known actin binding proteins as well as the cytoskeletal regulatory factors fall into one of those localisation classes.

In general terms, all the proteins showing cortical localisation and any level of translocation to the cortex upon cAMP stimulation, provide a positive validation of proteomic results from the SILAC experiments.

All of the unknown proteins, which were shown to localise to the cell cortex and respond to cAMP stimulation are validated novel cytoskeletal components identified in this study. These proteins need to be further investigated in order to determine their role in the regulation of cytoskeleton functions. Some of them exhibit very strong translocation to the cortex and other interesting characteristics. Most of these newly identified cytoskeletal proteins, together with several known structural and regulatory factors will be described in greater detail in the following chapter.

### 4.1.3. Microtubular proteins

Three of the unknown proteins were showing a localisation suggesting that they colocalise with microtubules (Fig. 4.3). Microtubular cytoskeleton is not in the main focus of this study; nevertheless it is interesting to see few novel microtubular proteins identified with this assay. Microtubules are known to interact with the cell cortex in a dynein/dynactin dependent fashion [234, 235]. It has been reported that microtubules play an important role in force generation at the cortex and that microtubular plus-ends connections at the cortex are essential for nucleus transport within the cell [236, 237]. A *Dictyostelium* ortholog of human protein LIS1, involved in those interactions was found and reported to mediate cross-talk between microtubules and cortical cytoskeleton [238]. Nevertheless the exact contribution of microtubules to the regulation of acto-myosin cortical cytoskeleton and cell movement in general, is not fully understood.

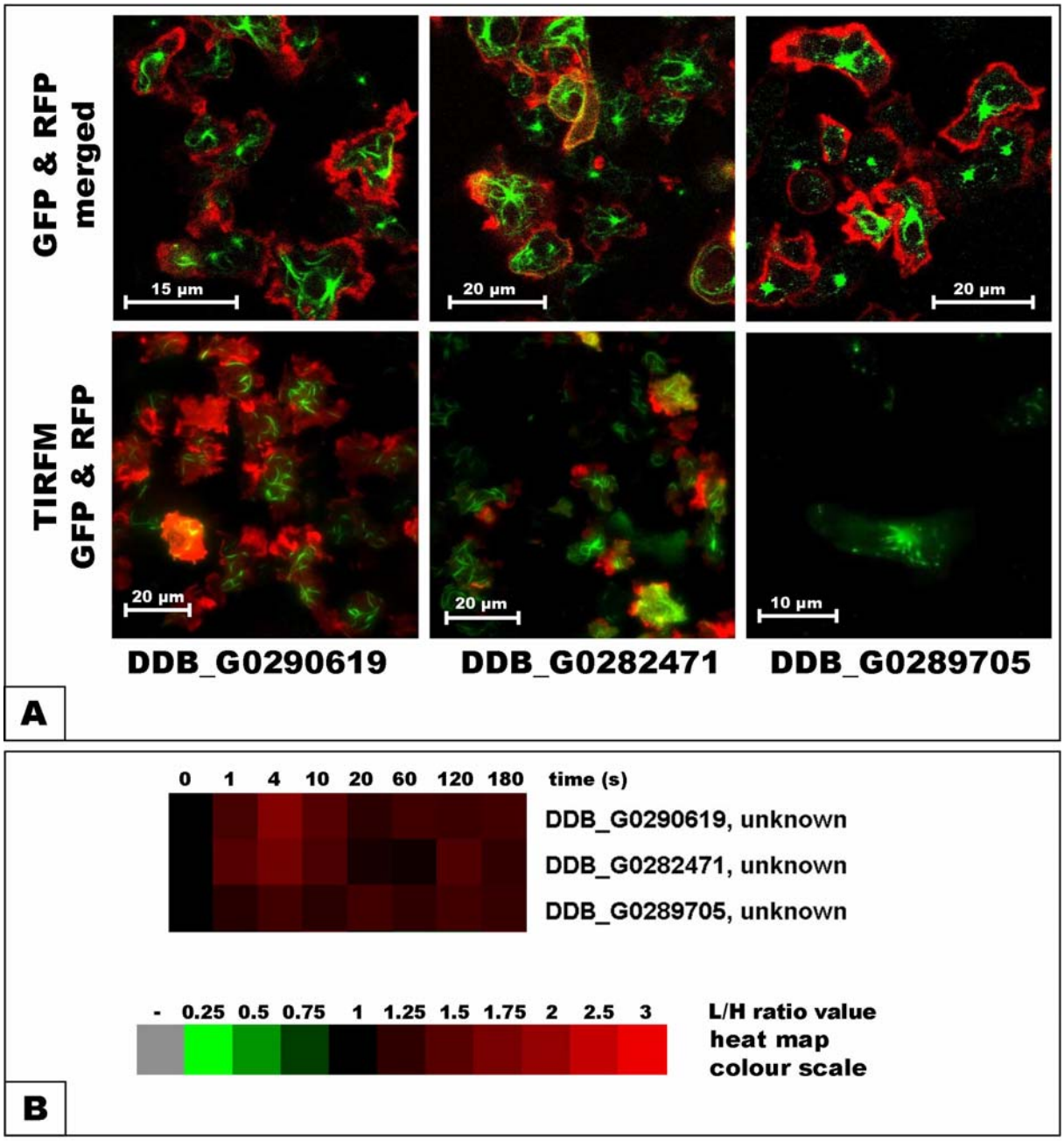


**Figure 4.3.** Proteins exhibiting microtubular localisation. **A)** Confocal (top) and TIRFM (bottom) images of proteins from this group. **B)** SILAC results for all the proteins shown in A with this type of localisation. **See also: Supplementary Materials \ Movies \ Microtubular proteins.**

Two of the newly identified microtubules associated proteins (DDB_G0290619 and DDB_G0282471) were localised along their whole length and were easily observed with TIRFM, indicating that microtubules are present in the outer cortical region of the cell. The third protein classified as microtubular – DDB_G0289705, showed a different type of localisation. On confocal images it is associated with part of the nuclear envelope and

structure of irregular shape in close proximity to the nucleus. This could be either a centrosome with short fragments of microtubules anchored to it, or a part of the Golgi apparatus. Confocal images do not provide enough detail to identify the precise localisation, but the star-like shape of those structures visible in some of the cells suggests that the protein is associated with a microtubule organising centre. Images obtained with TIRFM reveal more details of this structure showing a bundle of short filaments going out of one central point in all directions. They also reveal that some fraction of this protein, visible as single spots on the image shown above, moves along the microtubules. This dynamic character of interaction with microtubules is best noticeable in the movie format. The most likely interpretation of those imaging results is that this protein is dynamically associated with microtubules primarily at their minus-ends where they are anchored to the centrosome, except for the microtubules enfolding the nucleus, on which it localises further along the nuclear envelope.

Localisation of the first two proteins, which are uniformly distributed along the microtubules, does not tell us anything about their potential functions. On the other hand, the localisation observed for the third protein suggests, that it might be involved in anchoring microtubules to the centrosome and linking the whole structure to the nuclear envelope.

Even though both of the uniformly localised microtubular proteins share low actin-like biphasic dynamics in the SILAC experiment, none of the imaging data revealed any translocation or increase in the signal intensity following cAMP stimulation. This suggests that the dynamics observed in proteomic analysis might have been caused by the trapping mechanism described earlier. This would mean that the detected patterns are simply a representation of the variable efficiency, with which microtubular network is trapped in the cortex of intact cells in different time points, which is directly related to the thickness of the cortical actin cytoskeleton. None of those proteins has any identified domains and there are no known orthologs of those molecules in higher organisms. BLAST searches against human database revealed only short regions of medium similarity.

## 4.1.4. Contractile vacuole proteins

Another unexpected but interesting type of cellular localisation discovered among the cloned proteins, is the association with membranes of contractile vacuole system (Fig. 4.4.).

The contractile vacuole (CV) system is an osmoregulatory organelle which consists of tubules and vacuoles. It plays an essential role of maintaining the water balance in free-living cells exposed to hypotonic stress, by accumulating and expelling excess water out of the cell [239]. Membranes of the CV network are populated with vacuolar ATPases (V-ATPases), generating a proton gradient required for transporting other ions into CVs, which drives the inward flux of water [240]. V-ATPases are proton pumps present on many vacuolar and vesicular structures, and they consist of two individual subcomplexes: trans-membrane $V_0$ complex and peripheral catalytic $V_1$ complex, both of which contain several subunits [241]. Two components of the $V_1$ complex, subunits B and C, are known to have high affinity to actin filaments [242, 243]. This interaction between V-ATPases and actin cytoskeleton was found to be essential part of regulating lysosome neutralization and V-ATPase recycling from the lysosomes, driven by WASH (Wasp And Scar Homologue) dependent actin polymerisation [244].

In our results from the SILAC experiments several subunits of V-ATPases were showing strong enrichment in the insoluble fraction, mostly during the second phase of actin polymerisation, reaching L/H amplitudes of about 3. This type of enrichment pattern is very similar to myosin II dynamics and therefore is unlikely to be caused by the described trapping mechanism, which can only mimic the actin profile. The response shown by V-ATPase complex is presumably a result of direct interaction with actin filaments mentioned above. Two of V-ATPase subunits, VatA belonging to $V_1$ subcomplex and VatM which is a part of $V_0$ subcomplex, were tagged with GFP to verify the proteomic analysis.

## Contractile vacuole proteins

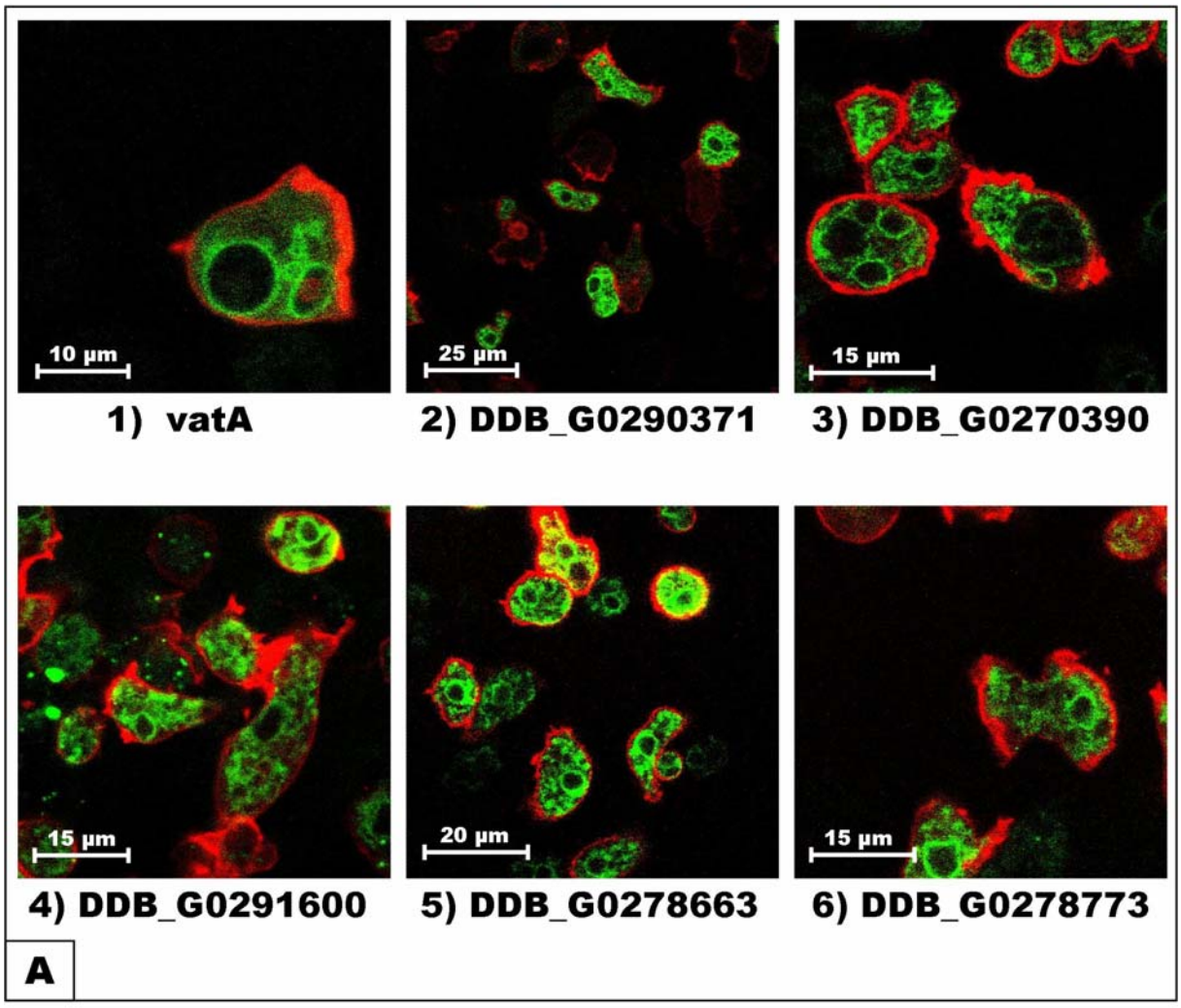


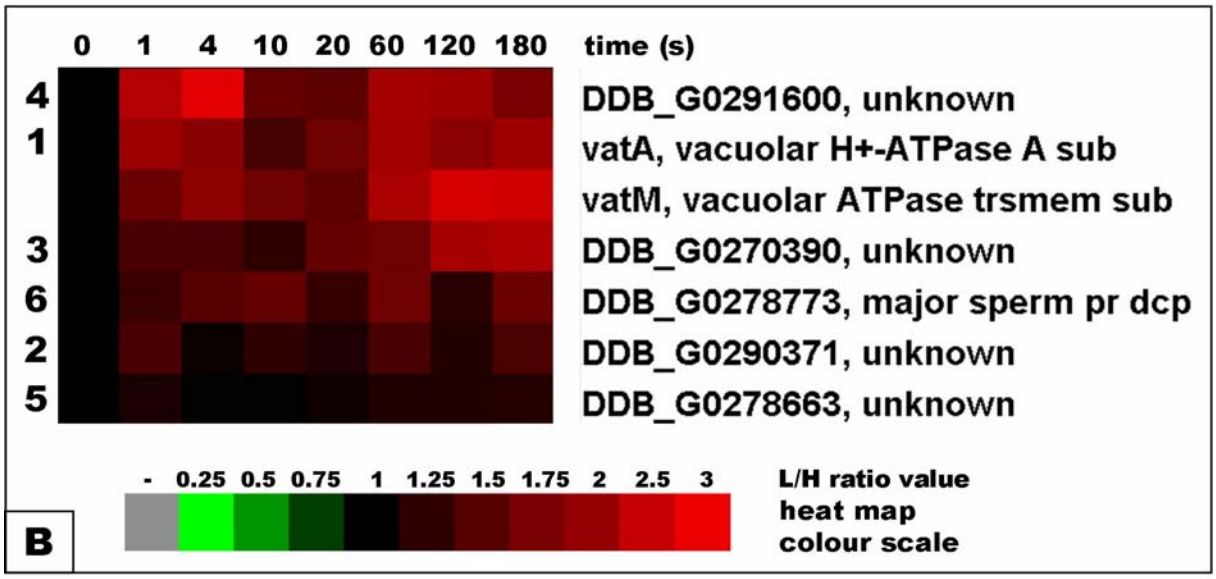


**Figure 4.4.** Proteins exhibiting localisation to contractile vacuole system. **A)** Confocal images of proteins from this group. Images were taken with different magnifications. **B)** SILAC results for all the cloned proteins with this type of localisation. **See also: Supplementary Materials \ Movies \ Contractile vacuole proteins.**

None of those proteins revealed any noticeable translocation or signal intensity changes upon stimulation with cAMP during confocal microscopy imaging (Suplementary Materials \ Movies \ Contractile vacuole proteins). Interestingly 5 of the unknown proteins also showed this type of localisation, and shared similar dynamics patterns to V-ATPase subunits in the SILAC experiment (Fig. 4.4. B).

One of those proteins – DDB_G0278773, has two domains identified as MSP (Major Sperm Protein) and VAP (Vesicle-Associated membrane Protein). This is a conserved protein with orthologs present in many higher organisms including human. Three other proteins: DDB_G0270390, DDB_G0291600 and DDB_G0290371, contain various transmembrane domains, the one in DDB_G0291600 being a multi-pass domain with 3 transmembrane regions. (all the information regarding protein domains and orthologs were obtained from http://dictybase.org/).

## 4.1.5. Vesicular proteins

Another collection of proteins with distinctive localisation, which contained the largest number of unknown proteins selected for cloning, was the vesicular proteins group (Fig. 4.5.). This group is also one of the most variable in appearance from all the types of cellular localisation found in these analyses. This observation is based on different characteristics, such as size, number and behaviour of vesicles labelled with different GFP-tagged proteins. This implies that many of the proteins in this class belong to different types of vesicular components of the cell. They might represent phagosomes, lysosomes at various stages of maturation, exosomes, different endosomes or even components of the Golgi network and possibly other unknown structures. The true identity of those vesicles cannot be determined

based on the confocal images and it will require additional co-staining with different vesicular markers.

There are 16 unknown proteins exhibiting vesicular localisation, most of which are comparatively small molecules, with only two proteins above 70kDa. None of those newly identified vesicular proteins contains any characterised domains and only two have orthologs in higher organisms: DDB_G0277011 and DDB_G0280801.

A couple of known proteins were also classified as vesicular. Prominent among those are clathrin heavy chain ChcA and its adaptor protein Ap2a1-1. A few proteins such as ponticulin related protein PonC3 and cell adhesion molecule CsaA unexpectedly were also found in vesicular structures. Both of these proteins are associated with membranes and those vesicles may be involved their membrane trafficking or recycling. Alternatively this may be an aberrant cellular localisation caused by the interference of the GFP tag.

Most of the vesicular proteins show biphasic dynamics with 10 s time point being the lowest point separating the two phases and the second peak having generally higher amplitudes than the first one. The average enrichment of those proteins was around 1.7 L/H and only two of them exceeded 2 L/H in their peaks. There are few possible explanations for this response shown by vesicular proteins. The trapping mechanism described earlier cannot be excluded, but due to small size and presumably low resistance to Triton X-100 lysis of those vesicles, trapping is not the most likely scenario.

A different approach would suggest that enrichment of those proteins observed in proteomic analysis is a result of their interaction with the components of the cytoskeleton. It is known that many types of vesicles exhibit actin-dependent movement inside the cell and that certain factors present in vesicular membranes, such as the previously described V-ATPase, bind to actin filaments. It is therefore possible that some of these proteins represent novel factors involved in vesicular trafficking in an acto-myosin dependent manner.

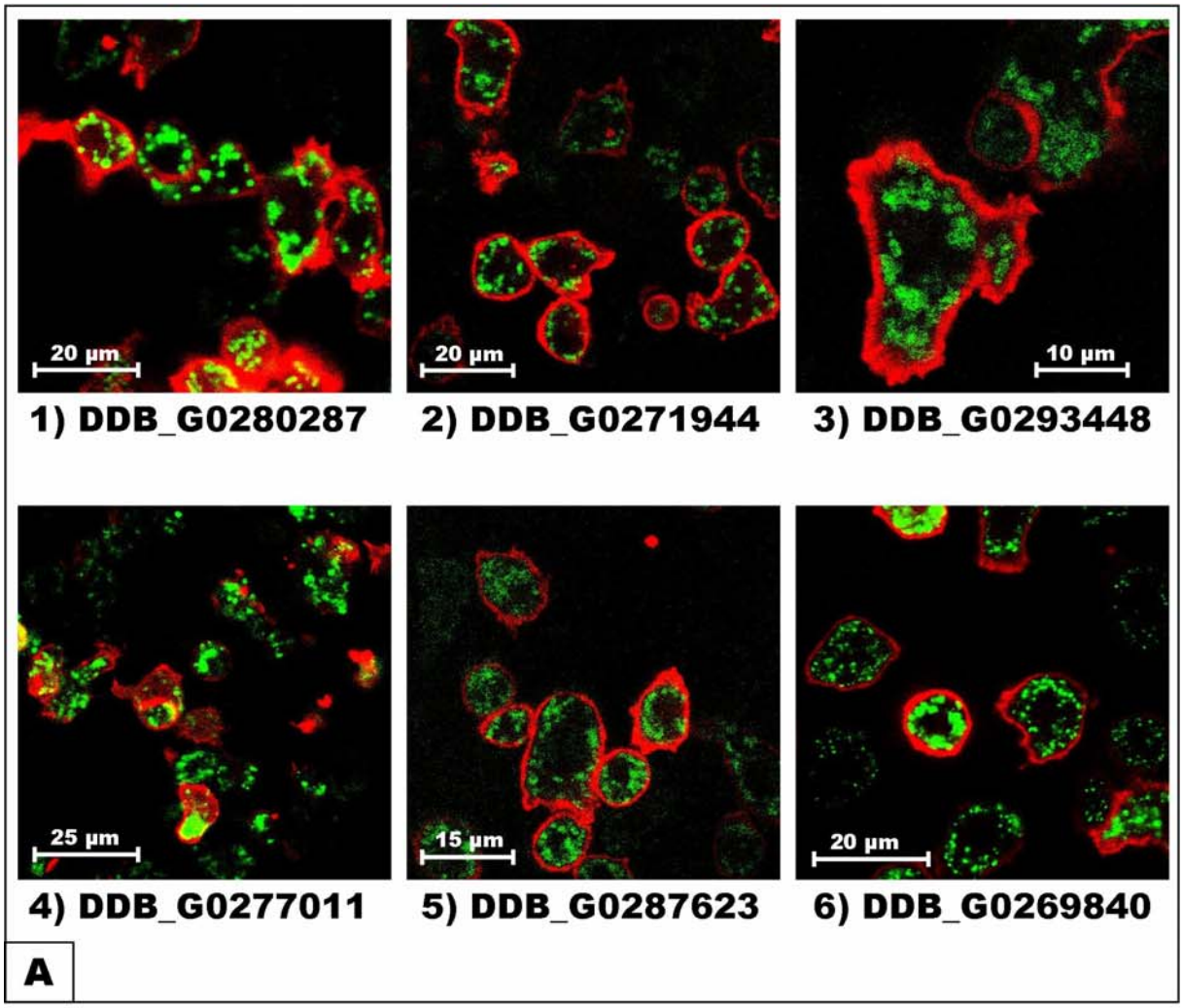


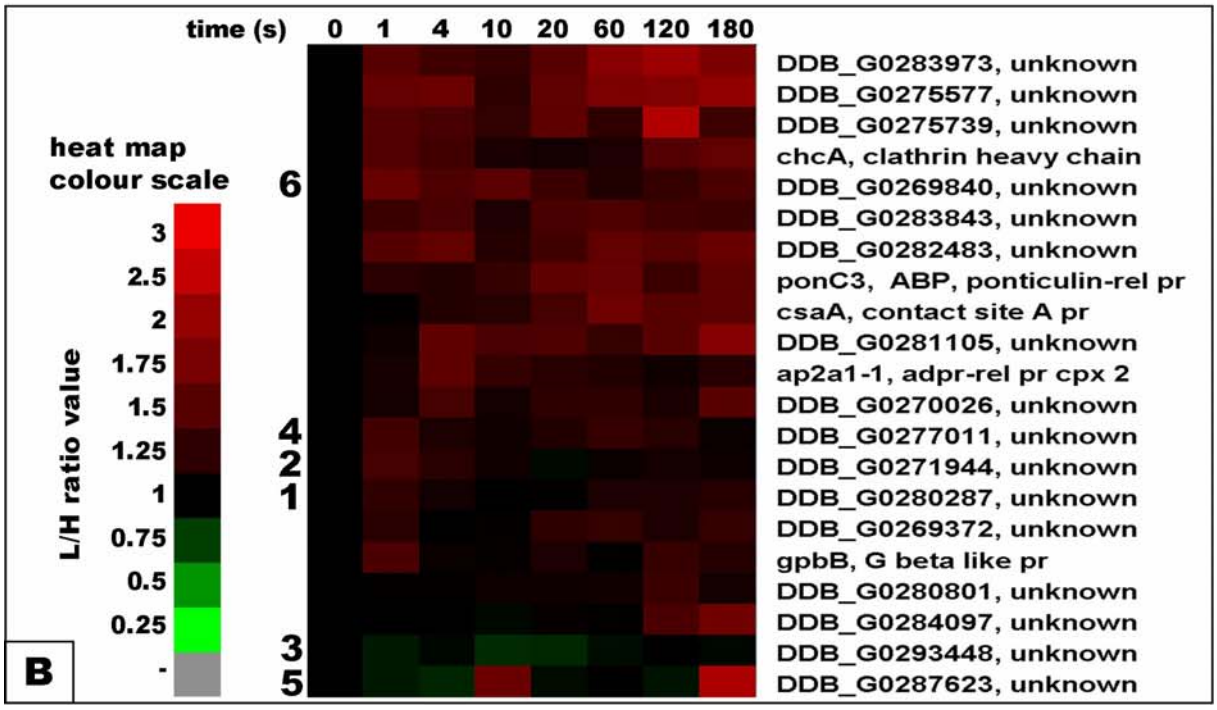


**Figure 4.5.** Proteins exhibiting vesicular localisation. **A)** Confocal images of 6 examples of proteins from this group. Images were taken with different magnifications. **B)** SILAC results for all the cloned proteins with this type of localisation. **See also: Supplementary Materials \ Movies \ Vesicular proteins.**

## 4.1.6. Nuclear proteins

The final group of proteins showing a distinct cellular localisation is formed by nuclear proteins (Fig. 4.6.). This group also contains substantial part of all the unknown proteins analysed. There are 12 uncharacterised proteins that fall into this class, providing a variety of novel nuclear markers. It is interesting to note that most of those proteins are not homogenously spread within the nucleus, but are rather confined to specific structures within the nucleus with variable background levels in the nucleoplasm. Many of those structures resemble nucleoli but some, such as the one revealed by DDB_G0267882 (Fig. 4.6. A3), do not match the typical nucleoli characteristic shown by DDB_G0289345 (Fig. 4.6. A5).

None of the unknown nuclear proteins contains any identified domains. Two proteins, DDB_G0289345 and DDB_G0284587, have orthologs in humans.

There are two previously characterised proteins that showed nuclear localisation. The first one is a heat shock protein HspC, which is a known nuclear factor and was selected for cloning to validate the dynamics measured in the SILAC experiment. The second one is a guanine nucleotide binding protein Gnl3, which is annotated as an intracellular protein (Gene Ontology annotation).

The SILAC results for most of the proteins in this group show only a weak increase in abundance after cAMP stimulation with peaks usually at 10 s and 3 min time points, and some proteins show depletion during the first minute after stimulation. Only one protein – DDB_G0283697, follows closely actin dynamics with the first peak reaching almost 2.5 L/H. None of those dynamics patterns was confirmed by *in vivo* imaging upon cAMP stimulation.

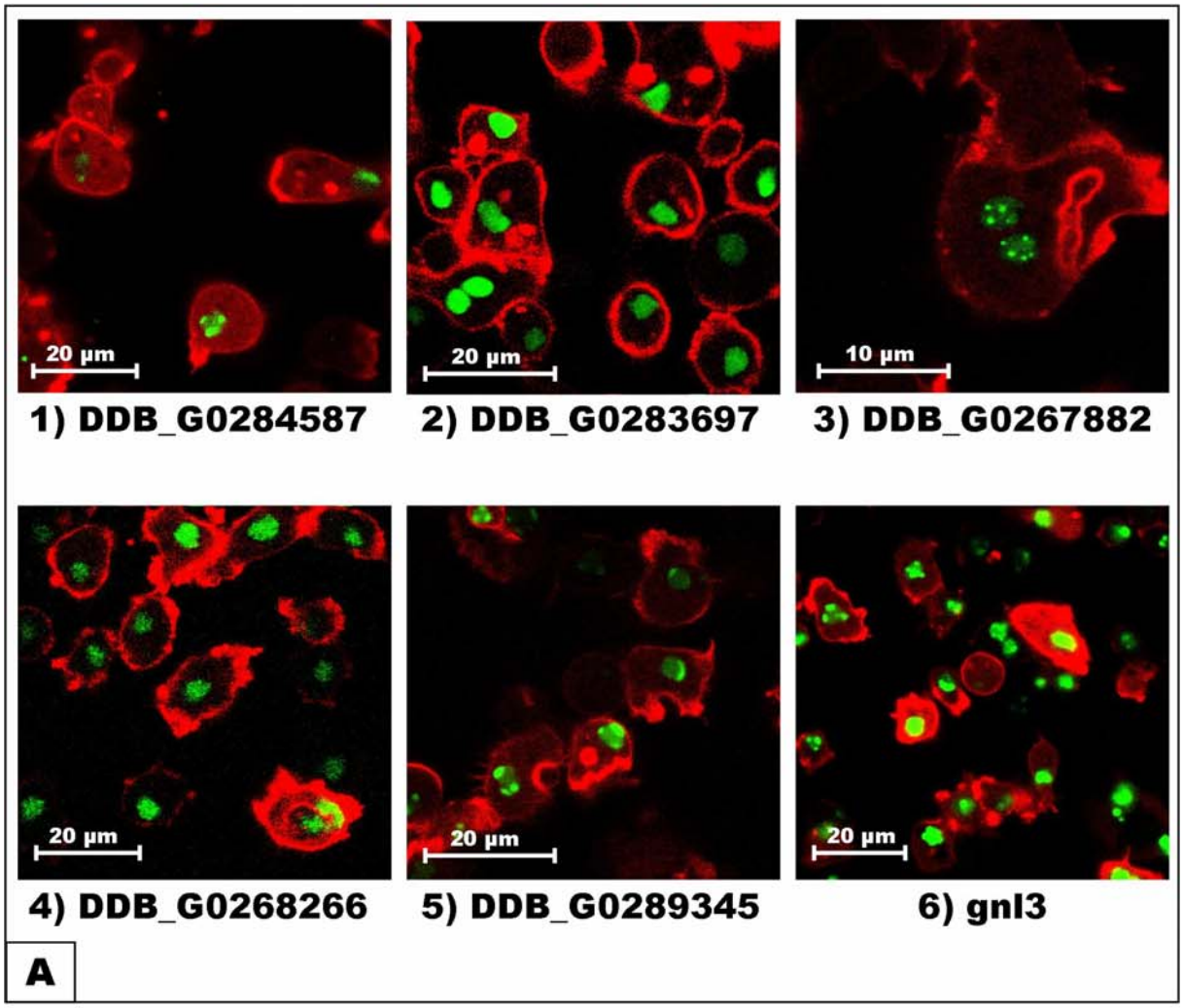


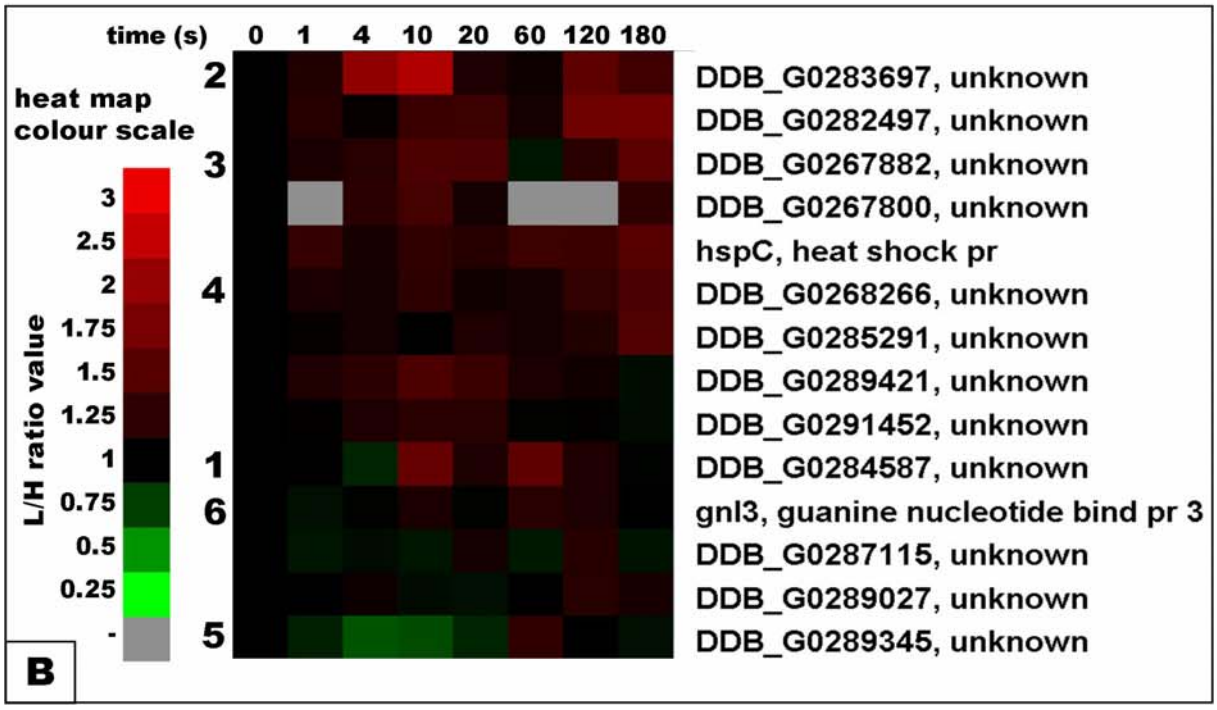


**Figure 4.6.** Proteins exhibiting nuclear localisation. **A)** Confocal images of 6 examples of proteins from this group. Images were taken with different magnifications. **B)** SILAC results for all the cloned proteins with this type of localisation. **See also: Supplementary Materials \ Movies \ Nuclear proteins.**

To summarize this general description of *in vivo* imaging analysis of selected proteins, there were 6 groups of distinct cellular localisation described: strong cortical, weak cortical, microtubular, contractile vacuolar, vesicular and nuclear. Out of 109 proteins successfully tagged with GFP and analysed by fluorescence microscopy, 55 were showing at least partial cortical localisation and were classified into one of the first two groups. Most of those proteins were known or suspected cytoskeletal components and were cloned for validation of the SILAC experiments results and for a further detailed analysis of cortical actin dynamics.

Out of 54 unknown proteins tagged with GFP, 12 showed a clear cortical localisation and translocation triggered by cAMP. 4 proteins contain identifiable actin binding domains, 2 contain a GEF or GAP domain, and 6 are truly novel cytoskeletal factors identified for the first time as associated with the cytoskeleton in this study.

All the other analysed proteins fell into one of the remaining groups. There are 3 novel microtubular proteins identified, 5 novel proteins localising to the contractile vacuole system, 16 novel proteins localising to various types of vesicles and also 12 novel nuclear proteins with various subnuclear localisations. The remaining 6 unknown proteins analysed by fluorescence microscopy were showing very weak signal with homogenous cytosolic localisation, suggesting that their stability and localisation may have been affected by the GFP tag (data not shown).

Even though many of those proteins represent potentially very interesting functions, for the purpose of this project all the proteins showing other than cortical localisation will not be described in any further detail.

# 4.2. Detailed characterisation of selected individual proteins

Selected proteins showing cortical localisation and cAMP dependent translocation are introduced and described in a greater detail. For each protein confocal images of GFP alone and merged GFP and RFP fluorescence are shown from 4 time points corresponding to pre-stimulation phase, peak of the first phase, depolymerisation phase and peak of the second phase of actin response to cAMP stimulation. A quantification of those confocal imaging series is also provided.

Confocal images were quantified as described in Materials and Methods by selecting a region of interest (ROI) covering a fragment of the cell cortex and reslicing the average signal intensity of those ROIs as a function of time. The intensity profile was generated giving a temporal dynamics for both GFP and RFP signals within this fragment of the cortex. This type of local quantification of cortical signals provides a good indication of translocation timing and colocalisation of both proteins but is limited by a great variability of response on such a local level. The actin response to cAMP stimulation is very reproducible at the level of cell populations and even at the level of the whole cell, but less so at the subcellular level.

While the first global phase of actin polymerisation is distinguishable on most of the quantifications, the second localised phase shows great variability in timing and intensity between different cells and parts of the cortex selected for quantification. Different levels of protein expression between the analysed cells also contribute to the big variability in quantifications. This type of analysis is also disturbed by cells moving out of or into the ROI during the course of imaging session. For all these reasons the quantifications were not combined, and instead two separate quantifications are presented for each protein. For proteins showing strong colocalisation with actin structures both GFP and RFP signals will

be following the same temporal dynamics at those quantifications, while proteins with weaker colocalisation will display greater mismatch between those two signals.

TIRFM images are also presented for each analysed protein. These images show much greater detail of the cortex than confocal microscopy and many proteins reveal a clear filamentous structure of the actin cortical meshwork. Sequences captured only for GFP fluorescence with constant rate of 2 fps were also quantified with ROIs selected in the middle of visualised cells. These quantifications were generally found to be much more reproducible and informative than the ones performed on confocal imaging series. Nevertheless there was still significant variability in signal intensities between the cells and in individual character of the late response to cAMP stimulation, therefore three independent measurements are represented in one graph instead of an averaged profile.

Quantification graphs for both confocal and TIRFM sequences show time plots of fluorescence signal intensity, which in confocal 8-bit images has a maximum value of 255 and in TIRFM 16-bit images has a maximum value of 65,025 and for the purpose of graph spatial organisation it is divided by 1000. In all the graphs the time point of cAMP stimulation, which is around 7-10 s from the beginning of imaging session, is clearly distinguishable by strong shift in signal intensity. Unfortunately the TIRFM sequences captured for both green and red channels simultaneously turned out to be incompatible with fast temporal analysis and these sequences are not quantitatively analysed.

Finally, all the proteins described have their dynamics profiles from the proteomic analysis, represented as a time plots of L/H values from two combined SILAC experiments with standard error bars, and whenever available also separate profile from the results of cross-linked SILAC. All the figures in jpeg format and both confocal and TIRFM imaging sessions in avi movie format for each protein described below are presented on the attached CD : Supplementary Materials \ Movies \ Individual Proteins.

# 4.2.1. Structural components of the cytoskeleton

## 4.2.1.1. Coronin A; CorA

Coronins are a highly conserved family of multifunctional actin binding proteins, which was originally discovered in *Dictyostelium discoideum* and named after its localisation to crown-like protrusions within the cell cortex [18]. It was later identified in all eukaryotes examined, and it is always involved in the cytoskeleton regulation.

Coronins form two distinct subfamilies, short coronins subfamily including CorA and the long subfamily, which is represented in *Dictyostelium* by CorB. All coronins contain a core domain of WD40 repeats, but members of the first subfamily contain only one such domain, while the long coronins contain two [245]. The WD40 domain is a versatile motif acting as a platform for simultaneous protein-protein interactions in a wide range of proteins, including several important cytoskeletal components. Proteins containing WD40 repeats often serve as mediators of interaction between other factors in diverse cellular processes including signal transduction, transcriptional regulation, remodeling of the cytoskeleton and vesicular trafficking [246].

Coronins were characterised as cross-linkers of actin filaments and also as factors binding to Arp2/3 complex in mammalian cells [247] and in yeast [248]. This direct interaction was found to have an inhibitory effect on Arp2/3 driven actin polymerisation, by stabilising this complex in an inactive open conformation [249].

Two coronins found in *Dictyostelium* are involved in processes controlling cytoskeleton function but instead of acting in a redundant fashion, they seem to have antagonistic effects. While CorA is proposed to be involved in actin filament disassembly [250] and act as a

negative regulator of actin polymerisation [251], the reported function of CorB is prevention of actin depolymerisation by stabilising the filaments [252]. *Dictyostelium* cells lacking CorA protein exhibited aberrant cytokinesis and cell morphology and decreased motility rate [253], while CorB knock-outs had aberrations in phagocytosis, increased lateral pseudopod formation and cell-substrate adhesion [252].

Our results confirm cortical localisation of CorA and indicate the strong translocation of this protein to the cortex in both phases of actin polymerisation (Fig. 4.7.). Only small fraction of the signal comes from the cytosol in unstimulated cells and in 5 s time point after stimulation it is almost completely depleted, which coincides with the increase of cortical signal thickness and intensity. Cells overexpressing CorA-GFP constructs seemed to have aberrant morphology on confocal images, compared to more round shaped WT cells, which is also indicated by very rough profiles of cortical signal quantification of those cells (Fig. 4.7. A, B). TIRFM images of those cells also reveal strong translocation of CorA to the cortex upon stimulation. They also indicate that CorA distribution within the cortex is not homogenous but rather concentrated within defined regions (Fig. 4.7. C, D).

Coronin A is one of the most abundant proteins detected in the SILAC experiments and shows more than 4 times higher abundance than CorB. The translocation dynamics measured for this protein is therefore very reliable and reproducible between both standard SILACs and is also well conserved in the cross-linked SILAC experiment. CorA exhibits the general actin-like dynamics with the first peak reaching about 1.6 L/H and the second peak about 1.3 L/H in the standard and 1.6 L/H in the cross-linked SILAC (Fig. 4.7. E). This protein is one of several positive controls, which served to validate the SILAC results with *in vivo* analysis of protein translocation to the cortex.

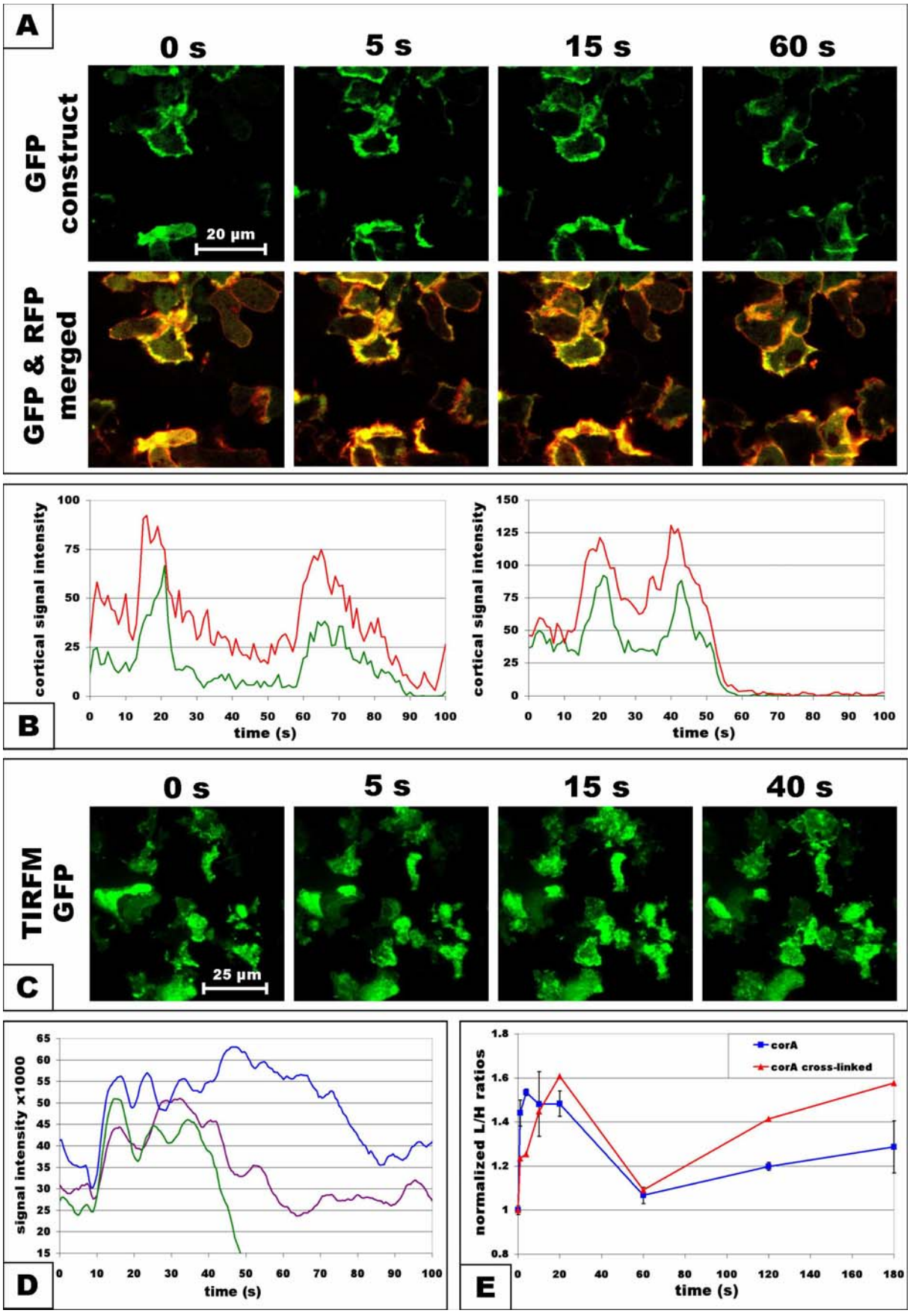


**Figure 4.7.** Results for CorA protein. **A)** Confocal images of 4 stimulation time points with GFP alone (top) and merged GFP and RFP signals (bottom). **B)** Quantifications of both GFP (green) and RFP (red) intensity dynamics from two separate fragments of the cortex in confocal images. **C)** TIRFM images of GFP signal at 4 stimulation time points. **D)** Signal quantification for 3 separate ROIs within cells from TIRFM images. **E)** Translocation dynamics measured in the standard SILAC (blue) and cross-linked SILAC (red) experiments.

## 4.2.1.2. Subunit of actin capping protein Cap32/34; AcpA

Cap32/34 is a heterodimeric actin capping protein composed of two subunits, a 32kDa AcpA and 34kDa AcpB proteins. Cap32/34 binds to fast growing barbed ends of actin filaments only in heterodimeric conformation and in a MgATP dependent manner [62]. This inhibitor of actin polymerisation was previously found to enter the cytoskeleton and follow the biphasic actin dynamics after chemoattractant stimulation [60].

There have been several regulatory interactions with other factors described for this protein. A 70kDa heat shock cognate protein (Hsc70) was copurified with Cap32/34 and found to act as a chaperone stimulating refolding of the denaturated subunits of the capping protein [254, 255]. There is some controversy regarding Hsc70 interaction with the capping activity of the Cap32/34 complex, since one research group described that Hsc70 significantly increased this activity during *in vitro* assays [254], while the other group reported that it had no influence on Cap32/34 dependent inhibition of actin polymerisation [256].

$PI(4,5)P_2$, which is a highly abundant factor on the inner side of the cell membrane, was demonstrated to inhibit Cap32/34 activity and therefore protect the very peripheral actin filaments from being capped [62]. Another important inhibitor of this capping protein is a different actin binding protein – coactosin (CoaA). This protein has no effect on dynamics of actin polymerisation alone, but was found to almost completely counteract the inhibitory effect of Cap32/34 on actin filament elongation [257].

Interestingly, CoaA was detected in our SILAC experiments and showed a strong enrichment above 3 L/H in the earliest 1 s time point. It then decreases to about 1.5 L/H until the second phase, when it rises reaching the same level above 3 L/H at 3 min (Fig. 4.8.). This first short peak was conserved in the cross-linked SILAC with amplitude about 2 L/H, and the second phase also reached similar level at the 3 min time point. This result suggests that CoaA

inhibits Cap32/34 protein in the very beginning of the first phase of actin polymerisation, maintaining undisturbed elongation of all the newly formed filaments, but then rapidly leaves the actin structures allowing Cap32/34 to inhibit the filaments elongation. This result indicates that coactosin plays important role in actin dynamics regulation also during the late response to cAMP stimulation.

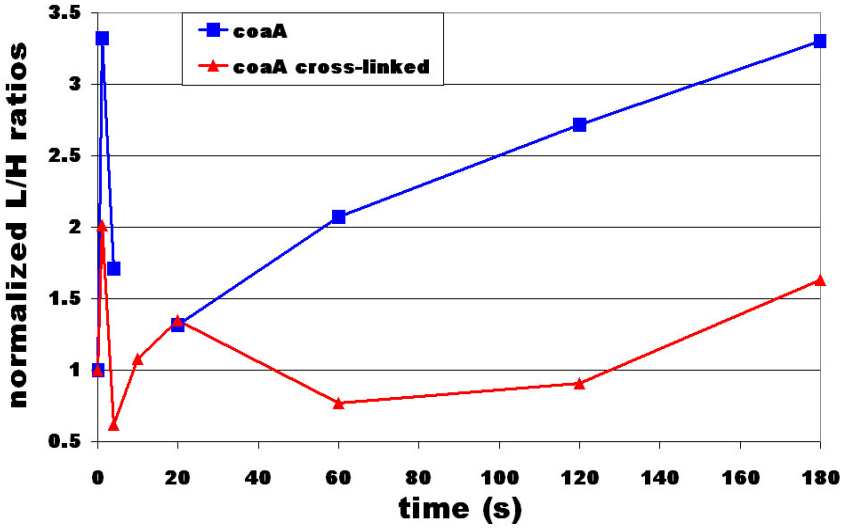


**Figure 4.8.** SILAC results showing translocation dynamics of CoaA protein to the cytoskeleton. Standard SILAC (blue) and cross-linked SILAC (red) experiments show similar patterns with the highest enrichment at 1 s time point. Cross-linked SILAC results have lower amplitudes, which is a very common difference between the two types of SILAC preparations.

Our imaging results of AcpA protein tagged with GFP confirm that Cap32/34 shows strong translocation to the cortex upon cAMP stimulation (Fig. 4.9. A). There is still a substantial level of signal coming from the cytosol even at the peak of translocation, which might come from the excess of AcpA protein generated by overexpression that could not be dimerised with AcpB subunit present at the endogenous levels.

Cap32/34 translocation during the first phase is very transient and virtually the whole cortical signal retreats to the cytosol during depolymerisation phase, and then reappears at the local actin-rich protrusions during the second phase.

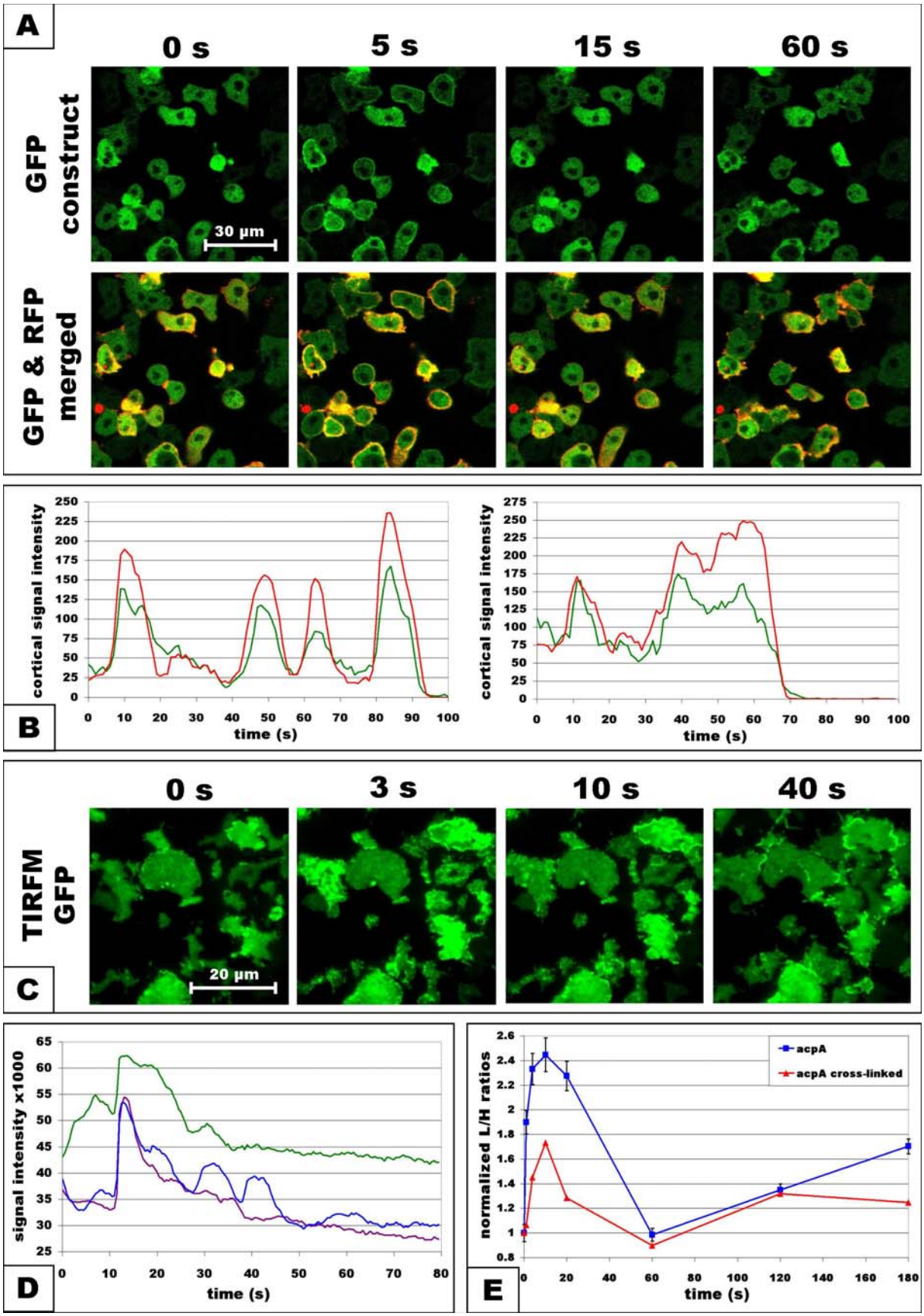


**Figure 4.9.** Results for AcpA protein. **A)** Confocal images of GFP alone (top) and merged GFP and RFP signals (bottom). **B)** Two separate quantifications of confocal GFP (green) and RFP (red) cortical intensity dynamics. **C)** TIRFM images of GFP signal. **D)** TIRFM signal quantification for 3 separate ROIs. **E)** Translocation dynamics measured in the standard SILAC (blue) and cross-linked SILAC (red) experiments.

The SILAC results for both subunits of Cap32/34 were described earlier. Both of those proteins follow closely the profile of actin dynamics in both types of SILAC experiments. TIRFM imaging reveals the same character of strong and rapid translocation in the first phase of response to cAMP stimulation (Fig. 4.9. C, D). The second phase of response is generally not well represented in this type of microscopy. This is most likely caused by the very limited pseudopod formation at sites of contact with the substrate. This means that cells do not extend protrusions in the direction of the cover slip, which makes the second phase hardly detectable by TIRFM imaging.

In order to obtain quantifiable results, these images were taken only for the GFP signal and therefore lack direct reference to the actin dynamics. Actin response was measured separately with TIRFM and quantified (Fig. 4.10.). This measurement of actin dynamics shows few unexpected features, which do not correlate exactly with the results from confocal microscopy and proteomic analysis. The peak of this response is around 10 s after cAMP stimulation, which is about two times slower than the actin response measured with confocal microscopy. The rising slope of this actin dynamics profile shows a distinct breaking point forming a plateau at about one third of the peak's amplitude.

This characteristic is conserved within all the cells quantified in this measurement, but has never been reported or detected in any other assay for actin dynamics. This observation might be related to the fact that the cells, in which the actin dynamics was measured were overexpressing the actin bundling protein alpha actinin, AbpA. This protein present in a great abundance could have affected the polymerisation dynamics in response to cAMP stimulation generating this distinct pattern. Nevertheless, in the absence of any more reproducible actin measurement from TIRFM analysis, this profile of actin dynamics will be used as a reference for other proteins.

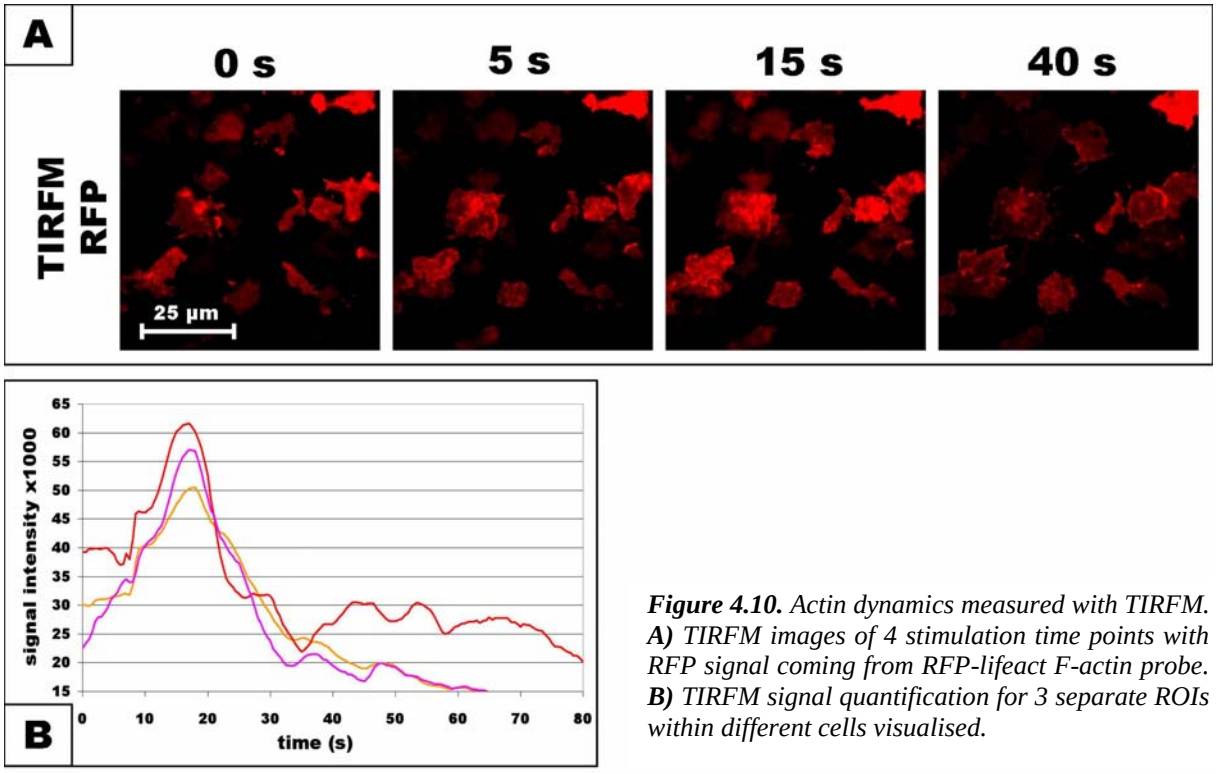


***Figure 4.10.*** *Actin dynamics measured with TIRFM.* ***A)*** *TIRFM images of 4 stimulation time points with RFP signal coming from RFP-lifeact F-actin probe.* ***B)*** *TIRFM signal quantification for 3 separate ROIs within different cells visualised.*

## 4.2.1.3. Myosin II heavy chain; MhcA

Myosin II is a major component of cortical cytoskeleton and it is involved in a variety of cellular processes such as cytokinesis, uropod and pseudopod retraction, cell polarisation and organisation of the actin cytoskeleton. It is an actin-based ATP-dependent motor molecule capable of generating force needed for the mentioned functions. Myosin II is a hexamer consisting of 2 myosin heavy chains (MHC), 2 regulatory light chains (RLC) and 2 essential light chains (ELC). These myosin II complexes spontaneously assemble into bipolar filaments made of 10-20 hexamers, which is the only form in which they can perform their cellular functions (reviewed in [72]).

Myosin II filament assembly is negatively regulated through MHC phosphorylation by MHCKs [73], and induced by dephosphorylation performed by MHC phosphatase PP2A

[74]. Myosin II filaments are assembled in the cytosol and then translocated to the cortex by two separate and independent mechanisms [75]. Myosin II function and motor activity are controlled by cGMP signalling pathway [76, 77] and other factors, such as p-21 activated kinase PakA [78, 79].

Our imaging results for the GFP tagged *Dictyostelium* MHC, MhcA protein, generally confirm the results of proteomic analysis. All the components of myosin II, as described earlier, shared similar biphasic dynamics with the first transient peak at 1 s and the main peak, with 3 L/H values, lasting from 1 min to 3 min time points (Fig. 4.11. E). This result is in agreement with previously published data, which describe the same pattern of translocation dynamics for myosin II in response to cAMP stimulation [258].

Confocal imaging confirms this behaviour, showing that the highest enrichment of MhcA at the cortex, occurs during the late response to cAMP stimulation (Fig. 4.11. A, B). TIRFM imaging provides much greater detail and reproducibility of myosin II dynamics analysis. It also reveals one unexpected characteristic of myosin II dynamics, showing sudden drop in fluorescence intensity directly following cAMP stimulation, which then returns to pre-stimulation levels and follows the canonical pattern of myosin II translocation. Except for this initial drop of signal intensity, the rest of the TIRFM signal time plot resembles closely the results from the SILAC experiments. It shows a small and transient first peak of myosin II translocation followed by the disassembly phase and then gradual constant increase in cortical localisation, forming a strong and long lasting peak in the late response to cAMP stimulation (Fig. 4.11. C, D).

This sudden drop of fluorescence intensity is only observed by TIRFM and, as it will be described later, it is shared by several other proteins analysed. The most likely explanation is that it represents a TIRFM specific phenomenon, related to the very unusual way by which cells are visualised with this method. To understand it, we need to imagine the processes that are happening at the very periphery of the cell cortex.

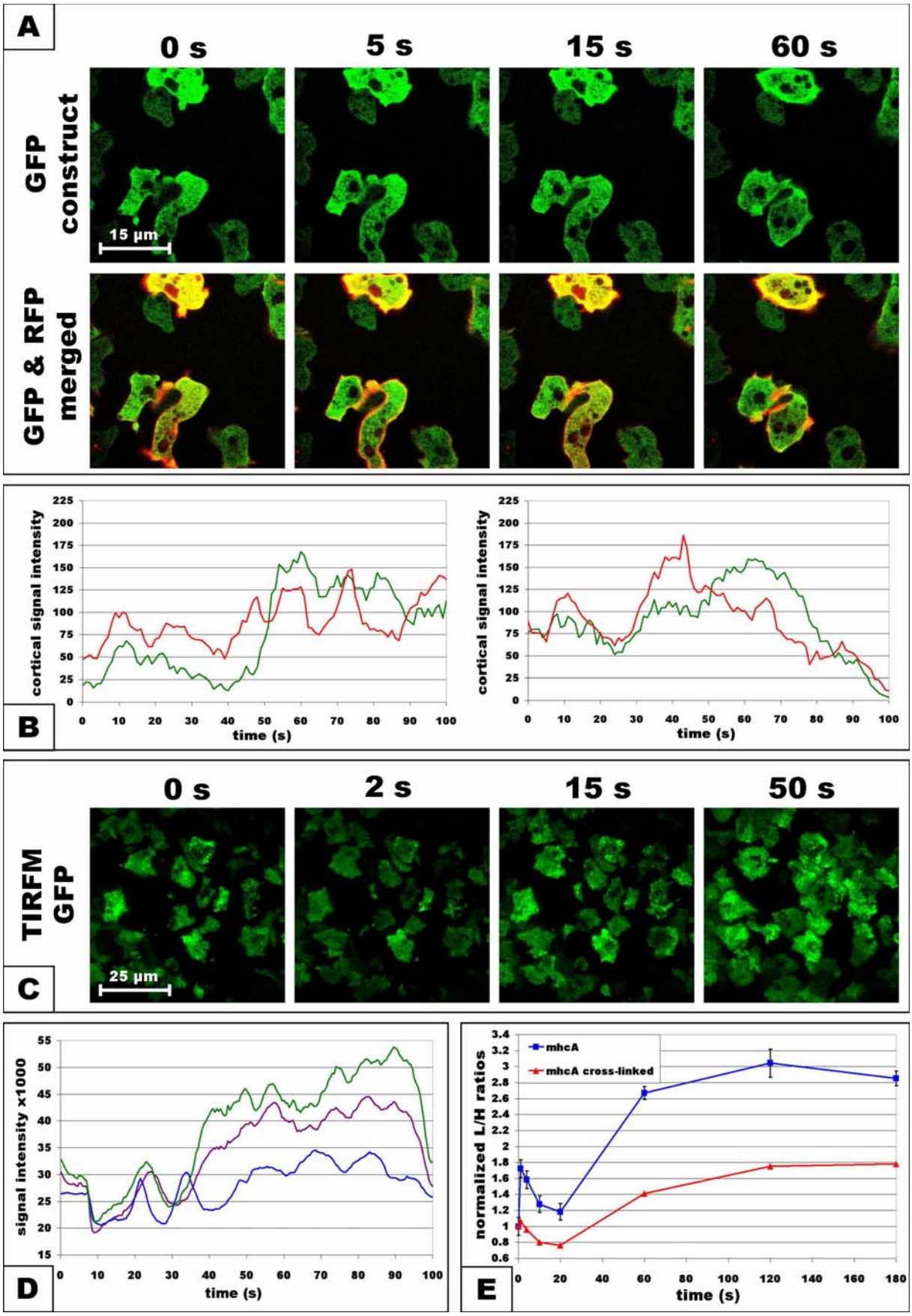


**Figure 4.11.** Results for MhcA protein. **A)** Confocal images of GFP alone (top) and merged GFP and RFP signals (bottom). **B)** Two separate quantifications of confocal GFP (green) and RFP (red) cortical intensity dynamics. **C)** TIRFM images of GFP signal. **D)** TIRFM signal quantification for 3 separate ROIs. **E)** Translocation dynamics measured in the standard SILAC (blue) and cross-linked SILAC (red) experiments.

In unstimulated cells we are observing a relatively stable network of cytoskeletal components existing in a dynamic equilibrium, with constant endogenous fluctuations of different factors. At the point of cAMP stimulation this whole equilibrium collapses and an explosion of actin polymerisation is triggered, generating massive amount of new actin filaments. Those new filaments are generated within the first 3 – 5 s almost exclusively at the outer cortex, and are equivalent of more than all the filamentous actin present in those cells before stimulation. This new F-actin population has to form a thick layer at the outer part of the cortex, pushing the old cortical structure deeper inside the cell.

The average length of actin filaments was previously determined to be constant throughout the whole response to cAMP stimulation and was calculated as about 350 nm ±100 nm [60]. Taking into account that TIRFM is efficiently illuminating a layer of only about 200 nm of the cell cortex, it is easy to understand that proteins which do not associate instantly with freshly formed ATP-rich actin filaments, will be pushed away from the cortex periphery and at the same time from the illumination field of TIRFM. This mechanism could explain the sudden drop of fluorescence intensity, which correlates with the burst of actin polymerisation, and then the following slow recovery of this fluorescence would indicate the gradual loss of this new outer layer of actin filaments during the depolymerisation phase.

The alternative explanation, that proteins exhibiting this type of behaviour are actually depleted from the cortex instantly after the stimulation, is not supported by any other available data.

## 4.2.1.4. Kinesin Family member; Kif5

Kinesins are molecular motors which move along microtubules driven by ATP hydrolysis, in the direction of the plus end, which means that they travel from the centre of the cell to the

cell periphery. These proteins are involved in diverse cellular processes such as vesicles and organelles transport and chromosome segregation. *Dictyostelium* genome encodes 13 members of this superfamily, given the acronym 'kif' followed by a number [259].

Kif5 is a kinesin-1 family protein and it is a very interesting member of this superfamily. It contains a conserved head domain at the N-terminus, central coiled coil region and a C-terminal tail domain. This protein has already been studied by Iwai *et al.* (2004) and found to colocalise with actin at the cortex [260]. The motor domain was shown to have ATP-dependent affinity to microtubules and the C-terminal domain was shown to bind directly and bundle actin filaments [260]. Based on those findings it has been proposed, that Kif5 might function as a cross-linker between actin filaments and microtubules associated with cortical structures.

Our results confirm cortical localisation of this protein and add interesting feature to its characteristic. In our study Kif5 was found to be localised predominantly at the uropod of polarised cells (Fig. 4.12. A). It actually showed only limited colocalisation with cortical actin, which was mainly present at the front of those cells. The reason why this uropod localisation was not reported in the previous study might be due to the fact, that those analysis were performed on vegetative cells by immunofluorescence microscopy, while our data represent *in vivo* imaging of GFP-tagged proteins in developed polarised cells.

Confocal microscopy revealed that this protein was translocated from the cytosol to the cortex after stimulation, but this translocation only slightly increased the initially strong cortical signal. In addition to cortical localisation, Kif5 was also present on short fragments of the microtubules around the centrosomes, which gave a visible signal from the centre of the cells. TIRFM imaging revealed a very homogenous distribution of Kif5-GFP fusion proteins within cortical filamentous structure, which also confirms a specific binding of this protein to actin filaments. These filamentous structures visualised with TIRFM showed very rapid dynamics, but it was difficult to notice any long range movement along microtubules

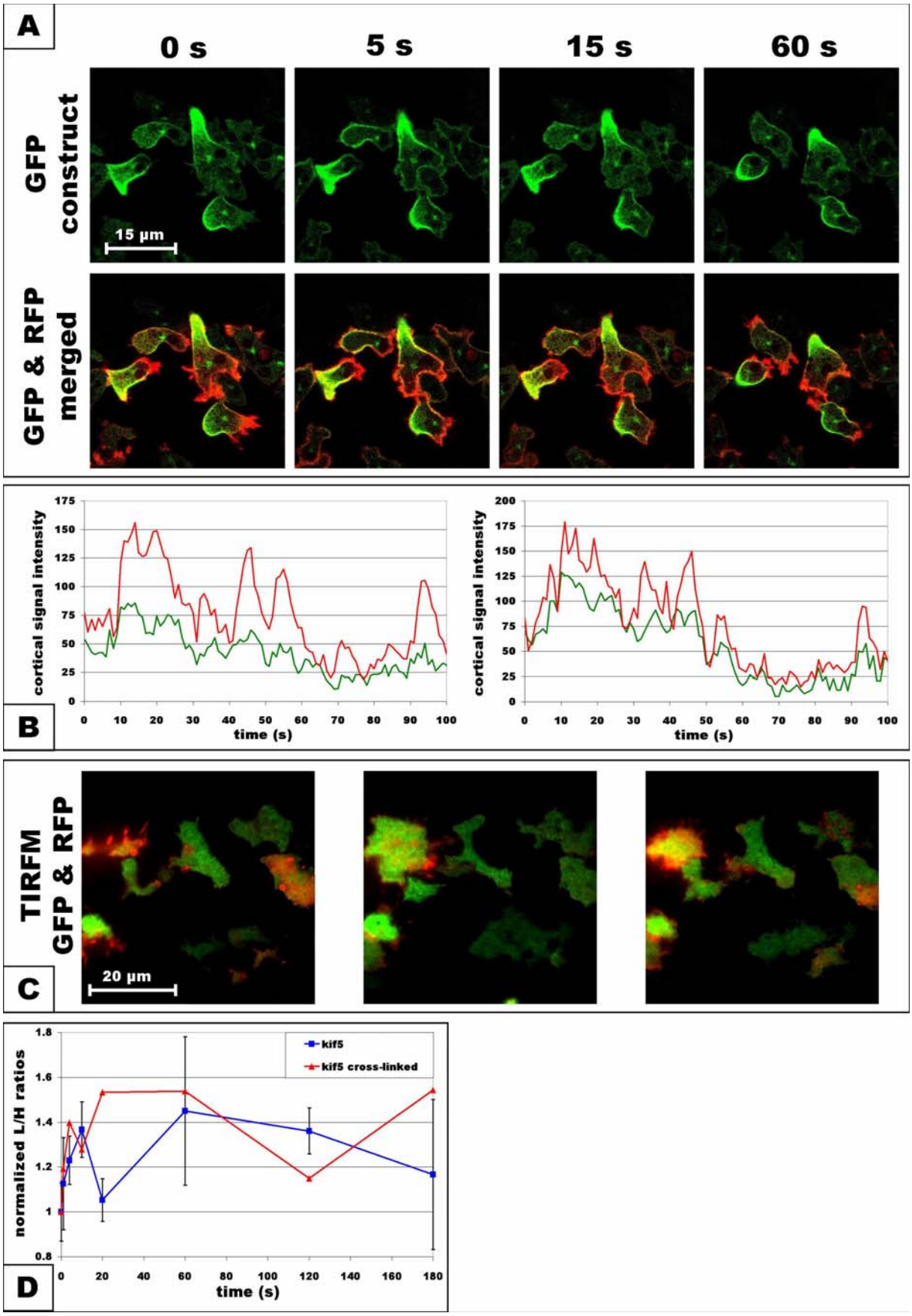


**Figure 4.12.** Results for Kif5 protein. **A)** Confocal images of GFP alone (top) and merged GFP and RFP signals (bottom). **B)** Two separate quantifications of confocal GFP (green) and RFP (red) cortical intensity dynamics. **C)** TIRFM images of merged GFP and RFP signals. **D)** Translocation dynamics measured in standard SILAC (blue) and cross-linked SILAC (red) experiments.

expected for kinesin protein (Supplementary Movies). It is important to indicate that even though both C-terminal and N-terminal GFP fusions were localised to the cortex, the N-terminal construct generated stronger fluorescence, suggesting that it was more stable, and it was the only one to stain microtubules close to the centrosome.

SILAC results for Kif5 show biphasic response with the first peak at 10 s and about 1.4 L/H, the second phase peaking at 60 s shows big variability between two experimental replicas. Results from the cross-linked SILAC are not consistent with the standard experiment.

# 4.2.2. Regulatory components of the cytoskeleton

## 4.2.2.1. Unconventional Rac GEFs; DocA and DocB

Both DocA and DocB are Rac GEFs which activate Rac GTPases by catalysing dissociation of GDP from those proteins, allowing binding of GTP and switching to an active form. Both of those proteins are related to human Dock180 protein and belong to evolutionarily conserved family of unconventional Rho GEFs containing CZH (CDM-zizimin homology) domain [261, 262]. They feature two CZH domains, CZH1 which can bind phospholipids such as $PI(3,4,5)P_3$ [263], and CZH2 which is responsible for activation of GTPases [264]. In addition to those two CZH domains DocA also contains N-terminal SH3 (Src homology 3) domain, which makes it closer homolog to human Dock180, than DocB [138].

There are 4 Dock180-related proteins in *Dictyostelium*. Two of them, which show highest homology to human ortholog, DocA and DocD, were previously investigated and characterised as having redundant functions [138]. Cells lacking either of those proteins were

showing reduced cell motility, which was further impaired in double knock-out. Morover, overexpression of DocD was shown to enhance actin polymerisation leading to increase in membrane protrusions. This protein was also described to translocate to the cortex after cAMP stimulation in a PI3K dependent fashion, which suggests its role in signal transduction from $PI(3,4,5)P_3$ accumulation to activation of the Arp2/3 complex [138].

Standard SILAC experiment detected only DocA and DocB members of Dock180-related proteins, which both shared interesting translocation dynamics and were selected for further investigation. Imaging analysis also revealed very similar characteristic of those two proteins (Fig. 4.13. and 4.14.). Both of them showed very rapid and transient translocation to the cortex in the first phase of response to cAMP stimulation, and then partially colocalised with actin structures during the second phase of response. Both types of SILAC experiments revealed that they have enrichment specific for the first phase of cAMP-induced actin polymerisation (sections E).

Both SILAC and TIRFM analysis reveal very rapid character of DocA and DocB translocation, reaching their peaks around 1 s after stimulation, except for the cross-linked SILAC with the firs peak between 4 – 10 s time points for both proteins. Interestingly, these proteins show relatively uniform localisation within the filamentous cortical structure visualised by TIRFM imaging (sections C; Suplementary Movies). Another important feature detected by imaging analysis, is that cells overexpressing each of those GFP-tagged proteins showed enhanced levels of cortical actin polymerisation leading to increased membrane protrusions and abnormal motion characteristic, which can be described as hectic and over agitated (sections A, B; Suplementary Movies). These observations are in agreement with phenotypes reported for cells overexpressing DocD-GFP fusion protein [138] and indicate their active role in positive regulation of actin polymerisation.

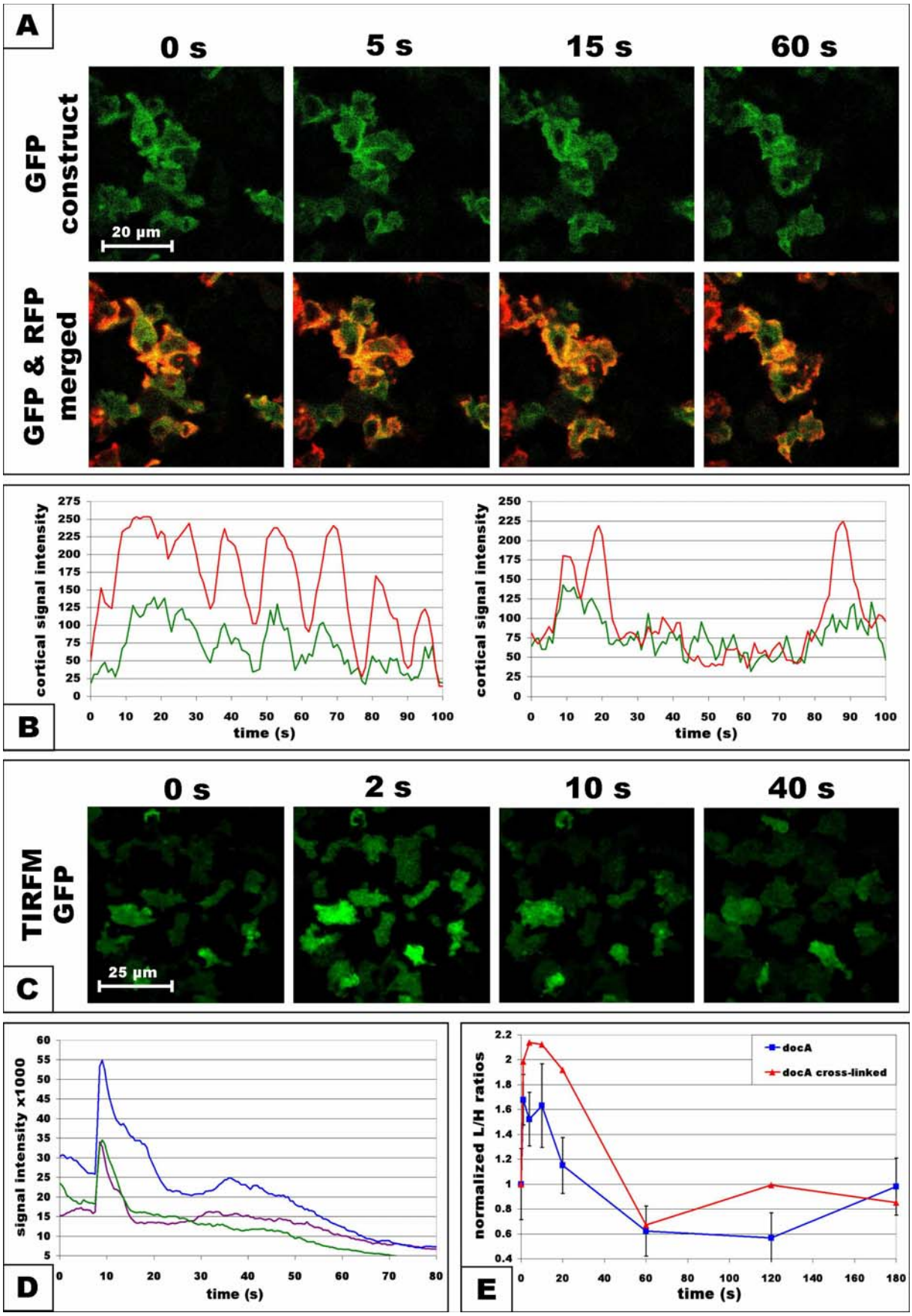


**Figure 4.13.** Results for DocA protein. **A)** Confocal images of GFP alone (top) and merged GFP and RFP signals (bottom). **B)** Two separate quantifications of confocal GFP (green) and RFP (red) cortical intensity dynamics. **C)** TIRFM images of GFP signal. **D)** TIRFM signal quantification for 3 separate ROIs. **E)** Translocation dynamics measured in the standard SILAC (blue) and cross-linked SILAC (red) experiments.

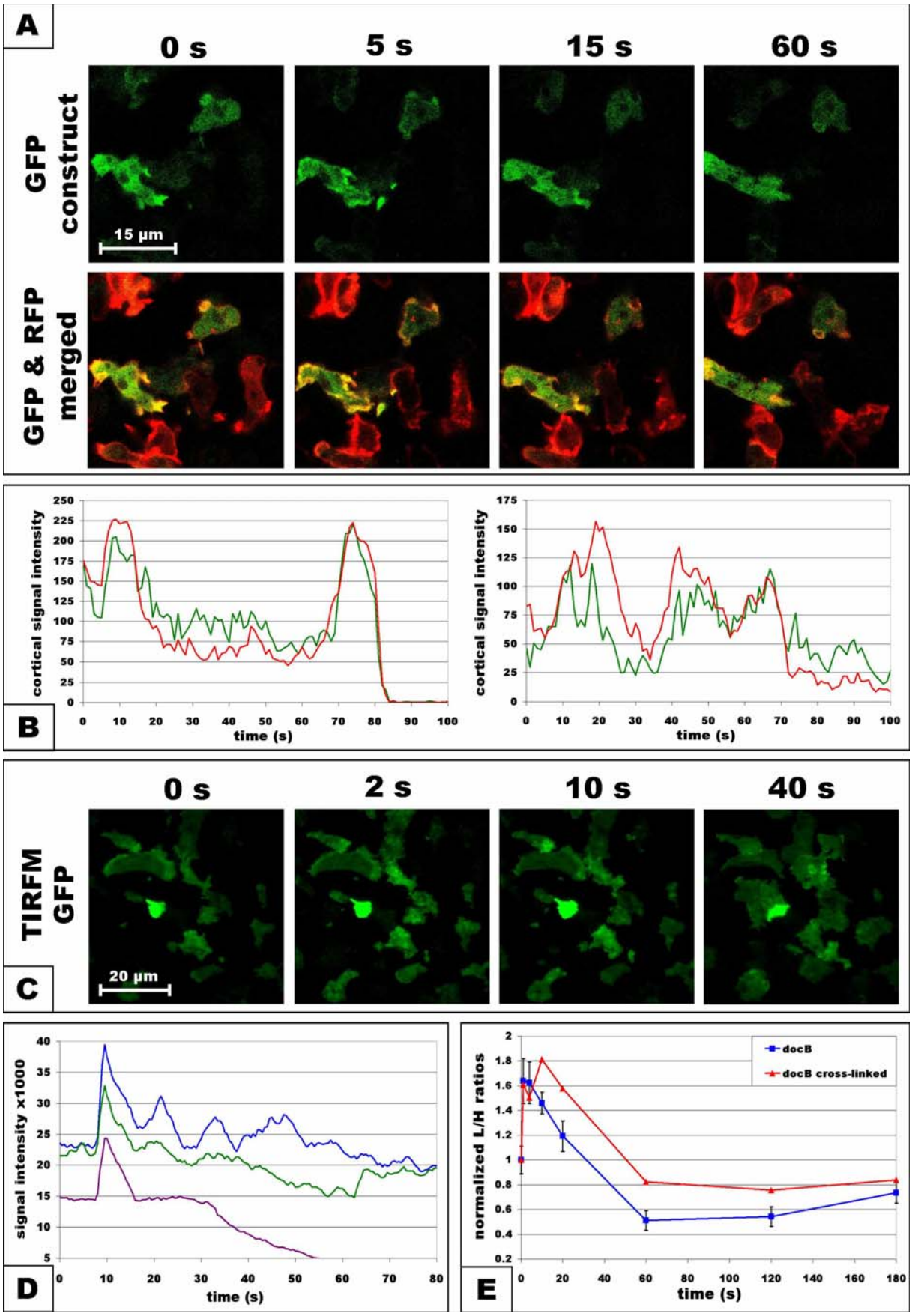


**Figure 4.14.** Results for DocB protein. **A)** Confocal images of GFP alone (top) and merged GFP and RFP signals (bottom). **B)** Two separate quantifications of confocal GFP (green) and RFP (red) cortical intensity dynamics. **C)** TIRFM images of GFP signal. **D)** TIRFM signal quantification for 3 separate ROIs. **E)** Translocation dynamics measured in the standard SILAC (blue) and cross-linked SILAC (red) experiments.

The fact that those two proteins have very high sequence similarity and share virtually the same characteristics in all the types of analyses performed, suggests that they also have redundant functions acting in the same processes.

The very rapid translocation to the cortex and higher enrichment during the first than the second phase of actin polymerisation would make those proteins a strong candidates for specific activators of fast actin response to cAMP stimulation. On the other hand, their translocation to the cortex is likely to be PI3K dependent, based on the previously mentioned study of their close homolog – DocD, which would exclude them from the list of potential factors mediating the PI3K independent response during the first phase.

### 4.2.2.2. Zizimin-related protein; ZizA

ZizA is a Zizimin-related protein which belongs to the same CZH family of unconventional Rho GEFs as Dock180-related proteins and it also contains two characteristic domains: CZH1 and CZH2. The difference between Dock-related and Zizimin-related proteins in humans is that they regulate different subfamilies of Rho GTPases. Dock proteins activate proteins belonging to the Rac subfamily while Zizimins activate the Cdc42 subfamily of the Rho GTPases [261]. Interestingly, *Dictyostelium* has 4 Zizimin-related proteins while there are no members of the Cdc42 family of Rho GTPases found in this organism [101]. Zizimins present in *Dictyostelium* are thought to be involved in development but not in chemotaxis to cAMP [261].

Our results of ZizA analysis give somehow inconsistent picture of this protein's dynamics. On one hand the standard SILAC experiment indicates that ZizA follows the generic actin dynamics with a first peak of 1.8 L/H at the 4 s time point, going down the to pre-stimulation level at 60 s and then increasing again at the second phase to 1.3 L/H (Fig. 4.15. E).

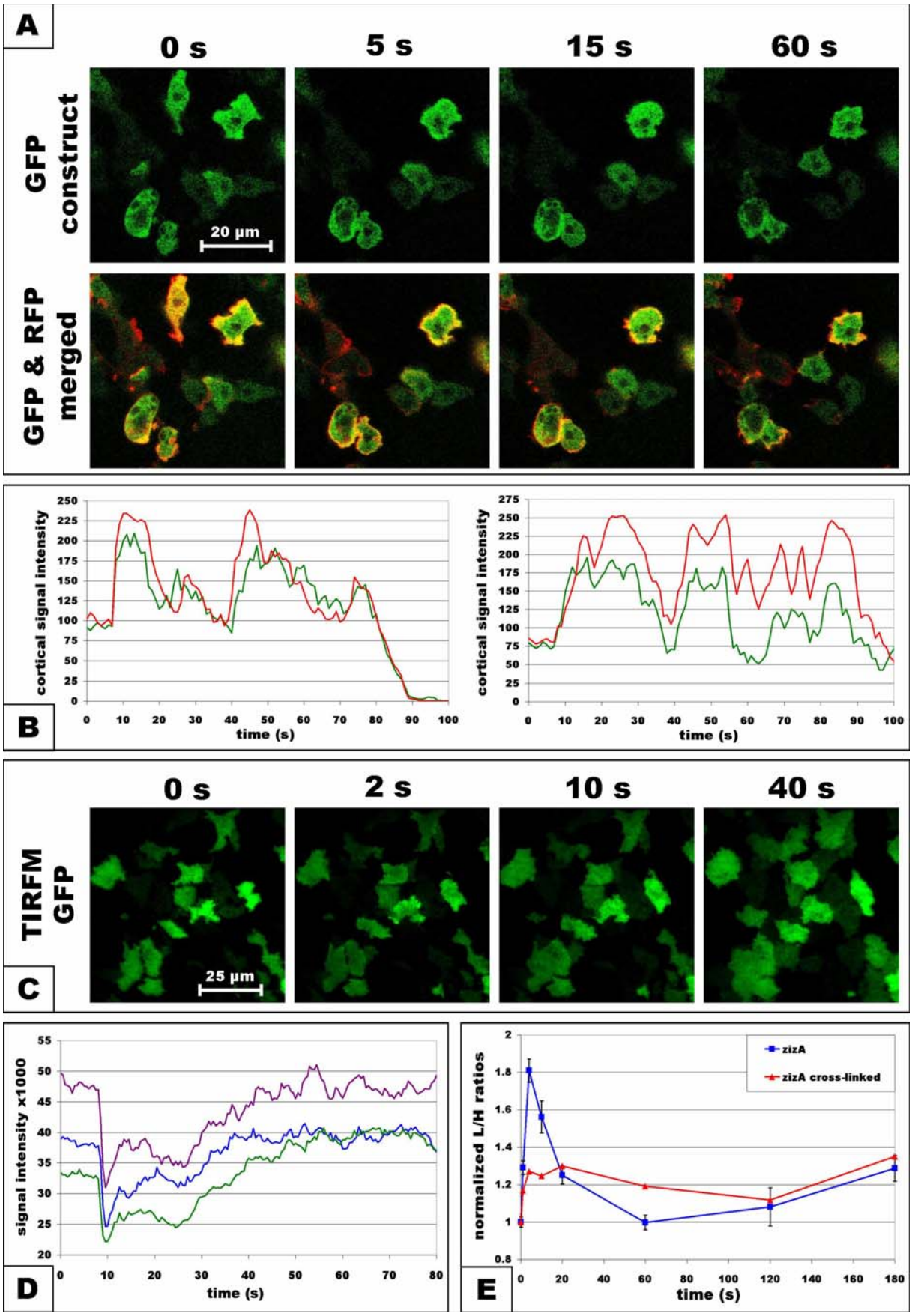


**Figure 4.15.** Results for ZizA protein. **A)** Confocal images of GFP alone (top) and merged GFP and RFP signals (bottom). **B)** Two separate quantifications of confocal GFP (green) and RFP (red) cortical intensity dynamics. **C)** TIRFM images of GFP signal. **D)** TIRFM signal quantification for 3 separate ROIs. **E)** Translocation dynamics measured in the standard SILAC (blue) and cross-linked SILAC (red) experiments.

This result is generally supported by the confocal imaging, showing weak cortical localisation with a lot of cytosolic signal, but also clear colocalisation with actin structures and cAMP-induced translocation (Fig. 4.15. A, B). On the other hand the cross-linked SILAC shows only mild enrichment after stimulation with no prominent pattern noticeable, which does not generate a major inconsistency alone, as there are many proteins with no correlation between the two types of SILAC experiments.

The major discrepancy comes from the TIRFM imaging analysis, showing a rapid and strong drop of fluorescence intensity after stimulation, which then recovers slowly reaching pre-stimulation levels after about 30 s (Fig. 4.15. C, D). This type of behaviour was described earlier for MhcA and it indicates that this protein is not present at the newly generated peripheral part of the cell cortex, consisting of actin filament formed in the first phase of actin polymerisation.

The most likely overall interpretation of those results is that ZizA is enriched in actin structures at the cortex and does respond to cAMP stimulation, but it translocates only to the old pre-existing network of actin filaments and does not bind to newly polymerised ones. This interpretation would suggest that ZizA plays some role specific only to pre-existing structure of cortical actin filaments, such as stabilisation or reorganisation of those filaments.

### 4.2.2.3. Ras-like GTPase; Roco7

Roco7 belongs to a superfamily of multidomain proteins containing a Ras-like GTPase domain called Roc (Ras of complex proteins) followed by a characteristic COR (C-terminal of Roc) domain. This superfamily was first identified in *Dictyostelium* [265] and later members of Roco family were detected in many other organisms including humans, where one of them (LRRK2) was found to be involved in development of Parkinson disease [266].

There are 11 members of Roco family in *Dictyostelium,* all containing a kinase domain belonging to MAPKKK subfamily of kinases, which follows directly the COR domain. Many of those proteins also contain other domains such as WD40, LRR or Rho GEF and Rho GAP domains [14, 265]. These proteins were described to play important roles in various cellular processes such as organisation of myosin II filaments, chemotaxis and development [14, 267]. Interestingly, it has been shown that the GTP binding to Roc domain is necessary for activation of the MAPKKK domain kinase activity, suggesting that these proteins may act as independent signal transduction units, performing tasks which normally require several proteins [268, 269].

Roco7 is the only roco protein in *Dictyostelium* which does not contain LRR (Leucin-Rich Repeat) domain at the N-terminus. Apart from the 3 common domains shared by all the members (Roc, COR and MAPKKK) it contains only WD40 repeat domain at the C-terminus, which makes it one of the most simple proteins in this family [265]. Expression of this protein is developmentally regulated and, similarly to many other proteins involved in chemotaxis, it shows the highest expression levels after 4 hours of starvation corresponding to the aggregation stage of development (http://www.ailab.si/dictyexpress/). Knock-out cells lacking *roco7* gene did not display any major developmental defects, neither did most of other *roco* single knock-out strains [267].

Our SILAC experiments detected 4 members of the Roco family, Roco5, Roco7, Roco9, and Roco10, most of which followed the basic actin dynamics with Roco7 showing the highest amplitude in the first phase (Fig. 3.5.). First three of them were selected for tagging with GFP, but because of the very big sizes of the genes encoding those proteins, only Roco7 was successfully cloned. This is unfortunate because Roco5 and Roco9 are more complex and potentially more interesting regulators of the cytoskeleton containing additional Rho GEF and Rho GAP domains respectively [265].

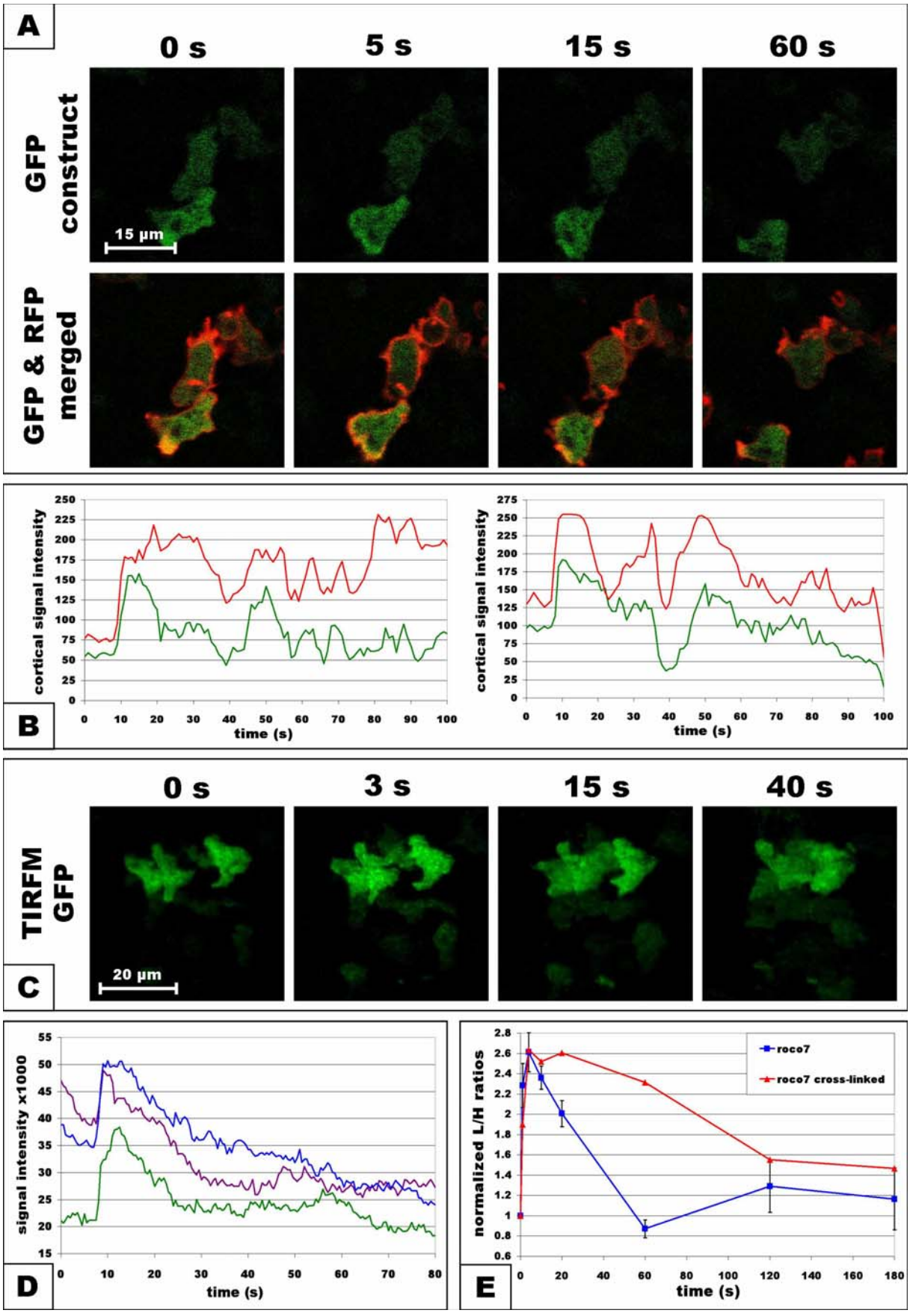


**Figure 4.16.** Results for Roco7 protein. **A)** Confocal images of GFP alone (top) and merged GFP and RFP signals (bottom). **B)** Two separate quantifications of confocal GFP (green) and RFP (red) cortical intensity dynamics. **C)** TIRFM images of GFP signal. **D)** TIRFM signal quantification for 3 separate ROIs. **E)** Translocation dynamics measured in the standard SILAC (blue) and cross-linked SILAC (red) experiments.

The SILAC results for Roco7 protein revealed an interesting dynamics pattern with rapid translocation reaching peak of about 2.6 L/H at 4 s after stimulation. In the standard SILAC it then followed actin dynamics decreasing linearly to slightly below pre-stimulation level at 60 s time point and was enriched during the second phase to around 1.3 L/H. The cross-linked SILAC experiment also revealed rapid translocation with a peak of 2.6 L/H at 4 s time point, but here instead of falling down it stayed at this level until 20 s and then gradually decreased to about 1.5 L/H at 2 and 3 min time points (Fig. 4.16. E).

This difference between dynamics patterns detected in two types of SILAC preparations can be easily explained for such a big and compex protein. As a multidomain factor, Roco7 is presumably involved in different interactions with several other proteins. The standard SILAC experiment can only detect translocation dynamics mediated through stable protein-protein interactions, while cross-linked version of the sample preparation is capable of fixing and maintaining also the weaker interactions. This type of difference in the SILAC results as observed for Roco7 might illustrate the fact that this protein changes interaction characteristic and partners in the course of response to chemoattractant stimulation.

In spite of this promising SILAC result showing strong enrichment, confocal imaging showed only weak cortical localisation of this protein (Fig. 4.16. A). This is one of the examples illustrating that those two assays measure slightly different aspects of protein dynamics and do not always correlate with each other.

TIRFM imaging results have higher correlation to the dynamics detected with the SILAC experiment. In TIRFM analysis Roco7 shows comparatively uniform distribution in the cortex and a rapid enrichment upon cAMP stimulation, with relatively long lasting effect (Fig. 4.16. C, D). These combined results indicate that Roco7 is involved in regulation of the cytoskeleton dynamics during response to cAMP stimulation.

## 4.2.2.4. p21-activated protein kinase; PakB

PakB belongs to a conserved family of p21-activated protein kinases, which are important regulators of the cytoskeleton and cell motility in a diverse range of organisms. This family of kinases is characterised by the presence of two domains, a PBD (p21-binding domain) and a C-terminal Ser/Thr protein kinase domain. In the inactive conformation the PBD inhibits the kinase activity of the catalytic domain, and this autoinhibitory effect is disrupted by interaction with active forms of Rac GTPases [270].

PakB from *Dictyostelium* was found to interact directly with Rac1a/b/c, RacA, RacB, RacC and RacF1 [99, 101]. PakB was originally identified as an activator of unconventional type I myosin – MyoD, which is phosphorylated by this kinase at a site located in the motor domain [271]. MyoD is a single-headed non-filamentous myosin, which is localised to the cell leading edge [272]. MyoD contains a membrane binding domain at the C-terminus and therefore may function as a cross-linker between actin filaments and cell membrane and it could also move those two structures relatively to each other [273, 274].

PakB has been previously investigated including *in vivo* localisation analysis and was shown to be enriched at the cell cortex and in a phagocytic cup structures, which is consistent with its role in regulation of MyoD [275]. PakB-null cells did not display any significant phenotypes, but overexpression of constantly active PakB resulted in cytokinesis defects and higher rates of phagocytosis and pinocytosis [275].

Our imaging results of GFP-tagged PakB confirm the cortical localisation of this protein. In fact this construct was showing one of the strongest translocation and colocalisation with actin structures after stimulating with cAMP (Fig. 4.17. A, B). What is noticeable, the GFP signal coming from this construct matched almost precisely the intensity of RFP-lifeact

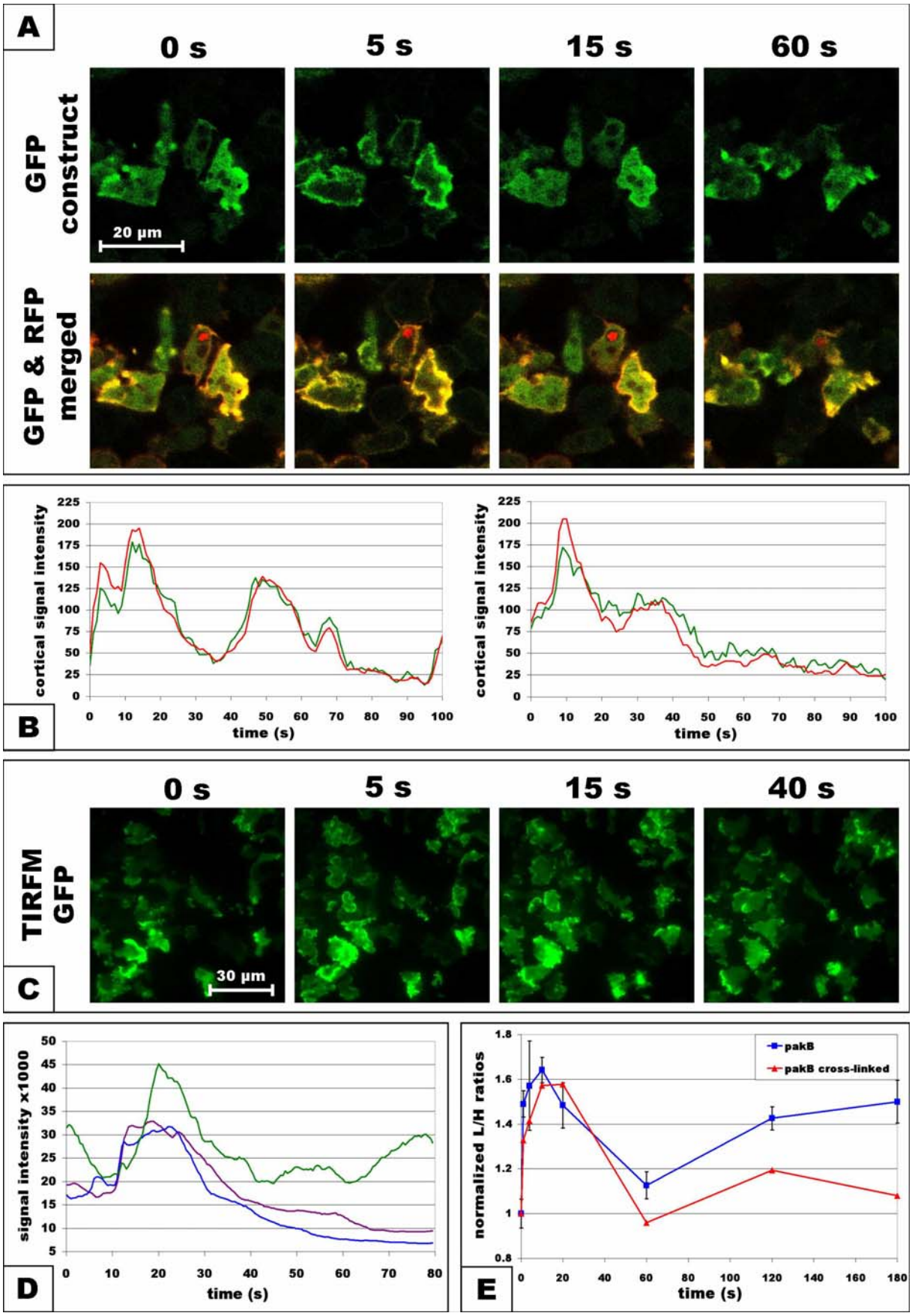


**Figure 4.17.** Results for PakB protein. **A)** Confocal images of GFP alone (top) and merged GFP and RFP signals (bottom). **B)** Two separate quantifications of confocal GFP (green) and RFP (red) cortical intensity dynamics. **C)** TIRFM images of GFP signal. **D)** TIRFM signal quantification for 3 separate ROIs. **E)** Translocation dynamics measured in the standard SILAC (blue) and cross-linked SILAC (red) experiments.

fluorescence in the cortex (Fig. 4.17. B), while most of the other cortical proteins showed weaker fluorescence than the F-actin probe.

TIRFM imaging also reveals increase in cortical signal intensity following cAMP stimulation and lasting for about 20 s (Fig. 4.17. C, D). Both types of microscopy analyses provide a good validation of the SILAC results, which show that PakB follows closely actin dynamics in both native and cross-linking conditions (Fig. 4.17. E).

MyoD was also detected in the SILAC experiments and it displayed a different dynamics pattern than PakB, showing no response in the early time points and then slow and gradual enrichment with a peak at the second phase of actin polymerisation. This pattern was consistent between both standard and cross-linked SILAC results (Fig. 3.8. 22$^{nd}$ profile from the bottom). The fact that PakB follows actin dynamics very closely, which is not shared by its main known substrate – MyoD, suggests that this kinase might also participate in the regulation of other cytoskeletal components upon cAMP stimulation.

## 4.2.2.5. Rac GAP; GacR

GacR (GTPase activating factor for Rac) is a Rho GAP domain containing protein. It activates the intrinsic catalytic activity of Rac GTPases leading to hydrolysis of GTP into GDP and thus inactivating those molecular switches. The family of Rho GAPs has generally attracted much less attention than the activators of those small GTPases, Rho GEFs. Only very few proteins containing Rho GAP domain were individually investigated and therefore the interaction partners for most of them remain unknown [100]. GacR has not been yet individually characterised with functional analysis.

GacR apart from Rho GAP domain also contains a BAR domain at the N-terminus. This type of domain is responsible for dimerisation, lipid binding and membrane curvature sensing.

BAR domains form dimers that bind to membranes and can induce or detect membrane bending and curvature, they may also be involved in protein-protein interactions [276]. This domain composition makes this protein an interesting molecule, which might be involved in local cytoskeleton regulation at sites of specific membrane structures, such as actin based protrusions or invaginations.

SILAC results show rapid enrichment of this protein after stimulation. It reaches a peak of about 1.5 L/H at 1 s, which then slowly decreases. The 60 s time point is missing but at 120 s it indicates protein abundance below the pre-stimulation level, which then goes up to 1.4 L/H in 180 s time point (Fig. 4.18. E). This protein was not detected in the cross-linked SILAC experiment.

Confocal imaging reveals a primarily cytosolic localisation in unstimulated cells and a strong translocation to the cortex after cAMP stimulation. GacR exhibits strong colocalisation to actin cortical structures in both phases of actin polymerisation (Fig. 4.18. A, B).

TIRFM imaging also indicates very rapid and strong enrichment of this protein at the peripheral cell cortex after stimulation, with characteristic biphasic dynamics, which is rather unusual for TIRFM analysis. The first rapid phase peaks only about 2-3 s after stimulation and the second lower peak comes at about 12-15 s (Fig. 4.18. C, D), which does not correlate with the two phases of actin response, but might represent a specific character of this protein's dynamics. It is also noticeable that GacR is not uniformly distributed, but rather concentrates locally at distinct patches throughout the cell cortex.

All the acquired results suggest, that this Rac GAP might play an important role in both phases of actin polymerisation. Based on the very strong translocation of GacR to actin structures, it is potentially one of the crucial regulatory factors of the cytoskeleton.

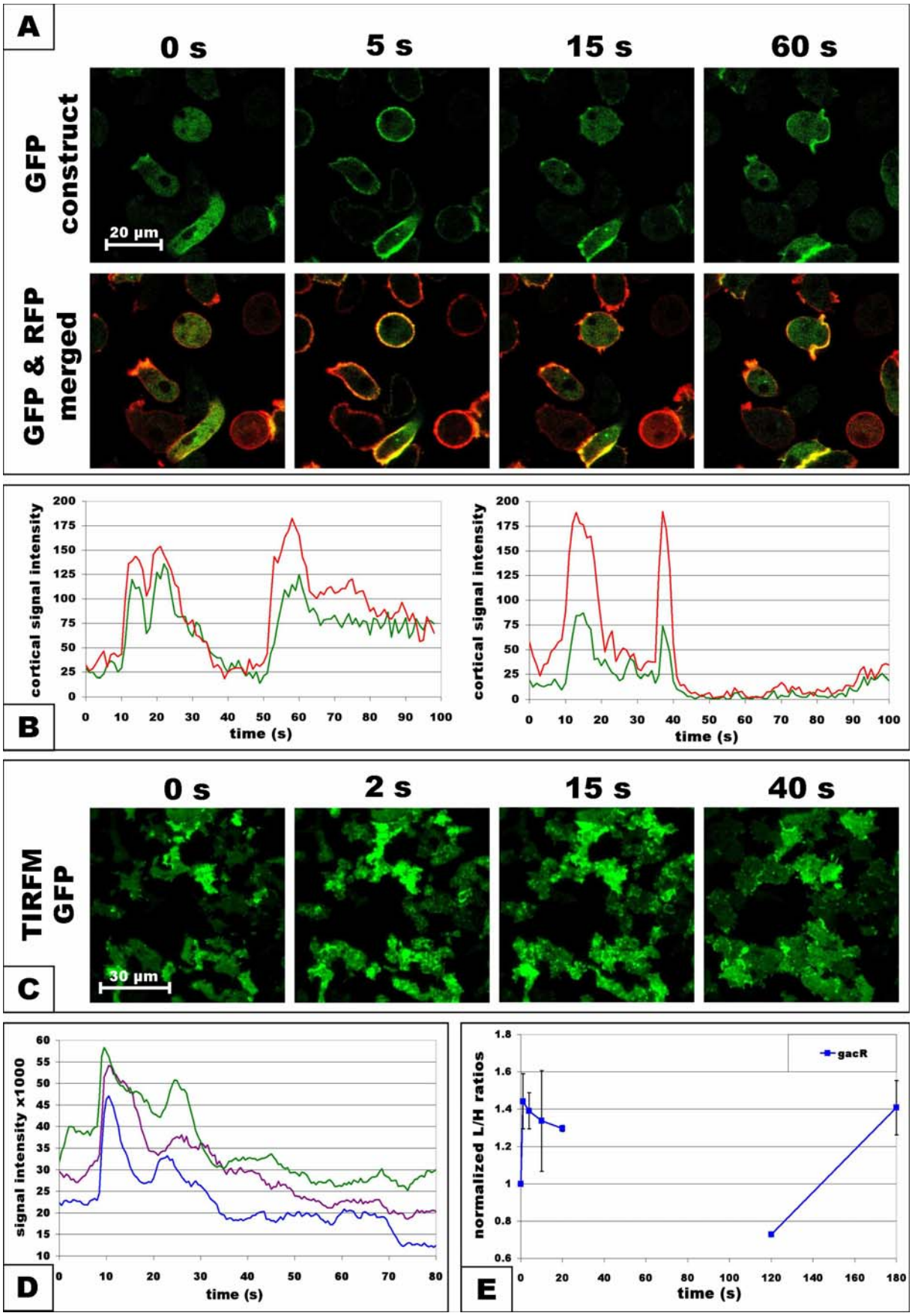


**Figure 4.18.** Results for GacR protein. **A)** Confocal images of GFP alone (top) and merged GFP and RFP signals (bottom). **B)** Two separate quantifications of confocal GFP (green) and RFP (red) cortical intensity dynamics. **C)** TIRFM images of GFP signal. **D)** TIRFM signal quantification for 3 separate ROIs. **E)** Translocation dynamics measured in the standard SILAC.

## 4.2.2.6. Rho GAP; GacA

GacA is another example of a Rho GAP domain containing protein. It is a relatively simple and small (37kDa) protein, which does not have any additional identified domains and has not been previously investigated.

Results from the standard SILAC experiment show initial depletion after stimulation, followed by enrichment to about 1.2 L/H at 20 s, which corresponds to the beginning of the depolymerisation phase. Indeed, this protein was selected for cloning as a potential factor involved in triggering actin depolymerisation at the end of the first phase. This pattern was not reproduced in the cross-linked SILAC experiment, which revealed instant enrichment after stimulation with a peak of 1.8 L/H at 20 s going down to below pre-stimulation level at 120 s and rising again to 1.3 L/H at 180 s (Fig. 4.19. E). This profile resembles the actin biphasic dynamics with a certain time delay and correlates with the imaging analysis much better than the standard SILAC results.

Confocal imaging shows strong translocation from the cytosol to the cortex triggered by cAMP stimulation. GacA exhibits partial colocalisation with actin structures leaving some of the cortical actin without GFP signal and staining some parts of the cortex with no actin present (Fig. 4.19. A). Cells overexpressing GacA showed greatly reduced second phase of actin polymerisation, which is in agreement with its function as an inhibitor of Rac signalling. TIRFM imaging also indicates cAMP dependent increase in cortical localisation of GacA corresponding to actin dynamics (Fig. 4.19. C, D).

These results show that GacA is another Rac GAP which follows actin dynamics after cAMP stimulation and the overexpression phenotype observed for this protein suggests, that it is capable of regulating the actin cytoskeleton globally.

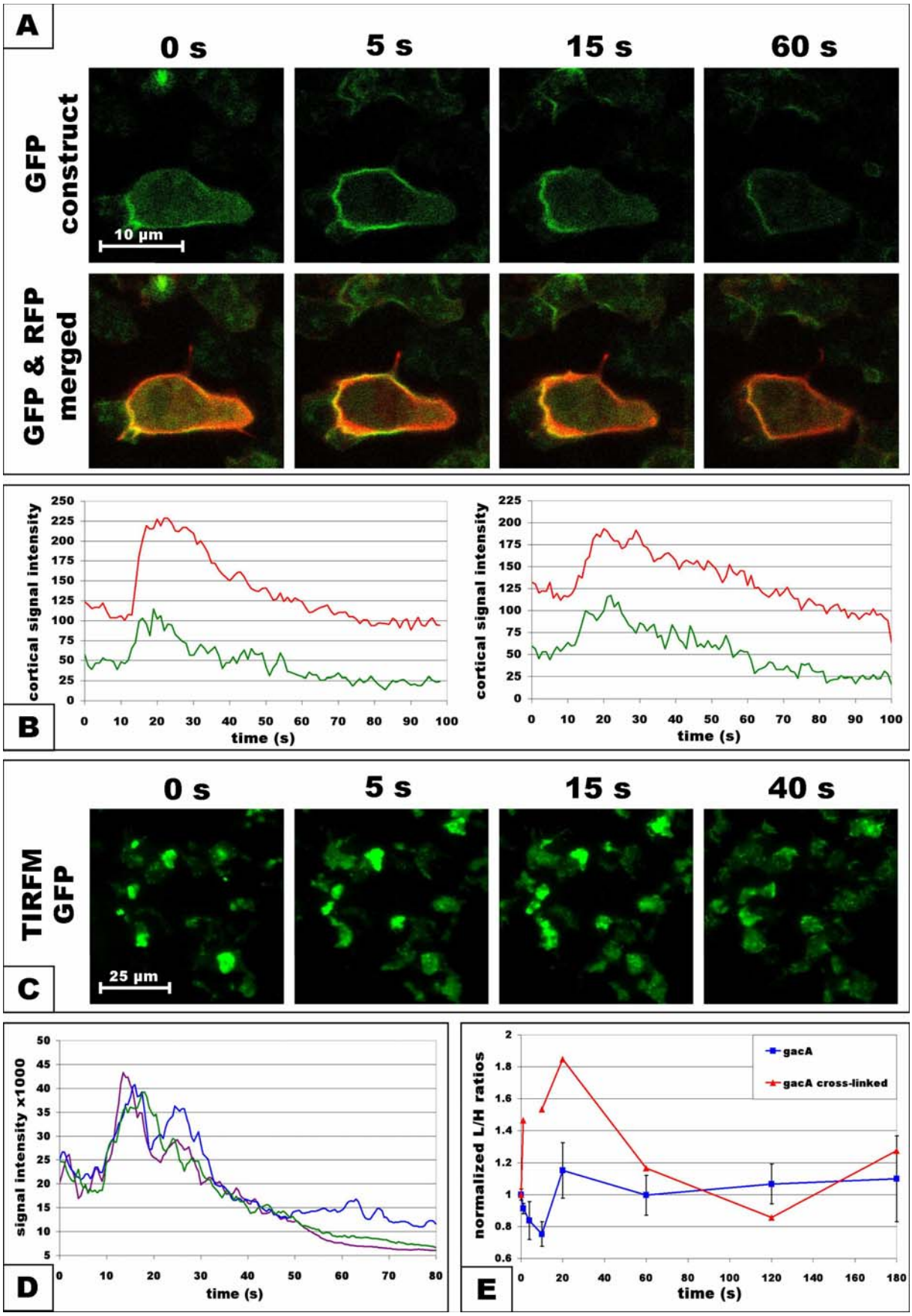


**Figure 4.19.** Results for GacA protein. **A)** Confocal images of GFP alone (top) and merged GFP and RFP signals (bottom). **B)** Two separate quantifications of confocal GFP (green) and RFP (red) cortical intensity dynamics. **C)** TIRFM images of GFP signal. **D)** TIRFM signal quantification for 3 separate ROIs. **E)** Translocation dynamics measured in standard SILAC (blue) and cross-linked SILAC (red) experiments.

It is interesting to observe those two Rho GAPs being translocated to the cortex after cAMP stimulation with very similar timing to that displayed by Rho GEFs. This indicates that both activators and inhibitors of small GTPases signalling are working with the same temporal and spatial dynamics.

## 4.2.2.7. Rho GEF / Rho GAP; XacB

XacB (Exchange and activating factor for Rac) is a complex 143kDa multidomain protein. It is one of three proteins in *Dictyostelium* containing both Rho GEF and Rho GAP domains. Its Rho GEF domain belongs to the canonical family comprised of DH (Dbl-homology) domain followed by PH (Plecstrin-homology) domain acting as a membrane anchor and as a mediator of interactions with other signalling components [100]. Those two subdomains belonging to the classical Rho GEF domain are followed by the Rho GAP domain at the C-terminus. The Rac GTPases which are controlled by each of those domains has not been identified and the XacB protein has not been yet functionally characterised.

Even though this protein domain composition seems to belong to the big repertoire of *Dictyostelium* specific cytoskeletal components, it does have identified orthologs in human and mouse (http://dictybase.org/gene/DDB_G0278417). XacB gene expression is like many other cytoskeletal factors developmentally regulated and it is most highly transcribed in the slug stage of development after 16 h of starvation.

XacB measured in the SILAC experiments exhibits biphasic dynamics with shifted timing relative to actin profile. The first peak of about 1.4 L/H ends at 20 s time point and then the gradual enrichment follows reaching about 1.5 L/H at 3 min time point (Fig. 4.20. E).

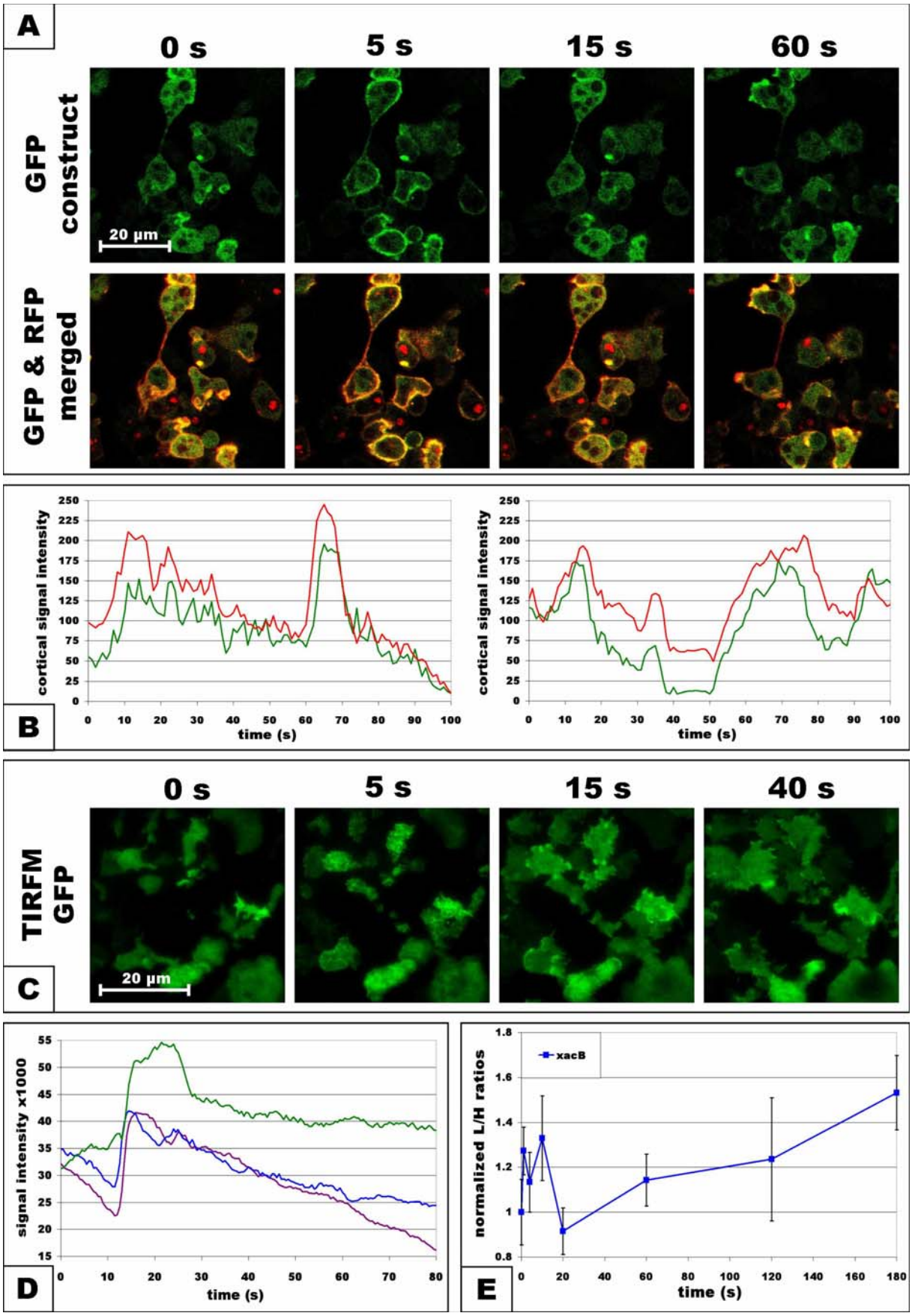


**Figure 4.20.** Results for XacB protein. **A)** Confocal images of GFP alone (top) and merged GFP and RFP signals (bottom). **B)** Two separate quantifications of confocal GFP (green) and RFP (red) cortical intensity dynamics. **C)** TIRFM images of GFP signal. **D)** TIRFM signal quantification for 3 separate ROIs. **E)** Translocation dynamics measured in the standard SILAC.

Confocal imaging reveals strong translocation from the cytosol to the cortex in the first phase of actin response. This cortical enrichment is almost completely reversed into the cytosol during the depolymerisation phase and then occurs again in the actin-rich cortical structures during the second phase (Fig. 4.20. A). Cells overexpressing XacB construct had both phases of actin polymerisation well represented and did not show any obvious aberrant phenotypes related to this overexpression. XacB shows comparatively uniform distribution along filamentous structures in the cortex of unstimulated cells, which is then followed by more localised enrichment after cAMP stimulation as visualized by TIRFM imaging, which also confirms the translocation triggered by this chemoattractant (Fig. 4.20. C, D).

These results indicate that XacB is involved in the chemotactic response to cAMP stimulation. The fact that it contains a PH domain suggests that the translocation of this protein might be driven by $PI(3,4,5)P_3$ accumulation at the membrane. It is not clear from the results which of the two domains, Rho GEF or Rho GAP, plays a primary role in the cellular functions of this protein, since both of those classes of regulatory factors share the same type of actin-like dynamics.

# 4.2.3. Uncharacterised cytoskeletal factors

## 4.2.3.1. DDB_G0283827; WASP-related protein

DDB_G0283827 is one of two WASP-related proteins found in *Dictyostelium* in addition to the conventional WASP. It contains a CRIB (Cdc and Rac Interactive Binding) domain at the N-terminus and a WH2 (WASP homology 2) domain at the C-terminus. The CRIB domain suggests that this protein is a putative effector of Rho GTPases signalling. Proteins

containing CRIB domains usually exist in a folded inactive conformation which has an autoinhibitory effect on its function. This conformation is disrupted by interaction with activated GTPases exposing the catalytic domain or allowing formation of further interactions with other proteins [48]. The WH2 domain is a monomeric actin binding motif, which facilitates the assembly of actin monomers into filaments, but by itself is not sufficient to establish interactions with F-actin or the Arp2/3 complex [49, 277].

This protein, together with the other WASP-related protein, was recently investigated and both were found to colocalise with clathrin coated vesicles, which suggests their potentially redundant function in the clathrin based endocytosis [50].

The standard SILAC experiments show a moderate increase of this protein's abundance during the first phase with a level of about 1.3 L/H at the 4 s and 10 s time points. It then goes down to prestimulation level at 20 s, and increases again up to 1.3 L/H at the last 3 min time point (Fig. 4.21. E). Results from the cross-linked SILAC are inconsistent with the standard experiment and show less coherent translocation profile.

This WASP-related protein shows very strong translocation to the cortex upon cAMP stimulation as observed with confocal imaging. It colocalises with most of the actin cortical structures in both phases of cAMP stimulated actin polymerisation response (Fig. 4.21. A, B). Apart from the cell cortex it also localises to circular structures resembling a phagocytic ring, which is best visible at the confocal images from the 60 s time point. This observation suggests that DDB_G0283827 might be also involved in the process of phagocytosis.

TIRFM imaging also reveals a strong translocation to the cortex after stimulation. This enrichment shows non-homogenous distribution and is present throughout the whole duration of the first phase of actin polymerisation (Fig. 4.21. C, D).

All the results show that this WASP-related protein colocalises strongly with actin structures in response to cAMP stimulation. This indicates a potential role in the regulation of the cytoskeleton, but the exact function of this component remains to be determined.

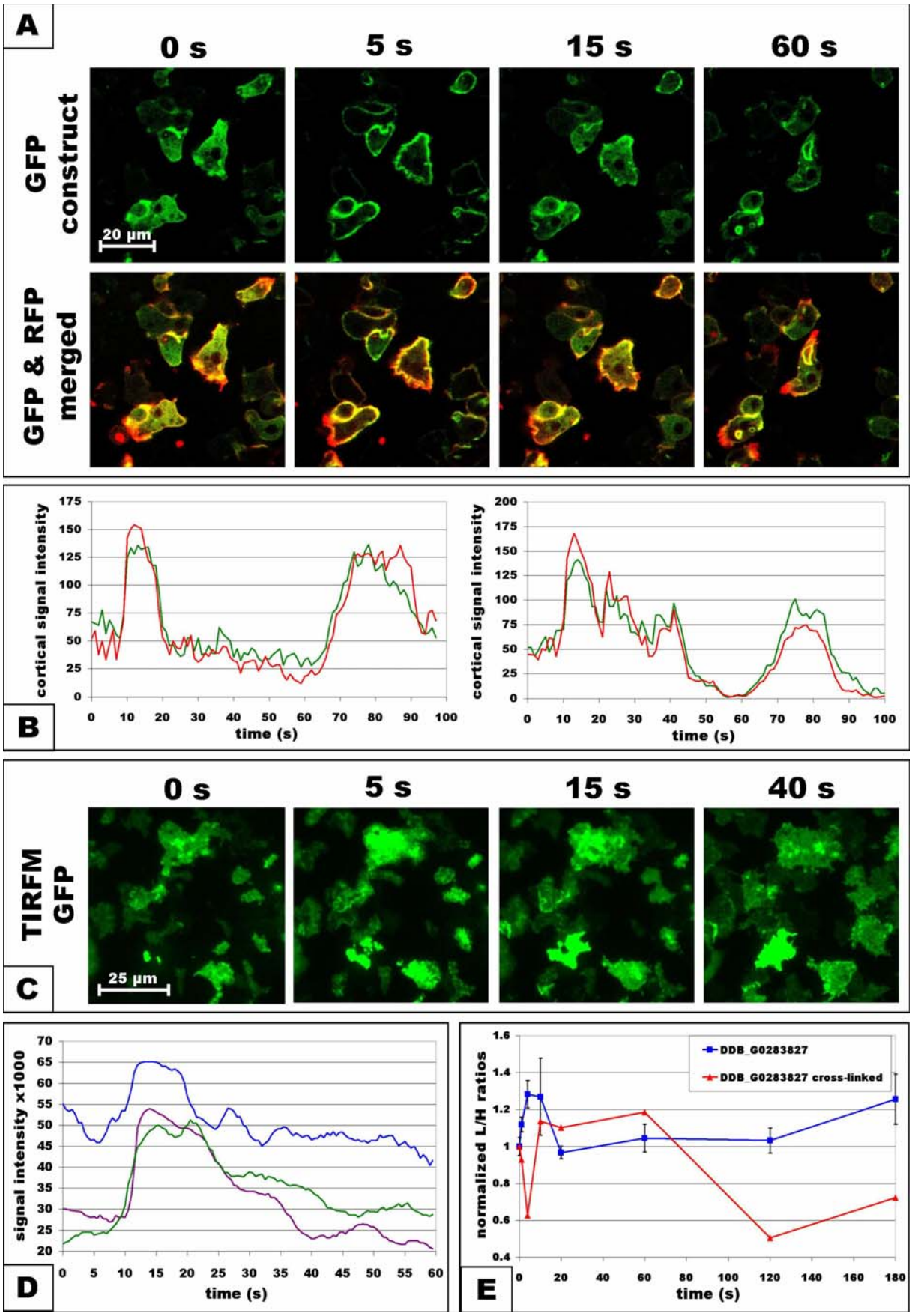


**Figure 4.21.** Results for DDB_G0283827 protein. **A)** Confocal images of GFP alone (top) and merged GFP and RFP signals (bottom). **B)** Two separate quantifications of confocal GFP (green) and RFP (red) cortical intensity dynamics. **C)** TIRFM images of GFP signal. **D)** TIRFM signal quantification for 3 separate ROIs. **E)** Translocation dynamics measured in the standard SILAC (blue) and cross-linked SILAC (red) experiments.

## 4.2.3.2. DDB_G0295683; ADF-H dcp

DDB_G0295683 is a big 190kDa protein containing two conserved domains: one ADF-H (Actin Depolymerising Factor Homology) domain and one LIM type Zinc finger domain.

ADF-H domain can bind both actin monomers and filaments and is found in three distinct classes of ABPs. A single ADF-H domain is found in ADF/cofilins which bind both G-actin and F-actin and promote rapid filament turn-over by depolymerising/fragmenting actin filaments. Twinfilins, which are actin monomer sequestering proteins, contain two ADF-H domains [278]. Drebrins, proteins that bind to actin filaments, but do not promote actin depolymerisation, contain one ADF-H domain followed by a C-terminal SH3 domain [279]. It therefore appears that the ADF-H domain mainly acts as an actin binding domain, but that it is not enough to specify a protein's function, since it is found in a diverse range of proteins playing very different roles in actin dynamics.

The LIM domain consists of two zinc finger motifs, which can coordinate one or more zinc atoms. This is a versatile domain which can mediate various interactions such as binding to nucleic acids or other proteins. It is found in factors involved in a wide range of cellular functions including gene expression, cytoskeleton organisation and development [280].

Protein BLAST search also revealed a region at the N-terminus, which shows similarity to several ATPases including V-ATPase, few bacterial SMC (structural maintenance of chromosomes) chromosome segregation ATPases and DNA repair ATPase SbcC. Its domain composition makes this protein a complex and potentially interesting ABP. The gene encoding this protein has a relatively low endogenous level of expression, which does not change significantly during development.

The standard SILAC results show enrichment of about 1.4 L/H at the 10 s time point, which then stays at this level almost constantly for the remaining time-points. The cross-linked

experiment shows a peak of 1.4 L/H at 10 s, but then shows depletion to 1.1 L/H at 60 s followed by a second lower peak at the 2 min time point (Fig. 4.22. D). This protein was among the most abundant factors detected in the SILAC experiments, which suggests that it might have a significant role in the cytoskeleton dynamics.

The GFP-tagged DDB_G0295683 protein displays a strong translocation to the cortex after cAMP stimulation as visualised by confocal microscopy, but interestingly it is localised only to the rear and sides of chemotaxing cells and it is virtually absent from the leading edge. It shows limited colocalisation with actin structures and appears to be enriched in cortical regions depleted of F-actin (Fig. 4.22. A).

TIRFM imaging was performed for both green and red channels simultaneously, which means that there is no accurate quantification of the translocation dynamics available, as explained before. Nevertheless it still provides useful information, visualising a clearly filamentous structure labelled uniformly with this construct. It also reveals stronger labelling of this structure by GFP construct than by the RFP-lifeact probe (Fig. 4.22. C).

The fact that both types of microscopy show a certain degree of exclusion between regions of GFP and RFP signal localisation suggests that the DDB_G0295683 protein might be involved in actin filament depolymerisation in accordance with the presence of an ADF-H domain. The very strong uropod localisation of this protein implies that it might be playing role in cell polarisation, myosin II filament assembly or inhibition of lateral pseudopod formation.

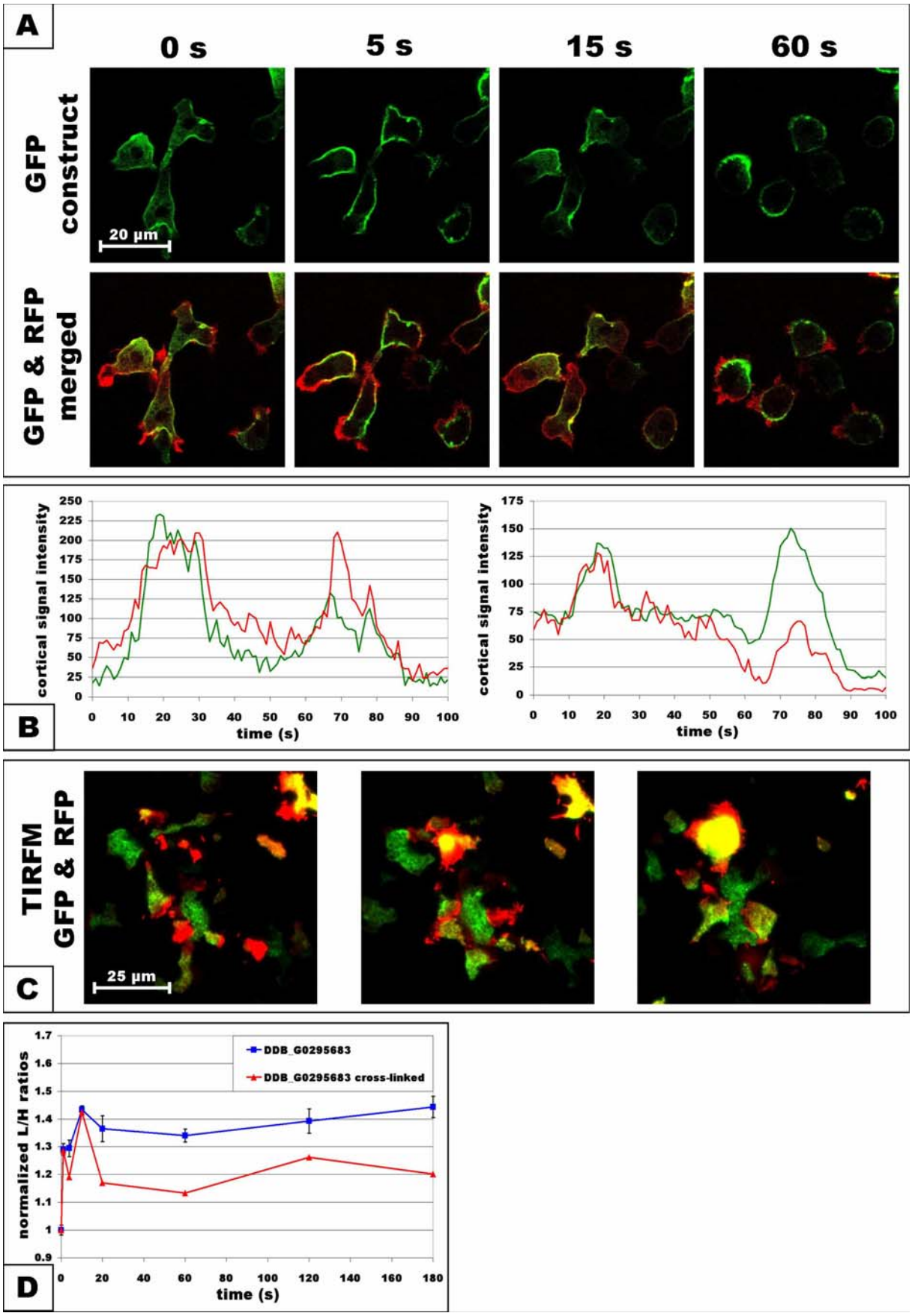


**Figure 4.22.** Results for DDB_G0295683 protein. A) Confocal images of GFP alone (top) and merged GFP and RFP signals (bottom). **B)** Two separate quantifications of confocal GFP (green) and RFP (red) cortical intensity dynamics. **C)** TIRFM images of merged GFP and RFP signals. **D)** Translocation dynamics measured in the standard SILAC (blue) and cross-linked SILAC (red) experiments.

## 4.2.3.3. DDB_G0277615; ADF-H dcp

DDB_G0277615 is another ADF-H domain containing protein (dcp). It actually contains three of those domains, each about 150 amino acids long, covering almost the entire sequence of this 56kDa protein. This type of domain architecture is not found in any of the protein families containing ADF-H domains described earlier and this particular protein does not have any clear orthologs in higher organisms

The gene shows very high levels of expression, which is developmentally regulated and reaches the highest level at the last stage of development, when it shows about 100 times higher gene expression than DDB_G0295683 described before. Interestingly, the detection of these two proteins in the proteomic data reveals a reversed abundance. The proteomic abundance factor was calculated as the total peptide count for each protein in the whole experiment divided by the size of this protein in kDa, to avoid overrepresentation of large proteins. Even with this normalisation to the protein size the DDB_G0295683 protein shows about 4 times higher abundance than the DDB_G0277615, which is more than 3 times smaller molecule and shows between 20 and 100 times higher levels of mRNA with 800 – 4000 counts detected by RNA sequencing (http://www.ailab.si/dictyexpress/).

DDB_G0277615 protein has been previously detected by proteomic analysis of the purified phagocytic vesicles [281] and also centrosomes [282], which suggests that it displays interactions with various cellular components.

Our image analysis does not confirm any centrosomal or vesicular localisation, but instead reveals a cAMP dependent translocation to the cortex and colocalisation with actin-rich structures. It is localised to the distinct and narrow cortical band, which determined its classification as a strong cortical protein, even though there is a substantial part of the signal coming from the cytosol at the peak of the first phase (Fig. 4.23. A).

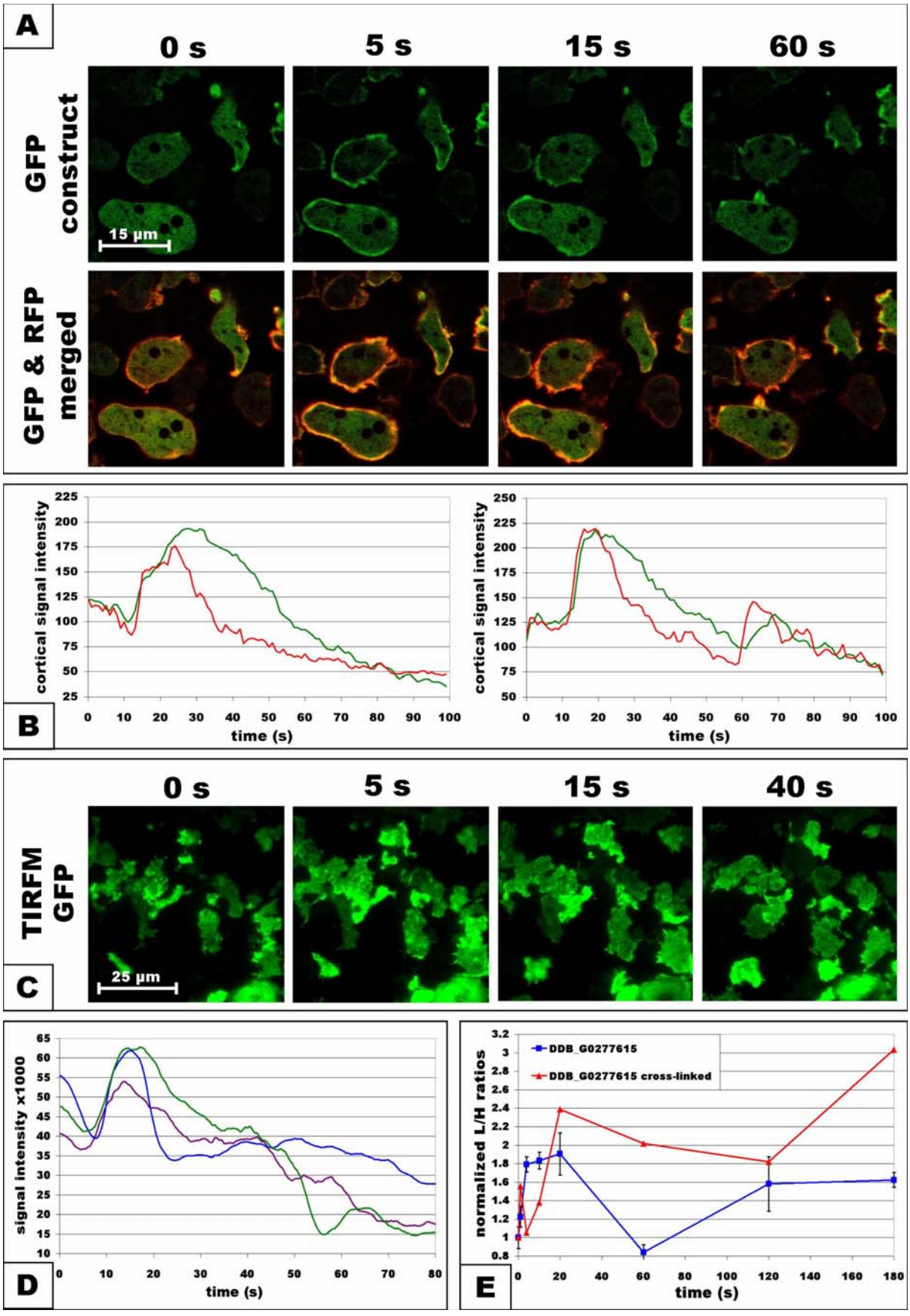


**Figure 4.23.** Results for DDB_G0277615 protein. **A)** Confocal images of GFP alone (top) and merged GFP and RFP signals (bottom). **B)** Two separate quantifications of confocal GFP (green) and RFP (red) cortical intensity dynamics. **C)** TIRFM images of GFP signal. **D)** TIRFM signal quantification for 3 separate ROIs. **E)** Translocation dynamics measured in standard SILAC (blue) and cross-linked SILAC (red) experiments.

The interesting and unusual characteristic of its translocation is its timing. DDB_G0277615 protein enrichment at the cortex is triggered at the same time as actin polymerisation but it seems to stay in the cortex still after the peak of the first phase when actin is being depolymerised. This is best noticeable in the quantification of the confocal images (Fig. 4.23. B) and in the movie format (Supplementary Materials \ Movies \ Individual Proteins \ DDB_G0277615). TIRFM imaging also reveals a strong translocation to the cortex after cAMP stimulation (Fig. 4.23. C, D). This analysis lacks the internal actin reference, but comparison to the actin dynamics measured for other cells does not indicate any significantly prolonged residence of this protein at the cortex.

The translocation to the cortex and colocalisation with actin observed by imaging analysis correlates with the standard SILAC results. In this experiment DDB_G0277615 protein follows closely the actin dynamics with the first peak reaching about 1.9 L/H at 4 – 20 s followed by depletion to prestimulation levels at 60 s and rising to 1.6 L/H at 2 and 3 min time points (Fig. 4.23. E). The cross-linked SILAC experiment does not reproduce this pattern and is less consistent with the imaging analysis.

The translocation dynamics of DDB_G0277615 validates this protein as an actin binding protein responsive to cAMP stimulation. The prolonged cortical localisation in comparison to actin polymerisation during the first phase, which was detected with confocal microscopy, suggests that this protein might be playing role in a disassembly of the actin filaments in the depolymerisation phase, in line with its domain architecture of three ADF-H motifs.

## 4.2.3.4. DDB_G0267974; CH dcp

DDB_G0267974 is an uncharacterised protein containing a single CH (Calponin Homology) domain at the N-terminus followed by three subsequent coiled coil regions. CH domains are

found usually as tandem repeats in cytoskeletal proteins and in signal transduction factors. There are several types of CH domains and some of them are functioning as actin binding modules, while others have no detectable affinity to actin [283].

The CH domain found in DDB_G0267974 protein belongs to the CH3 type, which is characteristic of many signalling factors such as Rho GEFs and is thought to be unable to bind actin [283]. There are no other conserved domains identified in the sequence, which makes the single CH domain insufficient to predict any potential function of this protein.

The SILAC results from both standard and cross-linked experiments show very similar biphasic response with the first peak reaching about 1.3 L/H and lasting for 10 s. The 20 s time point shows depletion to about the prestimulation level and is followed by a gradual enrichment rising to about 1.5 L/H in the last time point (Fig. 4.24. E).

Confocal imaging shows strong cortical localisation even in unstimulated cells. This cortical signal is enriched after stimulation by the cytosolic fraction of the protein translocating to the cortex (Fig. 4.24. A). It partially colocalises with actin structures, but noticeably the strongest enrichment of this protein is found at the uropod cortical regions, which show only limited amount of F-actin making a GFP signal almost excusive at those sites. In contrast in the leading edge of chemotaxing cells the RFP signal dominates over the weak GFP fluorescence. The imaging sequence shown below shows that this region of strong GFP fusion protein localisation is first established in the middle of the elongated cell at the 5 s time point, which then becomes the uropod of this cell as it retracts the left part of the body and moves rightwards at 60 s after stimulation (Fig. 4.24. A). The uropod localisation of this protein is most noticeable in the movies and also in another confocal image sequence discussed later.

TIRFM imaging reveals that this is one of the proteins showing a sudden drop of fluorescence after stimulation. Interestingly, it displays only partial signal recovery, never reaching the prestimulation level of fluorescence intensity in this experiment (Fig. 4.24.).

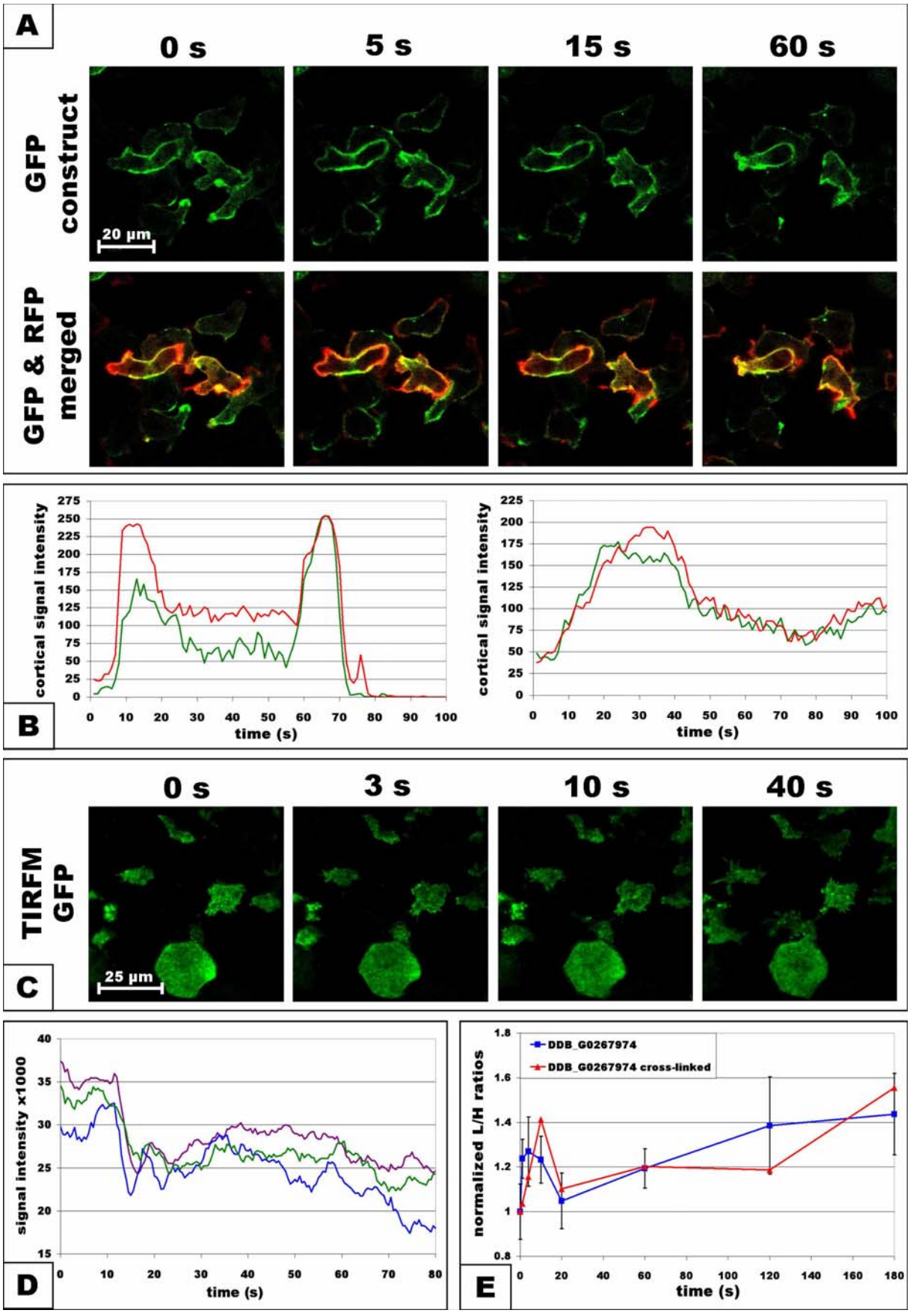


**Figure 4.24.** Results for DDB_G0267974 protein. **A)** Confocal images of GFP alone (top) and merged GFP and RFP signals (bottom). **B)** Two separate quantifications of confocal GFP (green) and RFP (red) cortical intensity dynamics. **C)** TIRFM images of GFP signal. **D)** TIRFM signal quantification for 3 separate ROIs. **E)** Translocation dynamics measured in the standard SILAC (blue) and cross-linked SILAC (red) experiments.

On the other hand, TIRFM also clearly shows that this protein does bind to actin filaments, which is best visible at the protrusions of cells in the centre of TIRFM images (Fig. 4.24. C). These observations indicate that DDB_G0267974 is an actin binding protein, which is not binding to the freshly polymerised actin filaments and during the translocation it localises only to the inner part of the cell cortex. This result together with the uropod localisation of this protein suggests that it might be another factor involved in actin depolymerisation or in inhibition of pseudopod formation at the back of the cell, rather than play a role in the process of cAMP dependent actin polymerisation.

This protein clearly binds to actin filaments either directly or indirectly, but the domain that mediates this interaction remains elusive. The CH3 domain found in this protein has been shown to be unable to bind F-actin [283, 284]

## 4.2.3.5. DDB_G0284825; Rap/Ran GAP dcp

DDB_G0284825 is a 186kDa protein containing one Rap/Ran GAP domain at the C-terminus and one ARM (armadillo) domain at the N-terminus. It has orthologs identified in higher organisms including human and mouse. Rap/Ran GAP domain is involved in the negative regulation of the Rap and/or Ran GTPases signalling. Ran GTPases are the major regulators of transport between the nucleus and the cytosol [285]. The Rap subfamily is involved in a wide range of cellular functions. Rap1 is the only Rap GTPase found in *Dictyostelium* and it was reported as an important regulator of cytoskeletal dynamics, chemotaxis, cell adhesion and phagocytosis [286-288]. It was found to be rapidly activated at the leading edge of chemotaxing cells, similarly to Ras GTPases but with slower kinetics [289].

The ARM domain is a versatile motif involved in protein-protein interactions found in a large variety of proteins including beta-catenins, importins, clathrin heavy chain and the regulatory subunit of V-ATPase [290].

Confocal imaging reveals only very weak cortical localisation and cAMP mediated translocation, with the majority of the protein being present in the cytosol (Fig. 4.25. A).

TIRFM analysis show very uniform distribution with no sign of binding to any type of filamentous structures. It does however reveal an increase in cortical localisation after cAMP stimulation. This enrichment is relatively small and has very sharp and narrow peak, lasting only about 3-4 s after which the signal drops to prestimulation level and does not show any further fluctuations apart from photobleaching (Fig. 4.25. C, D). This rapid translocation to the cortex detected by TIRFM confirms the SILAC results for this protein. Both types of experimental preparations indicate very early peak of enrichment after stimulations. Standard SILAC shows peak of 1.4 L/H at 1 s and 4 s, which drops down at 10 s followed by a second peak reaching 1.5 L/H at 60 s. Cross-linked SILAC shows lower amplitudes with the first peak of 1.2 L/H at 1 s and the second peak with the same level at 20 s (Fig. 4.25. E).

All the results obtained for the DDB_G0284825 protein indicate that it translocates to the cortex after cAMP stimulation, but it presumably does not bind to actin filaments directly. Based on the dynamics observed with TIRFM, it is likely to be involved in the very early events following detection of cAMP by the membrane receptors. The domain architecture of this protein suggests that it plays a role in regulation of Rap1 signalling, which is an important factor in chemotaxis.

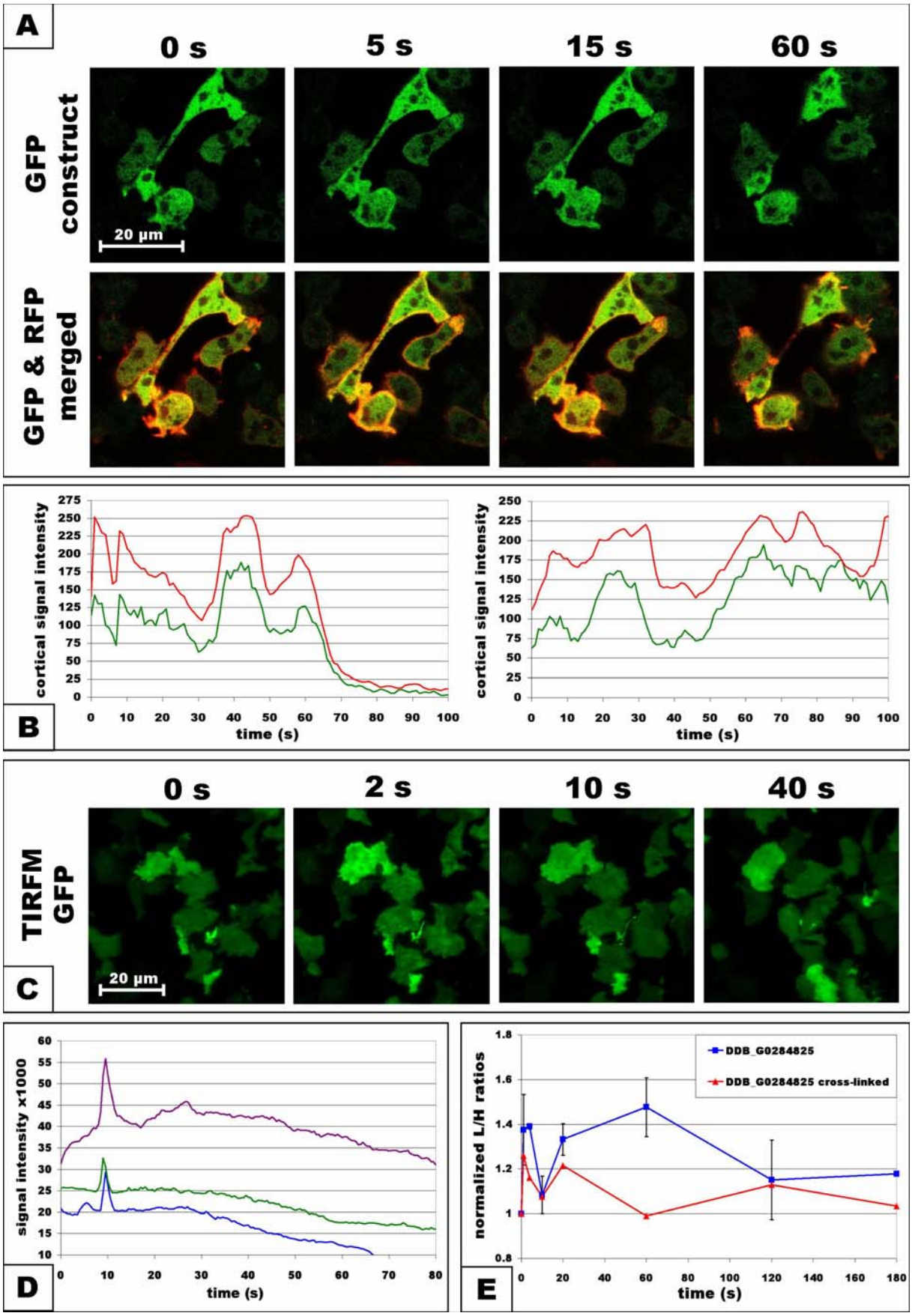


**Figure 4.25.** Results for DDB_G0284825 protein. **A)** Confocal images of GFP alone (top) and merged GFP and RFP signals (bottom). **B)** Two separate quantifications of confocal GFP (green) and RFP (red) cortical intensity dynamics. **C)** TIRFM images of GFP signal. **D)** TIRFM signal quantification for 3 separate ROIs. **E)** Translocation dynamics measured in the standard SILAC (blue) and cross-linked SILAC (red) experiments.

## 4.2.3.6. DDB_G0275305; Fry homolog

DDB_G0275305 is a very big protein with molecular weight over 320kDa. The only conserved domain identified in this protein is an ARM repeat, but based on the sequence homology it has predicted kinase activity. Expression of the gene encoding this protein is developmentally regulated and reaches the highest levels of transcription after 8 hours of starvation and does not decrease substantially until the end of development (http://dictyexpress.biolab.si/). This protein is an ortholog of a Fry (furry) protein and has two long regions of 800 and 500 amino acids showing very high similarity and one region of 200 amino acids with lower similarity to Fry protein and its homologs in fruit fly and human.

Furry is a conserved protein, which was first discovered in *Drosophila* and later found in many higher eukaryotes. It is proposed to play a key role in generating and maintaining extensions of polarised cells during morphogenesis of multicellular organisms [117] and is also involved in patterning dendritic fields of sensory neurons by limiting dendritic branching [118]. It performs those functions during development by regulating the actin cytoskeleton [291, 292]. The original Fry protein found in fly was reported to regulate the Trc (tricornered) Ser/Thr kinase and to localise to the cell cortex [293].

Our imaging results indicate that this protein has a very distinct localisation. It is localised at the cell boundary and only at the attachment sites with the substrate. This localisation is best analysed by TIRFM imaging (Fig. 4.26. A, D). The confocal imaging with Z-sectioning revealed that there is hardly any signal coming from the cortex at the upper part of the cells above the cover slip surface and confirmed the exclusive localisation of this protein to the cell boundary at the bottom of the cell (data not shown).

TIRFM analysis also showed that the DDB_G0275305 protein is enriched at those sites after stimulation with cAMP. It revealed an initial minor depletion of the fluorescence intensity

followed by gradual increase in protein abundance. This translocation displayed rather slow kinetics reaching its peak at about 40 s after stimulation (Fig. 4.26. B).

Interestingly, this type of dynamics is shared only with the cross-linked SILAC results showing the main enrichment of about 1.9 L/H during the late response to cAMP stimulation. The standard SILAC results indicate a different pattern with an early enrichment peak of around 1.4 L/H lasting until 20 s and then staying at the level of 1.2 L/H (Fig. 4.26. C).

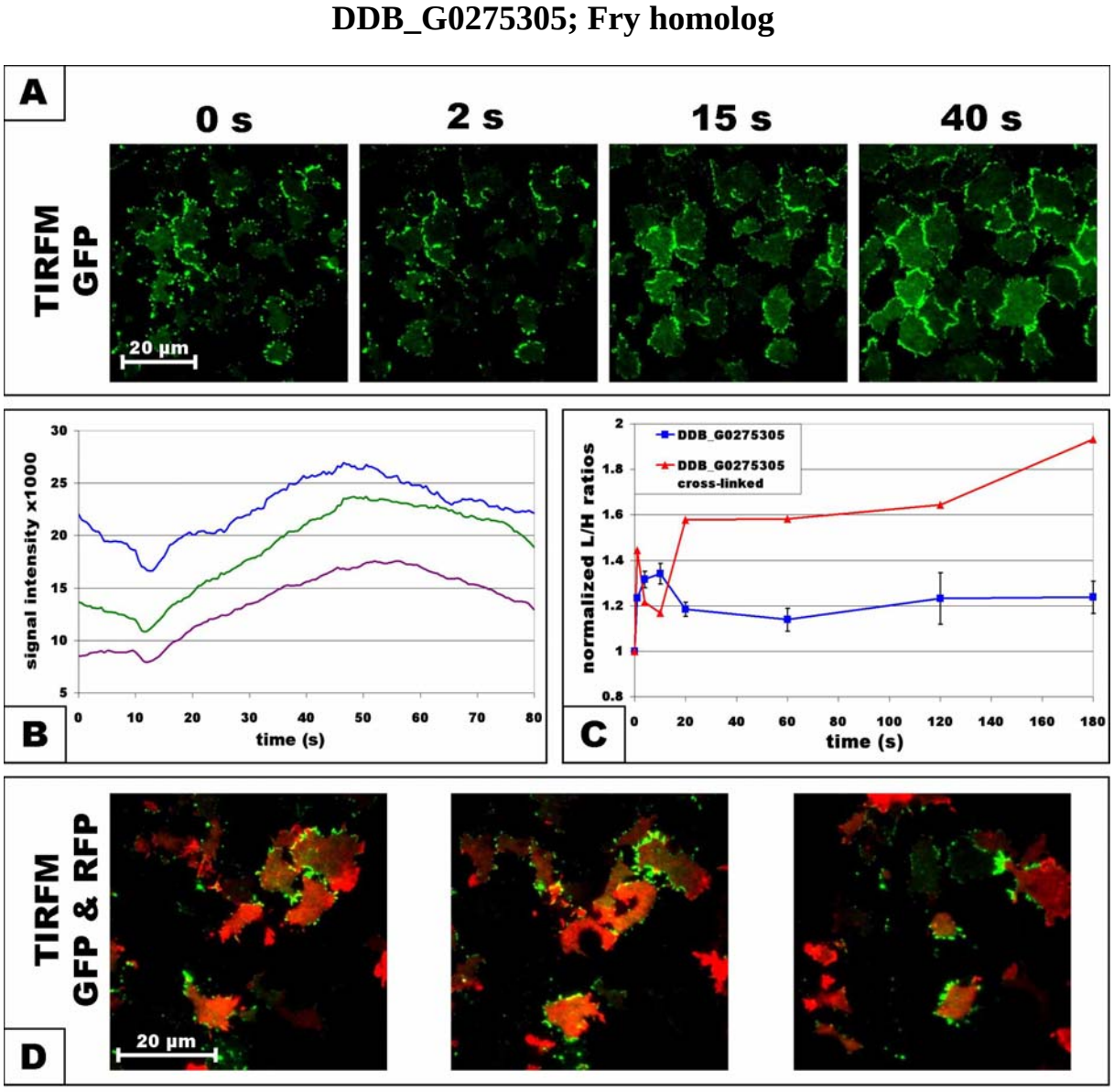


**Figure 4.26.** Results for DDB_G0275305 protein. **A)** TIRFM images of GFP fluorescence alone. **B)** TIRFM signal quantification for 3 separate ROIs. **C)** Translocation dynamics measured in standard SILAC (blue) and cross-linked SILAC (red) experiments. **D)** TIRFM images of merged GFP and RFP fluorescence. Cells were not stimulated with cAMP.

Another session of TIRFM imaging for both GFP and RFP fluorescence revealed another characteristic of this protein's localisation. This imaging analysis was performed on developed and polarised cells which were not stimulated with the chemoattractant and were performing a random walk. In these cells it is apparent that the cortical localisation of DDB_G0275305 is confined mainly to the back and sides of moving cells and almost absent from the leading edge (Fig. 4.26. D). In a few occasions when the localisation spot does occur at the front of the cell it is noticeable that it is not displaced by the protruding pseudopods, but instead the membrane protrusions have to go around it in order to move forward. This behaviour is best visible by watching a movie of this imaging sequence (Supplementary data \ Movies \ Individual proteins \ DDB_G0275305).

There is also another striking characteristic of this cortical localisation observed by TIRFM. Even though it does not colocalise with actin filaments it shows a protrusion-like rough pattern at the cell boundary. This is rather unusual, compared to other proteins showing cortical localisation at the uropod, which always form smooth band of signal detection.

All these results suggest that this protein is involved in establishment of the cell-substrate adhesion at the cell boundary. This localisation shows also certain similarity to the one observed for other protein involved in focal adhesion – paxillin PaxB [294]. The major difference between those two proteins is that PaxB was found not only at the cell boundary, but also in the focal points located throughout the whole cell surface touching the substrate. It will therefore be interesting to investigate this possibly specialised form of cell-substrate adhesion molecule.

## 4.2.3.7. DDB_G0292230

DDB_G0292230 is another very big protein of unknown function. This 334kDa protein is annotated as a hypothetical kinase based on the sequence homology analysis. The expression of this gene reaches its highest level of transcription after 8 hours of starvation and then slowly decreases during the remainder of development.

BLAST analysis of the protein sequence against human database revealed three regions of low similarity to various proteins. The longest fragment is less than 200 amino acids at the N-terminus and it shows similarity to several Rho GAPs. The second fragment of about 80 amino acids has homology to TRP (tetratricopeptide repeat) domain, which is responsible for protein-protein interactions in various proteins such as protein phosphatases and mediates binding of the heat shock protein hsp90 to a series of proteins containing TRP domain [295, 296]. The last region is about 50 amino acids long and it shows similarity to several isoforms of $Ca^{2+}$ transporting ATPase type 2C. This composition of homology regions indicates that it might be an interesting multidomain factor potentially involved in cytoskeleton regulation through Rho GTPase activity and calcium signalling.

The standard SILAC experiments show with high reproducibility that DDB_G0292230 follows closely actin dynamics with the first peak reaching 1.6 L/H at 4 s followed by depletion to about 0.8 L/H at 60 s time point and the second phase of enrichment to 1.2 L/H at the last two time points (Fig. 4.27. E). The cross-linked SILAC did not reproduce this result showing a depletion of this protein after stimulation with incoherent and noisy pattern, which indicates that interactions formed by this protein are disrupted rather than cross-linked by the formaldehyde treatment.

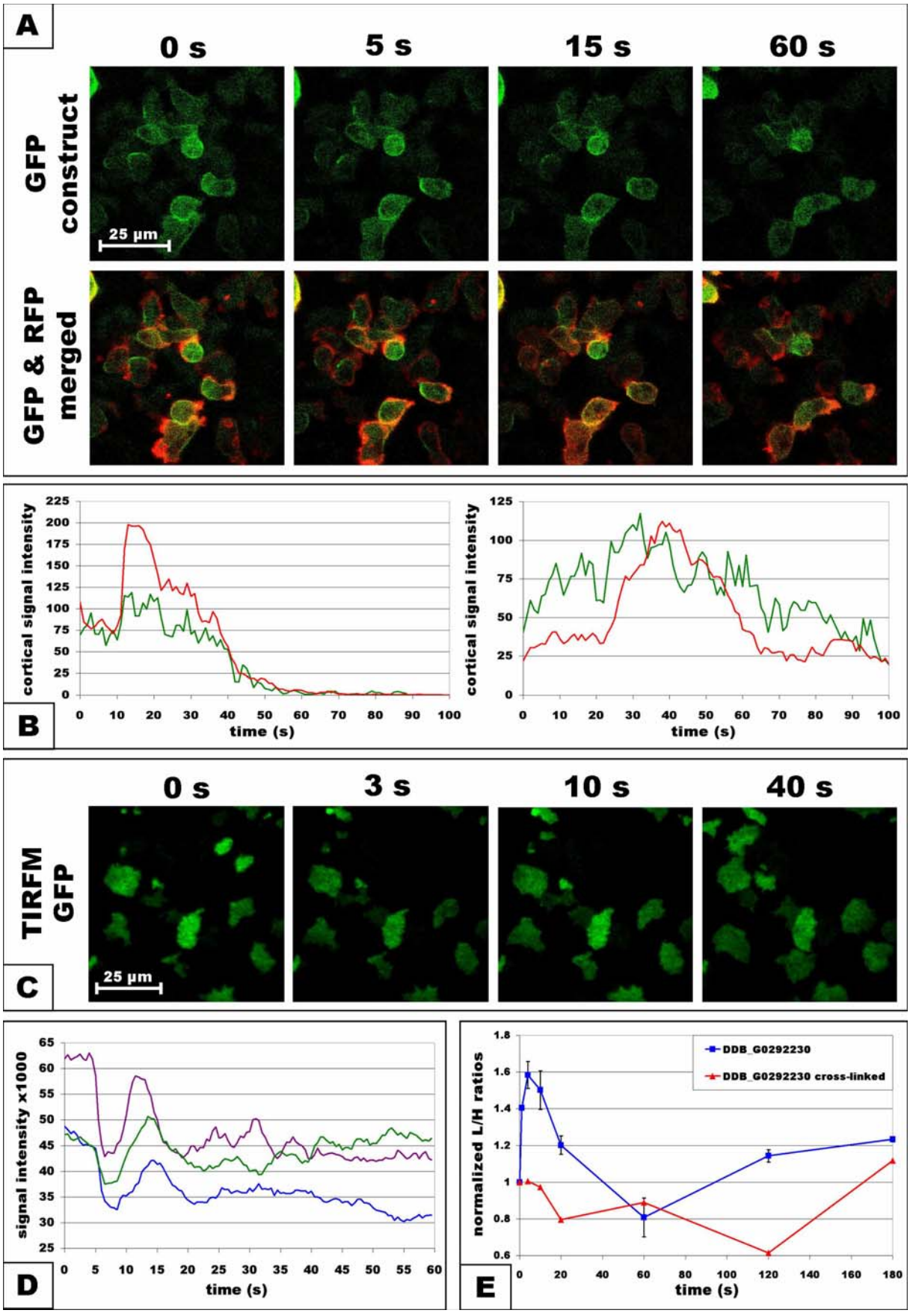


**Figure 4.27.** Results for DDB_G0292230 protein. **A)** Confocal images of GFP alone (top) and merged GFP and RFP signals (bottom). **B)** Two separate quantifications of confocal GFP (green) and RFP (red) cortical intensity dynamics. **C)** TIRFM images of GFP signal. **D)** TIRFM signal quantification for 3 separate ROIs. **E)** Translocation dynamics measured in the standard SILAC (blue) and cross-linked SILAC (red) experiments.

Confocal imaging analysis shows that this protein displays weak cortical localisation with hardly noticeable translocation to the cortex after cAMP stimulation. Most of the protein was present in the cytosol and the cortical fraction seems to almost completely disappear in the late phase of response to cAMP stimulation represented by a 60 s time point (Fig. 4.27. A, B). Interestingly, this weak enrichment at the cortex is mainly observed at the uropod of moving cells. TIRFM imaging reveals a comparatively uniform localisation to a filamentous structure at the cell cortex. The DDB_G0292230 GFP construct shows rapid depletion of fluorescence intensity after cAMP stimulation in TIRFM analysis. This initial depletion is followed by a relatively fast and transient recovery to the prestimulation level at around 10 s time point and then by a second phase of depletion, which does not recover during the experiment (Fig. 4.27. C, D). The first rapid depletion is an indication that the analysed protein belongs to the class of factors, which do not bind to newly polymerised actin filaments and the recovery could indicate a role in actin depolymerisation. The secondary depletion however, is a more unusual characteristic and presumably represents an actual loss of this protein from the cortical cytoskeleton, which is in agreement with the confocal imaging data but not with the SILAC results.

The proteomic data indicating an actin-like dynamic of this protein are generally not reproduced by the *in vivo* localisation analysis. The cortical enrichment during the first phase is hardly detectable on the confocal imaging and not possible to analyse by TIRFM due to the absence in the freshly generated periphery of the cortex. The enrichment in the second phase detected by the standard SILAC experiment is in contradiction to both types of imaging data, which indicate depletion of the cortical signal during the late response to the cAMP stimulation. The discrepancy between those results is another indication that the proteomic and the microscopy analysis are measuring different characteristics of protein translocation dynamics and do not necessarily correlate with each other. The dynamics measured by the SILAC experiments represent changes in type and stability of the protein-protein

interactions, which might involve only a fraction of the entire protein pool and might not always be detectable in the overexpression system used for *in vivo* localisation analyses.

Even though the imaging analyses do not confirm the type of dynamics indicated by the SILAC results, they do validate that DDB_G0292230 is a cytoskeleton interacting protein. The confocal microscopy shows cortical enrichment mostly at the uropod, while the TIRFM imaging shows binding of this protein to the filamentous structures at the cortex. All these results together indicate that DDB_G0292230 is a cytoskeletal factor most likely involved in the negative regulation of the actin polymerisation, which is also supported by the sequence homology analysis described before.

## 4.2.3.8. DDB_G0293032

DDB_G0293032 is a 180kDa protein which has two conserved domains identified in its sequence. It contains an AAA+ (ATPase Associated with a wide variety of cellular Activities) domain and a WD40 repeat domain. It has orthologs present in higher eukaryotes including human. It shows low level of gene expression, which is not increased during development.

The AAA+ superfamily represents an ancient group of ATPases belonging to the P-loop NTPase fold characterised by the conserved alpha-beta-alpha core domain and the Walker A and B motifs. The AAA+ ATPases function as molecular chaperons, ATPase subunits of proteases, helicases or nucleic-acid-stimulated ATPases. Several eukaryotic members of this family have adaptations related to cytoskeletal functions [297].The WD40 repeat, as described before, is a versatile domain acting as a platform for simultaneous protein-protein interactions in a wide range of proteins, including several important cytoskeletal components [246].

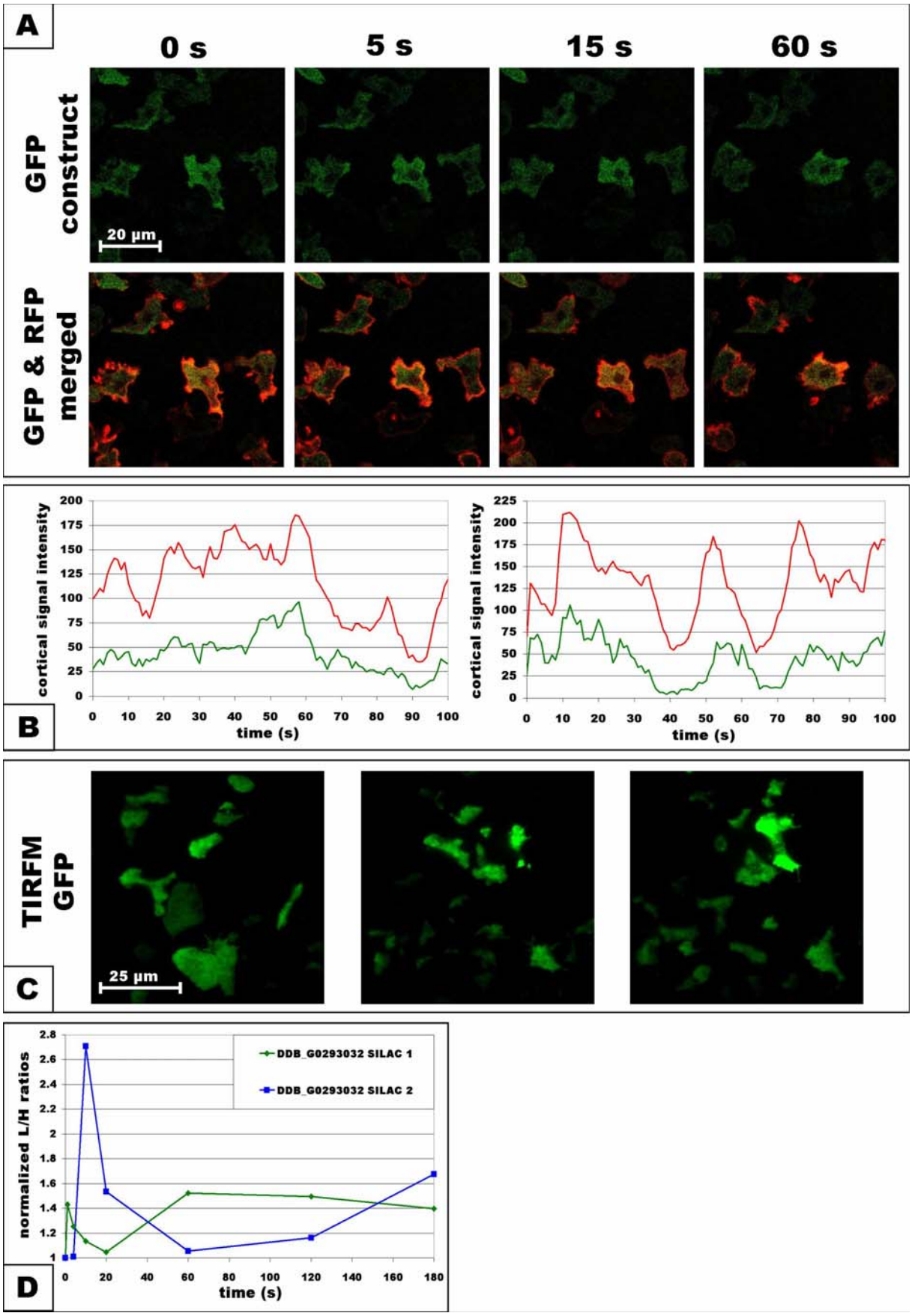


**Figure 4.28.** Results for DDB_G0293032 protein. **A)** Confocal images of GFP alone (top) and merged GFP and RFP signals (bottom). **B)** Two separate quantifications of confocal GFP (green) and RFP (red) cortical intensity dynamics. **C)** TIRFM images of GFP signal. **D)** Translocation dynamics measured in the first (green) and the second (blue) standard SILAC experiments.

The translocation dynamics pattern of the DDB_G0293032 protein showed substantial differences between the two standard SILAC experiments. The first experiment, which was used for selection of the proteins for cloning, showed a rapid first peak of 1.4 L/H at 1 s time point followed by depletion until 20 s and then enrichment to about 1.5 L/H at the rest of the time points. The second standard SILAC experiment also revealed a biphasic response to cAMP stimulation, but with different timing. In those results the first phase had a peak of 2.7 L/H at 10 s, the lowest depletion point at 60 s and the second peak reaching 1.6 L/H at 3 min time point (Fig. 4.28. D).

Confocal imaging revealed that this protein is mainly present in the cytosol, but it colocalises with actin at the tips of pseudopodia in unstimulated cells and during the second phase of actin polymerisation, and shows weak translocation to the whole cortex in the first phase of response to cAMP stimulation (Fig. 4.28. A).

TIRFM imaging was performed for both GFP and RFP simultaneously and therefore could not be quantified afterwards, but it indicated cortical localisation similar to filamentous structures visualised with other actin binding proteins. The individual filaments are not as easily distinguishable in the merged images as with some other constructs, but they become noticeable when observed in the GFP fluorescence images (Fig. 4.28. C).

These results suggest that DDB_G0293032 is one of the novel cytoskeletal factors identified in this study, but they do not provide enough information to speculate about the potential function of this protein.

# 5. Discussion

Chemotaxis is a fundamental cellular process playing a key role in a big variety of biological phenomena. It is involved in nearly all aspects of unicellular organisms, such as nutrient finding and avoidance of environmental stress. It also plays a crucial role during the development of multicellular organisms and in adult life in wound healing and the immune response. Chemotaxis also plays a key role in several pathological processes, e.g. the metastasis and invasion of cancer cells.

Chemotaxis is a highly conserved process and the principal mechanisms of cellular movement in gradients of chemical signals are virtually identical in all eukaryotes. This allows us to investigate this process in a simple model organism, which is genetically and biochemically tractable, and then translate key findings to a better understanding of this process in higher organisms. *Dictyostelium discoideum* is an ideal organism in which to investigate chemotaxis, indeed many crucial cytoskeletal components and regulatory factors were first discovered in this organism and subsequently identified in higher eukaryotes.

Even though chemotaxis has been studied for a few decades, there are still many fundamental aspects of this process that are not fully understood. There are several signalling pathways known to be involved in regulation of chemotactic movement, but none of them has been fully analysed and the cross-talk between them still needs to be delineated. All of those signalling pathways work in parallel and make different contributions to the regulation of this complex process.

One of the major aspects of this process that is still poorly understood is the biphasic character of the actin polymerisation in response to chemoattractant stimulation. This is a universal characteristic, which can be detected with certain variability in both *Dictyostelium*

amoebas and human cells such as neutrophils and fibroblasts. It is thought that the existence of the initial rapidly excitable actin polymerisation can enhance the spatial detection of the source of stimulation, but the exact physiological relevance of this type of dynamics remains unclear. It has been shown that those two phases of actin polymerisation have different characteristics and are independent to a certain extent, but a differential regulatory mechanism has not yet been identified.

There has been recently a great improvement of various techniques used in the quantitative proteomics, driven mainly by advancements in technology of the MS analysis. Orbitrap is a new type of mass spectrometer performing mass determinations with a very high resolution and accuracy and a large dynamic range. This allowed development of a new method for global quantitative proteomic analysis, based on a Stable Isotope Labelling by Amino acids in Cell culture. This relatively straightforward yet powerful procedure has been successfully used in many areas of research, mainly for analysis of protein expression dynamics in response to various treatments and for discovering interaction partners of investigated factors.

We have adapted this versatile technique to analyse fast protein translocation dynamics of the cytoskeletal components in response to stimulation with chemoattractant. This approach was focused on the quantitative examination of changes in the composition of the cytoskeletal fraction, in response to cAMP stimulation. Our experimental procedure was based on the crude purification of the Triton X-100 insoluble cytoskeletal fractions from various time points after cAMP stimulation, followed by the quantitative MS proteomic analysis.
We have performed two biological replicas of the standard SILAC experiment using native cell lysis conditions and one cross-linked SILAC experiment with formaldehyde fixation during lysis, followed by the thermal reversal of the cross-linking. Merged results from the

standard SILAC experiments form a main dataset of this proteomic analysis of fast translocation dynamics, while the cross-linked SILAC results serve as a complementary dataset.

## 5.1. SILAC allows simultaneous quantitative measurements of translocation dynamics for hundreds of proteins

The standard SILAC experiments have detected over 1800 proteins with a minimum detection of two peptides per time point in at least 4 out of 8 time points taken. It revealed that the analysed insoluble fraction of the cell lysate was composed, apart from the cytoskeletal factors, of proteins belonging to many different cellular compartments including nucleus, mitochondria, cell membranes, ribosomes and phagocytic vesicles. There was also a big fraction of uncharacterised proteins with no function determined, which contained about a quarter of all the identified proteins. Most of the proteins from those different groups exhibited some changes in abundance with various amplitudes and pattern persistency.

There are more than 200 known cytoskeletal proteins composing 11% of the whole number of identified proteins and they make up 17% of the total protein abundance detected in those samples. These 200 proteins contain members of different classes of effectors including all known families of actin binding proteins as well as regulatory factors such as Rho GTPases, GEFs, GAPs and various kinases. Nevertheless they represent only a fraction of all the known cytoskeletal factors. Based on the Gene Onthology annotation there are almost 800

proteins with a cytoskeletal annotation, including regulatory factors, in *Dictyostelium discoideum.*

This partial detection of about 25% of all the cytoskeletal proteins present in this organism is a result of several factors. The most important factor is protein abundance determining the likelihood with which a protein will be identified by MS analysis. Proteins with a low abundance have much lower probability of detection and are usually represented by only few peptides, which makes their measurement less reliable. Many of those low abundant proteins are detected only in a few time points, making their patterns not informative enough to be used in our analysis. In fact the total number of cytoskeletal factors identified in those experiments is more than 300, but about one third of them had L/H ratios in less than 4 time points or had no ratios available at all (proteins detected with a single peptide) and were therefore deleted from the final dataset. This detection rate could have been improved by further fractionation of protein samples decreasing the complexity and dynamic range of individual samples. Presumably using two different types of fractionation in parallel on the same samples and analysing them separately with several technical replicas on the MS, would generate much better coverage and reliable quantification of all the proteins. Unfortunately this ideal experiment would require much more MS runs and would exceed the resources available for this project.

A crucial factor influencing the protein detection in our experiments, besides abundance of expression, is the stability of the interactions formed with other cytoskeletal proteins. Only proteins which maintain their interactions after cell lysis and during the whole preparation procedure will be present in the final samples. The ones that form only transient interactions will be lost during purification and therefore not represented in the final results. The importance of this behaviour is illustrated by the number of cytoskeletal proteins detected only in the cross-linked SILAC experiment. This type of experiment was performed especially to detect those weakly binding proteins, which could not be detected in the

standard procedure. It showed a generally slightly higher detection of proteins, but the cytoskeletal fraction was the most strongly enriched in comparison to the standard experiment. 90 additional cytoskeletal components were detected, some of which are known to play key roles in chemotaxis, such as activators of the Arp2/3 complex, the Scar and WASP proteins.

These observations indicate that the proteins identified in the SILAC experiments represent mostly abundant proteins, which form stable interactions through direct or indirect binding to the cytoskeletal core components. Even though these characteristics imply that our analysis is limited to a subset of all the cytoskeletal proteins, it will still be very informative and give insights in their relative performance and regulation.

The stability of interactions formed by detected proteins can be to a certain extent assessed by comparing the results from the standard and cross-linked preparations. Proteins forming weak interactions are likely to show better or even exclusive detection in the cross-linked SILAC experiment. Some of the most prominent components that share this characteristic are unconventional myosins. There are 4 unconventional myosins that were detected in both types of SILAC experiment and these were: MyoA, MyoD, MyoI and MyoJ. Another 5 members of this family were detected only in the cross-linked preparation, including MyoB, MyoC, MyoE, MyoF and MyoK, suggesting that their binding to actin filaments is relatively unstable. This might be related to the ATP-depended character of this binding, which will be disrupted by dilution of the ATP after cell lysis.

For proteins belonging to the same class of cytoskeletal factors, which share similar function and are involved in the same process, we can assume that the ones present in a greater abundance are more likely to have higher significance for this particular process. Based on this correlation between protein's abundance and its relative importance, we can speculate

that the components detected in our SILAC experiments are likely to play more significant roles than members of the same families, which are not present in the final results. We can only discuss this relative contribution during the early development in which the cells were analysed.

Based on these assumptions, 3 out of 8 formins found in *Dictyostelium*, ForA, ForB and ForH are the most likely to mediate the cellular function of this family in the stage analysed. Formins belong to the class of actin nucleators, which elongate actin filaments at the barbed ends in contrast to Arp2/3, which is present at the pointed end. The only members of this family detected in the standard SILAC experiments were ForB and ForH showing low abundance, while ForA was detected only in the cross-linked experiment. These results also indicate that formins play only minor role in cAMP-induced actin polymerisation, compared to the Arp2/3 complex which is present at much higher abundance and shows stronger enrichment.

Similarly, we have detected only 4 out of 7 PI3 kinases identified in *Dictyostelium*. PikA and PikH were showing the highest abundance factors, while PikB and PikF were detected at lower levels. The remaining PikC, E and G proteins were not detected, which suggests that they have less significant contribution to the $PI(3,4,5)P_3$ signalling during the aggregation stage of development.

Following the same logic we suggest, that among the whole battery of GEFs and GAPs present in *Dictyostelium* cells, the ones that were detected through the proteomic analysis of the cytoskeletal fractions are potentially the most important regulators of the cytoskeleton dynamics during the early stage of development.

This approach of using the very fact of protein detection as an indicator of protein abundance and therefore significance in comparison to other undetected homologs, can only be used with limited confidence due to the big number of factors that can influence this detection rate. It can be affected by different protein composition of individual fractions, variable

efficiency of tryptic digest for different proteins or variable efficiency of peptide extraction from different parts of a gradient gel.

The abundance factor calculated for all the detected proteins is another way of comparing the relative contribution of different components to the function of the cytoskeleton. It was determined for each protein as the ratio of total number of peptides detected and the protein size in kDa. It is not the same as the absolute protein quantification but it represents an estimation of protein abundance. It is also affected by the variable character of several aspects described before and, similarly to the L/H quantifications, it is more reliable for the most abundant proteins.

One interesting outcome of the abundance factors analysis for all the cytoskeletal proteins is the list of factors showing the highest association with the cytoskeletal fraction (Table 5.1.). This list includes all the major structural components of the acto-myosin framework such as actin, myosin II complex, Arp2/3 complex, Cap32/34 complex, and several ABPs.

This list represents the key structural constituents of the cytoskeleton and the most abundant effectors regulating cytoskeletal dynamics. It is important to notice that the differences of the abundance factors exhibited by the subunits of the same complex do not necessarily represent a real variability in their abundance, but might just indicate the error levels of this estimation. The largest difference shown by components of myosin II complex is also likely caused by the very big difference in the size of those subunits, which results in different numbers of generated tryptic peptides and influences the relative representation of those proteins.

It is interesting to observe that one of the most abundant actin binding proteins is a translational elongation factor EfaAII, which is also a known actin bundling protein. This protein did not show any translocation dynamics in response to cAMP stimulation, displaying virtually identical L/H values in all the time points (data not shown). It is therefore

a good indication that the most abundant proteins are resistant to the noise fluctuations affecting quantification of less abundant molecules.

- **Actin** (34);
- **Myosin II** subunits : MHC (7.7), RLC (3.7), ELC (2);
- **Arp2/3** subunits : ArcB (4.3), ArpB (3.5), ArcD (3.2), ArpC (2.5), ArcE (2.4), ArcA (2), ArcC (1.6);
- **Cap32/34** subunits : AcpA (2.4), AcpB (1.6);
- **EfaAII** (10) – elongation factor, ABP involved in F-actin bundle assembly;
- **CorA** (4.4) – coronin A, ABP, cross-linker of actin filaments, negative regulator of actin polymerisation also involved in F-actin disassembly;
- **ComA** (3) – comitin A, ABP connecting actin filaments to the Golgi apparatus;
- **DDB_G0295683** (2.7) – uncharacterised protein containing ADF-H and LIM domains, potential factor involved in F-actin depolymerisation;
- **CofB** (2.2) – cofilin identical with CofA, F-actin depolymerising factor;
- **MhkA** (1.6) – MHC kinase A, promotes myosin II filament disassembly.

**Table 5.1.** The list of the most abundant proteins detected in the standard SILAC experiments. Abundance factors were calculated as a ratio of a total peptide count divided by protein MW in kDa and then normalised to the average of all the abundance factors. Values shown in brackets are representation of two combined abundance factors from the standard SILAC experiments.

Another important characteristic is that most of the highly abundant ABPs detected in those experiments are involved in actin filament disassembly. This includes cofilin, short coronin and also DDB_G0295683. This is a previously uncharacterised protein, which was analysed in this study and was found to localise to the cortex at the uropod and sides of moving cells. This observation illustrates the significance of the endogenous actin turn-over cycle in the maintenance of the cytoskeletal functions.

The translocation dynamics patterns revealed by the highly abundant structural components of the cytoskeleton form the most reliable part of the SILAC results. These patterns represent the global dynamics of the myosin and actin filaments and the major direct regulators of F-actin polymerisation in response to cAMP stimulation (Fig. 5.1.).

Even though there is certain variability between the individual subunits of the protein complexes forming the described structures, these complexes can be analysed as a whole unities, which is the best representation of their endogenous mode of action (Fig. 3.4.).

The biphasic actin dynamics is followed by both Arp2/3 and Cap32/34 complexes. There is however a substantial difference in the profiles displayed by those two components. While the capping protein shares almost the same levels of enrichment as actin in both phases of polymerisation, the Arp2/3 complex shows significantly higher levels of translocation during the first phase. Actin and Cap32/34 both reach the amplitude of about 2.4 L/H at the peak of the first phase and the Arp2/3 complex is enriched to about 3.2 L/H at the same time. This means that the increase in F-actin amount and Cap32/34 attached to it during the first phase of actin polymerisation equals to only 75% of the enrichment shown by the nucleator of actin filaments – the Arp2/3 complex.

To fully understand the profound implications of this observation we need to recall the characteristic of F-actin polymerisation reported previously. It has been shown in two independent studies, that the actin filament length distribution does not change during the whole process of chemoattractant induced actin polymerisation, but that the number of actin filaments increases [60, 298]. The average length of actin filaments was determined in both of those studies to be about 300 nm +/- 100 nm at all steps of cAMP stimulation.

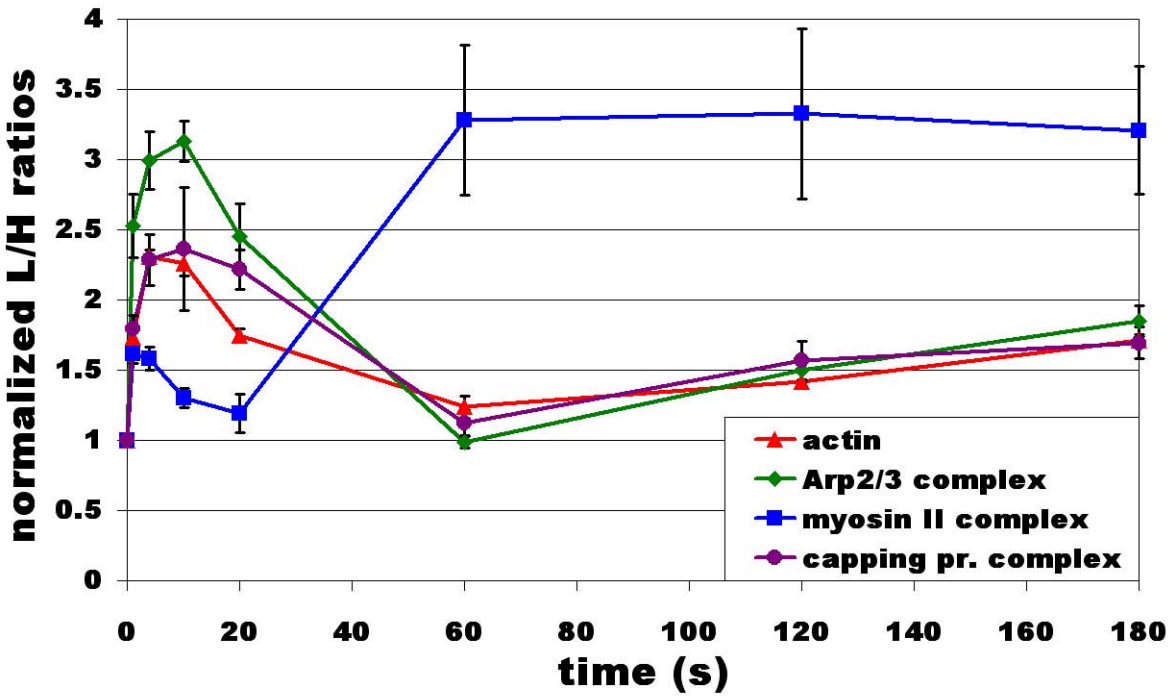


**Figure 5.1.** Translocation dynamics of the main structural components of the cytoskeleton measured in the standard SILAC experiments. Patterns are representation of combined results for all the subunits of the protein complexes: actin (red); Arp2/3 complex (green); Cap32/34 complex (violet); myosin II complex (blue).

This means that the 2.4 fold increase in F-actin in the first phase of chemotactic response actually represents the increase in the number of actin filaments generated during this process. Obviously the Arp2/3 and Cap32/34 enrichment also directly represents the numbers of those complexes bound to actin filaments. This finally means that we can analyse those enrichment factors as direct and proportional indicators of relative amounts of each of those components, including actin filaments.

With this feature established, we can now interpret these results and see the implications. The first implication is that all of the actin filaments, generated by the Arp2/3 complex during the first phase of polymerisation, are capped by the Cap32/34 complex. Another important conclusion is that there is about 25% excess of the Arp2/3 complex molecules in relation to the newly generated actin filaments. This implies that about one quarter of all the incorporated Arp2/3 complexes do not trigger actin polymerisation.

This could be related to some specific regulatory mechanism which has not yet been described, or might be a result of the whole process reaching the maximum capacity of actin

filament generation. There are several possible limiting factors that could be depleted during the first phase of actin polymerisation, the most obvious one being actin monomer availability.

The two activities exhibited by the Arp2/3 complex, binding actin filaments and filament nucleation, have been shown to be tightly coupled and perhaps inseparable events [39, 43], but the exact mechanism linking those activities *in vivo* has not been determined.

A different interesting observation is the faster depletion rate of F-actin compared to capping protein during the depolymerisation phase. This is clearly visible at the 20 s time point where F-actin level is almost in the middle of the falling slope, while Cap32/34 is still close to the peak level. This is related to the character of actin depolymerisation process and it illustrates that actin filaments are still capped at the barbed ends, and also interconnected with other filaments by cross-linking factors, while being depolymerised from the pointed ends.

All of those actin structures, which were generated during the first 10 s after stimulation with cAMP, are completely disassembled during the next 50 s and all of the structural components of actin filaments reach almost the pre-stimulation levels at 60 s time point. During the second phase of actin polymerisation all of those components share virtually the same enrichment levels. This indicates that during this slow and localised phase each Arp2/3 complex nucleates one actin filament, which is then capped by the Cap32/34 complex.

The majority of the cytoskeletal factors detected in the SILAC experiments can be divided into three groups, based on their translocation dynamics profiles.

The most commonly found group shows a typical actin-like biphasic incorporation profile in response to cAMP stimulation. This pattern is shared by a diverse range of proteins from different classes of cytoskeletal factors including effectors and both positive and negative

regulators of actin polymerisation. It is displayed with variable amplitude and sometimes slightly different timing by all those proteins.

This type of profile can represent a passive dynamics exhibited by many ABPs, which have constant affinity to F-actin and their incorporation levels simply mirror the amount of actin filaments. It can also represent an active type of translocation dynamics, characteristic for many regulatory components and mediators of the signalling pathways, which bind to the cytoskeleton after activation following the cAMP stimulation. Due to this generic character, this profile alone is not informative enough to indicate protein's function or specificity.

The other two groups are formed by proteins that show exclusive or primary enrichment during either the first or the second phase of actin polymerisation. These types of patterns are much less common, but are more informative as they indicate the specific role of the protein in one of the two phases.

Proteins from the first group show strong translocation during the rapid phase and are almost absent during the second slow phase of actin polymerisation (Table 5.2.). Some of the proteins in this group reach the highest point of enrichment in the earliest 1 s time point after cAMP stimulation, which strongly suggests their involvement in the earliest events following detection of this chemoattractant. This characteristic is shown by two Dock180-related Rho GEFs, DocA and DocB, and also by coactosin CoaA. This inhibitor of the Cap32/34 complex activity shows strong enrichment in both phases of actin polymerisation, but was classified in the group of early factors due to its distinct peak at the 1 s time point. This observation indicates CoaA dependent inhibition of actin filaments capping during the initiation of the first phase of cAMP mediated actin polymerisation, promoting elongation of actin filaments.

It is very striking that nearly all of the factors showing unambiguous specificity to the first phase are the activators of small GTPases signalling. This however does not necessarily mean, that they all induce only the positive regulation of actin polymerisation, since Ras GTPases could also activate the effectors responsible for actin depolymerisation.

- **DocA** – Dock180-related Rac GEF from unconventional CZH family;
- **DocB** – Dock180-related Rac GEF from unconventional CZH family;
- **GxcD** – DH family Rac GEF, contains CH and VHP domains;
- **ZizC** – Zizimin-related Rac GEF from unconventional CZH family;
- **GefA** – Ras GEF (Aimless) involved in chemotaxis and activation of ACA;
- **GefR** – Ras GEF, gefR null cells do not exhibit any observable phenotype;
- **CoaA** – coactosin, ADF-H domain containing inhibitor of Cap32/34 complex.

**Table 5.2.** The list of proteins showing incorporation to the cytoskeletal fraction specific to the first phase of actin polymerisation. These factors are the most likely candidates involved in the earliest events following cAMP stimulation.

All of the Rho GAPs detected in the SILAC experiments were showing certain enrichment during the late response to cAMP stimulations and therefore were not classified into this group. Nevertheless few of them had much stronger translocation during the first phase or reached the first peak in the 1 s time point, suggesting their involvement in the earliest events. These factors included two Rac GAPs, GacR and GacV, and one putative Rap/Ran GAP protein – DDB_G0281809.

The second group of proteins showing translocation specific to the second phase of actin polymerisation was poorly represented in the standard SILAC experiments. The most prominent component of the cytoskeleton exhibiting this type of dynamics is myosin II. This major F-actin based molecular motor is responsible for force generation during several cellular processes including uropod retraction and cytokinesis. It is also involved in inhibition of the pseudopod formation at the uropod of chemotaxing cells. There were only two regulatory factors characterised by this type of dynamics detected in the standard experiments: Rho GEF – GxcQ, and Rho GAP – GacHH (Table 5.3.).

- **GxcQ** – DH family Rac GEF, contains PH domain;
- **GacHH** – Rac GAP, contains Kelch repeat domain;
- **Myosin II** – conventional filamentous myosin, actin based molecular motor involved in stabilisation and retraction of the cell uropod;

**Proteins detected only in the cross-linked SILAC**

- **RacC** – Rac GTPase, direct activator of WASP, involved in PI3K activation and translocation to the cortex in response to cAMP stimulation;
- **GxcC** – DH family Rac GEF, contains PH and ARM domains;
- **RdiA –** Rho GDI, negative regulator of Rac GTPases;
- **PLC** – involved in PIP2 depletion, negative regulator of chemotaxis;
- **PTEN** – responsible for PIP3 hydrolysis, involved in chemotaxis and cell polarity;
- **CadA –** responsible for establishment of calcium-dependent cell-cell adhesion;
- **SevA** – severin responsible for calcium-dependent F-actin fragmentation;
- **MyoK –** class I myosin regulating cortical tension and phagocytosis;
- **CtxB –** cortexilin II involved in cytokinesis and cell morphogenesis.

**Table 5.3.** The list of proteins showing incorporation to the cytoskeletal fraction exclusively during the second phase of actin polymerisation. These factors are the most likely candidates involved specifically in the formation of localised protrusions in the late response following cAMP stimulation.

The cross-linked SILAC experiment on the other hand, revealed a large group of proteins detected only in this type of preparation, which exhibited incorporation to the cytoskeleton exclusively during the late response to cAMP stimulation. Some of those proteins are regulatory factors and some are effectors involved in cytoskeletal dynamics.

One of the most interesting members of this group is a RacC protein. This Rac GTPase was found to be a functional equivalent of mammalian Cdc42 in *Dictyostelium,* responsible for direct activation of WASP leading to stimulation of actin polymerisation [299]. Importantly, the incorporation dynamics detected by our SILAC analysis showed specific enrichment during the second phase of actin response, which is in agreement with the previous studies of

this protein. Cells with a disrupted *racC* gene have been reported to show almost wild type level of the first phase of actin polymerisation, but have completely lost the second peak following cAMP stimulation [299]. This result therefore confirms the previous findings of RacC specificity to the second phase and reversibly, also serves as a validation of this dynamics pattern detected with the cross-linked SILAC experiment.

RacC was also reported in the same study to be involved in activation and translocation of PI3K to the cortex after cAMP stimulation [299]. This activity also links RacC to the second phase of actin polymerisation, which contrary to the first phase is dependent on PI3K signalling. This regulation of PI3K activity by RacC could also to some extent explain the lack of the second phase of actin polymerisation observed in *racC* null cells.

There are also two other factors classified to this group, which are related to the PI3K signalling. PLC and PTEN are both involved in the metabolism of phosphatidylinositol and are negative regulators of $PI(3,4,5)P_3$ accumulation at the membrane [125, 133, 300]. Both of those proteins are associated with the membrane, which explains their absence from the standard SILAC results, and both of them show enrichment only during the second phase in the cross-linked SILAC.

There are also few proteins involved in the organisation and turn-over of the actin cytoskeleton, which show this type of late enrichment in response to cAMP stimulation. These include: severin involved in actin filament fragmentation [301, 302]; cortexilin II belonging to the alpha-actinin superfamily of actin bundling proteins [303]; calcium-dependent cell-adhesion molecule CadA playing role in Ras mediated cell-cell adhesion formation [304, 305]; class I unconventional myosin MyoK with characterised actin filament cross-linking activity affecting cortical tension and involved in phagocytosis [306, 307].

Our SILAC results provide for the firs time a basic characterisation of the cytoskeletal factors and mediators of the signal transduction, specific for each of the two phases of cAMP

induced actin polymerisation. It does not fully delineate the differential regulation of those processes, but it contributes significantly to the identification of the components determining the independent character of the fast and slow phases of actin polymerisation.

These factors need to be further investigated and functionally characterised in order to verify their involvement in the specific regulation of those two phases of cytoskeletal dynamics.

## 5.2. *In vivo* microscopy analysis validate the SILAC results and provide additional characterisation of the cytoskeletal components translocation dynamics

In order to validate the dynamic patterns detected with the SILAC experiments and further analyse the translocation dynamics of the cytoskeletal proteins, 55 suspected components of the cytoskeleton were tagged with GFP and visualised *in vivo*. Each of the cloned proteins was tagged with GFP on both C-terminus and N-terminus separately and coexpressed with RFP-lifeact F-actin probe from a single extrachromosomal vector. *Dictyostelium* cells overexpressing those constructs were developed in suspension and imaged by confocal and TIRF microscopy.

The majority of analysed proteins showed expected localisation consistent with the previous findings and with the reported or expected function of those components. Most of them exhibited cortical localisation classified as either strong or weak, based on the level of cAMP dependent translocation from the cytosol to the cortex. The dynamics of this translocation observed *in vivo* was generally in agreement with the proteomic data, although the results from those two types of assays were not always directly correlated.

Some of the proteins with strong enrichment in the SILAC results, such as Roco7, was showing only weak translocation in the imaging analysis, while some proteins with small changes in proteomic analysis, for example GacR, was found to strongly translocate to the cortex *in vivo.* This is related to the different character of those two assays, which detect slightly different aspects of protein translocation dynamics. The SILAC results are based on the changes in protein-protein interactions and their stability in the insoluble cytoskeletal fraction only, while the imaging analysis are based only on protein localisation and can detect the protein in all cellular compartments.

Nevertheless, all of the analysed known cytoskeletal factors, which followed the actin-like profile of enrichment in the SILAC experiments, were found to colocalise with actin structures at the cortex, providing a positive validation of the quantitative proteomic analysis. The imaging data also provide a characterisation of the cellular localisation and translocation for the proteins that have not previously been visualised *in vivo,* such most of the GEFs and GAPs investigated in this study.

The strength of cAMP induced translocation from the cytosol to the cortex observed with the confocal analysis is an indication of protein's binding affinity and availability of its binding sites in the cytoskeletal structures. This factor alone cannot determine the importance of protein's function, but it can be used as a basis for comparison of proteins from the same class of cytoskeletal factors.

We postulate that for proteins playing similar function in the regulation of the cytoskeletal dynamics, the strength of cortical translocation is a good indication of their relative importance. Therefore, within the group of all the GEFs and GAPs analysed in this study, the ones showing strong incorporation to the cortex during cAMP induced actin polymerisation are likely to play more significant role in this process than the ones displaying weak

incorporation. The list of those potentially most important regulatory factors includes 6 GEFs, 3 GAPs and one protein containing both GEF and GAP domains (Table 5.4.).

Most of those were not individually investigated before. GxcA is the only conventional Rac GEF from this group, that was functionally characterised. It was shown to activate RacB during chemotaxis and to colocalise with sites of actin polymerisation at the cortex [308].

RapGAP1 is the only GAP from this group that was previously investigated. It has been shown to regulate cell adhesion at the front of moving cells via Rap1 signalling and to translocate to the cortex after cAMP stimulation [286].

Both of those proteins were found to have significant effect on actin polymerisation process and cells lacking one of them or overexpressing the mutant forms of those components were showing aberrations in actin dynamics and defects in chemotaxis [286, 308].

**GEFs showing strong cortical localisation**

- **GxcW** – DH family Rac GEF, contains PH and FYVE zinc finger domains;
- **KxcB** – DH family Rac GEF, contains PH and STE group kinase domains;
- **GxcBB** – DH family Rac GEF, contains PH and CH domains;
- **GxcA** – DH family Rac GEF, contains PH and CH domains;
- **XacB** – DH family Rac GEF, Rac GAP, contains PH domain;
- **DocA –** CZH family Dock180-related Rac GEF, contains SH3 domain;
- **DocB** – CZH family Dock180-related Rac GEF;

**GAPs showing strong cortical localisation**

- **GacR** – Rac GAP, contains BAR domain;
- **GacA –** Rac GAP;
- **RapGAP1** – Rap/Ran GAP, inhibitor of Rap1 signalling;

**Table 5.4.** The list of GEFs and GAPs showing a strong translocation to the cortex after cAMP stimulation. These regulatory factors of the small GTPases are likely to play the most significant roles in the regulation of the cytoskeletal dynamics during response to cAMP stimulation.

The interaction partners for the rest of those regulatory factors have not yet been determined. The significant role of those proteins in the regulation of the actin cytoskeleton is also indicated by the fact, that in this study cells overexpressing most of those factors were displaying observable aberrations in actin dynamics compared to the wild type cells.

A common tendency was that cells overexpressing the proteins with Rac GEF activity were exhibiting enhanced actin polymerisation at the cortex, leading to increase in membrane protrusions and somewhat motile behaviour. On the other hand, overexpression of Rac GAPs was correlated with decrease in actin polymerisation and protrusion formation, leading to less prominent second phase of chemotactic response and generally calm cortical dynamics. These observations are in agreement with the expected roles of those regulatory components, but will need to be further characterised.

TIRFM imaging provided much better spatial and temporal resolution of protein localisation and incorporation dynamics. Components binding F-actin were clearly visible in the cortical filamentous structures, while others associating for instance with $PI(3,4,5)P_3$ at the membrane or with other cortical compartments, did not exhibit filamentous patterns.

One of the most informative contributions of the TIRFM analysis and the great advantage over the confocal microscopy was the ability to precisely measure the timing of the cAMP induced translocation to the cortex in a reproducible and easily quantifiable way. This allowed identification of the fastest responding regulatory factors and determination of the precise duration of their association with the cortex. All of the regulatory proteins analysed quantitatively by TIRFM, which showed enrichment at the cortex after cAMP stimulation, could be divided into two distinct groups based on the translocation dynamics (Fig. 5.2.).

The first group consists of proteins, which show very rapid translocation to the cortex periphery, reaching their peaks at about 1-2 s after cAMP stimulation. These proteins are also very rapidly depleted after the peak of translocation and most of them return to the pre-

stimulation levels within 10 s from the starting point, even before actin reaches its peak of polymerisation (Fig. 5.2. A).

The second group contains proteins which show the same rate of translocation as the initial actin dynamics and reach their peaks at about 3-5 s after cAMP stimulation. These components are characterised by slow depletion from the cortex and most of them reach the pre-stimulation levels at the same time or slightly after actin does at 20 s (Fig. 5.2. B).

It is important to note that the actin dynamics profile used in this analysis was measured in cells overexpressing alpha actinin – AbpA, and shows some unusual characteristics. It has a distinct plateau at a rising slope of polymerisation phase and reaches the peak at 10 s after the cAMP stimulation, which is about two times slower than the dynamics measured by the confocal microscopy, showing the first peak at 5 s for almost all the clones analysed.

This characteristic is most likely related to the overexpression of AbpA or alternatively to some other unidentified phenomenon. It is presumably not the best representation of the universal actin dynamics for TIRFM imaging, but due to the time constrains these measurements could not be repeated. Nevertheless, despite the nonuniversal character of this actin polymerisation profile, it can still serve as a good reference of incorporation timing for other proteins, allowing separation of the fast and slow factors.

Each of those groups contains both positive and negative regulators of actin polymerisation. The first group includes two GEFs – DocA and DocB, and two GAPs – GacR and DDB_G0284825 Rap/Ran GAP.

DocA and DocB display almost the same timing of association, which is consistent with their dynamics patterns measured in the SILAC experiments. They reach the peak of enrichment at 1.5 s after stimulation, which is followed by a rapid depletion reaching pre-stimulation levels at around 7 s time point. This result indicates that those two unconventional Rac GEFs are the earliest responding activators of the actin polymerisation after cAMP stimulation, suggesting that they might be involved in triggering the first phase of the chemoattractant

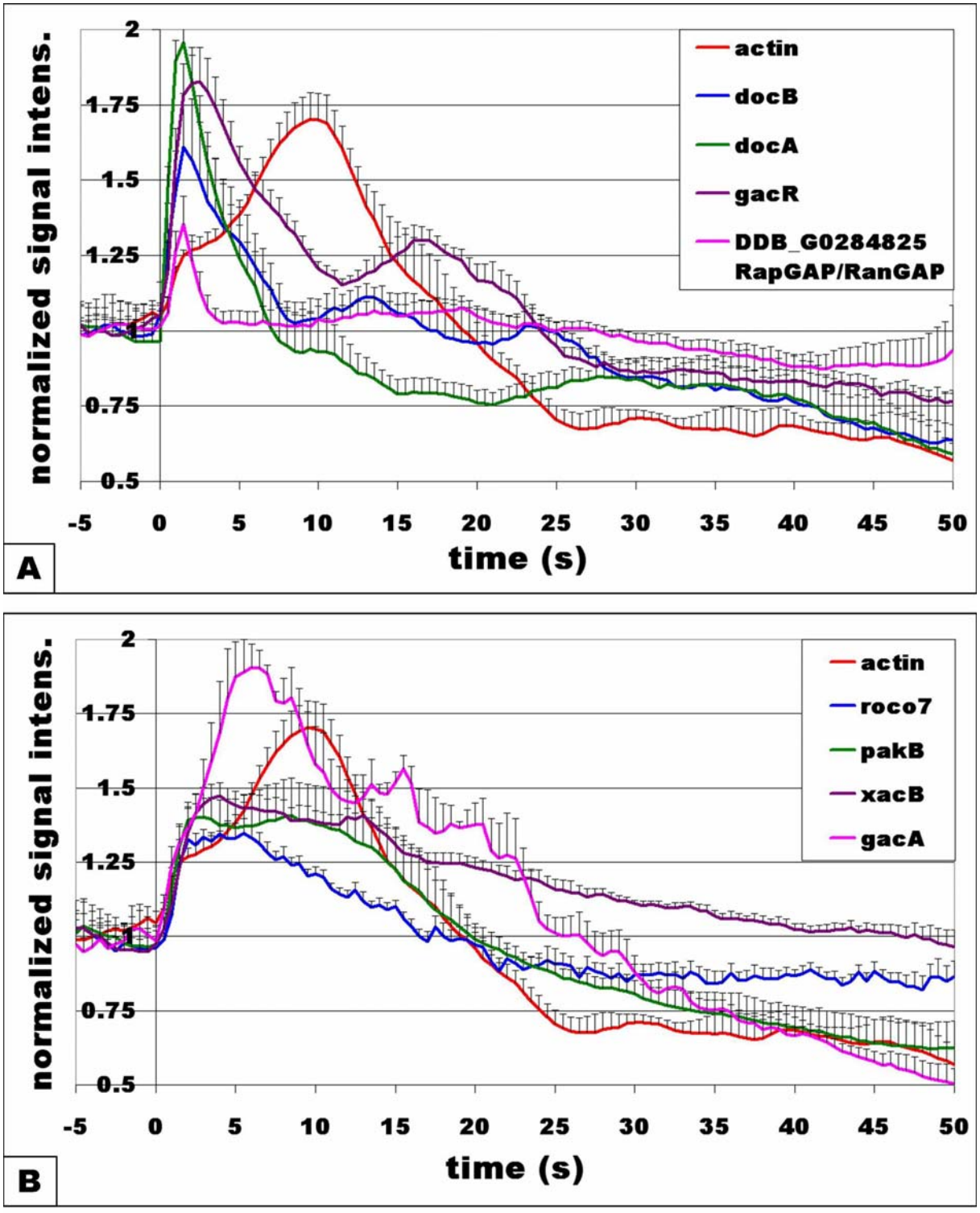


**Figure 5.2.** Translocation dynamics of the cytoskeletal regulatory components measured by the TIRFM analysis. Graphs represent a time plots of the GFP fluorescence intensity changes following cAMP stimulation. Each curve is an average of three measurements of different cells from a single imaging session. Individual measurements for each construct were first normalised to their average, then combined and finally normalised to the prestimulation period. Standard errors were calculated adequately to these normalisations. **A**) Proteins showing the fastest response to the cAMP stimulation. They reach the peak of enrichment at 1.5-2 s followed by a rapid depletion. **B**) Proteins showing slower rate of incorporation, equal to the actin dynamics. They reach the peak of translocation at 3-6 s after cAMP stimulation followed by a slow depletion usually matching the actin depolymerisation rate.

induced actin polymerisation. This very rapid character of translocation dynamics displayed by the Dock proteins is in agreement with the observations made by a different research group (Douwe Veltman and Robert Insall, personal communications).

DDB_G0284825 Rap/Ran GAP shows even more transient translocation to the cortex. It reaches peak at the same time as Dock proteins, but it shows much lower intensity and is completely depleted at 4 s. GacR shows slightly slower pace of incorporation reaching the peak at 2 s after stimulation, which lasts longer and has slower depletion rate the other proteins from this group. It displays biphasic dynamics, which is unusual for TIRFM analysis. It reaches close to pre-stimulation level at 12 s followed by a minor second peak at 16 s and then the final depletion lasting till the end of the measurement.

Proteins from the second group show slower enrichment kinetics, which matches the initial actin polymerisation rate. They reach the peak of translocation at 3-5 s after cAMP stimulation and exhibit a relatively long lasting occupation at the cortex, covering the whole period of the first phase of actin polymerisation. All four proteins belonging to this group of translocation dynamics represent cytoskeletal regulatory factors, but only two contain GEF or GAP domains.

Roco7 is a multidomain complex protein acting as a complex signal transduction unit. It contains Ras-like GTPase domain called Roc, which regulates the activity of the protein kinase domain sitting further downstream on this protein. The downstream effectors of this kinase have not been identified. This regulatory factor shows the lowest enrichment and shortest occupancy at the cortex from all the proteins in this group (Fig. 5.2. B). Its depletion starts at 6 s and reaches the pre-stimulation level at 20 s after cAMP stimulation, which correlates with the actin depolymerisation phase also reaching the pre-stimulation level.

PakB is another protein kinase showing this type of translocation dynamics. It belongs to the family of p21-activated protein kinases, which are regulated by the Rac GTPases. It is known

to interact directly with several Rac GTPases in *Dictyostelium* and to regulate activity of class I myosin MyoD [101, 271]. This protein reaches the peak of incorporation at 3 s and shows a plateau lasting until 12 s and its depletion matches exactly the timing of actin depolymerisation (Fig. 5.2. B). Another protein forming a very similar plateau is XacB, containing both Rac GEF and Rac GAP domains. The unusual characteristic of this protein's translocation is the slow rate of depletion. Even though the depletion phase starts at the same time as for PakB – around 13 s after stimulation, it lasts much longer than for any other protein in this group and reaches the pre-stimulation level at around 40 s, which is much later than the actin depolymerisation phase has finished.

GacA is the last protein from this group and it shows the highest amplitude of enrichment in response to cAMP stimulation. This Rac GAP reaches the peak of incorporation at 5 s and has relatively short occupation period in the cortex. Interestingly, this protein shows slightly biphasic depletion phase, similar to that of GacR in the first group discussed earlier. It is first depleted to about 1.5 of pre-stimulation signal intensity at 12 s and then shows very small secondary peak around 16 s, which is then followed by the final depletion lasting till the end of the measurement (Fig. 5.2. B). This second peak is much less prominent than the one showed by GacR, but it has the same timing corresponding to actin depolymerisation phase. This indicates that those two inhibitors of Rac signalling and potentially also XacB, showing prolonged occupation at the cortex relative to actin, are likely to play role in regulating actin depolymerisation phase and therefore adaptation of the cytoskeletal response to cAMP stimulation.

Proteins from this group, showing translocation timing correlating with actin polymerisation during the first phase, are most likely to be involved in maintenance of actin cytoskeleton dynamics and some of them in promoting a shift from polymerisation to depolymerisation mode of action.

There are few interesting insights into the nature of the first phase of cAMP-induced actin polymerisation coming from these observations. The first and most general one is that the regulatory factors can be divided into two distinct groups of translocation dynamics. The ones showing very rapid and transient incorporation into the cortical cytoskeleton are most likely responsible for triggering the actin polymerisation response. The ones showing slower and long lasting translocation are supposedly involved in regulating persistence and timing of this response. We have investigated only a fraction of all the regulatory factors functioning in this process and presumably many others would fall into one of those groups after this type of analysis.

Another important observation, which may help to understand the character of the first phase, is the presence of both activators and inhibitors of small GTPases in each of the groups showing different translocation dynamics. In the first group of early regulators there are two Rac GEFs – DocA and DocB, and two GAPs – Rac GAP GacR and Rap/Ran GAP DDB_G0284825. This indicates that both excitatory and inhibitory reactions are triggered at the same time and the response observed in actin polymerisation is the outcome of balancing those two contrary activities.

An intuitive way to understand the detailed process of chemoattractant mediated actin polymerisation is by describing the response profile in terms of an excitation adaptation mechanism. The first phase of actin polymerisation represents the primary response to cAMP stimulation followed by adaptation to this signal, which allows the secondary phase to occur and drive the chemotactic movement. This type of excitation response coupled with the adaptation to the stimulus is a common characteristic of the majority of signal induced reactions. In general the excitatory pathways generating the response are easier to investigate and therefore much better understood, while the inhibitory counterparts necessary for the adaptation remain elusive in most systems analysed.

One of the best established models describing this type of response coupled with adaptation is shown in Figure 5.3. It involves simultaneous activation of reactions leading to excitation and inhibition of the process. The excitation kinetics rises rapidly in response to the instantaneous change in signal and reaches a plateau level determined by the signal strength. The adaptation is characterised by a slower kinetics eventually reaching the same level as the excitation. The resulting actin polymerisation is proportional to the difference between excitation and adaptation. The result is a transient actin polymerisation response.

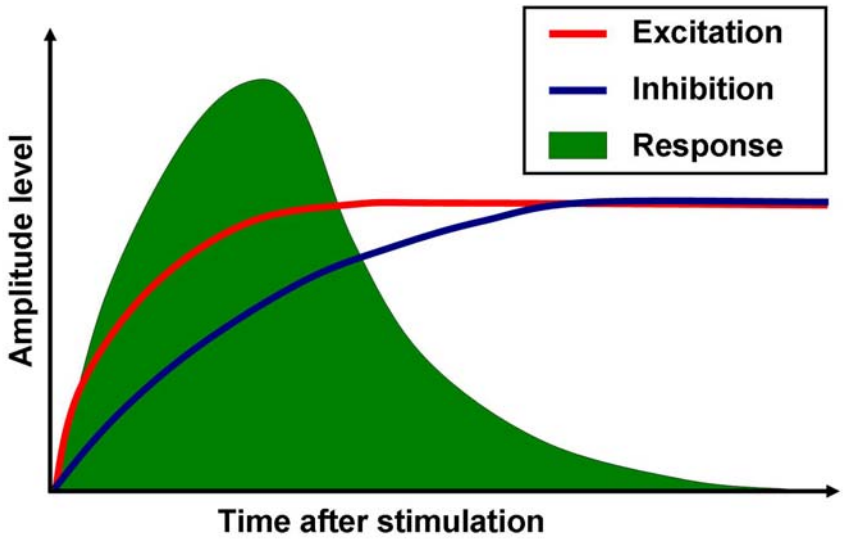


**Figure 5.3.** General model of the response perfect adaptation to stimulus. Both excitation and inhibition of the response are triggered at the same time by stimulation. These two processes have different kinetics and excitation reaches the plateau level much faster activating the response reaction. The inhibition rises slowly influencing the response level. When the inhibition reaches the same level as excitation the response is finished.

This model of adaptation has been proposed for several cellular processes. One of the best described is the adaptation of the adenylyl cyclase (ACA) during cAMP relay response in *Dictyostelium.* In this process both positive and negative regulators of ACA are thought to be activated by the same signal of $PI(3,4,5)P_3$ accumulation at the membrane, generated by PI3K after cAMP stimulation, and regulate ACA activity with different kinetics [309].

Our analysis of the translocation dynamics partially supports this model of adaptation of actin polymerisation response. We detect both activators and inhibitors of Rac signalling, regulating the actin polymerisation response, enriched at the cortex in almost the same time. We need to note again, that the translocation observed in our assay does not equal the activity of those components, which can differ in regulatory kinetics even when sharing the same incorporation dynamics.

Nevertheless, we can safely assume that the regulatory effect of one factor cannot exceed its occupancy at the site of the process being regulated, which in this case is the cell cortex. This generates a discrepancy between our results and the proposed model. All of the regulatory factors showing the fastest response to cAMP stimulation, display only transient incorporation to the cortex and therefore cannot provide the regulatory effect throughout the whole process of actin polymerisation. This indicates, that if this model of response adaptation is correct for this system, it requires the excitation function to be transferred from the earliest responding factors that initiate the response to the other factors, which are present at the cortex during the whole period of actin polymerisation and maintain the response. The inhibitory factors, GacR and GacA, might also exhibit similar type of temporal differentiation of activity. Even though they show a larger overlap of occupancy at the cortex than the excitatory components, the main peak of GacR is almost finished at 5 s which is when GacA reaches the peak of translocation. So these factors could also together provide a continuous inhibitory activity counterbalancing the excitatory reactions.

An alternative way of explaining the process of cAMP induced actin polymerisation on a different, more mechanistic level does not necessarily require the constant presence of excitatory reactions. It is plausible, that a single short peak of excitation generating a global activation of the Arp2/3 complex throughout the cell cortex, could initiate the process of formation of new filaments, which would then continue elongating and thereby increase the

mass of polymerised actin until inhibited by the capping protein, without the need of continuous excitation. In this model the excitation could be only transient and followed almost directly by the inhibition, which correlates closely with our results (Fig. 5.4.).

There is also another characteristic of actin polymerisation, which makes the adaptation of this response more complex processes. In actin polymerisation response, similarly to ACA activation, it is not enough to switch off the activity to generate the adaptation. During the cAMP relay response the cAMP produced needs to be removed, which is done by the constitutively active cAMP phosphodiesterases. In similar manner actin filaments, once polymerised, need to be actively depolymerised. This means that the perfect adaptation of the actin polymerisation response requires involvement of a different set of components, which will reverse the effects of this process. This depolymerisation process could be mediated by a constitutive activity of ADFs or could be more directly regulated during the adaptation phase.

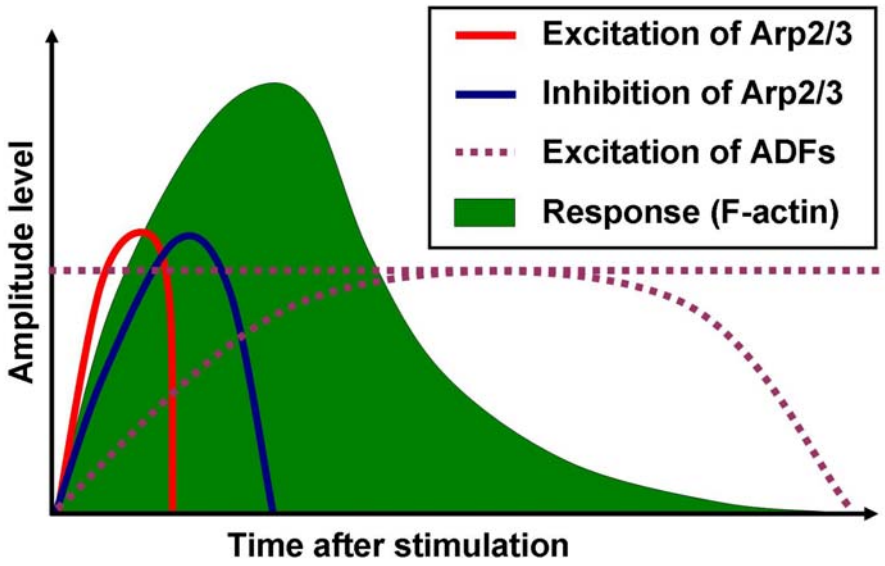


**Figure 5.4.** Mechanistic model of the perfect adaptation in the actin polymerisation response. Both excitation and inhibition of the Arp2/3 complex are transiently triggered at the same time by stimulation. These two processes have different kinetics and excitation reaches the peak level faster then inhibition, generating a short period of Arp2/3 activation and incorporation. This triggers the actin polymerisation process, which continues as an independent spontaneous reaction until inhibited by the capping protein. The adaptation of this system is mediated by the actin depolymerisation process, which is driven by ADFs. The activity of ADFs could be constitutive or could also be triggered by the initial signal and show slower kinetics.

The standard SILAC results did not detect any profound enrichment of cofilin, which is the major and most abundant ADF, during the depolymerisation phase (data not shown). The cross-linked SILAC experiment detected slightly higher incorporation of cofilin at 20 s corresponding to the depolymerisation phase, than at the peak of the first phase. This might suggest specific activation during the depolymerisation phase, but these data need to be further validated.

It is important to note that is a mechanistic model based on the results of the translocation dynamics analysis. The reactions responsible for excitation and inhibition of the Arp2/3 complex and excitation of ADFs represented in this model, are themselves regulated by some upstream regulatory reactions. This means that the translocation and activation of the components leading to downstream regulation of the actin polymerisation response, such as DocA, DocB or GacR, are all individually regulated responses to cAMP stimulation with their own excitatory and inhibitory reactions. All of those responses display their own adaptations (cortical enrichment of those proteins is followed by depletion reaching pre-stimulation levels) and it is likely, that their individual regulatory mechanisms follow the general model for response adaptation described before.

In this way of looking at the process of cAMP induced actin polymerisation, there is a whole layer of different individual responses to this stimulus, all showing different timing and adaptations, which function as regulatory reactions controlling all the aspects of actin polymerisation. The regulation of Arp2/3 will have its own activation and inhibition reactions, Cap32/34 will presumably be also individually regulated and similarly, all the factors involved in actin depolymerisation. From this point of view, the first phase of cAMP induced actin polymerisation emerges on a higher level from a multitude of individually controlled responses of different regulatory components to this global stimulation.

The model presented in the Figure 5.4., which requires only transient excitation of the Arp2/3 complex to drive the whole process of actin polymerisation, is based on the TIRFM imaging analysis of the translocation dynamics of different regulatory factors, especially DocA, DocB and GacR. It is also in agreement with the spontaneous character of the actin filament elongation following the nucleation by Arp2/3.

On the other hand this model is not supported by the SILAC analysis, which reveals gradual incorporation of the Arp2/3 complex during the whole period of the first phase, following similar dynamics as the changes of F-actin abundance. This model would predict an early peak of the Arp2/3 enrichment, forming a plateau until the depolymerisation phase.

This indicates that the whole process is more complex and that this simple model needs to be supplemented with additional regulatory levels. DocA and DocB do not activate the Arp2/3 complex directly, but this stimulation needs to go through Rac GTPases to NPFs, such as Scar and WASP, to eventually reach the actin nucleator. It is possible that this transient activity of Dock proteins detected by TIRFM analysis is capable of generating a long lasting activation of downstream NPFs, which will then activate Arp2/3 until the peak of the first phase. Alternatively, this activation can be maintained by other regulatory factors after the initial triggering ones have been depleted, as speculated before.

It is clear that these analyses are just a starting point of the long process of elucidating the mechanisms regulating the actin polymerisation response to cAMP stimulation. Many more components need to be individually investigated in order to provide further insight and feed the models of this process.

Nevertheless, we can already say which of the components are most likely to play certain roles during the cAMP induced actin polymerisation. DocA and DocB are the strongest candidates for the initial triggering of the response. XacB, PakB and Roco7 are likely to be involved in maintaining the regulatory signals and potentially contributing to the shift from

polymerisation to depolymerisation reactions. Finally, GacR and GacA are the most likely components involved in the inhibition of Rac signalling, switching off the whole excitation and allowing for the adaptation to take place.

The TIRFM imaging revealed that several of the analysed proteins were showing very distinct incorporation dynamics. These factors did not exhibit an increase in signal intensity upon cAMP stimulation, but instead they showed sudden drop of fluorescence to about 75% of the pre-stimulation level. This loss of the fluorescence intensity was typically followed by a gradual recovery showing different timing and dynamics patterns (Fig 5.5.).

The most likely explanation of this unusual behaviour is related to the specificity of this type of microscopy. TIRFM illuminates effectively only the very outer layer of about 200 nm of the cell cortex, which generally corresponds in scale to the cortex periphery newly generated during the first phase of actin polymerisation. This means that the proteins, which are incorporated to the cortical cytoskeleton but do not translocate to the newly polymerised fraction, will be pushed inside the cell and move partially out of the TIRFM illumination field, resulting in this type of fluorescence intensity decrease.

This interpretation is supported by the fact that the drop of signal intensity shows a very similar timing in all of those proteins, and it correlates with the initial actin polymerisation response. The recovery of this signal in case of ZizA is clearly correlated with actin depolymerisation at the end of the first phase, and it is one of two proteins that actually fully recover to the pre-stimulation level. The second one is MhcA, which is the only protein in this group showing strong enrichment in the late response following the initial drop of signal. In the other three proteins, this recovery is followed by a secondary fluorescence depletion, which does not recover and might represent a protein specific translocation dynamic required for a specific funtion.

Interestingly, all of components showing depletion were found to localise to cortical filamentous structures as observed by TIRFM and all of them showed actual translocation to the cortex revealed by the confocal imaging and also the SILAC analysis.

This leads to some interesting implications. All of those proteins apparently translocate to the cortex after cAMP stimulation and bind to actin filaments, but they are incorporated exclusively to the pre-existing cortical structures and do not localise to the very periphery of the cortex generated during the first phase of actin polymerisation. This indicates that these factors are playing role in processes that are specific to the pre-existing actin cytoskeleton and are not involved in the cAMP induced actin polymerisation.

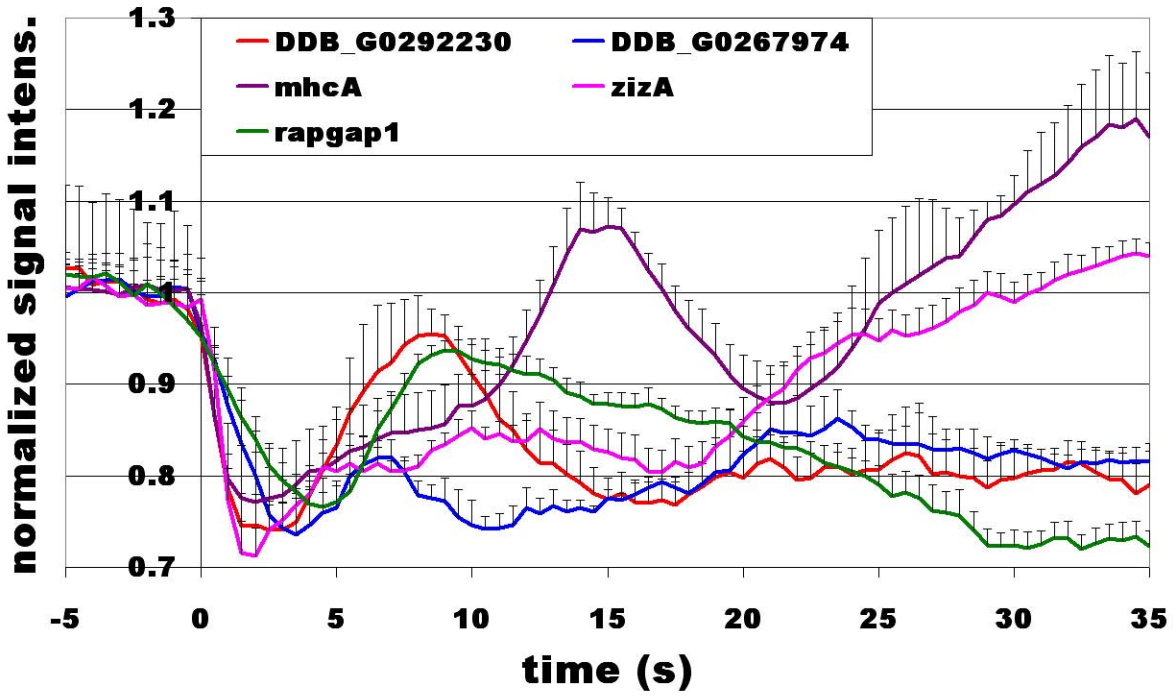


**Figure 5.5.** Translocation dynamics of the cytoskeletal components measured by the TIRFM analysis. These proteins revealed sudden drop of fluorescence intensity after cAMP stimulation, correlating with the burst of actin polymerisation. Graphs representing a time plots of the GFP fluorescence intensity changes following cAMP stimulation were averaged from three measurements and normalised as described for Figure 5.2.

This type of differential mechanisms working on those cortical actin structures of distinct origin have not yet been reported. It is likely caused by the fact that it is very challenging to distinguish *in vivo* between actin filaments that existed before and those generated after cAMP stimulation. The observation that this TIRFM based assay can indirectly distinguish

between those two types of actin structures was purely coincidental and it enabled the discovery of this novel class of cytoskeletal factors interacting or modulating specifically pre-existing cortical structures.

Three out of five proteins in this group share another interesting characteristic, which might relate to their specific functions. MhcA and two of the unknown proteins classified in this group, DDB_G0292230 and DDB_G0267974, are all found to localise to the uropod of moving cells as observed with the confocal analysis. Proteins showing this type of localisation are likely to be involved regulation of cell polarity and/or stabilisation of the cytoskeleton at the uropod and play a role in inhibition of pseudopod formation in this part of the cortex. They might also be involved in actin turn-over or in regulation and localisation of other components fount in this compartment such as myosin II filaments.
All of those potential functions are interesting candidates for processes that would need to be carried out specifically at the inner cortex composed of pre-existing cytoskeletal structures. The fact that those two proteins of unknown function show the same type of localisation as MhcA to the inner cortex at the cell uropod, suggests that they might be involved in some aspect of control of myosin II filament dynamics.

Another possibly important function of proteins from this group is the regulation of stability of the cytoskeletal structures. As discussed before, the regulation of the actin depolymerisation process during the response to cAMP stimulation is not well understood and we do not find reliable data elucidating this process in our analyses. One readily detectable, but not necessarily intuitive observation of this process shows that it brings the F-actin abundance back to pre-stimulation exactly at the end of the first phase. This suggests strongly that only the newly generated filaments are depolymerised, while the pre-existing filaments are not affected by this process. It is not clear why this global actin

depolymerisation phase occurring at the whole cortex would leave the old structures intact, while degrading the newly synthesised ones, rather than disassembling all of them.

Such character of depolymerisation specific only to the new filaments is also not in agreement with the general view of the ADF/cofilin dependent actin turn-over. This major depolymerising factor shows high affinity to older ADP-rich actin filaments and drives their depolymerisation, while fresh ATP-rich actin filaments are not processed by this protein [36]. This would suggest that the inner cortical structures based on older actin filaments, should be more susceptible to the actin depolymerisation process.

Nevertheless, our SILAC results reveal that all of the major structural constituents of the actin filaments, including Arp2/3, Cap32/34 and actin itself, are brought down to pre-stimulation levels, which is a strong indication that only the pre-existing structures are left intact. TIRFM analysis of the components localised to the inner cortex generally supports this notion. Firstly the structures labelled by the above described proteins do not show dramatic changes in shape, which would be noticeable if they were disassembled. Secondly by the correlation of the signal recovery for some of those proteins with the actin depolymerisation phase.

All these observations imply that there is some specific regulation during the depolymerisation phase, targeting this process to the freshly polymerised filaments and protecting the older structures. This function could be performed by this novel class of cytoskeletal components translocating specifically to the inner cortex. These proteins could stabilise the pre-existing actin filaments preventing their depolymerisation, or they could otherwise locally inhibit the factors responsible for actin filament disassembly. Alternatively, they could locally promote the depolymerisation process to occur on the border of pre-existing and cAMP induced structures, which would affect only the latter ones.

To summarise the whole picture of the biphasic process of the chemoattractant induced actin polymerisation, which emerges from these wide analysis of protein translocation dynamics, we will go through the major detected events.

Stimulation with cAMP triggers several signal transduction pathways, which lead to activation of the major actin nucleator the Arp2/3 complex. There are many positive regulators that show incorporation to the cortex during the first phase of actin polymerisation. The ones that exhibit the fastest translocation, and therefore are the most likely to act as the initial activators, are DocA and DocB Rac GEFs. These proteins show very transient incorporation to the cortex and they are followed by another set of regulatory factors, including XacB, PakB and Roco7, which show slower kinetics and longer occupancy lasting until the end of the first phase.

Activation of the Arp2/3 complex drives the whole process of actin polymerisation, leading to about 2.4 fold increase in F-actin abundance, which is proportional to the number of actin filaments. At the same time the Arp2/3 complex shows 3.2 fold enrichment, this indicates that about 25% of those nucleators incorporated to the cytoskeleton do not generate new actin filaments. This might be a regulated feature or result from some factors such as the actin monomers becoming limiting.

The major capping protein – Cap32/34, is likely to be inhibited at the very beginning of the first phase by CoaA, which then dissociates from the cytoskeleton before the peak of actin polymerisation, allowing the Cap32/34 complex to terminate filament elongation. Virtually all of the actin filaments are capped by the Cap32/34 complex and the entire polymerisation process stops after about 5 s at room temperature and 10 s at 12°C. At this point the excitatory reactions are switched off by Rac GAPs. Out of all the GAPs analysed in this study, GacR and GacA seem to be playing the most significant role in this process.

This rapid increase in the amount of actin filaments results in binding of a multitude of proteins associated with those structures, including many ABPs and regulatory factors.

The burst of actin polymerisation is then followed by the reverse reaction driving the disassembly of the generated filaments. The regulation of this depolymerisation phase is not well understood and there are not very many new insights into this process coming from our analysis. Depolymerisation appears predominantly to affect the newly generated filaments, leaving the older pre-existing actin structures intact. Such a specific targeting of this reaction could be mediated by the proteins translocating only to those pre-existing structures at the inner cortex Five proteins were discovered to exhibit this type of localisation in this study, including MhcA, RapGAP1, ZizA and two previously uncharacterised proteins DDB_G0292230 and DDB_G0267974.

At the end of the depolymerisation phase the whole actin cytoskeleton reaches perfect adaptation, which means that it has essentially the same composition as before cAMP stimulation. From this point onwards the process of cAMP induced actin polymerisation is taken over by a very different regulatory machinery. There are several regulatory factors that show specific enrichment during this phase, including RacC, GxcC, PLC and PTEN. This phase is thought to be mainly dependent on the PI3K signalling, which leads to local accumulation of $PI(3,4,5)P_3$ at the membrane guiding other components driving actin polymerisation.

Actin polymerisation during this phase is also driven by the Arp2/3 complex, but it leads to a completely different outcome. In this slow and long-lasting phase actin is polymerised only at local sites at the cortex, generating membrane protrusions and driving the actual chemotactic cell movement. Most of the proteins translocated to the cortex during the first phase are now colocalising with those local actin-based structures.

The regulatory network involved in this part of chemotactic response has been well characterised and it is very similar to the one operating at the pseudopod formation during a random walk in the absence of any chemoattractant stimulation [143]. Therefore it is

adequate to describe this phase of actin polymerisation as a guided regulation of a random motion.

The fact that the response is long lasting and low amplitude is the result of the process of pseudopod formation is only loosely coupled to the initial stimulus and happens at discrete times in different cells giving rise to slow, low amplitude kinetic in the population average.

In individual cells the response is fast as shown in several experiments. The time delay may reflect the pseudopod cycle (3/minute) that occurs independently of cAMP stimulation and may be part of the random movement response.

## 5.3. *In vivo* microscopy analysis validate the dynamics of several novel cytoskeletal components detected in the SILAC experiments

Apart from a detailed study of the translocation dynamics of many proteins simultaneoulsy in the same experiment this project was also aimed at identification of novel cytoskeletal components.

About 25% of all the proteins identified in the SILAC experiments, were proteins of unknown function. Most of those unknown proteins were showing changes in abundance following cAMP stimulation. 54 of those proteins, showing the strongest and most reliable patterns of translocation dynamics, were tagged with GFP and analysed by confocal and TIRFM imaging.

Most of those proteins revealed localisation to different cellular compartments and did not show any colocalisation with the cortex. This analysis led to identification of 3 novel

microtubule-associated proteins, 5 novel proteins localising to the contractile vacuole network, 16 novel vesicular proteins and 12 novel nuclear markers. There are few possible reasons for the changes in abundance of those factors detected by the SILAC analysis. Some of them might represent a real interaction with the cytoskeleton and some might be related to an unspecific co-purification for instance through trapping in the insoluble fraction.

There were also 12 proteins, which showed either strong or weak cortical localisation (Table 5.5.). 4 of those proteins had previously identified actin binding domains by sequence homology analysis, and 2 other proteins were identified as GAPs. The remaining 6 proteins have not been previously characterised as potential cytoskeletal factors.

6 of those proteins showing strong translocation to the cortex are most likely to play significant roles in the cytoskeleton dynamics. There are two proteins in this group containing ADF-H domains, suggesting that they might be involved in actin depolymerisation. Another factor showing strong cortical localisation is a WASP-related protein, which might be involved in activation of the Arp2/3 complex.

One of the most interesting proteins identified as cortical components is the homolog of Fry proteins. This family is suspected to play important roles during development of higher organisms, including humans, but the mechanism of action is poorly understood. We have found that Fry homolog is localised at the cell boundary at substrate attachment sites. This is presumably a multi-pass transmembrane protein. It is mostly enriched at the uropod of polarised cells and is clearly involved in establishing cell attachment to the substrate.

Two other proteins from this group were also showing localisation to the uropod. These were the factors discussed earlier as members of the characterised group of proteins translocating specifically to the inner cortex after cAMP stimulation.

The list of components showing weak cortical localisation includes two proteins containing GAP domains. One of them, DDB_G0284825 with Rap/Ran GAP domain, belongs to the group of proteins showing the fastest response to cAMP stimulation.

**Novel cytoskeletal components showing strong cortical localisation**

- **DDB_G0283827** – WASP-related protein, contains WH2 and CRIB domains;
- **DDB_G0277615** – contains 3 ADF-H actin binding domains;
- **DDB_G0295683** – contains ADF-H and LIM domains, localised at the uropod;
- **DDB_G0275305** – Fry homolog, localised at the uropod bottom cell boundary;
- **DDB_G0267974** – contains CH3 domain, localised at the uropod inner cortex ;
- **DDB_G0292230 –** contains regions of similarity to Rho GAPs and calcium transporting ATPases, localised at the uropod inner cortex;

**Novel cytoskeletal components showing weak cortical localisation**

- **DDB_G0279449** – contains VHP actin binding domain;
- **DDB_G0284825 –** contains Rap/Ran GAP domain;
- **DDB_G0274211** – contains Ras GAP domain;
- **DDB_G0280261 –** contains LisH/WD40 repeat domain;
- **DDB_G0293032 –** contains AAA+ ATPase and WD40 domains;
- **DDB_G0293724 –** contains regions of similarity to dynein heavy chains.

**Table 5.5.** The list of proteins of unknown function showing a strong or weak translocation to the cortex after cAMP stimulation. Some of those proteins have identified actin binding domains or other domains potentially involved in interaction with the cytoskeleton.

All of the unknown proteins with this type of localisation were showing uniform distribution at the cortex. On the other hand, surprisingly large proportion (4 out of 6) of the unknown proteins showing strong translocation to the cortex were found to localise to the uropod in polarised cells (Fig. 5.6.). Another protein, which was unexpectedly found to accumulate at

the uropod, was Kif5. This protein was previously found to localise to the cell cortex and in this study we further characterised this localisation, showing that Kif5 is found at the uropod of chemotaxing cells.

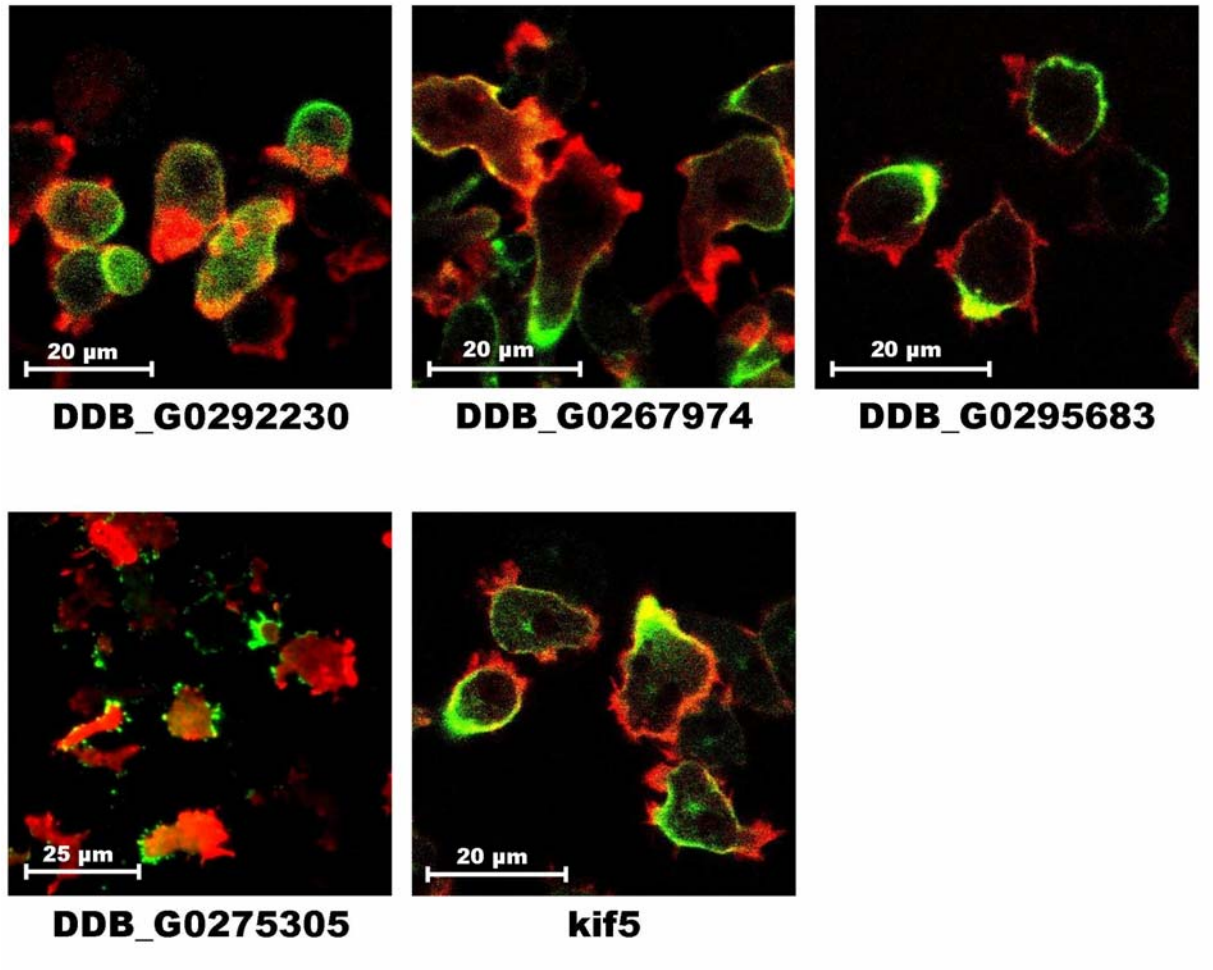


**Figure 5.6.** Protein showing cortical localisation at the uropod of polarised cells. Four of the unknown proteins were found to exhibit this characteristic localisation. Kif5 is a known protein, which was characterised as cortical protein and here we show that it is predominantly found at the uropod. All of the pictures represent confocal images, except for the DDB_G0275305 which was visualised by TIRFM.

All those proteins associated with the uropod, are most likely involved in one of the cellular processes that would require this type of localisation. They might be involved in establishing or maintaining cell polarisation, in regulation of other component's translocation or might play a role in stabilisation of the cytoskeleton and inhibition of lateral pseudopod formation.

In this study we have identified and briefly characterised a number of novel cytoskeletal components. They need to be further investigated individually by functional analysis in order to understand their roles in the cytoskeletal dynamics.

The next step in this process will be generation of knock-out strains for each of those factors followed by developmental phenotype characterisation and quantitative analysis of actin dynamics. In order to identify their interaction partners and regulatory factors, a series of immuno-precipitation preparations coupled with proteomic analysis will be performed.

Some of those factors might play a substantial role in the cytoskeleton, and their investigation and are expected to provide a new insight into the process of chemotaxis.

# ACKNOWLEDGMENTS

I would like to especially thank Prof. Kees Weijer, who had substantial influence on the final shape and outcome of this study. His close supervision and eagerness to discuss all the relevant matters, from technical issues to understanding the complexity of the entire system, provided an invaluable guidance throughout the whole period of this project.

I would also like to thank Dr. Kim Dale and Prof. Alan Fairlamb who supported me as my Thesis Committee and provided useful advices.

Many thanks go to the local proteomics experts, especially Sara ten Have who helped me patiently with countless technical problems. In this matter I would also like to thank all the stuff running the proteomics facility, especially Douglas Lamont and Kenny Beattie, who always ensured the high quality of MS analysis.

Finally I would like to thank everyone in the Weijer Lab, including all the present and past members, who always created a friendly atmosphere and served with useful assistance whenever needed.

# DECLARATION BY CANDIDATE

I hereby declare that this thesis is my own work and it presents my original research. It has not been submitted anywhere for any award. Whenever contributions of others are involved, every effort is made to state it clearly and references to the literature are provided.

Signature: …….

Date: ……

# DECLARATION BY SUPERVISOR

I hereby declare that this thesis is from the student's own work and effort and it presents his original research. It has been submitted with my approval.

Signature: …….

Date: ……

# 6. References


1. Vasiev, B., et al., *Modeling gastrulation in the chick embryo: formation of the primitive streak.* PLoS ONE, 2010. **5**(5): p. e10571.
2. Rubel, E.W. and K.S. Cramer, *Choosing axonal real estate: location, location, location.* J Comp Neurol, 2002. **448**(1): p. 1-5.
3. Martin, P. and S.M. Parkhurst, *Parallels between tissue repair and embryo morphogenesis.* Development, 2004. **131**(13): p. 3021-34.
4. Thelen, M., *Dancing to the tune of chemokines.* Nat Immunol, 2001. **2**(2): p. 129-34.
5. Moser, B. and P. Loetscher, *Lymphocyte traffic control by chemokines.* Nat Immunol, 2001. **2**(2): p. 123-8.
6. Tarrant, T.K. and D.D. Patel, *Chemokines and leukocyte trafficking in rheumatoid arthritis.* Pathophysiology, 2006. **13**(1): p. 1-14.
7. Le, Y., et al., *Chemokines and chemokine receptors: their manifold roles in homeostasis and disease.* Cell Mol Immunol, 2004. **1**(2): p. 95-104.
8. Charo, I.F. and M.B. Taubman, *Chemokines in the pathogenesis of vascular disease.* Circ Res, 2004. **95**(9): p. 858-66.
9. Wardlaw, A.J., et al., *Eosinophils in asthma and other allergic diseases.* Br Med Bull, 2000. **56**(4): p. 985-1003.
10. Murphy, P.M., *Chemokines and the molecular basis of cancer metastasis.* N Engl J Med, 2001. **345**(11): p. 833-5.
11. Condeelis, J., J. Jones, and J.E. Segall, *Chemotaxis of metastatic tumor cells: clues to mechanisms from the Dictyostelium paradigm.* Cancer Metastasis Rev, 1992. **11**(1): p. 55-68.
12. Condeelis, J., R.H. Singer, and J.E. Segall, *The great escape: when cancer cells hijack the genes for chemotaxis and motility.* Annu Rev Cell Dev Biol, 2005. **21**: p. 695-718.
13. Devreotes, P.N. and S.H. Zigmond, *Chemotaxis in eukaryotic cells: a focus on leukocytes and Dictyostelium.* Annu Rev Cell Biol, 1988. **4**: p. 649-86.
14. Marin, I., W.N. van Egmond, and P.J. van Haastert, *The Roco protein family: a functional perspective.* FASEB J, 2008. **22**(9): p. 3103-10.
15. Goldberg, J.M., et al., *Identification of four candidate cGMP targets in Dictyostelium.* Proc Natl Acad Sci U S A, 2002. **99**(10): p. 6749-54.
16. van Haastert, P.J., I. Keizer-Gunnink, and A. Kortholt, *Essential role of PI3-kinase and phospholipase A2 in Dictyostelium discoideum chemotaxis.* J Cell Biol, 2007. **177**(5): p. 809-16.
17. Chen, L., et al., *PLA2 and PI3K/PTEN pathways act in parallel to mediate chemotaxis.* Dev Cell, 2007. **12**(4): p. 603-14.
18. de Hostos, E.L., et al., *Coronin, an actin binding protein of Dictyostelium discoideum localized to cell surface projections, has sequence similarities to G protein beta subunits.* EMBO J, 1991. **10**(13): p. 4097-104.
19. Traynor, D., R.H. Kessin, and J.G. Williams, *Chemotactic sorting to cAMP in the multicellular stages of Dictyostelium development.* Proc Natl Acad Sci U S A, 1992. **89**(17): p. 8303-7.
20. Weijer, C.J., *Dictyostelium morphogenesis.* Curr Opin Genet Dev, 2004. **14**(4): p. 392-8.

21. Weeks, G. and C.J. Weijer, *The Dictyostelium cell cycle and its relationship to differentiation.* FEMS Microbiol Lett, 1994. **124**(2): p. 123-30.
22. Joseph, J.M., et al., *The actinome of Dictyostelium discoideum in comparison to actins and actin-related proteins from other organisms.* PLoS ONE, 2008. **3**(7): p. e2654.
23. Eichinger, L., et al., *The genome of the social amoeba Dictyostelium discoideum.* Nature, 2005. **435**(7038): p. 43-57.
24. Devreotes, P. and C. Janetopoulos, *Eukaryotic chemotaxis: distinctions between directional sensing and polarization.* J Biol Chem, 2003. **278**(23): p. 20445-8.
25. Chung, C.Y., S. Funamoto, and R.A. Firtel, *Signaling pathways controlling cell polarity and chemotaxis.* Trends Biochem Sci, 2001. **26**(9): p. 557-66.
26. Janetopoulos, C. and R.A. Firtel, *Directional sensing during chemotaxis.* FEBS Lett, 2008. **582**(14): p. 2075-85.
27. Inoue, Y. and T. Adachi, *Coarse-grained Brownian ratchet model of membrane protrusion on cellular scale.* Biomech Model Mechanobiol, 2011. **10**(4): p. 495-503.
28. de la Roche, M.A. and G.P. Cote, *Regulation of Dictyostelium myosin I and II.* Biochim Biophys Acta, 2001. **1525**(3): p. 245-61.
29. Fukui, Y., S. Yumura, and T.K. Yumura, *Agar-overlay immunofluorescence: high-resolution studies of cytoskeletal components and their changes during chemotaxis.* Methods Cell Biol, 1987. **28**: p. 347-56.
30. Girard, K.D., S.C. Kuo, and D.N. Robinson, *Dictyostelium myosin II mechanochemistry promotes active behavior of the cortex on long time scales.* Proc Natl Acad Sci U S A, 2006. **103**(7): p. 2103-8.
31. Lauffenburger, D.A. and A.F. Horwitz, *Cell migration: a physically integrated molecular process.* Cell, 1996. **84**(3): p. 359-69.
32. Sasaki, A.T. and R.A. Firtel, *Finding the way: directional sensing and cell polarization through Ras signalling.* Novartis Found Symp, 2005. **269**: p. 73-87; discussion 87-91, 223-30.
33. Affolter, M. and C.J. Weijer, *Signaling to cytoskeletal dynamics during chemotaxis.* Dev Cell, 2005. **9**(1): p. 19-34.
34. Charest, P.G. and R.A. Firtel, *Feedback signaling controls leading-edge formation during chemotaxis.* Curr Opin Genet Dev, 2006. **16**(4): p. 339-47.
35. Carlier, M.F. and D. Pantaloni, *Direct evidence for ADP-Pi-F-actin as the major intermediate in ATP-actin polymerization. Rate of dissociation of Pi from actin filaments.* Biochemistry, 1986. **25**(24): p. 7789-92.
36. Pollard, T.D. and G.G. Borisy, *Cellular motility driven by assembly and disassembly of actin filaments.* Cell, 2003. **112**(4): p. 453-65.
37. Blanchoin, L., et al., *Direct observation of dendritic actin filament networks nucleated by Arp2/3 complex and WASP/Scar proteins.* Nature, 2000. **404**(6781): p. 1007-11.
38. Machesky, L.M., et al., *Purification of a cortical complex containing two unconventional actins from Acanthamoeba by affinity chromatography on profilin-agarose.* J Cell Biol, 1994. **127**(1): p. 107-15.
39. Goley, E.D. and M.D. Welch, *The ARP2/3 complex: an actin nucleator comes of age.* Nat Rev Mol Cell Biol, 2006. **7**(10): p. 713-26.
40. Pollard, T.D. and C.C. Beltzner, *Structure and function of the Arp2/3 complex.* Curr Opin Struct Biol, 2002. **12**(6): p. 768-74.
41. Mullins, R.D. and T.D. Pollard, *Structure and function of the Arp2/3 complex.* Curr Opin Struct Biol, 1999. **9**(2): p. 244-9.
42. Amann, K.J. and T.D. Pollard, *Direct real-time observation of actin filament branching mediated by Arp2/3 complex using total internal reflection fluorescence microscopy.* Proc Natl Acad Sci U S A, 2001. **98**(26): p. 15009-13.

43. Bailly, M., et al., *The F-actin side binding activity of the Arp2/3 complex is essential for actin nucleation and lamellipod extension.* Curr Biol, 2001. **11**(8): p. 620-5.
44. Mullins, R.D., J.A. Heuser, and T.D. Pollard, *The interaction of Arp2/3 complex with actin: nucleation, high affinity pointed end capping, and formation of branching networks of filaments.* Proc Natl Acad Sci U S A, 1998. **95**(11): p. 6181-6.
45. Pantaloni, D., et al., *The Arp2/3 complex branches filament barbed ends: functional antagonism with capping proteins.* Nat Cell Biol, 2000. **2**(7): p. 385-91.
46. Higgs, H.N., L. Blanchoin, and T.D. Pollard, *Influence of the C terminus of Wiskott-Aldrich syndrome protein (WASp) and the Arp2/3 complex on actin polymerization.* Biochemistry, 1999. **38**(46): p. 15212-22.
47. Welch, M.D., et al., *Interaction of human Arp2/3 complex and the Listeria monocytogenes ActA protein in actin filament nucleation.* Science, 1998. **281**(5373): p. 105-8.
48. Bompard, G. and E. Caron, *Regulation of WASP/WAVE proteins: making a long story short.* J Cell Biol, 2004. **166**(7): p. 957-62.
49. Machesky, L.M. and R.H. Insall, *Scar1 and the related Wiskott-Aldrich syndrome protein, WASP, regulate the actin cytoskeleton through the Arp2/3 complex.* Curr Biol, 1998. **8**(25): p. 1347-56.
50. Veltman, D.M. and R.H. Insall, *WASP family proteins: their evolution and its physiological implications.* Mol Biol Cell, 2010. **21**(16): p. 2880-93.
51. Miki, H., S. Suetsugu, and T. Takenawa, *WAVE, a novel WASP-family protein involved in actin reorganization induced by Rac.* EMBO J, 1998. **17**(23): p. 6932-41.
52. Ibarra, N., A. Pollitt, and R.H. Insall, *Regulation of actin assembly by SCAR/WAVE proteins.* Biochem Soc Trans, 2005. **33**(Pt 6): p. 1243-6.
53. Buck, M., W. Xu, and M.K. Rosen, *A two-state allosteric model for autoinhibition rationalizes WASP signal integration and targeting.* J Mol Biol, 2004. **338**(2): p. 271-85.
54. Prehoda, K.E., et al., *Integration of multiple signals through cooperative regulation of the N-WASP-Arp2/3 complex.* Science, 2000. **290**(5492): p. 801-6.
55. Vartiainen, M.K. and L.M. Machesky, *The WASP-Arp2/3 pathway: genetic insights.* Curr Opin Cell Biol, 2004. **16**(2): p. 174-81.
56. Higgs, H.N. and T.D. Pollard, *Regulation of actin filament network formation through ARP2/3 complex: activation by a diverse array of proteins.* Annu Rev Biochem, 2001. **70**: p. 649-76.
57. Rohatgi, R., et al., *The interaction between N-WASP and the Arp2/3 complex links Cdc42-dependent signals to actin assembly.* Cell, 1999. **97**(2): p. 221-31.
58. Pantaloni, D., C. Le Clainche, and M.F. Carlier, *Mechanism of actin-based motility.* Science, 2001. **292**(5521): p. 1502-6.
59. Wear, M.A. and J.A. Cooper, *Capping protein: new insights into mechanism and regulation.* Trends Biochem Sci, 2004. **29**(8): p. 418-28.
60. Eddy, R.J., J. Han, and J.S. Condeelis, *Capping protein terminates but does not initiate chemoattractant-induced actin assembly in Dictyostelium.* J Cell Biol, 1997. **139**(5): p. 1243-53.
61. Hartmann, H., M. Schleicher, and A.A. Noegel, *Heterodimeric capping proteins constitute a highly conserved group of actin-binding proteins.* Dev Genet, 1990. **11**(5-6): p. 369-76.
62. Haus, U., et al., *F-actin capping by cap32/34 requires heterodimeric conformation and can be inhibited with PIP2.* Biochem Biophys Res Commun, 1991. **181**(2): p. 833-9.
63. Uribe, R. and D. Jay, *A review of actin binding proteins: new perspectives.* Mol Biol Rep, 2009. **36**(1): p. 121-5.

64. Revenu, C., et al., *The co-workers of actin filaments: from cell structures to signals.* Nat Rev Mol Cell Biol, 2004. **5**(8): p. 635-46.
65. Carlsson, A.E., *Stimulation of actin polymerization by filament severing.* Biophys J, 2006. **90**(2): p. 413-22.
66. Moon, A. and D.G. Drubin, *The ADF/cofilin proteins: stimulus-responsive modulators of actin dynamics.* Mol Biol Cell, 1995. **6**(11): p. 1423-31.
67. Pope, B., et al., *Characterisation of the F-actin binding domains of villin: classification of F-actin binding proteins into two groups according to their binding sites on actin.* FEBS Lett, 1994. **338**(1): p. 58-62.
68. Iwadate, Y. and S. Yumura, *Actin-based propulsive forces and myosin-II-based contractile forces in migrating Dictyostelium cells.* J Cell Sci, 2008. **121**(Pt 8): p. 1314-24.
69. Tafuri, S.R., et al., *Dictyostelium discoideum myosin: isolation and characterization of cDNAs encoding the regulatory light chain.* Mol Cell Biol, 1989. **9**(7): p. 3073-80.
70. Chisholm, R.L., et al., *Dictyostelium discoideum myosin: isolation and characterization of cDNAs encoding the essential light chain.* Mol Cell Biol, 1988. **8**(2): p. 794-801.
71. Warrick, H.M., et al., *Conserved protein domains in a myosin heavy chain gene from Dictyostelium discoideum.* Proc Natl Acad Sci U S A, 1986. **83**(24): p. 9433-7.
72. Bosgraaf, L. and P.J. van Haastert, *The regulation of myosin II in Dictyostelium.* Eur J Cell Biol, 2006. **85**(9-10): p. 969-79.
73. Yumura, S., et al., *Multiple myosin II heavy chain kinases: roles in filament assembly control and proper cytokinesis in Dictyostelium.* Mol Biol Cell, 2005. **16**(9): p. 4256-66.
74. Murphy, M.B. and T.T. Egelhoff, *Biochemical characterization of a Dictyostelium myosin II heavy-chain phosphatase that promotes filament assembly.* Eur J Biochem, 1999. **264**(2): p. 582-90.
75. Levi, S., M.V. Polyakov, and T.T. Egelhoff, *Myosin II dynamics in Dictyostelium: determinants for filament assembly and translocation to the cell cortex during chemoattractant responses.* Cell Motil Cytoskeleton, 2002. **53**(3): p. 177-88.
76. Veltman, D.M. and P.J. Van Haastert, *Guanylyl cyclase protein and cGMP product independently control front and back of chemotaxing Dictyostelium cells.* Mol Biol Cell, 2006. **17**(9): p. 3921-9.
77. Bosgraaf, L., et al., *A novel cGMP signalling pathway mediating myosin phosphorylation and chemotaxis in Dictyostelium.* EMBO J, 2002. **21**(17): p. 4560-70.
78. Muller-Taubenberger, A., et al., *Differential localization of the Dictyostelium kinase DPAKa during cytokinesis and cell migration.* J Muscle Res Cell Motil, 2002. **23**(7-8): p. 751-63.
79. Chung, C.Y. and R.A. Firtel, *PAKa, a putative PAK family member, is required for cytokinesis and the regulation of the cytoskeleton in Dictyostelium discoideum cells during chemotaxis.* J Cell Biol, 1999. **147**(3): p. 559-76.
80. Olson, M.F., H.F. Paterson, and C.J. Marshall, *Signals from Ras and Rho GTPases interact to regulate expression of p21Waf1/Cip1.* Nature, 1998. **394**(6690): p. 295-9.
81. Goi, T., et al., *Ral-specific guanine nucleotide exchange factor activity opposes other Ras effectors in PC12 cells by inhibiting neurite outgrowth.* Mol Cell Biol, 1999. **19**(3): p. 1731-41.
82. Yoshimura, T., et al., *Ras regulates neuronal polarity via the PI3-kinase/Akt/GSK-3beta/CRMP-2 pathway.* Biochem Biophys Res Commun, 2006. **340**(1): p. 62-8.
83. Lim, C.J., et al., *Loss of the Dictyostelium RasC protein alters vegetative cell size, motility and endocytosis.* Exp Cell Res, 2005. **306**(1): p. 47-55.
84. Oxford, G. and D. Theodorescu, *Ras superfamily monomeric G proteins in carcinoma cell motility.* Cancer Lett, 2003. **189**(2): p. 117-28.

85. Shields, J.M., et al., *Understanding Ras: 'it ain't over 'til it's over'.* Trends Cell Biol, 2000. **10**(4): p. 147-54.
86. Zhu, J.J., et al., *Ras and Rap control AMPA receptor trafficking during synaptic plasticity.* Cell, 2002. **110**(4): p. 443-55.
87. Bourne, H.R., D.A. Sanders, and F. McCormick, *The GTPase superfamily: conserved structure and molecular mechanism.* Nature, 1991. **349**(6305): p. 117-27.
88. Thomas, C., et al., *Structural evidence for a common intermediate in small G protein-GEF reactions.* Mol Cell, 2007. **25**(1): p. 141-9.
89. Quilliam, L.A., J.F. Rebhun, and A.F. Castro, *A growing family of guanine nucleotide exchange factors is responsible for activation of Ras-family GTPases.* Prog Nucleic Acid Res Mol Biol, 2002. **71**: p. 391-444.
90. Boguski, M.S. and F. McCormick, *Proteins regulating Ras and its relatives.* Nature, 1993. **366**(6456): p. 643-54.
91. Shutes, A. and C.J. Der, *Real-time in vitro measurement of intrinsic and Ras GAP-mediated GTP hydrolysis.* Methods Enzymol, 2006. **407**: p. 9-22.
92. Olofsson, B., *Rho guanine dissociation inhibitors: pivotal molecules in cellular signalling.* Cell Signal, 1999. **11**(8): p. 545-54.
93. Rommel, C. and E. Hafen, *Ras--a versatile cellular switch.* Curr Opin Genet Dev, 1998. **8**(4): p. 412-8.
94. Raimondi, F., M. Orozco, and F. Fanelli, *Deciphering the deformation modes associated with function retention and specialization in members of the Ras superfamily.* Structure. **18**(3): p. 402-14.
95. Chubb, J.R. and R.H. Insall, *Dictyostelium: an ideal organism for genetic dissection of Ras signalling networks.* Biochim Biophys Acta, 2001. **1525**(3): p. 262-71.
96. Kae, H., et al., *Chemoattractant-induced Ras activation during Dictyostelium aggregation.* EMBO Rep, 2004. **5**(6): p. 602-6.
97. Lim, C.J., G.B. Spiegelman, and G. Weeks, *RasC is required for optimal activation of adenylyl cyclase and Akt/PKB during aggregation.* EMBO J, 2001. **20**(16): p. 4490-9.
98. Bolourani, P., G.B. Spiegelman, and G. Weeks, *Delineation of the roles played by RasG and RasC in cAMP-dependent signal transduction during the early development of Dictyostelium discoideum.* Mol Biol Cell, 2006. **17**(10): p. 4543-50.
99. Rivero, F. and B.P. Somesh, *Signal transduction pathways regulated by Rho GTPases in Dictyostelium.* J Muscle Res Cell Motil, 2002. **23**(7-8): p. 737-49.
100. Vlahou, G. and F. Rivero, *Rho GTPase signaling in Dictyostelium discoideum: insights from the genome.* Eur J Cell Biol, 2006. **85**(9-10): p. 947-59.
101. Rivero, F., et al., *The Dictyostelium discoideum family of Rho-related proteins.* Nucleic Acids Res, 2001. **29**(5): p. 1068-79.
102. Manahan, C.L., et al., *Chemoattractant signaling in dictyostelium discoideum.* Annu Rev Cell Dev Biol, 2004. **20**: p. 223-53.
103. Schneider, I.C. and J.M. Haugh, *Mechanisms of gradient sensing and chemotaxis: conserved pathways, diverse regulation.* Cell Cycle, 2006. **5**(11): p. 1130-4.
104. Levchenko, A. and P.A. Iglesias, *Models of eukaryotic gradient sensing: application to chemotaxis of amoebae and neutrophils.* Biophys J, 2002. **82**(1 Pt 1): p. 50-63.
105. Xu, X., et al., *Coupling mechanism of a GPCR and a heterotrimeric G protein during chemoattractant gradient sensing in Dictyostelium.* Sci Signal, 2010. **3**(141): p. ra71.
106. Funamoto, S., et al., *Role of phosphatidylinositol 3' kinase and a downstream pleckstrin homology domain-containing protein in controlling chemotaxis in dictyostelium.* J Cell Biol, 2001. **153**(4): p. 795-810.
107. Comer, F.I., et al., *The PI3K-mediated activation of CRAC independently regulates adenylyl cyclase activation and chemotaxis.* Curr Biol, 2005. **15**(2): p. 134-9.

108. Meili, R., et al., *Chemoattractant-mediated transient activation and membrane localization of Akt/PKB is required for efficient chemotaxis to cAMP in Dictyostelium.* EMBO J, 1999. **18**(8): p. 2092-105.
109. Iijima, M. and P. Devreotes, *Tumor suppressor PTEN mediates sensing of chemoattractant gradients.* Cell, 2002. **109**(5): p. 599-610.
110. Kriebel, P.W., V.A. Barr, and C.A. Parent, *Adenylyl cyclase localization regulates streaming during chemotaxis.* Cell, 2003. **112**(4): p. 549-60.
111. Millard, T.H., S.J. Sharp, and L.M. Machesky, *Signalling to actin assembly via the WASP (Wiskott-Aldrich syndrome protein)-family proteins and the Arp2/3 complex.* Biochem J, 2004. **380**(Pt 1): p. 1-17.
112. Burgstaller, G. and M. Gimona, *Actin cytoskeleton remodelling via local inhibition of contractility at discrete microdomains.* J Cell Sci, 2004. **117**(Pt 2): p. 223-31.
113. Van Haastert, P.J. and P.N. Devreotes, *Chemotaxis: signalling the way forward.* Nat Rev Mol Cell Biol, 2004. **5**(8): p. 626-34.
114. Lai, F.P., et al., *Arp2/3 complex interactions and actin network turnover in lamellipodia.* EMBO J, 2008. **27**(7): p. 982-92.
115. Carlier, M.F., et al., *Actin-based motility as a self-organized system: mechanism and reconstitution in vitro.* C R Biol, 2003. **326**(2): p. 161-70.
116. Kortholt, A. and P.J. van Haastert, *Highlighting the role of Ras and Rap during Dictyostelium chemotaxis.* Cell Signal, 2008. **20**(8): p. 1415-22.
117. Sasaki, A.T., et al., *Localized Ras signaling at the leading edge regulates PI3K, cell polarity, and directional cell movement.* J Cell Biol, 2004. **167**(3): p. 505-18.
118. Huang, Y.E., et al., *Receptor-mediated regulation of PI3Ks confines PI(3,4,5)P3 to the leading edge of chemotaxing cells.* Mol Biol Cell, 2003. **14**(5): p. 1913-22.
119. Kolman, M.F., L.M. Futey, and T.T. Egelhoff, *Dictyostelium myosin heavy chain kinase A regulates myosin localization during growth and development.* J Cell Biol, 1996. **132**(1-2): p. 101-9.
120. Xiong, Y., et al., *Cells navigate with a local-excitation, global-inhibition-biased excitable network.* Proc Natl Acad Sci U S A, 2010. **107**(40): p. 17079-86.
121. Bosgraaf, L. and P.J. Van Haastert, *A model for cGMP signal transduction in Dictyostelium in perspective of 25 years of cGMP research.* J Muscle Res Cell Motil, 2002. **23**(7-8): p. 781-91.
122. van Haastert, P.J. and H. Kuwayama, *cGMP as second messenger during Dictyostelium chemotaxis.* FEBS Lett, 1997. **410**(1): p. 25-8.
123. Dembinsky, A., H. Rubin, and S. Ravid, *Chemoattractant-mediated increases in cGMP induce changes in Dictyostelium myosin II heavy chain-specific protein kinase C activities.* J Cell Biol, 1996. **134**(4): p. 911-21.
124. Loovers, H.M., et al., *Distinct roles of PI(3,4,5)P3 during chemoattractant signaling in Dictyostelium: a quantitative in vivo analysis by inhibition of PI3-kinase.* Mol Biol Cell, 2006. **17**(4): p. 1503-13.
125. Funamoto, S., et al., *Spatial and temporal regulation of 3-phosphoinositides by PI 3-kinase and PTEN mediates chemotaxis.* Cell, 2002. **109**(5): p. 611-23.
126. Bosgraaf, L., I. Keizer-Gunnink, and P.J. Van Haastert, *PI3-kinase signaling contributes to orientation in shallow gradients and enhances speed in steep chemoattractant gradients.* J Cell Sci, 2008. **121**(Pt 21): p. 3589-97.
127. Andrew, N. and R.H. Insall, *Chemotaxis in shallow gradients is mediated independently of PtdIns 3-kinase by biased choices between random protrusions.* Nat Cell Biol, 2007. **9**(2): p. 193-200.
128. Van Haastert, P.J., *A stochastic model for chemotaxis based on the ordered extension of pseudopods.* Biophys J, 2010. **99**(10): p. 3345-54.

129. Bagorda, A., V.A. Mihaylov, and C.A. Parent, *Chemotaxis: moving forward and holding on to the past.* Thromb Haemost, 2006. **95**(1): p. 12-21.
130. Neilson, M.P., et al., *Chemotaxis: a feedback-based computational model robustly predicts multiple aspects of real cell behaviour.* PLoS Biol, 2011. **9**(5): p. e1000618.
131. Kim, J.Y., J.A. Borleis, and P.N. Devreotes, *Switching of chemoattractant receptors programs development and morphogenesis in Dictyostelium: receptor subtypes activate common responses at different agonist concentrations.* Dev Biol, 1998. **197**(1): p. 117-28.
132. Prabhu, Y. and L. Eichinger, *The Dictyostelium repertoire of seven transmembrane domain receptors.* Eur J Cell Biol, 2006. **85**(9-10): p. 937-46.
133. Kortholt, A., et al., *Phospholipase C regulation of phosphatidylinositol 3,4,5-trisphosphate-mediated chemotaxis.* Mol Biol Cell, 2007. **18**(12): p. 4772-9.
134. Iijima, M., et al., *Novel mechanism of PTEN regulation by its phosphatidylinositol 4,5-bisphosphate binding motif is critical for chemotaxis.* J Biol Chem, 2004. **279**(16): p. 16606-13.
135. Keizer-Gunnink, I., A. Kortholt, and P.J. Van Haastert, *Chemoattractants and chemorepellents act by inducing opposite polarity in phospholipase C and PI3-kinase signaling.* J Cell Biol, 2007. **177**(4): p. 579-85.
136. Okaichi, K., et al., *Amino acid substitutions in the Dictyostelium G alpha subunit G alpha 2 produce dominant negative phenotypes and inhibit the activation of adenylyl cyclase, guanylyl cyclase, and phospholipase C.* Mol Biol Cell, 1992. **3**(7): p. 735-47.
137. Inoue, T. and T. Meyer, *Synthetic activation of endogenous PI3K and Rac identifies an AND-gate switch for cell polarization and migration.* PLoS ONE, 2008. **3**(8): p. e3068.
138. Para, A., et al., *Dictyostelium Dock180-related RacGEFs regulate the actin cytoskeleton during cell motility.* Mol Biol Cell, 2009. **20**(2): p. 699-707.
139. Blagg, S.L., et al., *PIR121 regulates pseudopod dynamics and SCAR activity in Dictyostelium.* Curr Biol, 2003. **13**(17): p. 1480-7.
140. Sasaki, A.T. and R.A. Firtel, *Regulation of chemotaxis by the orchestrated activation of Ras, PI3K, and TOR.* Eur J Cell Biol, 2006. **85**(9-10): p. 873-95.
141. Merrifield, C.J., et al., *Neural Wiskott Aldrich Syndrome Protein (N-WASP) and the Arp2/3 complex are recruited to sites of clathrin-mediated endocytosis in cultured fibroblasts.* Eur J Cell Biol, 2004. **83**(1): p. 13-8.
142. Kamimura, Y., et al., *PIP3-independent activation of TorC2 and PKB at the cell's leading edge mediates chemotaxis.* Curr Biol, 2008. **18**(14): p. 1034-43.
143. Sasaki, A.T., et al., *G protein-independent Ras/PI3K/F-actin circuit regulates basic cell motility.* J Cell Biol, 2007. **178**(2): p. 185-91.
144. Merlot, S. and R.A. Firtel, *Leading the way: Directional sensing through phosphatidylinositol 3-kinase and other signaling pathways.* J Cell Sci, 2003. **116**(Pt 17): p. 3471-8.
145. Hoeller, O. and R.R. Kay, *Chemotaxis in the absence of PIP3 gradients.* Curr Biol, 2007. **17**(9): p. 813-7.
146. Rericha, E.C. and C.A. Parent, *Steering in quadruplet: the complex signaling pathways directing chemotaxis.* Sci Signal, 2008. **1**(22): p. pe26.
147. Schaloske, R. and D. Malchow, *Mechanism of cAMP-induced Ca2+ influx in Dictyostelium: role of phospholipase A2.* Biochem J, 1997. **327 ( Pt 1)**: p. 233-8.
148. Veltman, D.M., I. Keizer-Gunnik, and P.J. Van Haastert, *Four key signaling pathways mediating chemotaxis in Dictyostelium discoideum.* J Cell Biol, 2008. **180**(4): p. 747-53.
149. Lee, S., et al., *TOR complex 2 integrates cell movement during chemotaxis and signal relay in Dictyostelium.* Mol Biol Cell, 2005. **16**(10): p. 4572-83.

150. Charest, P.G., et al., *A Ras signaling complex controls the RasC-TORC2 pathway and directed cell migration.* Dev Cell, 2010. **18**(5): p. 737-49.
151. Cai, H., et al., *Ras-mediated activation of the TORC2-PKB pathway is critical for chemotaxis.* J Cell Biol, 2010. **190**(2): p. 233-45.
152. Chen, L., et al., *Two phases of actin polymerization display different dependencies on PI(3,4,5)P3 accumulation and have unique roles during chemotaxis.* Mol Biol Cell, 2003. **14**(12): p. 5028-37.
153. Langridge, P.D. and R.R. Kay, *Mutants in the Dictyostelium Arp2/3 complex and chemoattractant-induced actin polymerization.* Exp Cell Res, 2007. **313**(12): p. 2563-74.
154. Orelio, C. and T.W. Kuijpers, *Shwachman-Diamond syndrome neutrophils have altered chemoattractant-induced F-actin polymerization and polarization characteristics.* Haematologica, 2009. **94**(3): p. 409-13.
155. Somesh, B.P., et al., *RacG regulates morphology, phagocytosis, and chemotaxis.* Eukaryot Cell, 2006. **5**(10): p. 1648-63.
156. Van Haastert, P.J. and D.M. Veltman, *Chemotaxis: navigating by multiple signaling pathways.* Sci STKE, 2007. **2007**(396): p. pe40.
157. Cravatt, B.F., G.M. Simon, and J.R. Yates, 3rd, *The biological impact of mass-spectrometry-based proteomics.* Nature, 2007. **450**(7172): p. 991-1000.
158. Ong, S.E. and M. Mann, *Mass spectrometry-based proteomics turns quantitative.* Nat Chem Biol, 2005. **1**(5): p. 252-62.
159. Hu, Q., et al., *The Orbitrap: a new mass spectrometer.* J Mass Spectrom, 2005. **40**(4): p. 430-43.
160. Olsen, J.V., et al., *Parts per million mass accuracy on an Orbitrap mass spectrometer via lock mass injection into a C-trap.* Mol Cell Proteomics, 2005. **4**(12): p. 2010-21.
161. Scigelova, M. and A. Makarov, *Orbitrap mass analyzer--overview and applications in proteomics.* Proteomics, 2006. **6 Suppl 2**: p. 16-21.
162. McLafferty, F.W., et al., *Top-down MS, a powerful complement to the high capabilities of proteolysis proteomics.* FEBS J, 2007. **274**(24): p. 6256-68.
163. Witze, E.S., et al., *Mapping protein post-translational modifications with mass spectrometry.* Nat Methods, 2007. **4**(10): p. 798-806.
164. Nita-Lazar, A., H. Saito-Benz, and F.M. White, *Quantitative phosphoproteomics by mass spectrometry: past, present, and future.* Proteomics, 2008. **8**(21): p. 4433-43.
165. Kim, S.C., et al., *Substrate and functional diversity of lysine acetylation revealed by a proteomics survey.* Mol Cell, 2006. **23**(4): p. 607-18.
166. Parker, C.E., et al., *Mass spectrometric determination of protein ubiquitination.* Methods Mol Biol, 2008. **446**: p. 109-30.
167. Andersen, J.S., I. Matic, and A.C. Vertegaal, *Identification of SUMO target proteins by quantitative proteomics.* Methods Mol Biol, 2009. **497**: p. 19-31.
168. Parker, C.E., et al., *Mass Spectrometry for Post-Translational Modifications.* 2011.
169. Jensen, O.N., *Interpreting the protein language using proteomics.* Nat Rev Mol Cell Biol, 2006. **7**(6): p. 391-403.
170. Wepf, A., et al., *Quantitative interaction proteomics using mass spectrometry.* Nat Methods, 2009. **6**(3): p. 203-5.
171. Trinkle-Mulcahy, L., et al., *Identifying specific protein interaction partners using quantitative mass spectrometry and bead proteomes.* J Cell Biol, 2008. **183**(2): p. 223-39.
172. Vasilescu, J., X. Guo, and J. Kast, *Identification of protein-protein interactions using in vivo cross-linking and mass spectrometry.* Proteomics, 2004. **4**(12): p. 3845-54.
173. Gingras, A.C., et al., *Analysis of protein complexes using mass spectrometry.* Nat Rev Mol Cell Biol, 2007. **8**(8): p. 645-54.

174. Link, A.J., et al., *Direct analysis of protein complexes using mass spectrometry.* Nat Biotechnol, 1999. **17**(7): p. 676-82.
175. Boisvert, F.M., et al., *A quantitative spatial proteomics analysis of proteome turnover in human cells.* Mol Cell Proteomics, 2011.
176. Walther, T.C. and M. Mann, *Mass spectrometry-based proteomics in cell biology.* J Cell Biol, 2010. **190**(4): p. 491-500.
177. Pagliuca, F.W., et al., *Quantitative proteomics reveals the basis for the biochemical specificity of the cell-cycle machinery.* Mol Cell, 2011. **43**(3): p. 406-17.
178. Lucitt, M.B., et al., *Analysis of the zebrafish proteome during embryonic development.* Mol Cell Proteomics, 2008. **7**(5): p. 981-94.
179. Kierszniowska, S., B. Seiwert, and W.X. Schulze, *Definition of Arabidopsis sterol-rich membrane microdomains by differential treatment with methyl-beta-cyclodextrin and quantitative proteomics.* Mol Cell Proteomics, 2009. **8**(4): p. 612-23.
180. Morandell, S., et al., *Quantitative proteomics and phosphoproteomics reveal novel insights into complexity and dynamics of the EGFR signaling network.* Proteomics, 2008. **8**(21): p. 4383-401.
181. Yan, W. and S.S. Chen, *Mass spectrometry-based quantitative proteomic profiling.* Brief Funct Genomic Proteomic, 2005. **4**(1): p. 27-38.
182. Ong, S.E. and M. Mann, *A practical recipe for stable isotope labeling by amino acids in cell culture (SILAC).* Nat Protoc, 2006. **1**(6): p. 2650-60.
183. Shevchenko, A., et al., *In-gel digestion for mass spectrometric characterization of proteins and proteomes.* Nature Protocols, 2006. **1**(6): p. 2856-2860.
184. Chenau, J., et al., *Peptides OFFGEL electrophoresis: a suitable pre-analytical step for complex eukaryotic samples fractionation compatible with quantitative iTRAQ labeling.* Proteome Sci, 2008. **6**: p. 9.
185. Wisniewski, J.R., et al., *Universal sample preparation method for proteome analysis.* Nat Methods, 2009. **6**(5): p. 359-62.
186. Wisniewski, J.R., A. Zougman, and M. Mann, *Combination of FASP and StageTip-based fractionation allows in-depth analysis of the hippocampal membrane proteome.* J Proteome Res, 2009. **8**(12): p. 5674-8.
187. Fenn, J.B., et al., *Electrospray ionization for mass spectrometry of large biomolecules.* Science, 1989. **246**(4926): p. 64-71.
188. March, R.E., *Quadrupole ion traps.* Mass Spectrom Rev, 2009. **28**(6): p. 961-89.
189. Ouyang, Z., et al., *Quadrupole ion traps and trap arrays: geometry, material, scale, performance.* Eur J Mass Spectrom (Chichester, Eng), 2007. **13**(1): p. 13-8.
190. Sadygov, R.G., D. Cociorva, and J.R. Yates, 3rd, *Large-scale database searching using tandem mass spectra: looking up the answer in the back of the book.* Nat Methods, 2004. **1**(3): p. 195-202.
191. Cox, J. and M. Mann, *MaxQuant enables high peptide identification rates, individualized p.p.b.-range mass accuracies and proteome-wide protein quantification.* Nat Biotechnol, 2008. **26**(12): p. 1367-72.
192. Gerisch, G. and A. Muller-Taubenberger, *GFP-fusion proteins as fluorescent reporters to study organelle and cytoskeleton dynamics in chemotaxis and phagocytosis.* Methods Enzymol, 2003. **361**: p. 320-37.
193. Miyawaki, A., A. Sawano, and T. Kogure, *Lighting up cells: labelling proteins with fluorophores.* Nat Cell Biol, 2003. **Suppl**: p. S1-7.
194. Chudakov, D.M., S. Lukyanov, and K.A. Lukyanov, *Fluorescent proteins as a toolkit for in vivo imaging.* Trends Biotechnol, 2005. **23**(12): p. 605-13.
195. Shimomura, O., F.H. Johnson, and Y. Saiga, *Extraction, purification and properties of aequorin, a bioluminescent protein from the luminous hydromedusan, Aequorea.* J Cell Comp Physiol, 1962. **59**: p. 223-39.

196. Prasher, D.C., et al., *Primary structure of the Aequorea victoria green-fluorescent protein.* Gene, 1992. **111**(2): p. 229-33.
197. Inouye, S. and F.I. Tsuji, *Aequorea green fluorescent protein. Expression of the gene and fluorescence characteristics of the recombinant protein.* FEBS Lett, 1994. **341**(2-3): p. 277-80.
198. Chalfie, M., et al., *Green fluorescent protein as a marker for gene expression.* Science, 1994. **263**(5148): p. 802-5.
199. Heim, R., A.B. Cubitt, and R.Y. Tsien, *Improved green fluorescence.* Nature, 1995. **373**(6516): p. 663-4.
200. Tsien, R.Y., *The green fluorescent protein.* Annu Rev Biochem, 1998. **67**: p. 509-44.
201. Ormo, M., et al., *Crystal structure of the Aequorea victoria green fluorescent protein.* Science, 1996. **273**(5280): p. 1392-5.
202. Yang, F., L.G. Moss, and G.N. Phillips, Jr., *The molecular structure of green fluorescent protein.* Nat Biotechnol, 1996. **14**(10): p. 1246-51.
203. Heim, R. and R.Y. Tsien, *Engineering green fluorescent protein for improved brightness, longer wavelengths and fluorescence resonance energy transfer.* Curr Biol, 1996. **6**(2): p. 178-82.
204. Pedelacq, J.D., et al., *Engineering and characterization of a superfolder green fluorescent protein.* Nat Biotechnol, 2006. **24**(1): p. 79-88.
205. Nagai, T., et al., *A variant of yellow fluorescent protein with fast and efficient maturation for cell-biological applications.* Nat Biotechnol, 2002. **20**(1): p. 87-90.
206. Lukyanov, K.A., et al., *Innovation: Photoactivatable fluorescent proteins.* Nat Rev Mol Cell Biol, 2005. **6**(11): p. 885-91.
207. Chudakov, D.M., et al., *Photoswitchable cyan fluorescent protein for protein tracking.* Nat Biotechnol, 2004. **22**(11): p. 1435-9.
208. Patterson, G.H. and J. Lippincott-Schwartz, *A photoactivatable GFP for selective photolabeling of proteins and cells.* Science, 2002. **297**(5588): p. 1873-7.
209. Zacharias, D.A., et al., *Partitioning of lipid-modified monomeric GFPs into membrane microdomains of live cells.* Science, 2002. **296**(5569): p. 913-6.
210. Miesenbock, G., D.A. De Angelis, and J.E. Rothman, *Visualizing secretion and synaptic transmission with pH-sensitive green fluorescent proteins.* Nature, 1998. **394**(6689): p. 192-5.
211. Ando, R., et al., *An optical marker based on the UV-induced green-to-red photoconversion of a fluorescent protein.* Proc Natl Acad Sci U S A, 2002. **99**(20): p. 12651-6.
212. Shaner, N.C., et al., *Improved monomeric red, orange and yellow fluorescent proteins derived from Discosoma sp. red fluorescent protein.* Nat Biotechnol, 2004. **22**(12): p. 1567-72.
213. Shaner, N.C., P.A. Steinbach, and R.Y. Tsien, *A guide to choosing fluorescent proteins.* Nat Methods, 2005. **2**(12): p. 905-9.
214. Hutter, H., *Fluorescent protein methods: strategies and applications.* Methods Cell Biol, 2012. **107**: p. 67-92.
215. Gunkel, M., et al., *Dual color localization microscopy of cellular nanostructures.* Biotechnol J, 2009. **4**(6): p. 927-38.
216. Wallace, W., L.H. Schaefer, and J.R. Swedlow, *A workingperson's guide to deconvolution in light microscopy.* Biotechniques, 2001. **31**(5): p. 1076-8, 1080, 1082 passim.
217. Dailey, M., et al., *Concepts in imaging and microscopy. Exploring biological structure and function with confocal microscopy.* Biol Bull, 1999. **197**(2): p. 115-22.

218. Fink-Puches, R., et al., *Confocal laser scanning microscopy: a new optical microscopic technique for applications in pathology and dermatology.* J Cutan Pathol, 1995. **22**(3): p. 252-9.
219. Itoh, J., et al., *Three-dimensional imaging of hormone-secreting cells and their microvessel environment in estrogen-induced prolactinoma of the rat pituitary gland by confocal laser scanning microscopy.* Appl Immunohistochem Mol Morphol, 2001. **9**(4): p. 364-70.
220. Shotton, D. and N. White, *Confocal scanning microscopy: three-dimensional biological imaging.* Trends Biochem Sci, 1989. **14**(11): p. 435-9.
221. Keller, P.J. and E.H. Stelzer, *Digital scanned laser light sheet fluorescence microscopy.* Cold Spring Harb Protoc, 2010. **2010**(5): p. pdb top78.
222. Keller, P.J., et al., *Reconstruction of zebrafish early embryonic development by scanned light sheet microscopy.* Science, 2008. **322**(5904): p. 1065-9.
223. Axelrod, D., *Total internal reflection fluorescence microscopy.* Methods Cell Biol, 1989. **30**: p. 245-70.
224. Axelrod, D., *Total internal reflection fluorescence microscopy in cell biology.* Traffic, 2001. **2**(11): p. 764-74.
225. Schmoranzer, J., et al., *Imaging constitutive exocytosis with total internal reflection fluorescence microscopy.* J Cell Biol, 2000. **149**(1): p. 23-32.
226. Gerisch, G., *Imaging actin cytoskeleton dynamics in Dictyostelium chemotaxis.* Methods Mol Biol, 2009. **571**: p. 385-400.
227. Patel, H., et al., *The multi-FERM-domain-containing protein FrmA is required for turnover of paxillin-adhesion sites during cell migration of Dictyostelium.* J Cell Sci, 2008. **121**(Pt 8): p. 1159-64.
228. Axelrod, D., *Cell-substrate contacts illuminated by total internal reflection fluorescence.* J Cell Biol, 1981. **89**(1): p. 141-5.
229. de Hoon, M.J., et al., *Open source clustering software.* Bioinformatics, 2004. **20**(9): p. 1453-4.
230. Saldanha, A.J., *Java Treeview--extensible visualization of microarray data.* Bioinformatics, 2004. **20**(17): p. 3246-8.
231. Kim, J.Y., et al., *Random mutagenesis of the cAMP chemoattractant receptor, cAR1, of Dictyostelium. Mutant classes that cause discrete shifts in agonist affinity and lock the receptor in a novel activational intermediate.* J Biol Chem, 1997. **272**(4): p. 2060-8.
232. Veltman, D.M., et al., *A new set of small, extrachromosomal expression vectors for Dictyostelium discoideum.* Plasmid, 2009. **61**(2): p. 110-8.
233. Franke, J. and R. Kessin, *A defined minimal medium for axenic strains of Dictyostelium discoideum.* Proc Natl Acad Sci U S A, 1977. **74**(5): p. 2157-61.
234. Hestermann, A. and R. Graf, *The XMAP215-family protein DdCP224 is required for cortical interactions of microtubules.* BMC Cell Biol, 2004. **5**: p. 24.
235. Tai, C.Y., et al., *Role of dynein, dynactin, and CLIP-170 interactions in LIS1 kinetochore function.* J Cell Biol, 2002. **156**(6): p. 959-68.
236. Dogterom, M., et al., *Force generation by dynamic microtubules.* Curr Opin Cell Biol, 2005. **17**(1): p. 67-74.
237. Adames, N.R. and J.A. Cooper, *Microtubule interactions with the cell cortex causing nuclear movements in Saccharomyces cerevisiae.* J Cell Biol, 2000. **149**(4): p. 863-74.
238. Rehberg, M., et al., *Dictyostelium LIS1 is a centrosomal protein required for microtubule/cell cortex interactions, nucleus/centrosome linkage, and actin dynamics.* Mol Biol Cell, 2005. **16**(6): p. 2759-71.
239. Du, F., et al., *Regulation of contractile vacuole formation and activity in Dictyostelium.* EMBO J, 2008. **27**(15): p. 2064-76.

240. Heuser, J., Q. Zhu, and M. Clarke, *Proton pumps populate the contractile vacuoles of Dictyostelium amoebae.* J Cell Biol, 1993. **121**(6): p. 1311-27.
241. Forgac, M., *Structure and properties of the vacuolar (H+)-ATPases.* J Biol Chem, 1999. **274**(19): p. 12951-4.
242. Vitavska, O., H. Wieczorek, and H. Merzendorfer, *A novel role for subunit C in mediating binding of the H+-V-ATPase to the actin cytoskeleton.* J Biol Chem, 2003. **278**(20): p. 18499-505.
243. Holliday, L.S., et al., *The amino-terminal domain of the B subunit of vacuolar H+-ATPase contains a filamentous actin binding site.* J Biol Chem, 2000. **275**(41): p. 32331-7.
244. Carnell, M., et al., *Actin polymerization driven by WASH causes V-ATPase retrieval and vesicle neutralization before exocytosis.* J Cell Biol, 2011. **193**(5): p. 831-9.
245. Rybakin, V. and C.S. Clemen, *Coronin proteins as multifunctional regulators of the cytoskeleton and membrane trafficking.* Bioessays, 2005. **27**(6): p. 625-32.
246. Smith, T.F., et al., *The WD repeat: a common architecture for diverse functions.* Trends Biochem Sci, 1999. **24**(5): p. 181-5.
247. Machesky, L.M., et al., *Mammalian actin-related protein 2/3 complex localizes to regions of lamellipodial protrusion and is composed of evolutionarily conserved proteins.* Biochem J, 1997. **328 ( Pt 1)**: p. 105-12.
248. Humphries, C.L., et al., *Direct regulation of Arp2/3 complex activity and function by the actin binding protein coronin.* J Cell Biol, 2002. **159**(6): p. 993-1004.
249. Rodal, A.A., et al., *Conformational changes in the Arp2/3 complex leading to actin nucleation.* Nat Struct Mol Biol, 2005. **12**(1): p. 26-31.
250. Shina, M.C., et al., *Redundant and unique roles of coronin proteins in Dictyostelium.* Cell Mol Life Sci, 2010. **68**(2): p. 303-13.
251. Cvrckova, F., F. Rivero, and B. Bavlnka, *Evolutionarily conserved modules in actin nucleation: lessons from Dictyostelium discoideum and plants. Review article.* Protoplasma, 2004. **224**(1-2): p. 15-31.
252. Shina, M.C., et al., *A Coronin7 homolog with functions in actin-driven processes.* J Biol Chem, 2010. **285**(12): p. 9249-61.
253. de Hostos, E.L., et al., *Dictyostelium mutants lacking the cytoskeletal protein coronin are defective in cytokinesis and cell motility.* J Cell Biol, 1993. **120**(1): p. 163-73.
254. Haus, U., et al., *The heat shock cognate protein from Dictyostelium affects actin polymerization through interaction with the actin-binding protein cap32/34.* EMBO J, 1993. **12**(10): p. 3763-71.
255. Eddy, R.J., R.A. Sauterer, and J.S. Condeelis, *Aginactin, an agonist-regulated F-actin capping activity is associated with an Hsc70 in Dictyostelium.* J Biol Chem, 1993. **268**(31): p. 23267-74.
256. Eddy, R.J., et al., *A major agonist-regulated capping activity in Dictyostelium is due to the capping protein, cap32/34.* Biochim Biophys Acta, 1996. **1314**(3): p. 247-59.
257. Rohrig, U., et al., *Coactosin interferes with the capping of actin filaments.* FEBS Lett, 1995. **374**(2): p. 284-6.
258. Lee, S., et al., *Involvement of the cytoskeleton in controlling leading-edge function during chemotaxis.* Mol Biol Cell, 2010. **21**(11): p. 1810-24.
259. Kollmar, M. and G. Glockner, *Identification and phylogenetic analysis of Dictyostelium discoideum kinesin proteins.* BMC Genomics, 2003. **4**(1): p. 47.
260. Iwai, S., et al., *A novel actin-bundling kinesin-related protein from Dictyostelium discoideum.* J Biol Chem, 2004. **279**(6): p. 4696-704.
261. Meller, N., S. Merlot, and C. Guda, *CZH proteins: a new family of Rho-GEFs.* J Cell Sci, 2005. **118**(Pt 21): p. 4937-46.

262. Cote, J.F. and K. Vuori, *Identification of an evolutionarily conserved superfamily of DOCK180-related proteins with guanine nucleotide exchange activity.* J Cell Sci, 2002. **115**(Pt 24): p. 4901-13.
263. Kobayashi, S., et al., *Membrane recruitment of DOCK180 by binding to PtdIns(3,4,5)P3.* Biochem J, 2001. **354**(Pt 1): p. 73-8.
264. Cote, J.F. and K. Vuori, *In vitro guanine nucleotide exchange activity of DHR-2/DOCKER/CZH2 domains.* Methods Enzymol, 2006. **406**: p. 41-57.
265. Bosgraaf, L. and P.J. Van Haastert, *Roc, a Ras/GTPase domain in complex proteins.* Biochim Biophys Acta, 2003. **1643**(1-3): p. 5-10.
266. Marin, I., *The Parkinson disease gene LRRK2: evolutionary and structural insights.* Mol Biol Evol, 2006. **23**(12): p. 2423-33.
267. van Egmond, W.N. and P.J. van Haastert, *Characterization of the Roco protein family in Dictyostelium discoideum.* Eukaryot Cell, 2010. **9**(5): p. 751-61.
268. Ito, G., et al., *GTP binding is essential to the protein kinase activity of LRRK2, a causative gene product for familial Parkinson's disease.* Biochemistry, 2007. **46**(5): p. 1380-8.
269. Korr, D., et al., *LRRK1 protein kinase activity is stimulated upon binding of GTP to its Roc domain.* Cell Signal, 2006. **18**(6): p. 910-20.
270. Bokoch, G.M., *Biology of the p21-activated kinases.* Annu Rev Biochem, 2003. **72**: p. 743-81.
271. Lee, S.F., et al., *Regulation of the p21-activated kinase-related Dictyostelium myosin I heavy chain kinase by autophosphorylation, acidic phospholipids, and Ca2+-calmodulin.* J Biol Chem, 1998. **273**(43): p. 27911-7.
272. Morita, Y.S., et al., *Localization of Dictyostelium myoB and myoD to filopodia and cell-cell contact sites using isoform-specific antibodies.* Eur J Cell Biol, 1996. **71**(4): p. 371-9.
273. De La Roche, M.A., S.F. Lee, and G.P. Cote, *The Dictyostelium class I myosin, MyoD, contains a novel light chain that lacks high-affinity calcium-binding sites.* Biochem J, 2003. **374**(Pt 3): p. 697-705.
274. Senda, S., et al., *Recruitment of a specific amoeboid myosin I isoform to the plasma membrane in chemotactic Dictyostelium cells.* J Biol Chem, 2001. **276**(4): p. 2898-904.
275. de la Roche, M., et al., *Cellular distribution and functions of wild-type and constitutively activated Dictyostelium PakB.* Mol Biol Cell, 2005. **16**(1): p. 238-47.
276. Frost, A., V.M. Unger, and P. De Camilli, *The BAR domain superfamily: membrane-molding macromolecules.* Cell, 2009. **137**(2): p. 191-6.
277. Paunola, E., P.K. Mattila, and P. Lappalainen, *WH2 domain: a small, versatile adapter for actin monomers.* FEBS Lett, 2002. **513**(1): p. 92-7.
278. Palmgren, S., et al., *Interactions with PIP2, ADP-actin monomers, and capping protein regulate the activity and localization of yeast twinfilin.* J Cell Biol, 2001. **155**(2): p. 251-60.
279. Lappalainen, P., et al., *The ADF homology (ADF-H) domain: a highly exploited actin-binding module.* Mol Biol Cell, 1998. **9**(8): p. 1951-9.
280. Matthews, J.M. and M. Sunde, *Zinc fingers--folds for many occasions.* IUBMB Life, 2002. **54**(6): p. 351-5.
281. Shevchuk, O., et al., *Proteomic analysis of Legionella-containing phagosomes isolated from Dictyostelium.* Int J Med Microbiol, 2009. **299**(7): p. 489-508.
282. Reinders, Y., et al., *Identification of novel centrosomal proteins in Dictyostelium discoideum by comparative proteomic approaches.* J Proteome Res, 2006. **5**(3): p. 589-98.

283. Friedberg, F. and F. Rivero, *Single and multiple CH (calponin homology) domain containing multidomain proteins in Dictyostelium discoideum: an inventory.* Mol Biol Rep, 2009. **37**(6): p. 2853-62.
284. Gimona, M. and R. Mital, *The single CH domain of calponin is neither sufficient nor necessary for F-actin binding.* J Cell Sci, 1998. **111 ( Pt 13)**: p. 1813-21.
285. Clarke, P.R. and C. Zhang, *Spatial and temporal coordination of mitosis by Ran GTPase.* Nat Rev Mol Cell Biol, 2008. **9**(6): p. 464-77.
286. Jeon, T.J., et al., *Regulation of Rap1 activity by RapGAP1 controls cell adhesion at the front of chemotaxing cells.* J Cell Biol, 2007. **179**(5): p. 833-43.
287. Seastone, D.J., et al., *The small Mr Ras-like GTPase Rap1 and the phospholipase C pathway act to regulate phagocytosis in Dictyostelium discoideum.* Mol Biol Cell, 1999. **10**(2): p. 393-406.
288. Rebstein, P.J., et al., *Mutational analysis of the role of Rap1 in regulating cytoskeletal function in Dictyostelium.* Exp Cell Res, 1997. **231**(2): p. 276-83.
289. Jeon, T.J., et al., *Rap1 controls cell adhesion and cell motility through the regulation of myosin II.* J Cell Biol, 2007. **176**(7): p. 1021-33.
290. Andrade, M.A., C. Perez-Iratxeta, and C.P. Ponting, *Protein repeats: structures, functions, and evolution.* J Struct Biol, 2001. **134**(2-3): p. 117-31.
291. Emoto, K., et al., *Control of dendritic branching and tiling by the Tricornered-kinase/Furry signaling pathway in Drosophila sensory neurons.* Cell, 2004. **119**(2): p. 245-56.
292. Cong, J., et al., *The furry gene of Drosophila is important for maintaining the integrity of cellular extensions during morphogenesis.* Development, 2001. **128**(14): p. 2793-802.
293. He, Y., et al., *The tricornered Ser/Thr protein kinase is regulated by phosphorylation and interacts with furry during Drosophila wing hair development.* Mol Biol Cell, 2005. **16**(2): p. 689-700.
294. Bukharova, T., et al., *Paxillin is required for cell-substrate adhesion, cell sorting and slug migration during Dictyostelium development.* J Cell Sci, 2005. **118**(Pt 18): p. 4295-310.
295. Russell, L.C., et al., *Identification of conserved residues required for the binding of a tetratricopeptide repeat domain to heat shock protein 90.* J Biol Chem, 1999. **274**(29): p. 20060-3.
296. Chen, M.S., et al., *The tetratricopeptide repeat domain of protein phosphatase 5 mediates binding to glucocorticoid receptor heterocomplexes and acts as a dominant negative mutant.* J Biol Chem, 1996. **271**(50): p. 32315-20.
297. Iyer, L.M., et al., *Evolutionary history and higher order classification of AAA+ ATPases.* J Struct Biol, 2004. **146**(1-2): p. 11-31.
298. Cano, M.L., D.A. Lauffenburger, and S.H. Zigmond, *Kinetic analysis of F-actin depolymerization in polymorphonuclear leukocyte lysates indicates that chemoattractant stimulation increases actin filament number without altering the filament length distribution.* J Cell Biol, 1991. **115**(3): p. 677-87.
299. Han, J.W., et al., *Role of RacC for the regulation of WASP and phosphatidylinositol 3-kinase during chemotaxis of Dictyostelium.* J Biol Chem, 2006. **281**(46): p. 35224-34.
300. Wessels, D., et al., *PTEN plays a role in the suppression of lateral pseudopod formation during Dictyostelium motility and chemotaxis.* J Cell Sci, 2007. **120**(Pt 15): p. 2517-31.
301. Summerscales, J. and J.F. Dawson, *Probing Dictyostelium severin structure and function by cross linking to actin.* Biochem Cell Biol, 2004. **82**(2): p. 343-50.
302. Yamamoto, K., et al., *Mechanism of interaction of Dictyostelium severin with actin filaments.* J Cell Biol, 1982. **95**(3): p. 711-9.

303. Faix, J., et al., *Cortexillins, major determinants of cell shape and size, are actin-bundling proteins with a parallel coiled-coil tail.* Cell, 1996. **86**(4): p. 631-42.
304. Secko, D.M., et al., *An activated Ras protein alters cell adhesion by dephosphorylating Dictyostelium DdCAD-1.* Microbiology, 2006. **152**(Pt 5): p. 1497-505.
305. Lin, Z., et al., *Solution structures of the adhesion molecule DdCAD-1 reveal new insights into Ca(2+)-dependent cell-cell adhesion.* Nat Struct Mol Biol, 2006. **13**(11): p. 1016-22.
306. Dieckmann, R., et al., *A myosin IK-Abp1-PakB circuit acts as a switch to regulate phagocytosis efficiency.* Mol Biol Cell, 2010. **21**(9): p. 1505-18.
307. Schwarz, E.C., et al., *Dictyostelium myosin IK is involved in the maintenance of cortical tension and affects motility and phagocytosis.* J Cell Sci, 2000. **113 ( Pt 4)**: p. 621-33.
308. Park, K.C., et al., *Rac regulation of chemotaxis and morphogenesis in Dictyostelium.* EMBO J, 2004. **23**(21): p. 4177-89.
309. Comer, F.I. and C.A. Parent, *Phosphoinositide 3-kinase activity controls the chemoattractant-mediated activation and adaptation of adenylyl cyclase.* Mol Biol Cell, 2006. **17**(1): p. 357-66.